NAT'L INST. OF STAND & TECH R.I.C.
A11104 411774
NIST
PUBLICATIONS

NISTIR 5499

ANNUAL CONFERENCE ON FIRE RESEARCH: Book of Abstracts October 17-20, 1994

Sheilda B. Smith, Editor

United States Department of Commerce
nology Administration
›nal Institute of Standards and Technology

QC
100
.U56
NO.5499
1994

NISTIR 5499

ANNUAL CONFERENCE ON FIRE RESEARCH: Book of Abstracts October 17-20, 1994

Sheilda B. Smith, Editor

September, 1994
Building and Fire Research Laboratory
National Institute of Standards and Technology
Gaithersburg, MD 20899

U.S. Department of Commerce
Ronald H. Brown, *Secretary*
Technology Administration
Mary L. Good, *Under Secretary for Technology*
National Institute of Standards and Technology
Arati Prabhakar, *Director*

TABLE OF CONTENTS

INTRODUCTION

The NIST Annual Conference on Fire Research has long been the prime forum for the presentation and discussion of the latest advances in the science of fire and the engineering of fire safety. Hundreds of billions of dollars of products and services are involved in fire safety decisions each year. New technology is changing the way those products are developed, manufactured, evaluated, and used. This conference enables all interested parties to hear of and discuss advances in fire science, with the intent of stimulating (a) new products that are more fire-safe and (b) new ways to capture that value in the ways products are tested and approved for use.

The Conference scope includes all fire research performed within Federal laboratories or sponsored by Federal agencies, as well as work from laboratories around the world. The Conference was organized with the assistance of representatives from those Federal agencies:

Mr. Donald Bathurst	General Services Administration
Mr. Michael Bennett	Wright-Patterson Air Force Base
Dr. Thor Eklund	Federal Aviation Administration
Mr. Kenneth Faulstich	Department of Veterans Affairs
Dr. Robert Friedman	NASA Lewis Research Center
Mr. William Haskell	U.S. Army Materials Technology Laboratory
Mr. James Hoebel	Consumer Product Safety Commission
Ms. Karla Kertis	U.S. Bureau of Mines
Mr. Dennis Kubicki	Department of Energy
Mr. Larry Maruskin	U.S. Fire Administration
Mr. Charles McGuire	Department of Transportation
Dr. Ronald Sheinson	Naval Research Laboratory
Mr. Phillip Tapper	NASA Goddard Space Flight Center
Capt. Thomas Tetta	Tyndall Air Force Base
Dr. Robert White	Forest Products Laboratory

This booklet contains the abstracts of the 84 papers focussing on the phenomenology of fire: fire extinguishment, chemistry and physics of material and product combustion, flame spread, flame structure, soot, fire signatures, fire-induced flows, pool fires, fire plumes, and fire hazard and risk. Discussion sessions will consider the status of our knowledge and the most important understanding yet to be developed. With this, we hope to continue cross-pollinating the elements of the fire research community while stimulating our members to new understanding that will lead to more fire-safe products and practices.

Richard G. Gann, Conference Chair
Chief, Fire Science Division
Building and Fire Research Laboratory
National Institute of Standards and Technology

FLAME SUPPRESSION EFFECTIVENESS OF HALON ALTERNATIVES[1]

William L. Grosshandler and Anthony Hamins
Building and Fire Research Laboratory
National Institute of Standards and Technology
Gaithersburg, MD 20899

The elimination of new production of halon 1301 has forced the manufacturers, owners, and users of aircraft to search for an alternative. The program described here developed performance screens for candidate agents as a means to identify the best chemicals for subsequent full-scale aircraft fire extinguishment evaluation at Wright-Patterson Air Force Base[2]. The discriminating factors could be lumped into four categories: agent dispersion characteristics, required storage volume, environmental factors, and operational issues. The results presented in this abstract are limited to the flame suppression experiments, which directly impact the storage volume of agent required. However, the dispersion of the agents in cold-flow experiments varied more extensively than the amount of the agent required for flame suppression. The behavior of the chemical as it leaves the storage vessel (typically pressurized with N_2 at 4.1 MPa) and subsequently flashes or breaks into droplets, evaporates, and mixes with ambient air is critical, and can render an agent which requires less mass to extinguish a laboratory flame less effective in suppressing an actual aircraft fire. The reader is referred to the thorough discussion by Pitts et al.[3] for details of the agent dispersion screening process.

Four different flame suppression facilities were designed with the objective of examining the flame extinction properties of the agents over the whole range of conditions likely to be encountered by aircraft in flight: (1) an opposed-flow diffusion flame (OFDF) burner, (2) a cup burner, (3) a turbulent spray burner, and (4) a detonation/deflagration tube. A core of eleven gaseous fluorocarbons (FCs), hydrofluorocarbons (HFCs), and hydrochlorofluorocarbons (HCFCs) were examined in all four facilities and compared to the performance of N_2 and CF_3Br. Iodotrifluoromethane and sodium bicarbonate powder were examined in three of the flames, and twenty additional compounds were evaluated in the cup burner alone. Air was the oxidizer and the fuels included ethene, propane, heptane, JP-5, JP-8, and two hydraulic fluids. While the absolute amount of agent necessary to quench the flames varied with the operating conditions in each facility, a single parameter called the volume factor, VF, was chosen to compare the relative suppression performance of the various agents. VF is an estimate of the liquid volume in the storage vessel for a given agent normalized by the liquid volume of halon 1301, and is found from the respective saturated liquid densities and the measurements of mass fraction, Y_i, found in each laboratory burner.

The cup burner apparatus produces a co-flowing flame burning gaseous and liquid fuels, and can handle gaseous, liquid and powder suppressants. CF_3I and the bromine containing compounds were generally very effective on both a mole and a mass basis. The absolute agent concentration at extinction was found to agree well with measurements made in the OFDF[4]. The turbulent spray burner was useful for comparing the performance of extinguishing agents in transient operation, with the agent delivery system able to control accurately the injection period between 20 and 910 ms. Of the chemicals evaluated in the turbulent spray burner, $NaHCO_3$ was the only compound more effective than halon 1301, and CF_3I required the least mass and volume of the gaseous agents. The gaseous agents performed better in the turbulent spray burner relative to halon 1301 than was

---

[1] Sponsored by Wright-Patterson AFB, the US Naval Air Systems Command, the Army Aviation and Troop Command, and the FAA Technical Center

[2] *Evaluation of Alternative In-flight Fire Suppressants for Full-scale Testing in Simulated Aircraft Engine Nacelles and Dry Bays*, W.L. Grosshandler, R.G. Gann and W.M. Pitts, editors, NIST Special Publication 861, Gaithersburg, MD, April 1994.

[3] "Fluid Dynamics of Agent Discharge," W.M. Pitts, J.C. Yang, G.Gmurczyk, L.Y. Cooper, W.L. Grosshandler, and C. Presser, Section 3, *ibid.*

[4] "Flame Suppression Effectiveness," A. Hamins, G. Gmurczyk, W.L. Grosshandler, R.G. Rehwoldt, I. Vazquez, T. Cleary, C. Presser and K. Seshadri, Section 3, *ibid.*

predicted from cup burner measurements. The experimental conditions in the deflagration/detonation tube differed significantly from those found in the other burners. The main qualitative difference was the occurrence of a strong shock wave ahead of the flame which influenced the chemical state of the pure combustible mixture in the driver section and the mixture containing an agent in the test section.

Table 1 compares the volume factors for each apparatus (sodium bicarbonate is expressed on a mass basis). The OFDF values were found from the ambient temperature experiments with JP-8, taken at a strain rate of 100 s^{-1}. The cup burner values were measured with heptane as the fuel. For the spray burner, VF was calculated from the mass of agent injected in the ambient temperature JP-8 experiments. The performance in the detonation tube was based upon the average of the mass of agent required to reduce the pressure ratio by one half and to 10% of the maximum increase, with data restricted to the lean experiments. The uncertainty in the values of VF is estimated to be $\pm$ 10%.

The following observations summarize the results of the flame suppression study:

- The relative ranking of the agents depends upon whether one uses a mass basis or a volume basis.
- The relative ranking of the agents varies only slightly among the three non-premixed burners, but a substantially different ranking results from the premixed deflagration/detonation apparatus.
- The relative ranking of the agents is not much affected by the fuel type or air temperature.
- The quantity of agent required to suppress a flame varies with the type of burner generally in the following order: cup burner $\approx$ low strain OFDF > spray burner > high strain OFDF > deflagration tube.
- The quantity of agent required to suppress a non-premixed flame varies somewhat with the type of fuel in the following order: propane > heptane > JP-8 > JP-5 > HF-5606 > HF-83282.
- The quantity of agent required to suppress the turbulent spray flame increases with decreasing rate of agent injection.
- The quantity of agent required to attenuate the shock wave speed and pressure ratio in the deflagration/ detonation tube varies with equivalence ratio, sometimes increasing as one goes from lean to stoichiometric and sometimes decreasing.

Table 1. Volume factors for flame suppression in different apparatus

Agent	OFDF	Cup Burner	Spray Burner	Deflag. Tube
$NaHCO_3$ (mass)	0.23	0.45	0.85	--
CF_3I	--	0.9	0.8	1.4
HCFC-124	2.5	2.2	1.8	1.5
HCFC-22	3.0	2.8	1.8	2.5
HFC-236fa	3.1	2.3	1.8	1.4
HFC-227	3.2	2.4	1.8	1.4
FC-218	3.6	2.8	2.1	1.2
FC-3110	3.9	2.6	2.1	1.4
HFC-134a	4.0	2.8	2.0	1.8
HFC-125	4.1	2.8	2.0	1.7
FC-318	4.1	2.6	2.0	1.4
HFC-32/125	5.3	3.5	2.5	2.5
FC-116	7.1	6.0	4.0	2.5

Chemical Inhibition of Methane-Air Diffusion Flames

K.Seshadri

Center for Energy and Combustion Research
Department of Applied Mechanics and Engineering Sciences
University of California at San Diego
La Jolla, California 92093-0310

Abstract

A numerical and experimental study is performed to clarify the mechanisms of chemical inhibition of methane-air diffusion flames. The counterflow configuration is employed for the study. Numerical calculations are performed to determine the structure of the two-dimensional, laminar, diffusion flames stabilized in the forward stagnation region of a porous cylinder. In the counterflow configuration the flame structure is influenced by the value of the strain rate a. The chemical-kinetic mechanism employed in the calculations contained 52 elementary reactions involving 29 chemical species excluding nitrogen. The values of the rate parameters for the reactions used in the calculations are those recommended by Peters and Rogg [1] and Westbrook [2]. The flame structure is calculated for various values of a with different amounts of CF_3Br added to air.

The results of the numerical calculations show the chemical reactions to occur in three zones. These zones are referred to as "fuel-consumption zone," the "product-formation zone" and the "CF_3Br-consumption zone." The fuel-consumption zone is found to be a sink for radicals and in this zone the predominant reactions are found to be those between the fuel and the radicals to form CO and H_2. The CF_3Br-consumption zone is found to be an additional sink for radicals and also a sink for H_2. A significant amount of oxygen is found to leak through the fuel-consumption zone into the fuel-stream. These qualitative observations are used as a guide for the asymptotic analysis.

An asymptotic analysis is performed to determine the influence of CF_3Br on the structure and extinction of nonpremixed methane-air flames. The inhibitor CF_3Br is again added to the air-stream of the diffusion flame. In the outer structure of the flame CH_4 and CF_3Br are presumed to be completely consumed in two different infinitely thin zones and the chemistry in these zones are represented by the global steps

$$CH_4 + 2O_2 \rightarrow CO_2 + 2H_2O. \qquad \text{GI}$$

$$CF_3Br + 2H_2O \rightarrow HBr + 3HF + CO_2. \qquad \text{GII}$$

It is noteworthy that the global step GII does not involve O_2. These infinitely thin reaction zones are separated by a chemically inert region. Previous analysis by Peters [3] has shown that these reaction zones must merge at conditions close to extinction. Therefore only the asymptotic structure of the merged flame is analyzed here.

In the inner structure of the flame, a reduced four-step mechanism is used to describe the chemistry taking place in the reaction zone. This four-step mechanism can be written as

$$
\begin{aligned}
CH_4 + O_2 &\rightarrow CO + H_2 + H_2O, && \text{I}\\
CO + H_2O &\rightleftharpoons CO_2 + H_2, && \text{II}\\
O_2 + 2H_2 &\rightarrow 2H_2O, && \text{III}\\
CF_3Br + 7H_2 + 3O_2 &\rightarrow 5H_2O + HBr + 3HF + CO. && \text{IV}
\end{aligned}
$$

The reaction rates of the overall reactions in the reduced mechanism can be related to the reaction rates of an appropriate elementary chemical-kinetic mechanism. For simplicity only the contributions of the principal elementary reactions are included in the asymptotic analysis. In the four-step mechanism, the overall reaction I is effectively a chain-breaking step and represents the reaction between the fuel and the radicals to form the intermediate products CO and H_2. The overall reaction II represents the oxidation of CO to form the final product CO_2. The overall reaction III represents the three-body recombination steps and is also responsible for a major fraction of the heat released in the flame. The overall reaction IV is also a net chain-breaking step and represents the reaction between the inhibitor CF_3Br and the radicals. In fact it is found that the chain-breaking effect of CF_3Br is greater than that of CH_4 [4]. It is interesting that H_2 is produced in the overall step I but is consumed in the overall step IV. The stoichiometry of the overall steps I and IV is found to be consistent with the numerically calculated profiles of CH_4, CF_3Br, H_2 and H. In the inner structure of the merged flame chemical reactions are presumed to take place in three distinct layers which were identified as the "fuel-consumption layer," the "oxidation layer" and the "CF_3Br-consumption layer". Following previous analysis of Seshadri and Ilincic [5] of the structure of uninhibited methane-air diffusion flames, oxygen is presumed to leak through the reaction zone to the leading order.

The results of the asymptotic analysis predicts the value of the scalar dissipation rate at extinction to decrease with increasing concentration of CF_3Br in the oxidizing stream. However the inhibiting effect of CF_3Br predicted by the asymptotic model is found to be weaker than that measured previously. The differences between the predictions of the asymptotic model and the measurements are attributed to the neglect of the contributions of additional inhibiting reactions to the rates of the overall reactions in the reduced chemical-kinetic mechanism. The asymptotic model predicts the value of the maximum flame temperature at extinction to increase with increasing concentration of CF_3Br in the air-stream which agrees qualitatively with the results of previous numerical calculations as well as with previous measurements. Research is in progress aimed at improving the predictions of the asymptotic analysis.

References

[1] Peters, N., and Rogg, B., (Eds.), Reduced Kinetic Mechanisms for Application in Combustion Systems, *Lecture Notes in Physics* m 15, Springer-Verlag, Berlin Heidelberg, 1993.

[2] Westbrook, C. K., *Combust. Sci. Tech.* 36: 201-225 (1983).

[3] Peters, N., *Twentieth Symposium (International) on Combustion,* The Combustion Institute, Pittsburgh, pp 353–360 (1984).

[4] Seshadri, K, Ilincic, N., "The Asymptotic Structure of Inhibited Nonpremixed Methane-Air Flames," Submitted for publication in *Combust. Flame,* 1994.

[5] Seshadri, K., and Ilincic, N., "The Asymptotic Structure of Nonpremixed Methane-Air Flames With Oxidizer Leakage of Order Unity," Submitted for publication in *Combust. Flame,* 1994.

SUPPRESSION OF SIMULATED ENGINE NACELLE FIRES

A. Hamins, D. Baghdadi, P. Borthwick, M. Glover,
W. Grosshandler, D. Lowe, L. Melton[1], and C. Presser[2]

Building and Fire Research Laboratory
National Institute of Standards and Technology

The engine nacelle encases the jet engine compressor, combustor and turbine. A nacelle fire is typically a turbulent diffusion flame stabilized behind an obstruction in a moderately high speed air flow. The most likely source for a fire in the nacelle are leaks in the fuel lines carrying jet fuel or hydraulic fluid, that can feed the fire either as a spray or as a pre-vaporized gas. Temperatures as high as 150 °C are common in normal operating engine nacelles.

Extinguishment occurs when a critical amount of agent is transported to the flame, where it is entrained into the primary reaction zone. The extinction process is affected by a number of parameters, including the velocity of the air flow, the type and quantity of fuel, the system temperature, agent properties and concentration, and the flow field geometry (e.g., the location of obstacles in the flow field). Re-ignition is also dependent on these system parameters and should be considered independently from the extinction phenomena.

Halon 1301, or trifluorobromomethane (CF_3Br), has been used as the fire extinguishing agent for protecting aircraft engine nacelles because of its many positive attributes. However, its production will cease at the end of this year, leaving many aircraft needing an alternative. The Air Force will soon begin testing three candidate alternatives to halon 1301 in its full scale Engine Nacelle Test Facility. Because testing cannot be performed for all possible aircraft and conditions, knowledge is needed which will provide guidance in the extension of the full-scale data to untested systems and conditions.

Recently, the Air Force funded an experimental study which involved simulating an idealized engine nacelle fire[1-3]. A coaxial turbulent spray burner was used, with jet fuel and hydraulic fluid as the fuels with the air at ambient and elevated temperatures. The research presented here extends that study to a broader range of suppression and re-ignition conditions, typical of in-flight engine nacelles.

The objective of the work is to document guidelines for fire suppression system performance based on improved understanding of the influence of various parameters on fire suppression in the engine nacelle. The primary objective of the proposed research is to produce organized guidance for adjusting the needed concentration of candidate fire suppressants over a range of engine nacelle fire conditions. This will be based on understanding the influence of various parameters on the flame extinction process in the engine nacelle.

Flame suppression measurements were conducted in a coaxial turbulent jet spray burner with JP8 fuel. The agents tested are CF_3I, HFC-125, and HFC-227. The mass and mass rate of application of agent required to achieve extinction of the spray flame is measured. A broad range of suppression and re-ignition condi tions are tested and the influence of a number of flow parameters are investigated including the fuel and air flow, air and agent temperature, system pressure, rate of agent application, and agent injection interval.

---

1. Department of Chemistry, University of Texas, Dallas, TX
2. CSTL, NIST, Gaithersburg, MD

Results show that as the agent delivery interval decreases, the mass of agent required for suppression increases. Measurements also show that the air flow has little impact on the required mass (see Fig. 1 below).

References

1. "A Turbulent Spray Burner for Assessing Halon Alternative Fire Suppressants", Grosshandler, W., Lowe, D., Rinkinen, B., Presser, C., ASME Paper No 93-WA/HT-23, 1993.

2. "Assessing Halon Alternatives for Aircraft Engine Nacelle Fire Suppression", Grosshandler, W., Presser, C., Lowe, D., and Rinkinen, W., to appear in J. Heat Transfer (1994).

3. "Suppression of Elevated Temperature Hydraulic Fluid and JP8 Spray Flames", Vazquez, I., Grosshandler, W., Rinkinen, W., Glover, M., and Presser, C., to appear in the Proceedings of the Fourth International Symposium on Fire Safety Science, 1994.

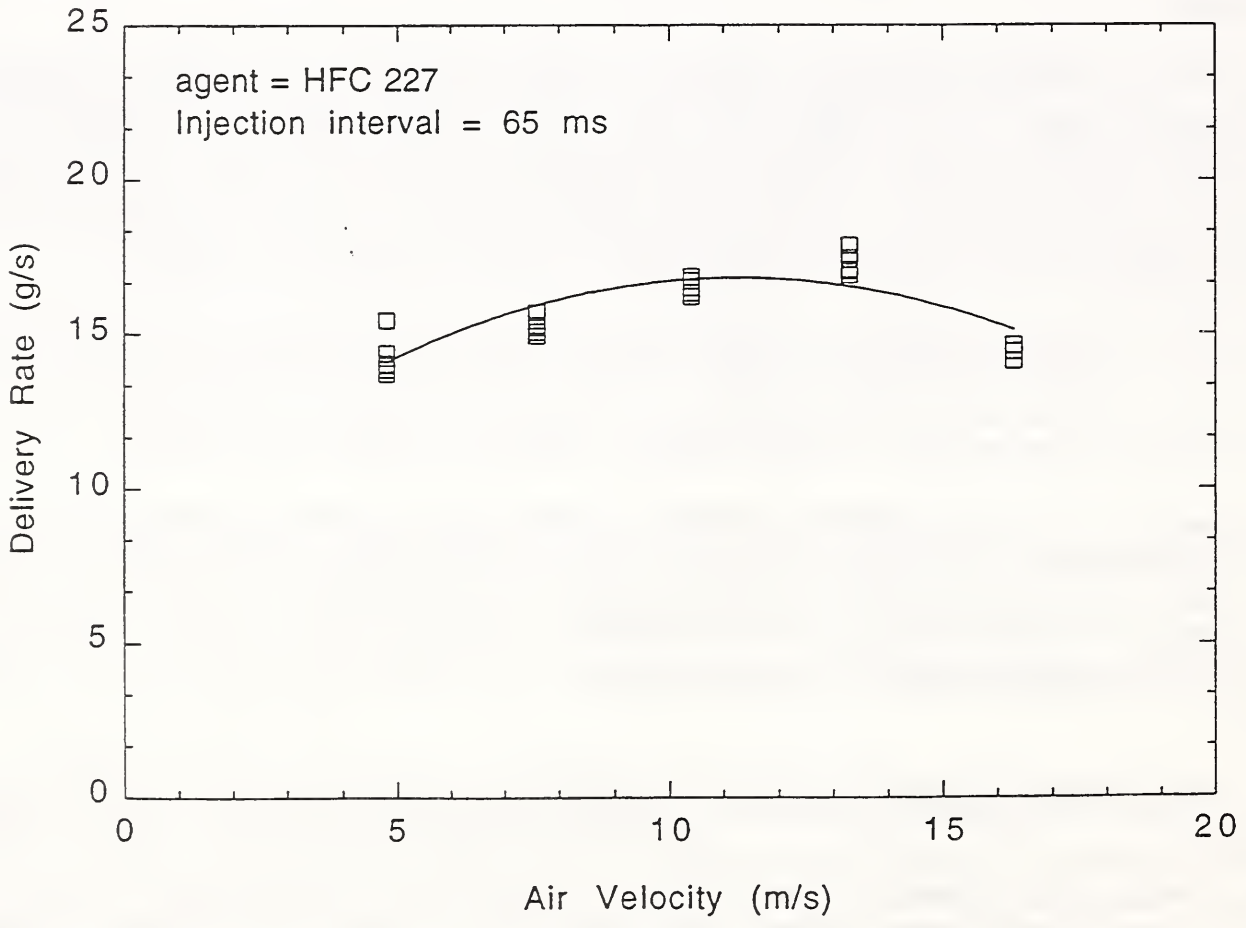

Figure 1 The mass delivery rate of agent required to extinguish the JP8 spray flame as a function of air velocity.

ABSTRACT

Halon 1301 Surrogates for Engine Nacelle Fire Suppression System Certification[1]

C.A. Womeldorf, J.Y. Yang, and W.L. Grosshandler

National Institute of Standards and Technology
Building and Fire Research Laboratory
Building 224, Room B356
Gaithersburg, MD 20899

Until recently halon 1301 has been regularly discharged in Navy aircraft engine nacelles to certify that the fire suppression systems distribute the fire suppressant effectively. Halon 1301 can no longer be used in this manner because of its high ozone depletion potential. In order to continue to certify the fire suppression systems of Navy aircraft a surrogate for halon 1301 must be found. Ideally, this simulant will have the physical and dynamical properties that will allow it to mimic halon 1301 in discharge behavior in any aircraft fire suppression system. This work presents the significant parameters relevant to agent discharge in an engine nacelle, as well as a discussion of the procedure and preliminary results of our search for a halon 1301 simulant.

The discharge of halon 1301 during the aircraft certification process is a complex combination of many factors. It can be broken into four primary areas:

- N_2 pressurized bottle and storage
- Two-phase flow through the piping
- Spray discharge into the nacelle
- Statham analyzer detection of the agent

The physical characteristics of halon 1301 affect how it behaves in each of these areas. Some of its properties are more critical in a specific area than others. For example, the solubility of halon with N_2 will be of critical concern during the storage and pressurization stage. And as a consequence, it is important to take the solubility of any possible simulant into account. Similarly, during the discharge process the boiling point, heat of vaporization, and liquid heat capacity must be taken into account; these properties can be considered individually or in the composite value of the Jakob number. Below is a table summarizing some of the properties we have considered important and the areas they influence

	Storage	Pipe Flow	Discharge	Statham
Boiling Point		X	X	
Critical Temperature	X		X	
Molecular Weight	X	X		
Critical Pressure	X			
Liquid Density	X			
Liquid Viscosity		X		
Solubility w/N_2	X		X	
Surface Tension			X	
Melting Point			X	
Heat of Vaporization		X	X	
Liquid Heat Capacity		X	X	
Vapor Pressure	X			
Jakob Number		X	X	
Vapor Viscosity		X		X
Thermal Conductivity				X

[1] Sponsored by U.S. Naval Air Systems Team, Lakehurst, New Jersey

The first three properties listed above (boiling point, critical temperature, and molecular weight) were used for an initial review of a large number of chemicals. If a chemical was found to have a boiling point and a critical temperature in the range of plus or minus 25°C from that of halon 1301, then it was carried over to the next round of criteria. At the second level the qualifying chemicals were examined for suitability for the application. They could not be flammable, toxic, corrosive, unstable, or difficult to obtain. In addition, it was essential that their ozone depletion potential was below the cutoff value of 0.2, preferably zero. And though not a factor that eliminated any acceptable candidates, the atmospheric lifetime was used as an indicator of the global warming potential and, eventually was considered in the determination of the final selection of three candidates.

The five possible candidates, shown here alongside halon 1301, are:

	Halon 1301	HCFC-22	HFC-125	FC-216	FC-218	SF_6
Chemical Form	CF_3Br	$CHClF_2$	C_2HF_5	C_3F_6	C_3F_8	SF_6
Molecular Weight, kg/mol	148.91	86.47	120.03	150.00	188.03	146.06
Normal boiling point, °C	-57.83	-40.86	-48.57	-29.65	-36.75	-63.90
Critical temperature, °C	67.05	96.15	66.18	94.80	71.95	45.54
Melting point, °C	-168.10	-157.42	-103.00	-156.60	-147.69	-50.70
Vapor pressure, kPa at 22°C	1508	949.1	1174	602.7	814.6	2268
Jakob number, at 20°C	.51	.31	.52	.40	.58	.67*
Ozone Depletion Potential	16	0.05	0	0	0	0
Atmospheric lifetime, years	110	16	41	2800*	10,000	3200

A thorough analysis of these and other parameters was conducted to determine which of these chemicals had the highest potential to serve as good simulants of halon 1301. This analysis as well as review of experiments performed by NAVSEA on SF_6, HCFC-22, and halon 1301[2] led to the selection of three candidate simulants. The chemicals NIST has recommended to the Navy for testing are HFC-125, SF_6, and HCFC-22, in that order of preference. The strengths and drawbacks of each are summarized below:

	Strengths	Drawbacks
HFC-125	Excellent Jakob Number Very good overall comparison More conservative than SF_6 Zero ozone depletion potential Short atmospheric lifetime	Low liquid density Low vapor pressure
SF_6	Excellent molecular weight Very good overall comparison Zero Ozone Depletion Potential	Potentially too high Jakob number Long atmospheric lifetime High melting point
HCFC-22	Satisfactory overall comparison Very low ALT	Very low molecular weight Low Jakob number Low vapor pressure Non-zero Ozone Depletion Potential

NIST and Walter Kidde Aerospace are currently testing these three candidates for similarities with halon 1301 in flow, discharge, and wind tunnel tests.

---

* Extrapolated value.

[2] "Hydraulic Performance Test of Halon 1301 Test Gas Simulants," P.J. DiNenno, E.W. Forssell, M.D. Starchville, H.W. Carhart, J.T. Leonard, *Fire Technology*, May 1990, pp. 121-140.

Pipe Flow Characteristics of Alternative Agent/Nitrogen Mixtures*

T.G. Cleary, M.D. King, J.C. Yang, and W.L. Grosshandler

Building and Fire Research Laboratory
National Institute of Standards and Technology
Gaithersburg, MD 20899 U.S.A

ABSTRACT

The evaluation of alternative agents for application in engine nacelle fire protection includes delivery efficiency of agent from a remote storage bottle through piping to the nacelle injection location. Present military requirements for halon systems specify a maximum discharge time from the remote bottle to the injection location of 1 second. A similar performance criterion for the replacement agent delivery will more than likely be required. The applicability of retro-fitting existing systems or optimal design of new systems necessitates a thorough understanding of the two-phase flow in piping. As part of the halon replacement project, an experimental pipe flow apparatus was constructed and is being used to examine alternative agent flow in various horizontal piping configurations and conditions. The selected agents for engine nacelle fire protection are CF_3I, HFC-227ea, and HFC-125. Halon 1301 is included in this study in order to establish a reference for comparison.

The experimental apparatus, shown in Fig. 1, consists of a 4.1 ℓ pressure vessel, a fast-opening valve connected to the bottom of the vessel, piping, agent recovery tanks, and nitrogen make-up tanks connected to the top of the pressure vessel and isolated by an electric solenoid valve. A test can be run either at constant head, where make-up nitrogen flows into the vessel during discharge to maintain the ullage pressure, or a standard test where no additional nitrogen is added to the ullage during discharge, as is the case for actual systems. Measurements include pipe and ullage pressure traces during discharge, and a limited number of high speed movies of the discharge viewed through a clear section of piping. Strain-gage type pressure transducers flush-mounted in the piping are used to record temporal pressure variation. An example of a pressure trace is shown in Fig. 2.

The effects of the initial vessel temperature, fill condition (amount of agent and nitrogen superpressurization), pipe diameter and length, and piping configuration are being studied.

A typical experiment consists of filling the pressure vessel with a known amount of agent to some fill condition (typically 1/2 or 2/3 filled); then nitrogen is added to the vessel from an access port in the fast-opening valve, allowing it to bubble through the liquid. The bubbling facilitates the dissolution of the nitrogen. If a constant-head test is to be run, the make-up tanks are pressurized slightly above the vessel pressure, and the valve from the make-up tanks to the vessel opens approximately 20 ms before the fast-opening valve to the piping. The contents from the pressure vessel flows through the piping to the recovery tanks (15 ℓ total volume) which are chilled with dry ice, allowing the agent to condense for reuse.

Tests performed with halon 1301 show the expected result that the pressure drop is non-linear; the pressure drop increases as the fluid travels down the piping. The pressure in the recovery tanks starts to increase almost as soon as the agent is released, and increases at an approximately constant rate until

*Sponsored by U.S. Air Force, U.S. Navy, and U.S. Army

the pressure reaches the final value at the end of the test. The increasing pressure in the recovery tanks has no significant effect on the flow during the constant-head tests. After the pipe fills with agent, the pipe pressures remain constant until presumably the liquid runs out, in which case a steady mass flow rate can be estimated. The pressure drop for a given pipe length in the constant-head tests are equivalent to the pressure drop in the standard tests when the bottle pressures are equal. Therefore, for the most part, one can assume that the standard test proceeds in a quasi-steady manner.

Two-phase pipe flow characteristics for other agents and under various experimental conditions will be presented and discussed.

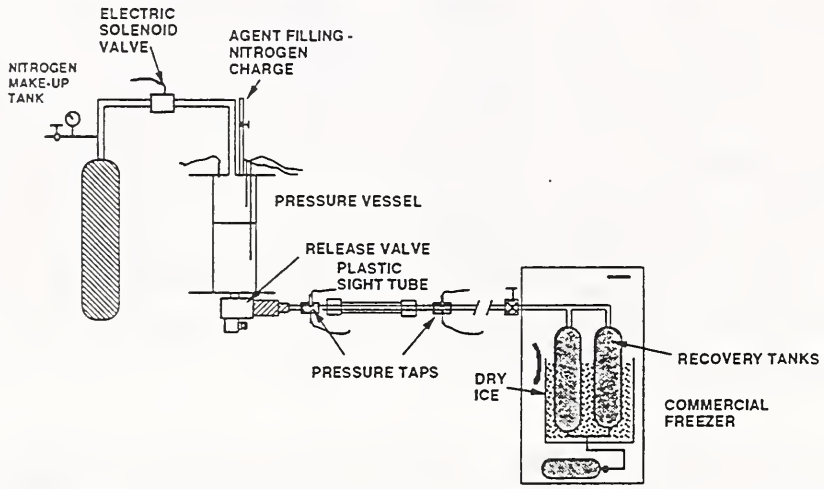

Figure 1. Schematic diagram of experimental apparatus.

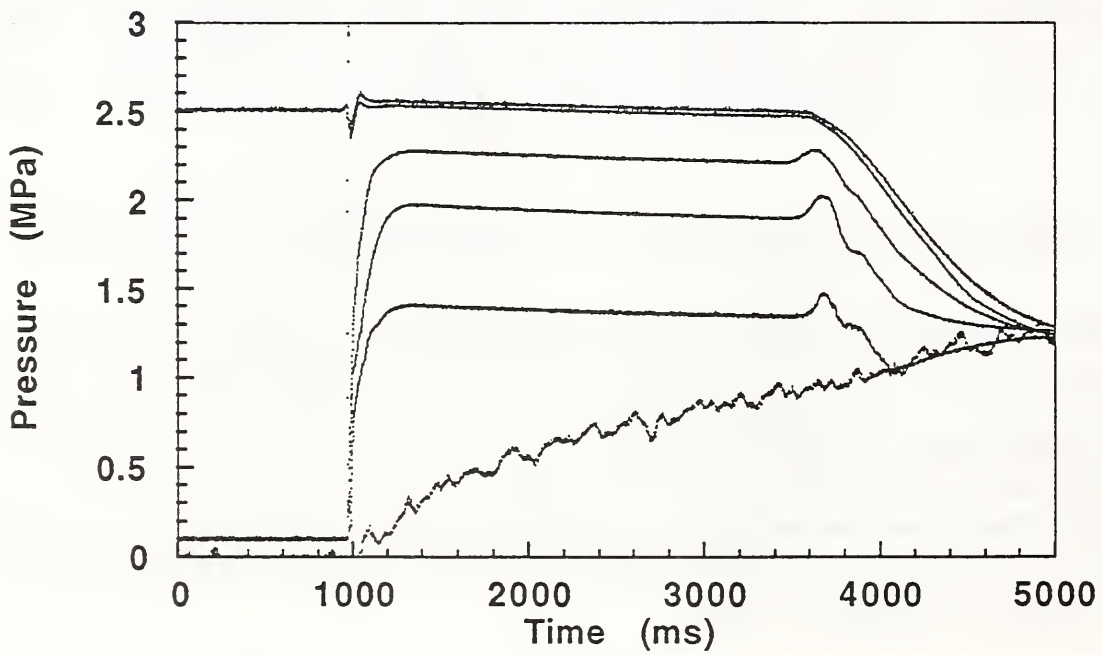

Figure 2. Pressure trace from a constant-head run with halon 1301 in 3 m of straight pipe, 95 mm in diameter. The top trace is the vesel ullage pressure, the next four traces are pipe pressure near the vessel exit then in 1 m increments, and the bottom trace is of the recovery tanks. The make-up tanks valve opened at 1 s, the vessel valve opened at 1.02 s and the make-up tanks valve closed at 3.5 s.

Measurements of Some Thermodynamic Properties of Alternative Agent/Nitrogen Mixtures[1]

I. Vazquez, C. Boyer, B. Breuel, L. Weber*, M. Huber**, and J. C. Yang

Building & Fire Research Laboratory
and
**Chemical Science & Technology Laboratory*
National Institute of Standards & Technology
Gaithersburg, MD 20899 U.S.A.
and
***Boulder, CO 80303 U.S.A.*

ABSTRACT

This study is a continuation of a U.S. Air Force/Navy/Army and FAA sponsored program, currently being conducted at NIST, to further evaluate some thermodynamic properties of the four selected alternative agents for in-flight aircraft fire protection in both dry bays and engine nacelles. The four selected agents are HFC-227ea, CF_3I, FC-218, and HFC-125.

To prepare a conventional halon 1301 bottle for in-flight fire protection, the bottle is normally filled with liquid halon 1301 to about half of the bottle volume and is then pressurized with nitrogen at room temperature. Depending on the applications, the charge pressure can vary (from 2.4 to 4.1 MPa or higher). The purpose of using the nitrogen to increase the ullage pressure is to provide extra driving force to facilitate the expulsion of the liquid agent from the bottle upon release. However, depending on the location of the bottle aboard an aircraft (which in turn determines the ambient temperature of the bottle), the total pressure in the bottle will change because the vapor pressure of the agent and the solubility of the nitrogen in the liquid agent vary with temperature. In addition, the final pressure at elevated temperature also depends on the fill density of the bottle (i.e., how much agent is dispensed into the bottle). When the bottle is exposed to very high ambient temperature (e.g., near an engine), the bottle pressure can be very high such that the structural integrity of the bottle may be compromised. On the other hand, when the bottle experiences very low temperature (e.g., at high altitude), the bottle has to have sufficient residual pressure to discharge the liquid agent from the bottle when needed. Therefore, measurements of the lower and upper limits for the bottle pressure are necessary in order to determine whether existing halon 1301 bottles can be used for "drop-in" replacement agents or to provide safety guidelines on bottle design for retrofitting for the alternative agents.

This study consists of several parts. The first part involved measurements of the amount of nitrogen required to pressurize the bottle, filled with a pre-determined amount of agent, to a specified pressure at room temperature. The second part of this work dealt with measurements of the final pressure of an agent/nitrogen mixture when the bottle was exposed to different ambient temperatures (from -60°C to 150°C). Finally, measurements obtained from the above experiments were used to fit the binary interaction coefficients in the computer program PROFISSY (Properties of Fire Suppression Systems). The code was developed to calculate pressure-temperature characteristics for the four selected agents. Other agents can also be incorporated easily into the program.

---

[1] sponsored by U.S. Air Force/Navy/Army and FAA

For measurements of the amount of nitrogen required to pressurize the vessel to a specified pressure and the thermodynamic properties of agent/nitrogen mixtures at -60°C, the experimental apparatus consisted of a stainless steel vessel equipped with a fill valve, a thermocouple and a pressure transducer. The experimental procedure is as follows. The set-up was evacuated for at least 10 minutes, and the vessel was then filled with an amount of agent equivalent to half or two-thirds of the vessel volume. By immersing the vessel in dry ice, liquid agent was dispensed into the vessel by condensing gaseous agent from the supply bottle. Attempt was made to remove noncondensible gases, if there were any, in the liquid agents by boiling off the liquid agent under low pressure and recondensing the agent vapor by using a liquid nitrogen trap. For CF_3I, an additional purification step was taken which involved passing of CF_3I vapor through beds of molecular sieves and potassium hydroxide before the agent vapor was condensed for collection. The vessel was then pressurized with nitrogen to either 2.75 or 4.1 MPa. Agitating the vessel constantly during pressurization facilitated reaching of the final equilibrium pressure. The amount of nitrogen was determined by weighing the apparatus. This amount corresponded to the sum of the nitrogen mass in the vapor phase as well as that dissolved in the liquid agent. The vessel was then immersed in a low temperature bath at -60°C. The final internal pressure of the vessel was recorded from the pressure transducer read-out when the internal temperature of the vessel had reached thermal equilibrium with the temperature of the bath.

For high temperature measurements, a high pressure stainless steel vessel with sight glass windows together with a pressure transducer and a circulating pump were used. The windows on the vessel and pump facilitated the filling of the vessel and the mixing of nitrogen with the agent respectively. The entire set-up was placed inside a temperature-controlled oven and heated to 150°C. The final pressure in the vessel was then recorded. The same pressures and fill densities as those in the cold temperature experiments were used.

The binary interaction coefficients in the computer code PROFISSY were then determined by matching the experimental results with those calculated by assuming different values for the binary interaction coefficients. Once the right binary interaction coefficients are established, the code can be used to generate pressure-temperature characteristics for the agent/nitrogen mixtures. Only four pieces of information are required to run the program: (1) agent mass, (2) vessel volume, (3) fill temperature, and (4) either nitrogen mass needed to pressurize the vessel or the fill pressure of the vessel.

Experimental Studies on Discharge of Alternative Agent/Nitrogen Mixtures in a Simulated Dry Bay [1]

J. C. Yang, T. G. Cleary, R. McLane, and W. L. Grosshandler

Building & Fire Research Laboratory
National Institute of Standards & Technology
Gaithersburg, MD 20899 U.S.A.

ABSTRACT

Discharge of the three selected alternative agents for aircraft dry bay fire protection has been conducted in a simulated dry bay (i.e., in an unconfined space). The three selected agents are CF_3I, FC-218, and HFC-125. Halon 1301 is also included in the study for the purpose of comparison.

The experimental set-up consists of a pressure vessel, a release mechanism, pressure transducers, a series of lasers and detectors, and a high speed movie camera. The experimental procedure involves the following. The vessel was initially filled with a fixed amount of agent and was then pressurized with nitrogen to a specified equilibrium pressure at room temperature. The use of nitrogen was to facilitate the discharge of agent from the container. For dry bay protection, it is required that the discharge time has to be less than fifty milliseconds upon detection of a fire. A quick-action solenoid valve or a squib which was located in the bottom of the vessel was used to release the agent from the pressure vessel. The temporal variation of the internal ullage pressure was measured during discharge. The dispersion dynamics of the agent external to the vessel were characterized by high speed photography. A laser attenuation technique was used to measure the global average speed of the dispersion at various locations downstream of the vessel exit. A pressure transducer was also placed at approximately 1.3 m downstream of the vessel exit in order to measure the impact force and to obtain some qualitative two-phase behavior of the flashing spray.

The studied experimental parameters include: (1) vessel geometry (spherical *vs.* cylindrical), (2) nitrogen charge pressure, (3) initial amount of agent, (4) temperature of liquid agent, and (5) discharge orifice size. A cylindrical pressure vessel with sight windows is also used to observe the process inside the vessel during discharge.

Three distinct regions are noted in the temporal variation of the ullage pressure. The first corresponds to the discharge of the liquid agent/nitrogen mixture from the vessel, followed by a sudden pressure recovery which signifies the degassing of dissolved nitrogen from the liquid mixture. The pressure recovery is due to expansion of the liquid level caused by the growth of nitrogen bubbles, thus compressing the ullage space. The third region corresponds to the discharge of the remaining vapor mixture from the vessel. The duration of each region and the degree of nitrogen degassing appear to be dependent on the initial amount of agent and the equilibrium nitrogen charge pressure. Since the rate of nitrogen degassing depends on the amount of nitrogen dissolved in the liquid agent, the extent of degassing is less apparent at lower nitrogen charge pressure given the same amount of agent in the vessel. This is further substantiated by the experimental results obtained by partially saturated the liquid agent with nitrogen. In this case, the rate of nitrogen degassing is much slower than the rate of liquid discharge such that no pressure recovery is noticeable in the pressure trace. Partial saturation was

---

[1] sponsored by U.S. Air Force/Navy/Army and FAA

obtained by simply bubbling nitrogen through the liquid agent to a specified pressure without attaining the final equilibration pressure.

Based on the observations from a high speed movie camera, the extent of flashing at the outlet of the solenoid valve during discharge at moderately low liquid temperature (-15°C) appears to be similar to that at room temperature. In addition, no discernable difference in the behavior of the flashing spray at the vessel exit was observed among the four agents studied when a large opening solenoid valve was used to discharge the agent at room temperature. Except at the beginning and close to the end of the liquid discharge, the spray angle at the valve exit remained close to 180° during a large portion of the liquid discharge time.

According to the measurements obtained from the laser attenuation, the dispersion of CF_3I was much slower compared to the other two selected agents when a quick-action solenoid valve was used to discharge the agent from the vessel.

Depending on the agent and nitrogen charge pressure, maximum downstream dynamic pressure could reach 2 MPa in some cases when a solenoid valve with a large opening was used.

Results obtained from a spherical bottle using a squib and other experimental parameters will be presented and discussed.

BURNING RATE OF PREMIXED METHANE-AIR FLAMES INHIBITED BY FLUORINATED HYDROCARBONS

G.T. Linteris
Fire Science Division
National Institute of Standards and Technology
Gaithersburg MD 20899
and
L. Truett
Wright-Patterson AFB
Dayton OH 45433

Introduction: The agents which are currently being considered as replacements for fire suppressant agent CF_3Br are mostly fluorinated hydrocarbons and perfluorinated alkanes. This abstract describes measurements of the reduction in burning rate of premixed methane-air flames with the addition of the single carbon inhibitors CF_4, CF_3H, CF_2H_2, and CF_3I. Early studies of the inhibitory effects of halogenated hydrocarbons on flames were conducted in premixed systems[1,2,3]. The premixed laminar burning rate is a fundamental parameter describing the overall reaction rate, heat release, and heat and mass transport in a flame. In addition, the reduction in the premixed flame burning rate is useful for understanding the mechanism of chemical inhibition of fires since diffusion flames often have a stabilization region which is premixed, and good correlation has been found between the reduction in burning rate and the concentration of inhibitors found to extinguish diffusion flames[4]. Premixed flame burners have flow fields which are relatively easily characterized, making interpretation of the inhibitor's effect on the overall reaction rate straightforward.

Experiment: In the present research, the flame speed measurements are performed using a nozzle burner[5]. The burner consists of a quartz tube 27 ± 0.1 cm long with an area contraction ratio of 4.7 ± 0.1 and a final nozzle diameter of 1.02 ± 0.005 cm. The nozzle contour is designed to produce straight-sided schlieren and visible images which are very closely parallel. The burner is placed in a square acrylic chimney 10 cm wide and 86 cm tall with provision for co-flowing air or nitrogen gas. Gas flows are measured with digitally-controlled mass flow controllers (Sierra Model 860*) with a claimed repeatability of 0.2 % and accuracy of 1 %, which are calibrated with bubble and dry (American Meter Co. DTM-200A) flow meters so that their accuracy is ± 1%. A frame-grabber board in an Intel 486-based computer digitizes the image from a 512 by 512 pixel CCD array for subsequent analysis, and the mass burning rate is determined using the total area method. The product gas temperature is measured with Pt/Pt 6% Rh - Pt/Pt 30% Rh thermocouples which are coated with Yttrium oxide to reduce catalytic reaction on the thermocouple surface. Measurements with two bead diameters (344 and 139 μm) allow correction for radiation losses.

Model: The structure of the inhibited premixed methane-air flame is calculated for CF_4, CF_3H, and CF_2H_2 using currently available techniques[6,7,8]. The equations of species and energy conservation are solved numerically for the initial gas compositions of the experiments. The calculations employ a chemical kinetic mechanism recently developed at NIST[9,10] for fluorine inhibition of hydrocarbon flames. The 85-species mechanism uses the Miller and Bowman[11] hydrocarbon sub-mechanism (140 reactions) and adds C_1 (200 reactions) and C_2 (400 reactions) fluorochemistry. Fluorinated-species reaction rates and thermochemical data are from the literature when available and are otherwise estimated.

---

*Certain commercial equipment, instruments, or materials are identified in this paper in order to adequately specify the experimental procedure. Such identification does not imply recommendation or endorsement by the National Institute of Standards and Technology, nor does it imply that the materials or equipment are necessarily the best available for the intended use.

Results and Discussion: The measured burning rate of the uninhibited methane-air flame as a function of equivalence ratio is in good agreement with previously published results[2,12] and with the prediction of the numerical model. The reduction in burning rate is determined for the fluorinated inhibitors CF_4, CF_3H, CF_2H_2, and CF_3I in near-stoichiometric premixed methane-air flames at inhibitor concentrations up to about 4%. Even at this early stage of development, the NIST fluorine-inhibition mechanism predicts the burning rate reduction quite well for these flames. The experiments and the modeling results indicate that CF_4, CF_3H, and CF_2H_2 all work somewhat better than if they act as inerts. The agent CF_3I reduces the burning rate about six times greater than the fluorinated agents. The inhibition index suggested by Fristrom and Sawyer[13] is 1.5 to 2.0 for the fluorinated agents and 11.0 for CF_3I. For comparison, this index is 16.0 for CF_3Br[14] and 0.86 for CO_2[4]. Future research will continue mechanism refinement and validation and examine the chemical kinetic mechanisms of inhibition of hydrocarbon flames by fluorinated species.

Acknowledgements: This research was supported by the US Naval Air Systems Command; US Army Aviation and Troop Command; Federal Aviation Administration Technical Center; and the US Air Force, under the direction of Mr. M. Bennett at the Wright Patterson AFB Flight Dynamics Laboratory, Survivability Enhancement Branch. The authors are grateful to Drs. D. Burgess, W. Tsang, P. Westmoreland, and M. Zachariah for helpful conversations and for making their mechanism and publications available prior to publication.

References:

[1] Garner, F.H., Long, R., Graham, A.J., and Badakhshan, A., *XIth Symposium (Int'l) on Combustion*, Reinhold Publishing Corp., New York, 1957, 802.

[2] Rosser, W. A., Wise, H., and Miller, J., *VIIth Symposium (Int'l) on Combustion*, Butterworths Scientific Publications, Butterworths, London, 1959, 175.

[3] Lask, G., Wagner, H.G., *VIIIth Symposium (Int'l) on Combustion*, Williams and Wilkins Co., Baltimore, 1961, 432.

[4] Hastie, J.W., *High Temperature Vapors: Science and Technology*, N. Y.: Academic Press, 332-350, 1975.

[5] Mache, H. and Hebra, A. (1941), *Sitzungsber. Osterreich. Akad. Wiss., Abt.* IIa, 150, 157, 1941.

[6] Smooke, M.D., *J. Comp. Phys.*, **B48**, 72, 1982.

[7] Kee, R.J., Miller, J.A. and Jefferson, T.H., "CHEMKIN: a General-Purpose, Transportable, Fortran Chemical Kinetics Code Package," *Sandia National Laboratories Report*, SAND80-8003, 1980.

[8] Kee, R.J., Warnatz, J., Miller, J.A., "A Fortran Computer Code Package for the Evaluation of Gas-Phase Viscosities, Conductivities, and Diffusion Coefficients," *Sandia National Laboratories Report*, SAND83-8209, 1983.

[9] Burgess, D., Jr., Tsang, W., Westmoreland, P.R., Zachariah, M.R., *Third International Conference on Chemical Kinetics*, Gaithersburg, MD, July 12-16, 119, 1993.

[10] Westmoreland, P.R., Burgess, D.F.R. Jr., Tsang, W., and Zachariah, M.R., *XXVth Symposium (Int'l) on Combustion*, The Combustion Institute, 1994.

[11] Miller, J.A., and Bowman, C.T., *Progress in Energy and Combust. Science*, **15**, 287, 1987.

[12] Law, C.K., "A Compilation of Experimental Data on Laminar Burning Rates," in *Reduced Kinetic Mechanisms for Application in Combustion Systems*, (Peters, N. and Rogg, B., eds.) Springer-Verlag, Berlin, 15, 1993.

[13] Fristrom, R.M. and Sawyer, R., *AGARD Conf. Proc. on Aircraft Fuels, Lubricants and Fire Safety*, AGARD-CP 84-71, 1981.

[14] Fristrom, R.M. and Van Tiggelen, P.J., *XVIIth Symposium (Int'l) on Combustion*, The Combustion Institute, 773, 1979.

LAMINAR FLAME SPEEDS OF CF_3H-PROPANE-AIR MIXTURES AT ELEVATED PRESSURES

Simone Hochgreb, Y. Ernest Hsin and Gregory T. Linteris*
Massachusetts Institute of Technology
*National Institute of Standards and Technology

INTRODUCTION

A fundamental property of interest in characterizing the effectiveness of fire suppressants is the effect of addition of inhibitors on the laminar flame speed of a fuel as a function of pressure and temperature of the unburned mixture. The effects of CF_3H and C_2F_6 on the laminar flame speed of mixtures of gaseous fuels and air are currently being investigated in a laminar combustion bomb (a constant volume combustion device amenable to flame speed measurements at elevated and reduced pressures). Preliminary results for CF_3H-propane-air mixtures are reported here. The data show little reduction in the burning rate at elevated pressures for addition of 1% CF_3H but about 25% reduction in the burning rate for 2% CF_3H.

EXPERIMENT AND DATA ANALYSIS

The experimental apparatus consists of a spherical container 15.24 cm in diameter with one inlet port through which the combustible mixture is introduced. Ignition is provided by two extended electrodes at the center of the bomb. A pressure transducer monitors the pressure of the device as the fuel is consumed. The surface of the bomb was coated with vacuum grease to avoid corrosion by the products of combustion. The bomb was initially evacuated, and precalculated partial pressures of inhibitor, fuel and air were added. Care was taken to remove the acid combustion products before evacuating the bomb for the next experiment. A more detailed description of the apparatus is given in [1]. After introduction of the combustible mixture in the bomb, the flame is ignited at the center and a calibrated pressure trace is obtained. Given the initial conditions, it is possible to relate the pressure signal to the extent of reaction, and thus to the flame speed as a function of the temperature and pressure of the adiabatically compressed, unburned mixture ahead of the flame by solving the energy and mass conservation equations assuming that the combustion products achieve equilibrium. Allowances for variable properties of burned and unburned gases with temperature, and of heat transfer to the wall are made. The data analysis program is being updated to calculate equilibrium flame temperatures more accurately including HF and F production.

RESULTS

Initial tests were conducted to acquire control data for flame speeds of uninhibited flames. Data were obtained for methane at ϕ = 1.0 and 1.3, and propane at ϕ = 0.8, 1.0, and 1.3 (nominal). Concentrations of 1.0 and 2.0% of the total mixture (by volume) of the inhibitor CF_3H were added to propane mixtures for flame speed comparison. Figure 1 shows the calculated burning velocity and chamber pressure as a function of the unburned gas temperature for a stoichiometric propane-air mixture with 0 and 2% CF_3H. The noise in the lower unburned gas temperature data is a result of the combined effects of the spark and the very low heat release rate, which lead to uncertainties in the final pressure derivative, from which the flame speed is calculated. The results for propane at ϕ=1.0 indicate that adding 1% CF_3H (not shown) slowed flame speeds negligibly; however, the addition of 2% of the agent decreased the flame speed by about 25% The reasons for this behavior are unclear at this point, but may be related to the changing stoichiometry with addition of the inhibitor. Increasing the CF_3H concentration also modifies the heat release per unit mass and overall rates of reaction. Chemical kinetic modeling of this flame will help to explain the observed behavior.

FUTURE WORK

A complete set of data at two or three initial pressures, equivalence ratios and concentrations will be produced for propane, and a similar set will be produced for methane flames. From these data it should be possible to derive a correlation or a table that can be interpolated over a relatively wide range of pressures (~1-8 atm), temperatures (~400-600 K) and equivalence ratios. Numerical calculations of the flame structure will performed and the results will be interpreted to determine the reasons for the observed behavior.

REFERENCE

1. Metghalchi, M. and Keck, J. C. , Combust. Flame 38,143 (1980).

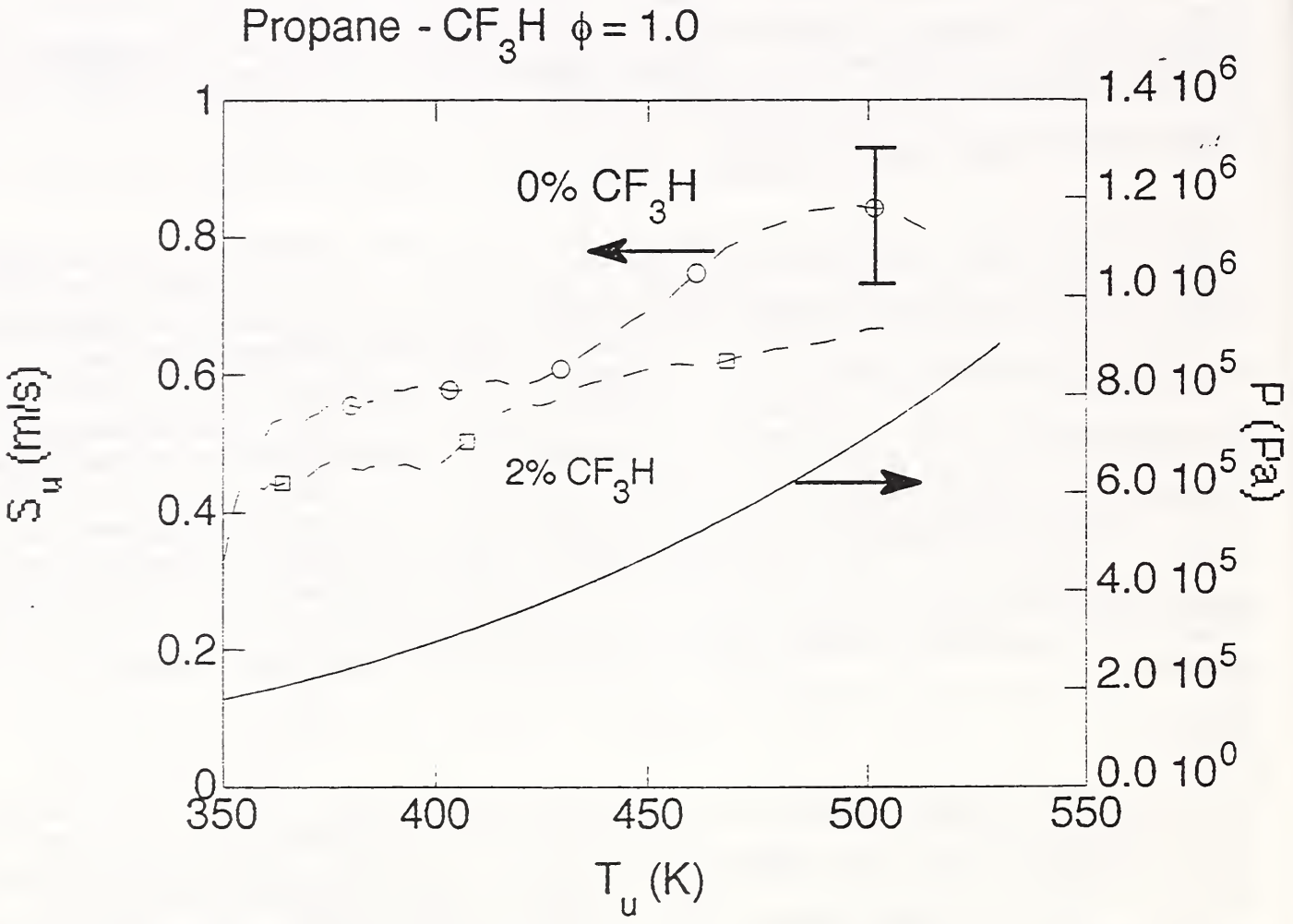

Figure 1 - Burning rate and chamber pressure as a function of unburned gas temperature for constant volume combustion of a stoichiometric propane-air mixture with 0 and 2% CF_3H added.

ACID GAS PRODUCTION IN INHIBITED PREMIXED FLAMES.

G.T. Linteris, M.D. King, A. Liu
National Institute of Standards and Technology
Gaithersburg, MD 20899

Introduction: Halogenated fire extinguishing agents such as CF_3Br decompose in flames to form hydrogen halides such as HF and HBr and other toxic and corrosive products.[1-8] Possible replacements for halon 1301 are required in significantly higher concentrations to extinguish fires; consequently, the post combustion gases in the inhibited flames may have higher concentrations of these undesirable species. Previous experiments and analyses have been preformed[9] to understand the phenomena important for HF production in inhibited propane-air diffusion flames. These tests have suggested that, for diffusion flames, both the rate of agent transport to the reaction zone and the chemical kinetic rates influence the formation of HF. In order to more clearly separate the importance of these processes and study HF formation in a more tractable configuration, the methods previously applied to diffusion flames are now extended in the present work to premixed flames.

Experiment: A Mache-Hebra nozzle burner (fabricated from a quartz tube with a final diameter 0.974 cm) is located concentrically in a 45 cm tall quartz chimney with a contraction to 3 cm diameter at the top. Calibrated mass flow controllers (Sierra Model 860*) under computer control meter the flows of fuel, air, and inhibitor and maintain an air co-flow of 25 l/min. A quartz probe, centered in the contraction of the chimney, extracts a measured fraction of the product gases, and directs the gases through polyethylene sample lines to two bubblers filled with water which trap the acid gases. The test duration is 4 minutes with a product gas sampling rate of 0.18 l/min. The bubbler water is weighed and then tested for F^- using an ion-selective electrode (Orion model 96-09). It should be noted that since COF_2 rapidly hydrolyzes in water, this technique for acid gas measurement includes F^- from both HF and COF_2.

The inhibitor is added to the premixed flow of fuel and air at a high concentration (one which reduces the burning rate by about a factor of two) and at a low concentration (about one tenth of the high concentration). The flames are operated at a unity fuel-air equivalence ratio ϕ (based on the oxygen demand of the fuel, but not on the inhibitor). For these tests, the heat loss rate to the burner is held constant by maintaining the flame at a constant height (1.24 cm) while changing the total mass flow rate and keeping the stoichiometry and inhibitor concentration as desired.

Results and Discussion: Figure 1 presents the measured number of moles of F^- per mole of fuel (points) as a function of the inhibitor concentration in the premixed stream for ϕ equal to 1.0 for CF_4, CF_3H, CF_2H_2, and C_2F_6 with methane and for C_2HF_5, C_3HF_7, and C_3F_8 with propane. Also shown is the amount of HF which would have been formed if all of the fluorine in the inhibitor were converted to HF. As shown, the conversion of the fluorine in the inhibitor to species which form F^- in the bubbler is nearly complete for these concentrations and stoichiometries for all of these agents except CF_4, for which there were kinetic limitations (although significant F^-, about 15% of the maximum, was detected). For near-stoichiometric premixed flames, HF formation is controlled by equilibrium thermodynamics at least up to inhibitor concentrations which give a factor of two reduction in burning rate for C_2F_6, C_3F_8, C_2HF_5, and C_3HF_7, and CF_3H. These results show that for these conditions, essentially all the fluorine in the inhibitors is converted to species which appear as F^- in the bubblers, and that the mechanism of inhibition of these agents is not one of an inert agent.

---

* Certain commercial equipment, instruments, or materials are identified in this paper in order to adequately specify the experimental procedure. Such identification does not imply recommendation or endorsement by the National Institute of Standards and Technology, nor does it imply that the materials or equipment are necessarily the best available for the intended use.

References

[1] Di Nenno, P.J., Forssell, E.W., Peatross, M.J., Wong, J.T., and Maynard, M., *Halon Alternatives Technical Working Conference*, Albuquerque, NM., May 11-13, 1993.

[2] Ferreira, M.J., Hanauska, C.P., and Pike, M.T., *Halon Alternatives Technical Working Conference*, New Mexico Engineering Research Institute, Albuquerque NM, May 1992.

[3] Ferreira, M.J., Hanauska, C.P., and Pike, M.T., *Halon Alternatives Technical Working Conference*, New Mexico Engineering Research Institute, Albuquerque NM, October 1992.

[4] Filipczak, R.A., *Halon Alternatives Technical Working Conference*, Albuquerque, NM., May 11-13, 1993.

[5] Sheinson, R.S. and Alexander, J.I., *Fall Meeting, Eastern States Section Meeting/The Combustion Institute*, Pittsburgh PA, Paper 62, 1982.

[6] Sheinson, R.S., Musick, J.K., and Carhart, H.W., *Journal of Fire and Flammability*, **12**, 229-235,1981.

[7] Sheinson, R.S., Penner-Hahn, J.E., and Indritz, D., *Fire Safety Journal* **15**, 437, 1989.

[8] Smith, W.D., Sheinson, R.S., Eaton, H.G., Brown, R., Salmon, G., Burchell, H., and St. Aubin, H.J., *Sixth International Fire Conference*, 1993.

[9] Linteris, G.T., King, M.D., Liu, A., Womeldorf, C., and Hsin, Y.E., *Halon Options Technical Working Conference*, Albuquerque, NM, May 35, 1994.

Acknowledgements: This research was supported by the US Naval Air Systems Command; US Army Aviation and Troop Command; Federal Aviation Administration Technical Center; and the US Air Force, under the direction of Mr. M. Bennett at the Wright Patterson AFB Flight Dynamics Laboratory, Survivability Enhancement Branch.

Figure 1 Moles of F^- per mole of fuel for CF_4, CF_3H, CF_2H_2, and C_2F_6 addition to a methane-air flame and for C_2HF_5, C_3HF_7, and C_3F_8 with propane. Symbols are the experimental results, and the solid lines are the predicted quantities based on equilibrium thermodynamics.

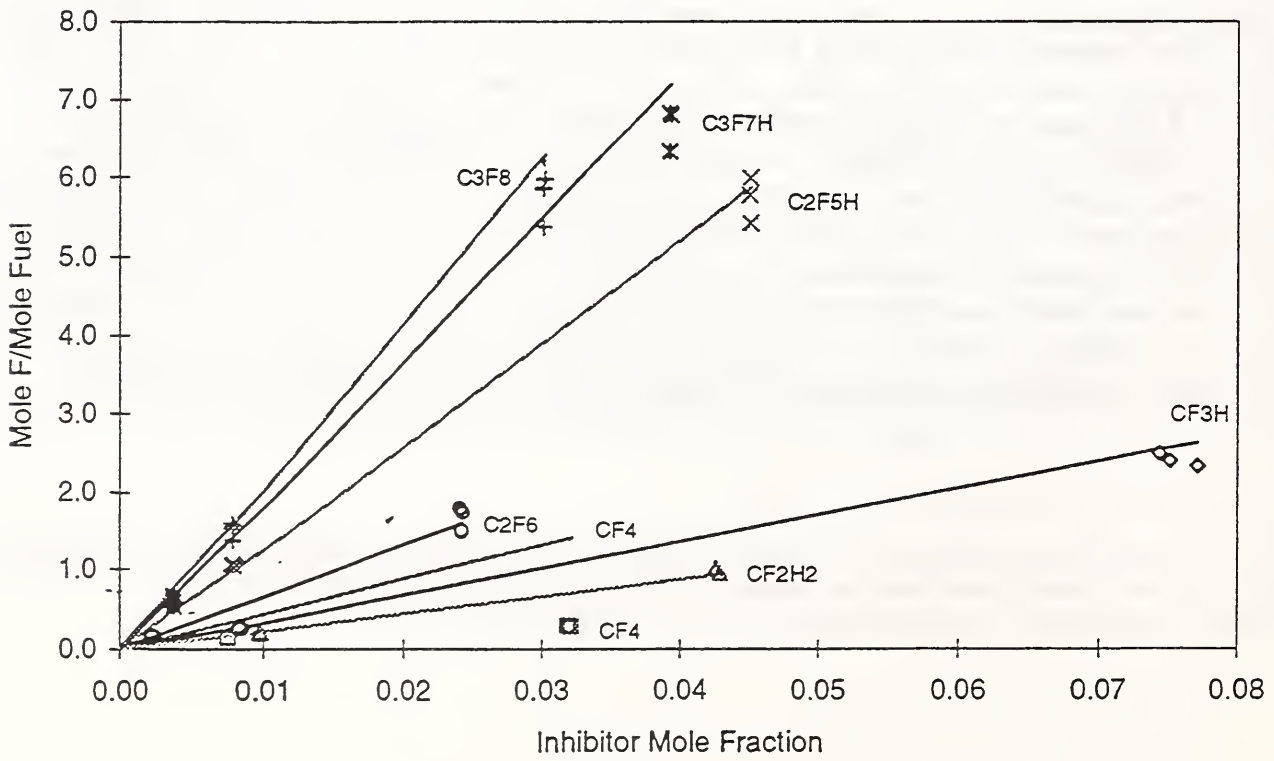

COMBUSTION SUPPRESSION THROUGH ENDOTHERMIC DECOMPOSITION OF AGENTS

V. I. Babushok*, D. R. F. Burgess and W. Tsang
National Institute of Standards and Technology
Gaithersburg, Maryland 20899

A. Miziolek
Army Research Laboratory
Aberdeen Proving Ground, MD 21005-5066

The inhibition and suppression of fire processes is of great practical importance. Currently, there is much interest in finding alternative flame retardants that do not deplete ozone. Many studies have been carried out to determine the controlling mechanisms without definitive results. It may well be that there are a variety of possibilities. In this paper we consider flame retardation caused through the endothermic decomposition of the retardant.

Our approach is to carry out simulation studies on the ignition delay resulting from the addition of a variety of possible flame suppressants, Br_2, HBr, CH_3Br, CF_3Br, CF_3H, CF_2H_2, CF_4, C_2F^6, C_2HF_5 and $C_2H_2F_4$ to a number of combustible gases; H_2, CH_4, CH_3OH and C_2H_6 with air at temperatures between 900-2000 K, 0.5-1.5 atm, equivalence ratios of 0.5-1.3 and additive concentrations ranging from 0 to 30% by volume. The simulations were carried out with the Sandia Chemkin code with a graphical post-processor that was written at NIST. The input data consists of three blocks of rate constant information that describe the C-H-O, C-H-O-F and C-H-O-Br systems and consists of approximately 900 reactions involving about 100 species.

We examined the relations between ignition delay and concentration of additives. The general features are:

a: initially, the ignition delay is decreased.
b: at concentrations 0.5-2.0 % there is a minimum.
c: subsequently, there is a continual increase in the ignition delay.

The last appears to be connected with a decrease in the heat release rate and is most likely due to the increasing capability of the additive to intercept reactive radicals and hence begin its own pyrolytic decomposition. At the lowest concentrations the instability of the agent can introduce radicals into the system and thus initiate the combustion process. A particularly

* On leave from the Institute of Chemical Kinetics and Combustion, Novosibirsk, Russia

interesting feature of the results are a sudden decrease in the temperature (as large as 200 degrees) in the course of the exothermic decomposition process. This is a manifestation of the very endothermic unimolecular decomposition process. In the case of CF_3Br and CF_3H a characteristic time of 1 msec is achieved near 1500 K.

These results are consistent with literature observations on the necessity of large concentration of additives near the fuel in order for extinguishment to occur. At such large concentrations it is necessary to consider the coupling of the agent and fuel decomposition mechanisms. Large concentrations of inhibitors generate by themselves thermal effects through reactions proceeding along endothermic decomposition channels as well as dilution. The latter can be expected to be much more important and in a sense can be considered as "chemical heat capacity". We have estimated the maximum temperatures achievable in systems with "chemical additives" in comparison with the inert case and arrived at values for an additional temperature decrease in the 100-200 degree range. Furthermore, the endothermic decomposition products may be less chemically active and thus can contribute to chemical inhibition through changes in reaction pathways and distribution of products. For CF_3Br the important transient products are CH_3Br, CF_3H and CF_2O. Results of reaction pathways analysis for ignition with large concentrations of retardants will be discussed.

HEPTANE INERTING CONCENTRATIONS OF CANDIDATE HALON 1301 REPLACEMENT AGENTS

Craig Hofmeister and Robert Zalosh
Center for Firesafety Studies
Worcester Polytechnic Institute
Worcester, MA 01609

INTRODUCTION

A few of the most promising Halon 1301 (CF_3Br) replacement agents include HFC-227ea (CF_3CHFCF_3), HFC-23 (CHF_3), INERGEN™ (N_2-Ar-CO_2), and CF_3I. These agents have zero, or in the case of CF_3I, near zero low ozone depletion potential and the first three have received EPA acceptance in the Significant New Alternatives Policy (SNAP) rulemaking for Halon replacement agents (1994).

According to NFPA 2001 (1993), applications involving a potential for explosion or post fire reflash should utilize a minimum design concentration based on inerting tests. Inerting data are available for flammable gases such as methane and propane, but there has not been any data reported for low vapor pressure flammable liquids such as heptane. It is also important to observe how the inerting data compare with cup burner and large scale minimum extinguishment concentrations. These are the objectives of the experiments being reported in this paper.

EXPERIMENTAL APPARATUS AND PROCEDURE

The experiments are being conducted in a 6.7 liter spherical vessel with much of the same procedure utilized by Zalosh and Edwards (1994) summarized and modified as follows. After evacuating the vessel, heptane, agent, and air are loaded sequentially by partial pressures to achieve the desired mixture composition. The partial pressure for heptane is converted to a volume of liquid which is injected using a syringe and air tight rubber gasket plug. The vessel pressure is monitored during this process. The ignition spark of 11 joules is generated at electrodes located near the center of the vessel and bridged by a carbon rod.

The presence of combustion is measured by a pressure transducer and a thermocouple. Both instrument signals are output to a computer data acquisition system for analysis.

The tests were conducted with an equivalence ratio of 0.98 ± 0.02. The test series begins with a sufficiently low concentration of agent to produce a substantial overpressure and the agent concentration is increased in subsequent tests until the overpressure is less than 1.0 psig in two successive tests.

INITIAL RESULTS and COMMENTS

Results to date, as well as reported minimum heptane cup burner

extinguishment concentrations from NFPA 2001 (1994) and comparisons are shown below.

AGENT	INERTING CONC.	EXTINGUISHMENT CONC. RANGE REPORTED	AVERAGE	RATIO INERT TO EXT.
HFC-227ea	7.7 v%	5.8-6.6 v%	6.2 v%	1.24
HFC-23	14.7 v%	12.0-12.7 v%	12.3 v%	1.20
CF_3I	5.1 v%	3.0 v%*	-	1.70
INERGEN™	40.0 v%	29.1 v%	-	1.37
CF_3Br	3.1 v%	2.9-3.9 v%	3.2 v%	0.97

*CF_3I extinguishment conc. taken from Heinonen and Skaggs (1992).

According to this data, the ratio of heptane inerting concentration to (the average reported) heptane extinguishment concentration for the various agents ranges from about 1.0 for Halon 1301 to 1.7 for CF_3I. Thus utilizing a single ratio such as the minimum cup burner extinguishing concentration plus a safety factor of 20% may not be sufficient to prevent an explosion or fire reflash for all the agents. Additionally, results reported by Zalosh and Edwards (1994) for propane inerting concentrations with HFC-227ea (11.7 v%) and HFC-23 (20.2 v%) indicate a much higher propane inerting concentration than that for heptane. These results suggest that inerting concentrations for flammable liquids should be based on liquid-specific inerting test data rather than "adjustment factors" based on cup burner extinguishment data or inerting data for flammable gases.

REFERENCES

Heinonen, E. and Skaggs, S., "Fire Suppression and Inertion Testing of Halon 1301 Replacement Agents," Proceedings, Halon Alternatives Technical Working Conference, New Mexico Engineering Research Institute, May 1992.

NFPA 2001, "Standard on Clean Agent Fire Extinguishing Systems", National Fire Protection Association, 1994.

Environmental Protection Agency Significant New Alternatives Policy for Ozone Depleting Substances, 59 CFR 13044, March 18,1994.

Zalosh, R. and Edwards, R., "Inerting of Propane-Air Mixtures with C_3F_7H-Nitrogen Blends," Proceedings, Halon Alternatives Technical Working Conference, New Mexico Engineering Research Institute, May 1994.

DYNAMICS OF FAST FLAMES, DETONATIONS AND THEIR SUPPRESSION IN C_2H_4/AIR AND C_3H_8/AIR PREMIXED SYSTEMS[1]

Grzegorz Gmurczyk and William Grosshandler

National Institute of Standards and Technology
Building and Fire Research Laboratory
Gaithersburg, MD 20899, USA

Experimental investigations of the effect of the fuel type, composition of the combustible mixture, geometry of the combustion system and concentration of the suppressing agent were investigated in a two-sectional 50 mm i.d. detonation tube (see Figure 1). Depending on the initial and boundary conditions, fast flames, quasi-detonations, Chapman-Jouguet detonations, and over-driven detonations were obtainable as possible modes of combustion. Each of such combustion modes constituted a reference state for further determination of the dynamic characteristics of the suppression processes. The 5 m long driver section of the tube was the auxiliary part of the set-up, serving as a flame generator. The essential part of the facility was the 2.5 m long test section separated from the driver part by a high-vacuum gate valve. A 44% blockage ratio spiral obstruction inserted into the tube was used optionally as a turbulence generator to broaden the gas dynamic conditions attainable by the flame. To produce the premixed flames, lean, stoichiometric, and rich C_2H_4/Air and C_3H_8/Air mixtures were employed as the combustible media. In all the cases, the initial pressure in the system was 100 kPa and the initial temperature was 295 K. The reference states were obtained when no suppressing agent was present in the test section. The suppression characteristics were taken in the presence of an extinguishant premixed with the combustible mixture in the test section of the tube. The composition of the mixtures in the two sections were prepared with the method of partial pressures. The combustible mixture was ignited due to a microexplosion of a tin droplet on the tips of an AC spark plug located at the end of the driver section.

A primary objective of the work has been to determine the suppression efficiencies of different agents under highly dynamic situations, without the undue influence of either the ignition event or the mixing of the agent into the flame front. The dynamic characteristics of the combustion and inhibition processes were determined by measurements of the velocity and pressure ratio as the shock/flame system entered the test section of the tube, which contained optionally a suppressant premixed with a fuel/air combination. Flame and shock wave velocities ranging from 300 m/s to 2200 m/s, pressure ratios across the shock fronts ranging from 18:1 to 45:1, and shock wave/flame spacings ranging from 1 mm to 100 mm were measured with piezo-electric pressure transducers and fast photodiodes. The experimental facility was successfully employed [1] to clearly discriminate among the dynamic characteristics of the extinguishing compounds, revealing behavior distinct from what was observed in companion studies using atmospheric non-premixed flames. It has been found that the dynamics of the

[1] The work sponsored by the U.S. Air Force, Navy, Army, and FAA.

combustion and suppression processes is strongly influenced by the concentration of an agent, the structure and composition of an agent molecule, the composition of the combustible mixture itself, the type of fuel used and the geometry of the combustion system.

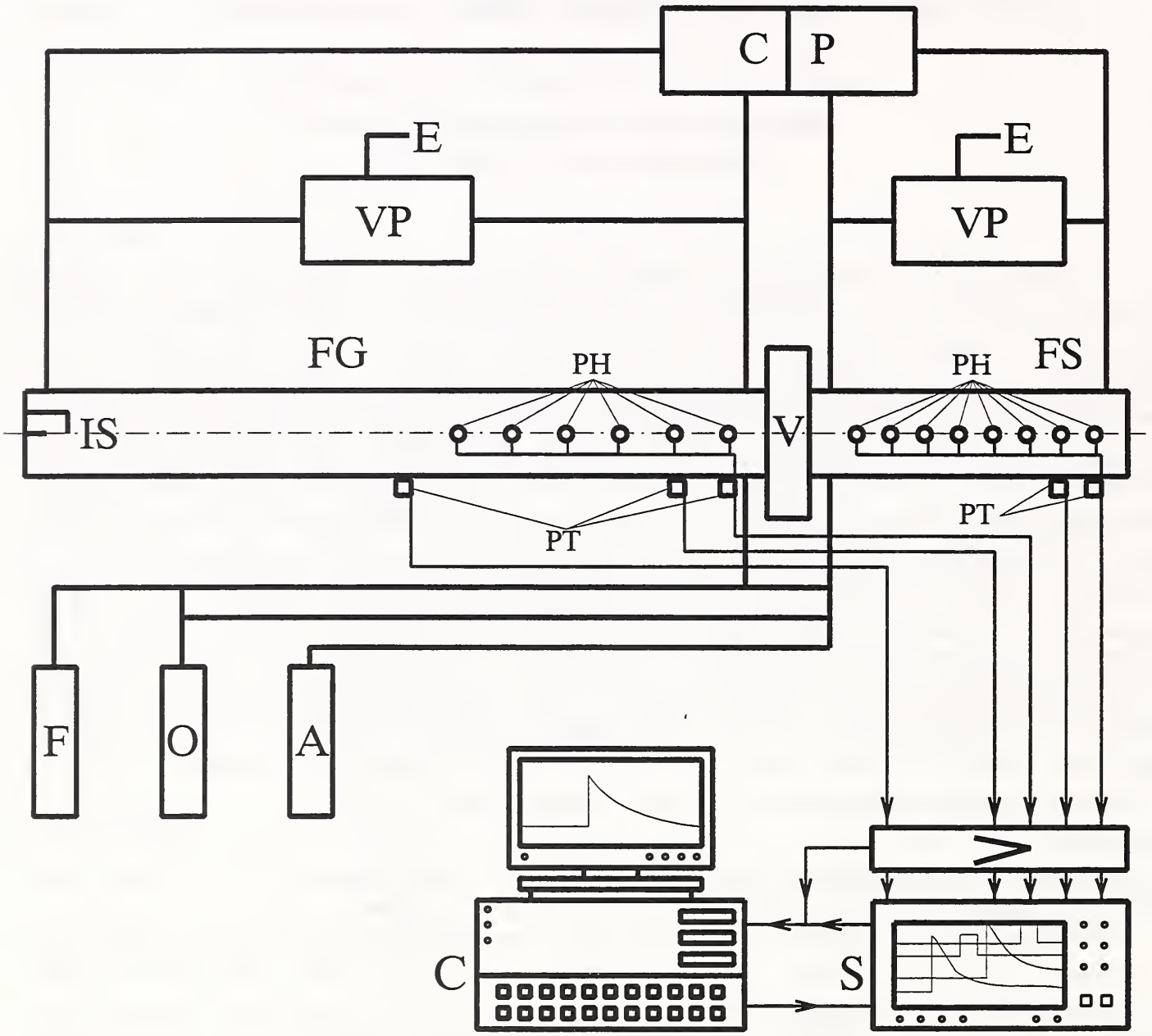

Figure 1. Schematic of the detonation tube facility: FG - flame generation section, FS - flame suppression section, V - high-vacuum gate valve, IS - ignition system, CP - dual circulation pump, VP - vacuum pump, E - exhaust, PH - fast photodiode, PT - piezoelectric pressure transducer, F - fuel, O - oxidizer, A - agent, C - computer, S - digital scope.

References

[1] Gmurczyk, G.W., Grosshandler, W.L. and Lowe D.L.: Suppression Effectiveness of Extinguishing Agents under Highly Dynamic Conditions. Fourth International Symposium on Fire Safety Science, Ottawa, Canada, 1994.

NUMERICAL ANALYSIS OF FIRE IN A LARGE COMPARTMENT

G.H. Yeoh , V. Chandrasekaran, M. Hildebrandt & S. Grubits
CSIRO, Division of Building, Construction & Engineering,
North Ryde, NSW, Australia.

ABSTRACT

Progressive improvements in the performance-cost ratio of computers has meant that field models based on Computational Fluid Dynamics (CFD) are rapidly becoming a viable tool for fire safety engineering. Such a tool is likely to meet the important requirement of fire safety engineers to reliably predict the fire phenomena and hence the hazard that it represents. Development of such analyses techniques will lead to the proper fire safety design of modern buildings. In recent times, there has been an increasing effort in providing solutions to fire safety engineering by developing various analytical techniques based on fire modelling. The main objectives have been to develop fire models capable of predicting fire growth and smoke spread.

In this paper, the primary features of a field model, FIRE3D, developed by CSIRO and based on CFD techniques are described. The model is being developed to deal with the initial fire ignition scenario together with the analysis of the growth of flame on various combustible materials. The model is capable of the detailed consideration of the complexities associated with the interaction of air flow with the pyrolysing material and the resultant growth of flame, the production of flaming products and the heat transfer mechanisms in a transient phenomena including gas-phase radiation. The combustion phenomena is treated using fast chemistry principles. The evaluation of the quantities of the combustion products and the tracking of their movements at various times has been one of the several important features associated with the computer program.

The FIRE3D computer code has been developed principally for predicting the heat transfer and the spread of combustion products in any arbitrary shaped single or multi-compartment enclosures. The code incorporated the fully compressible time averaged equations of motion and energy governing the turbulent gaseous flow. The velocity-pressure linkage was handled through the Pressure Implicit Splitting Operator (PISO) algorithm. A two-equation k-ε turbulence model was used, with wall functions for the momentum and heat fluxes in the near wall region. A diffusion flame was used, in which the fuel and oxidant are assumed always to unite in their stoichiometric proportions; the intermediate species were ignored. To predict the zone of chemical reaction, an assumption has been made that the shape of the probability density function is a blended beta function with two Dirac delta functions. Radiation from the flame has been modelled incorporating the spherical P_1 - approximation with Weighted Sum Of Gray Gases (WSGG) model. This model was formulated on spectral basis. The finite volume approach was employed to discretise the time-averaged conservation equations. The equations were solved iteratively using the Stone's fully-implicit procedure and the Preconditioned Conjugate Gradient method.

The predictions of the FIRE3D have been compared to a limited number of experiments that formed part of a series to study smoke-filling of single compartments. The studies were conducted in a 20 m × 17.5 m × 8 m compartment. For the purpose of computational solutions, the computational region is extended to eliminate the requirement of specifying boundary conditions at the doorway. The schematic diagram of

the experimental setup is shown in Fig 1. Alcohol was burnt in metal trays in the middle of the compartment. The exhaust fan flow rate was set at 45 m^3/s. Temperature measurements were made using thermocouple trees as illustrated in Fig 1.

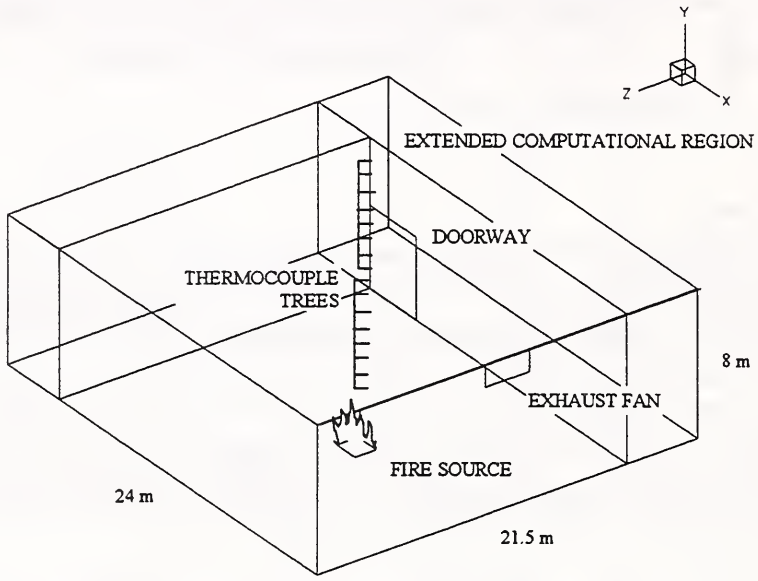

Figure 1. Schematic diagram of the laboratory experiment.

The velocity vectors and temperature field at 60 seconds can be seen in Fig 2(a) and Fig 2(b). The computed results showed good agreement with experimental observations of the turbulent flow in the compartment due to high induced door-jet velocities that could not be adequately modelled by zone models.

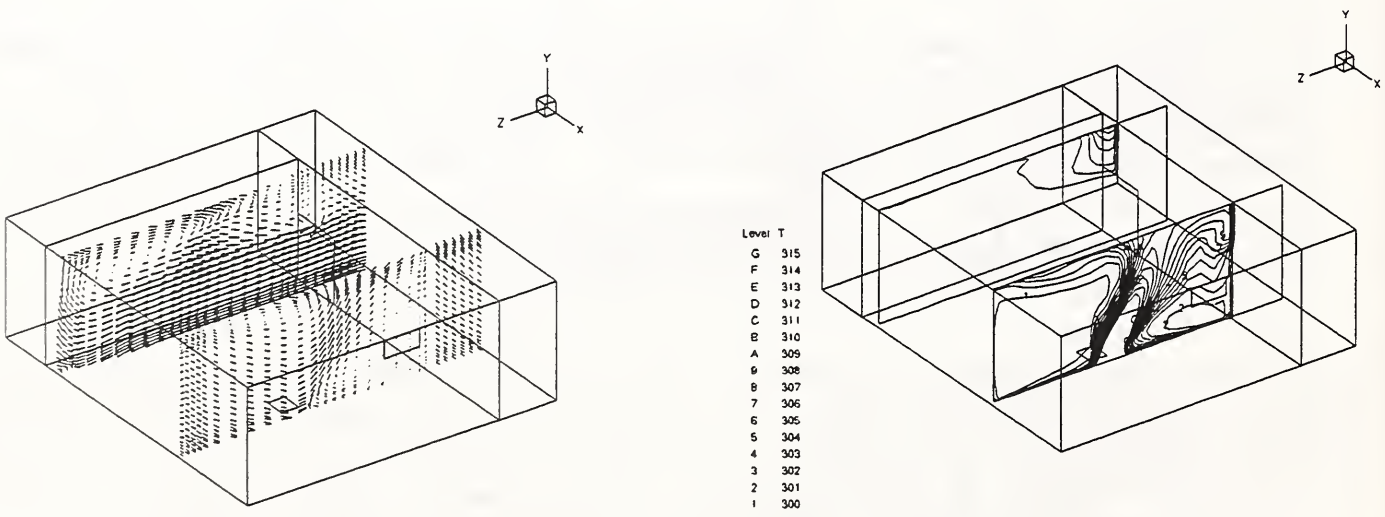

Figure 2. (a) Velocity vectors and (b) Temperature contours at two constant x planes at 60 seconds.

EXPERIMENTS AND MODELLING OF GAS AND DUST EXPLOSIONS

A.K. Rastogi, St. Schumann
Battelle Ingenieurtechnik GmbH, Germany

Gas Jet Explosions

In the Chemical and Petrochemical Industries large amounts of flammable hydrocarbons are handled and stored. In spite of the high safety-standards applied in these operations, accidents, with the release of flammable materials cannot be excluded entirely. In view of the hazards for on-site personnel and environment, it is necessary to develop methods by which the possible consequences of fire or explosion can be assessed. Based on such methods, safety-measures for the prevention of accidents with such consequences can be improved. An open question so far is the possible effect of an explosion after massive release of flammable hydrocarbons in the form of a single or two phase jet from the leak of a pressure vessel or pipe. In the case of large release rates, for example after the failure of a flange, a highly turbulent flammable cloud of air/gas mixture will be formed. Ignition of such a vapour cloud may result in explosion pressures with accordingly large damage potential especially when the jet is impinging on an obstacle.

The overall objective of the work presented has been to improve the knowledge about realistic accidental scenarios in an industrial plant and to develop further safety measures by performing propane jet release experiments into ambient air as well as against medium and large scale obstacles of 10 % volume blockage. The tests have been performed with openings of diameters between 32 mm and 78 mm for the gas and different slits for an additional release from the liquid in order to release large propane vapour clouds against a medium (dimensions: 4 m x 4 m x 2 m) or a large scale obstacle (dimensions: 8 m x 8 m x 4 m) configuration both having a volume blockage of 10 %. The concentration of the flammable mixture measured and in case of ignition the measured flame and pressure development will be presented. Explosion pressures of upto 3.4 bar and maximum flame speeds of upto 300 m/s have been measured.

Using BASSIM (BAttelle StrömungsSIMulator), a state-of-the-art CFD code developed at Battelle, computations to model the jet release without and with obstacle are presented. For these calculations only gas release is considered and calculation results are compared with the concentration measurements. Explosion computations are in progress and it is intended to present these also at the conference.

Dust Explosion Venting

Explosion venting is a common and frequently used measure in various industries such as food and catering to protect production facilities from being destroyed by dust explosions. The explosion inside a vented apparatus also causes secondary blast and fire effects outside, against which people or nearby installations and buildings have to be protected. Lack of information to quantify fire and blast effects outside vented vessels led to experimental investigations by Battelle, which will be presented.

Pressure development inside the vented vessel (primary explosion) is studied as a function of the time intervals between dust injection, ignition and initiation of disc bursting. Applying pressure transducers the explosion and blast pressure development in the environment of the vented vessel was measured as well as cloud formation and flame propagation outside the vented vessel using video cameras and ionization gauges. Venting experiments for vessel volumes from 0.3 m^3 up to 250 m^3 and scaled vent areas $A/V^{2/3}$ of 0.07 up to 0.39 have been performed. In addition to cornstarch with three different K_{St}-values for the primary explosion (varied via ignition time delay), the behaviour of other dust materials was investigated. All tests show, that for identically chosen experimental parameters two different types of secondary explosions can occur, which differ in respect to their peak pressures by a factor up to four. As empirical equations the most violent cases were included in the new VDI-guideline 3673.

To predict the parameters for the most violent dust explosion for the closed 1 m^3 vessel, unsteady premixed dust explosion computations have been performed using the Battelle-CFD code BASSIM, and the computed results are compared with the existing data for pressure and flame effects. Further computational work on vented dust explosions and dust jet ignition is planned.

EXPERIMENTAL OBSERVATIONS OF FULL SCALE HOUSE BURN TESTS: PART I - HOUSE BURN EXPERIMENTS

M.A. Ryan, M. Hildebrandt, N. McArthur, V. Chandrasekaran, G.C. Ramsay, S.J.Grubits
CSIRO, Division of Building, Construction and Engineering
P.O. Box 310, North Ryde, NSW, Australia

ABSTRACT

A group of houses scheduled for demolition in Anders Avenue, Marion (a suburb of Adelaide) were made available for experimental and investigative work. Two houses were selected for tests to be conducted in a collaborative venture by the Fire Technology Program of the CSIRO Division of Building, Construction and Engineering, the South Australian Fire Services Fire Safety Department, and the Adelaide University Fire Safety Research Unit.

In addition to the full house burns several preliminary room burn tests using various corner fires were conducted in Bedroom 2 of Building 2. Temperature and smoke density measurements were also made in several rooms and oxygen, carbon dioxide and carbon monoxide were measured in the room of fire origin (Bedroom 2). The purpose of these experiments and an ancillary purpose of the full house-burn tests was to generate data for comparison with and development of mathematical models of flame and smoke spread.

Another aim of the house-burn tests was to determine the effectiveness of two domestic fire safety systems. The effectiveness of the fire protection systems was to be measured by two criteria; life safety and property protection. Brand A comprised five domestic smoke detectors, three heat detectors and a passive infrared (P.I.R.) motion detector, all connected to a control panel located outside the house, and an audio/visual alarm sounder. The system also included a length of thermal conduit and a modem link to the Brand A central monitoring office. Brand B comprised two domestic smoke detectors and two sprinkler heads connected by a single pipe to the domestic water supply. The operation of the smoke detectors and sprinklers was monitored by a control panel outside the house. Only one house, Building 1, was fitted with the fire protection systems. The other house, Building 2, was left unprotected.

The houses were single storey and virtually identical in floor plan although mirror images of each other. "Bedroom 2" in each house was chosen to be the room of fire origin. A fuel load comprising a CSIRO "standard single chair" and CSIRO "standard three-seater sofa" in addition to a timber wardrobe and a timber chair and drawer unit was placed in each of these rooms. The rooms were partially carpeted with a polyurethane foam underlay with a polyolefin covering. The other rooms in each house were equipped with furniture and furnishings typically found in a house. The items of furniture and the furnishings in each house were chosen to be as similar as possible, in many cases identical.

The fire in each house was initiated by placing a lighted match on the back of the seat cushion closest to the wall on the three-seater sofa (in the centre of where the seat cushion meets the seat back) in Bedroom 2. Ignition was initiated simultaneously in each house.

Temperatures at various heights were measured at twenty locations throughout each house and at three locations in the ceiling space to monitor the progress of the fire and smoke through each house and monitor conditions in each room. Smoke meters were located in Bedroom 2 and the Entry to give an indication of the smoke densities in these rooms and the speed of the spread of smoke from the room of fire origin (Bedroom 2). Concentrations of CO, CO_2 and O_2 were measured in Bedroom 2. The progress of the fire was observed and recorded by two video cameras operated by two persons on an elevated platform halfway between the two houses, and by roving video cameras on the grounds around the house and in the room of fire origin in the early stages. The activation times of the various smoke detectors, heat detectors and the sprinkler heads were monitored and the results for three of the rooms are shown in Figure 1. The smoke detectors activated before any other alarm.

The fire developed in a similar way in the room of fire origin (Bedroom 2) in each house reaching temperatures indicative of flashover ($>800°C$) at approximately 5 minutes into the test. At 5 minutes into the test the automatic sprinklers located in the Loungeroom of Building 1 activated. This had the effect of curtailing the temperature rise in Bedroom 2 of this house presumably due to the conversion of the sprinkler water to steam by the hot smoke, enabling it to mix with the smoke and move through the house. In Building 2, which had no sprinklers, temperatures in Bedroom 2 continued to rise, the temperatures attained ($>1300°C$) suggesting that the room had reached ventilation controlled heat output levels. Temperatures measured at 2 m above the floor in three of the rooms of Building 1 are shown in Figure 1.

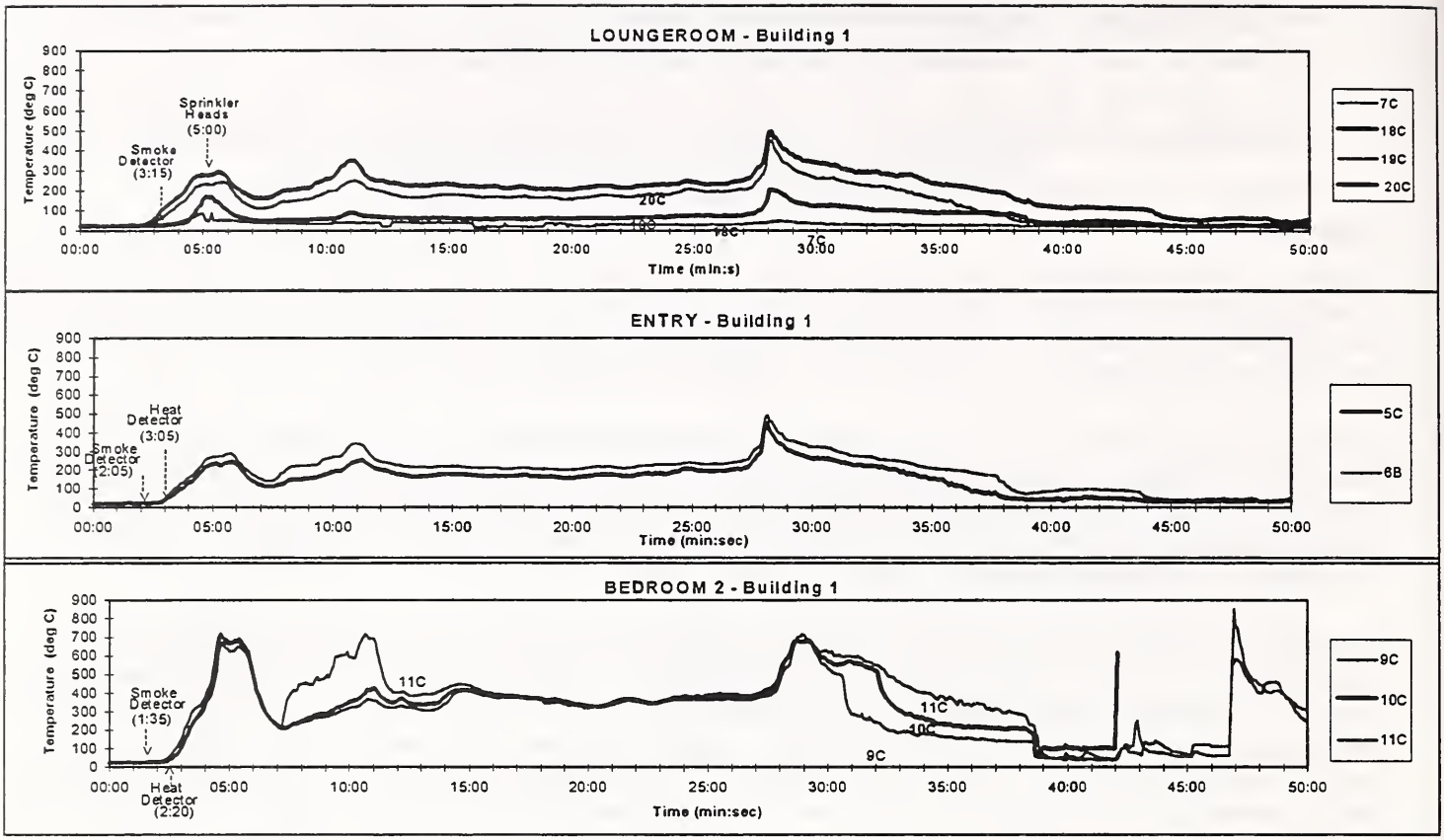

Figure 1: Temperatures at 2 m above floor level in Building 1

Smoke spread quickly through each house as evidenced by the short alarm activation times in Building 1 and temperatures in both houses. After sprinkler activation the fire in each house progressed differently. There was a noticeable drop in temperature in all rooms of Building 1 immediately following sprinkler activation. In Building 2, temperatures indicated that there was significant flaming in the ceiling space and and that this had contributed greatly to the spread of fire through the house. In Building 1, temperatures indicate that there was not significant flaming in the ceiling space.

Inspection of the two houses after the test revealed that in Building 1 the damage had mostly been confined to Bedroom 2. Some fire damage was observed on walls just outside the burnroom in the Hall and Entry at high levels. Soot damage extended as far as Bedrooms 1 and 3 at high levels. The furnishings in these rooms were virtually undamaged.

In Building 2, the roof had collapsed and all rooms had been gutted with the exception of the Loungeroom where the fire was extinguished by the fire brigade approximately 50 minutes into the test. The only furniture remaining was that at the far end of the Loungeroom and this was only due to fire brigade intervention.

The full report presents temperatures measured throughout each house, smoke densities and gas species concentrations in each room of fire origin and discusses the conditions in Building 1 in terms of the activation times of the various alarms and the sprinklers. The effect of the sprinkler system is discussed in terms of comparing the conditions in each house before and after sprinkler activation and in terms of the property damage to each house.

The performances of the two fire safety systems are compared in terms of life safety and property protection. The fire safety system referred to as Brand A would give occupants in Bedroom 2 approximately 75 seconds to get out, and the occupants of Bedroom 1 would have 110 seconds to get out. However, the Hall was untenable at 85 seconds following activation of the first (Bedroom 2) smoke detector so occupants may have had to egress via the bedroom windows if they were capable of doing so. The smoke detectors gave greater egress time than the heat detectors.

In general, this test confirms the life safety effectiveness of smoke detectors. The use of a sprinkler system only in the Loungeroom did significantly reduce property damage by containing the fire to the room of origin but did not contribute to life safety in this case, as at the time of activation of the sprinkler system conditions were already untenable throughout the house.

FIRE GROWTH RATES IN STRUCTURAL FIRES

G.M. Poole, E.J. Weckman, A.B. Strong
Department of Mechanical Engineering
University of Waterloo
Waterloo, Ontario
N2L 3G1

Introduction

The work reported in this paper represents one aspect of a cooperative project between the City of Kitchener Fire Department and the University of Waterloo aimed at developing design criteria for the construction of a fire fighter training facility. One particular criterion is that realistic training with respect to temperature, heat release and stratification be provided in such a facility. It is the purpose of this paper to compare existing analytical heat release and upper and lower layer gas temperature rise correlations and models with data from actual structures which were instrumented and burned in collaboration with the Kitchener Fire Department.

Description of the Models

The three mathematical models used in the prediction of the upper layer gas temperature rise were the ASET-B model as implemented in FPEtool, available through NIST [1], correlations of previous fire test data put forth by McCaffrey, Quintiere and Harkleroad [2], and the CFAST programs, also available through NIST [3]. The temperature rise in the lower layers of the rooms were also predicted using the CFAST programs. The inputs to the models include the physical room dimensions, the ventilation opening geometry, the thermophysical properties of the interior enclosure lining materials, the properties of the ambient air, and the transient heat release rate (HRR) from the fire.

Instrumentation and Experimental Conditions

The data base used for testing the correlations was obtained from full scale structural fire tests in which the temperature profiles of the upper and lower gas layers in selected rooms were recorded during development of a room fire. The fires were initiated in rooms of differing sizes, lining materials and fuel loadings in order to test the ability of the models to predict over a variety of inputs. For practicality, the test fires were allowed to develop only until the environment in the structure became too severe to allow entry of fire fighters, as indicated by measured lower zone gas temperatures. Computations were also truncated on this basis. Room lining materials included concrete, concrete block, wood panelling, plywood, and gypsum plaster. The fuels used in the tests were wooden pallets, liquid hydrocarbon fuels and polyurethane foam mattresses. The fires were non-ventilation controlled. Thermocouples were located at several positions on the ceiling and at the fire fighter level (FFL, one metre above floor) throughout the rooms. Heat release rates from the fuels were estimated for the wooden pallets, polyurethane foam mattresses and diesel fuel using models presented by Delichatsios [4], Orloff [5], Stensaas, Hovde and Magnussen [6] and Weckman [7] respectively, as appropriate.

Results

The measured and predicted upper and lower layer gas temperatures for typical tests are shown in Figures 1 and 2. Good agreement between the measured data and the predictions of the models is found for the temperature rise at the ceiling in the upper zone. The CFAST subroutines show fair agreement between the measured and predicted temperatures of the lower zone.

The sensitivity of the models to variations in the input parameters has been examined. Thomas and Bullen [8] have shown that the thermal properties, i.e. density, specific heat and thermal conductivity, of the interior enclosure lining materials have little effect on the time to reach critical conditions in the enclosure. The effect of varying the ventilation opening geometry and heat release rate from the fuel were examined and show that the models are extremely sensitive to the heat release rate predictions and moderately sensitive to the ventilation opening geometry.

Conclusions

As the models discussed in this paper have generally been tested under controlled laboratory conditions, there is a need to develop confidence in their ability to predict the conditions which exist in an uncontrolled environment. Given that the HRR of the fuels under consideration can be reasonably estimated, both the ASET-B and CFAST models, and the test fire data correlations demonstrate good agreement with the measured data and can be used with confidence for estimating the temperature rise in the upper layer of a room during the initial stages of a developing fire, at a minimum until such time that the environmental conditions within the structure become too severe to allow the entry of fire fighters. The ability to predict the HRR and temperature rise in a full scale structural fire finds application as a design tool for the development of a safe and realistic training facility. The results of this comparison also provide real fire validation of these models which in turn are also applied to fire protection engineering (pre-fire planning), fire cause determination and risk assessment.

References

1. Nelson, H., Center for Fire Research, NIST, Gaithersburg, MD.
2. McCaffrey, B.J. et al, Fire Technology, Vol. 17, No. 2, May 1981, p.98.
3. Peacock, R. D., et al, Nist Technical Note 1299, Feb., 1993
4. Delichatsios, M. A., Combustion and Flame, 27, 1976, p. 267.
5. Orloff, L., Modak, A.T. ed., Influence of Enclosures on Fire Growth, Volume II-Analysis, FMRC J. I. OAOR3.BU, RC78-BT-24, Factory Mutual Research Corp., Norwood, MA., 1978
6. Stensaas, J.P. et al, Proceedings of the Second International Symposium on Fire Safety Science, Hemisphere Publishing Corporation, 1989, p.215.
7. Weckman, E.J., Ph.D. Thesis, University of Waterloo, 1987
8. Thomas, P.., Bullen, L., Fire and Materials,Vol. 3, No. 2, 1979

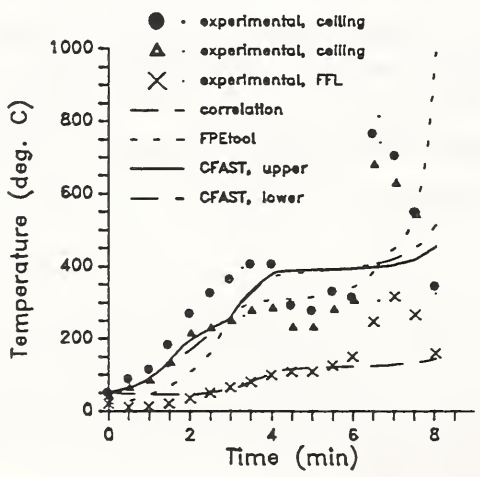

FIGURE 1

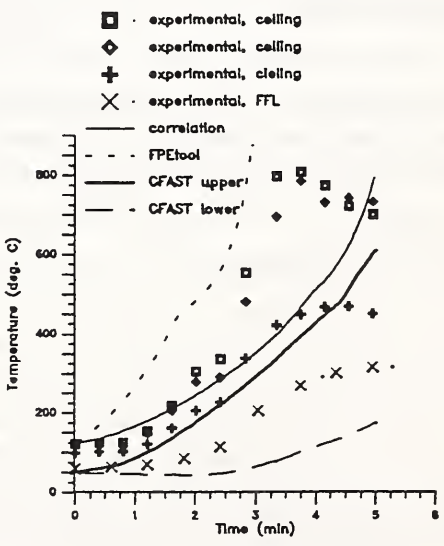

FIGURE 2

Fire Data Management System, FDMS 2.0

Rebecca W. Portier

Building and Fire Research Laboratory
National Institute of Standards and Technology
Gaithersburg, MD 20899

Introduction

A unified method of accessing data is crucial to both experimental and modeling efforts in the development of the science of fire. The FDMS concept is well founded, and very important to experimentalists acquiring data, as well as modelers and others using data related to fires and material properties. A standalone, PC version of the database, FDMS 1.0, currently exists which supports a limited number of fire test method types. This version is not portable across computer platforms and is dependent upon third-party software libraries which are no longer supported. A second generation of the database, FDMS 2.0, is in development which will remedy these problems and provide flexibility for future data needs. As an extension to FDMS 1.0, version 2.0 will play an important part in model verification. The design of FDMS 2.0 allows fire test data and model output data to be stored in the same database. Storage design provides for replicate data for standard test methods as well as compressed data for extensive real-scale tests.

Planned Implementation

FDMS 2.0 provides platform-independent storage, retrieval, and exchange of fire data. This data includes bench-scale and real-scale fire test results, results from available fire models as well as a variety of supplemental information including details on organizations, personnel, products evaluated and their related properties, and test method descriptions. Current development provides for two implementations of the database:

- A centralized database will be accessible to users worldwide with either a text-oriented interface or a MS-Windows style interface on the Internet. Data in the centralized database will be a compilation of data provided from internal and external sources. There will be no edit capabilities for users accessing this database. Import and editing will be handled by the individual(s) responsible for maintaining the database. The centralized database could be expanded in the future to access reports and documentation online as well as to view pictures and run movies using an interface similar to Mosaic.

- Users will also have access to a local, laboratory-specific implementation of the database. This implementation will be platform-independent (IBM PCs, Macintosh, MS-Windows, Unix, etc.) and will be the replacement for the existing FDMS software. The interface will be a superset of the MS-Windows style interface to the centralized database. New functionality provided will enable users to import, edit, and maintain their own database. Users will be able to exchange data with other FDMS users through the common format discussed in the "FDMS Programmer's Reference," NISTIR 5162. In addition, each laboratory will be encouraged to send results to be incorporated into the centralized database.

Additional implementations are under consideration.

Participation

Outside parties are encouraged to contribute available data to FDMS. Laboratories interested in providing test data to be imported into the FDMS centralized database should currently store their results in the FDMS import format to be presented. Any future versions of FDMS will be backwards-compatible in support of the import formats so that data generated today can be loaded once the centralized database is completed.

Software developers of complementary packages such as CFAST and HAZARD should consider supporting the FDMS import formats to be presented.

References

[1] Babrauskas, V., Janssens, M., Peacock, R.D., and Batho, N.E., Technical Documentation and User's Guide for FDMS, A Fire Data Management System, unpublished (1990).

[2] Babrauskas, V., Peacock, R.D., Janssens, M., and Batho, N.E., Standardizing the Exchange of Fire Data - The FDMS, *Fire and Materials* **15**, 85-92 (1991).

[3] FDMS 1.0 version software distributed by Fire Research Station, Borehamwood, Herts, WD6 2BL, England, attn: S.A. Ames.

[4] Portier, R.W., "A Programmer's Reference Guide to FDMS File Formats," National Institue of Standards and Technology Internal Report 5162, (1993).

[5] Portier, R.W., "Fire Data Management System, FDMS 2.0, Technical Documentation," National Institue of Standards and Technology Technical Note 1407, (1994).

Estimating the Fire Risk for an Industrial Facility

D. A. Coutts
Westinghouse Savannah River Company
Aiken SC 29808

The Westinghouse Savannah River Company (WSRC) is the prime contractor for the Department of Energy's Savannah River Site (SRS). This site has been involved in the production and processing of weapons grade nuclear materials since the early 1950s. The site has approximately 5600 buildings located on 800 km^2. In addition to production nuclear reactors, building functions include chemical processing facilities, machine shops, laboratories, offices, and warehouses.

The activities within many of the industrial structures at the SRS are changing. This represents a change in occupancy and the necessity to upgrade fire protection features. The Department of Energy has strict loss criteria Achieving strict compliance with these criteria is cost prohibitive and sometimes not feasible. In such instances the acceptability of alternatives must be evaluated. Demonstrating an equivalent level of fire protection features or evaluating the cost effectiveness of retrofitting fire protection systems requires quantification of the fire risk. Both the consequence (monetary loss, radiological release, etc.) and the frequency (times/year) must be estimated to quantify the risk. In addition, for nuclear facilities it is necessary to maintain a current safety analysis which includes a fire risk estimate. These needs have necessitated the development of a risk estimation technique that is applicable to general industrial facilities as well as facilities which handle radioactive materials.

WSRC uses event trees coupled with several different mechanistic models to develop plausible fire scenarios [1]. The event tree separates the accident into fire stages that are defined in terms of specific parameters and logical system responses. Both historical data and mechanistic models are used to evaluate the feasibility and probability of fire propagation to the next phase. The technique considers the non-uniform loading of combustibles normally found in most facilities. The event tree includes scenarios where the Maximum Credible Fire Loss (MCFL) could be exceed because of sprinkler system failure and the Maximum Possible Fire Loss (MPFL) could be exceeded because of barrier failure, adjacent fire exposures, or special activities (e.g., high value temporary storage). This allows comparisons between facilities that may have good fire barrier separation but do not have freestanding 4-hour (or better) fire walls. Additional comparisons based on occupant distributions and upgrade costs are possible.

The Fire Risk Assessment (FRA) event tree shown in Figure 1 contains several unique features. The probability of fire propagation (i.e., fire does not propagate) is calculated using a mechanistic model for the maximum ignition distance and a histogram of room combustibles as shown in Figure 2. The maximum ignition distance is based on the peak heat release rate (kW) for the first item ignited and the ease-of-ignition (kW/m^2) for the second item [2]. This technique provides an analytic method to demonstrate a considerable reduction in risk for facilities which contain few combustibles or hard-to-ignite materials.

While not shown in Figure 1, the event tree can be expanded to include intermediate fire barriers (e.g., 20 minute, 1 hour, etc.) which define fire zones within the facility. The success probability for each intermediate barrier can then be included in the overall facility risk estimate. The events in Figure 1 are sequential and resemble a timeline. This allows the success probability of multiple containment efforts by fire fighting personnel to be included in the event tree. This results in additional credit for proactive fire fighting efforts.

The presentation format of the event tree results is unique. Key outcomes are presented as the probability that a given loss is exceeded. This eliminates the disparity between the pass-fail frequency results presented by most event trees and historical fire data where the magnitude and frequency of fire losses are functionally dependent. The risk can be presented using the format shown in Figure 3. The results shown in Figure 3 can also be presented as a quantity of radioactive or toxic material released for use in a Safety Analysis Report.

References:

1. Coutts, D. A., 1994 *Fire Risk Assessment Methodology Generic Event Tree Description (U)*. Aiken, SC: Westinghouse Savannah River Company. (March) WSRC-TR-94-0188.

2. Bukowski, R. W., et. al. 1990. *Fire Risk Assessment Method: Description and Methodology*. Gaithersburg MD: Center for Fire Research, National Engineering Laboratory, National Institute of Standards and Technology (May) NISTIR 90-4242.

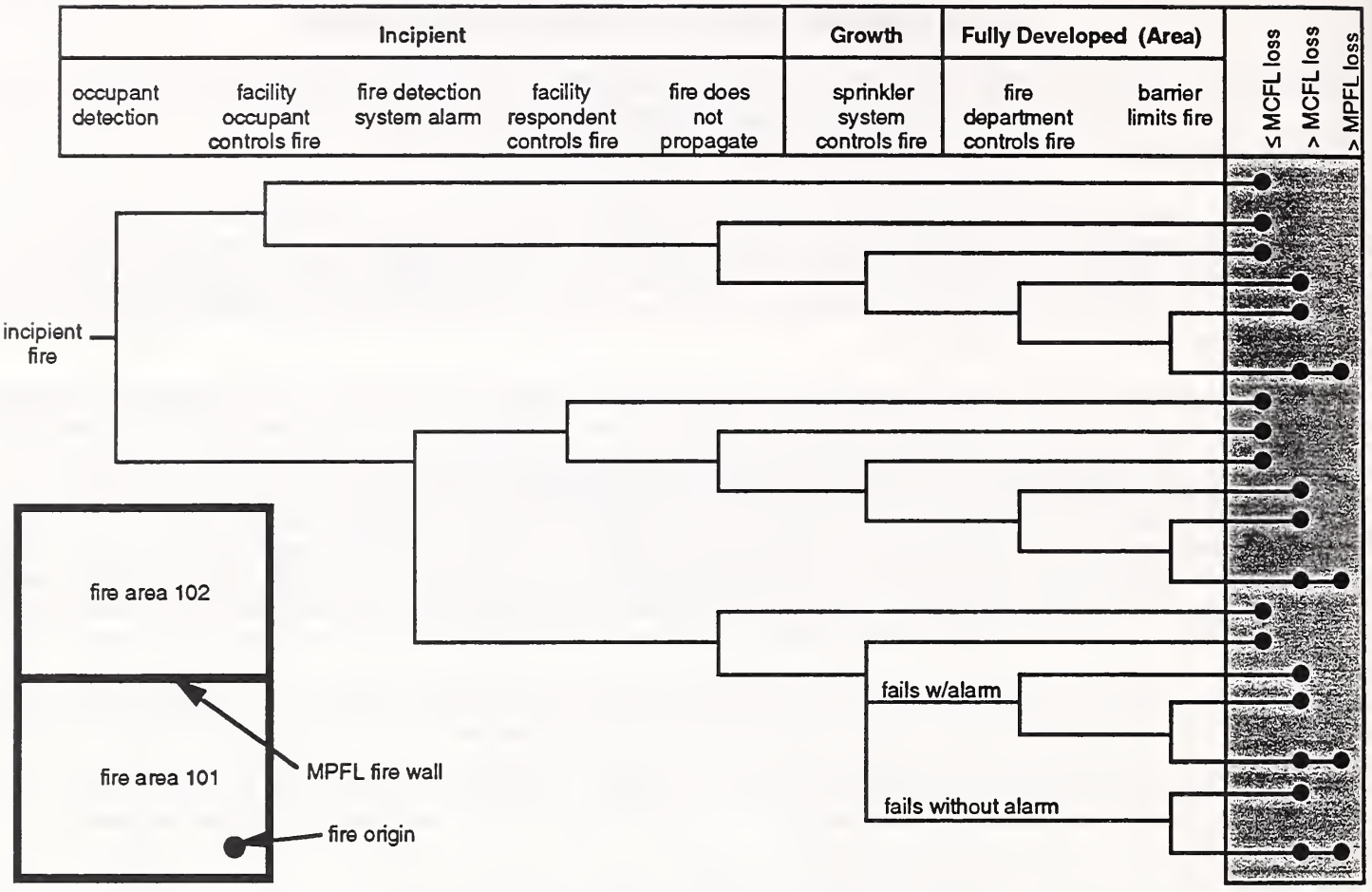

Figure 1, Fire event tree (MPFL is exceeded when fire from area 101 enters area 102).

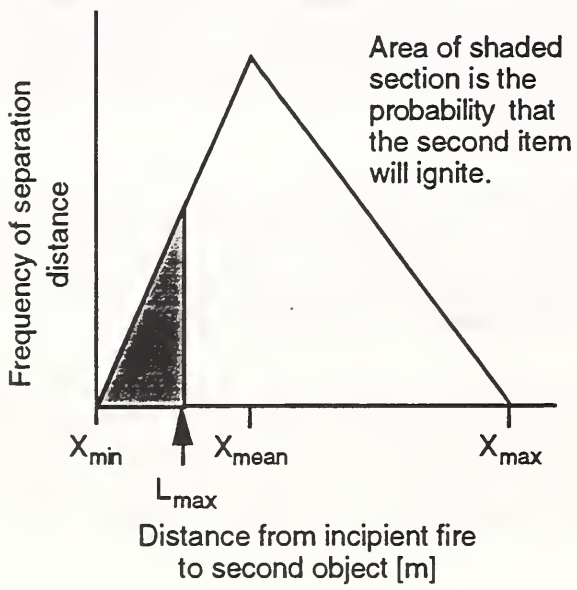

Figure 2, Combustible material histogram.

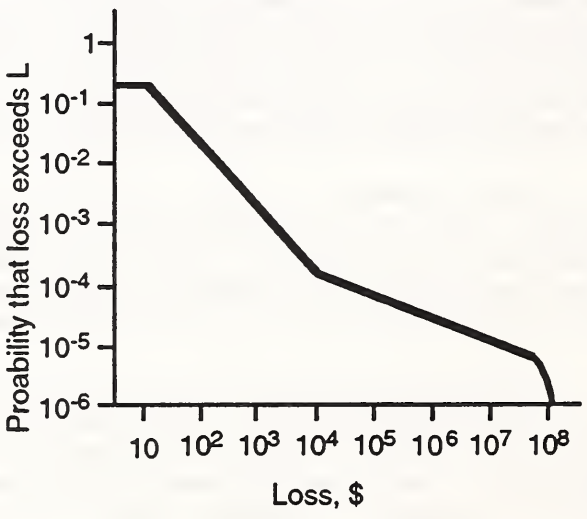

Figure 3, Loss probability diagram.

Submitted for presentation at the Annual Conference on Fire Research, Gaithersburg, MD, October 1994.

A RISK ASSESSMENT METHODOLOGY FOR FIRE SAFETY FACTORS IN PERFORMANCE-BASED DESIGN OF BUILDINGS

D.M. Karydas and M.A. Delichatsios
Factory Mutual Research Corporation
Norwood, MA 02062

Industrial safety standards, in particular loss prevention, property preservation and risk management standards, are traditionally developed on the basis of acceptable engineering principles addressing countermeasures against deviations from normality. Their implementation involves the specification of solutions tested by experience, and experimentation of small or large scale. By the nature of their development and acceptance such standards address the worst case scenarios. The uncertainty associated with limited experience of rare catastrophic events, -such as fires - and the prohibitively expensive repetition, in large numbers, of testing that considers all possible combinations of involved parameters and recreates design conditions for preventive and protective countermeasures is reflected in the introduction of liberal safety factors. The prescriptive approach of specification-based standards, therefore, provides sufficient coverage for many cases, suffers from excessive conservatism in many other situations, where less expensive protection may be sufficient, and becomes inflexible and restrictive in the selection of alternative solutions of satisfactory effectiveness. Generally, this approach addresses individual components of the system. It does not identify interactions of individual elements that may be contributory to the mitigation or, in other cases, the proliferation of undesirable consequences, thus, rendering the worst-case-scenario design basis into a dangerously misleading concept.

Recognizing the limitations of specification-based standards, efforts in individual countries, e.g., the U.S.A. (ASME, AICHE/CCPS, ISA(SP84), NFPRF, Factory Mutual Research, Bellcore, NIST, NRC), Australia (Warren Center), New Zealand (SANZ), Canada(NRCC), Japan, UK, Norway, and within international organizations, e.g., ISO (TC92/SC4/WG1), IEC (TC65A,WG10), CIB (W14) are being directed toward establishing performance-based standards using quantified risk as the basic performance parameter. The objective of these efforts is to establish a consistent and widely acceptable methodology to evaluate total system risks and propose alternative solutions that reduce risk to acceptable levels.

The risk assessment models adapted in the aforementioned areas of fire hazards, process safety and control, and in-service inspections, are characterized by many common elements. Deterministic and non-deterministic models are used in combination for the development of a systematic framework addressing:

- the likelihood of the occurrence of events when safety and control systems or system components operate successfully or fail,
- the timing and consequences of such events,
- the expression of results in terms of quantitative performance parameters.

The uncertainties of the models used, as well as the parameters considered by each model are treated systematically and expressed quantitatively. This analysis of uncertainty, combined with sensitivity and importance ranking studies, help to estimate the effects of data and models on the evaluation of risks, identify the effects of changes of component and sub-system level data to the overall system, and rank the individual parameters with respect to their contribution to the system performance.

The benefits of the performance-based approach using quantified risk as the performance parameter of safety and control systems can be summarized in the following topics:

- examination and evaluation of existing standards and practices with respect to their consistency and cost effectiveness,
- identification of alternative solutions with equivalent performance at a lower cost,
- flexibility in the design of alternative solutions with equal risk reduction,
- optimization of protection and control systems in terms of maximization of effectiveness at reduced cost,
- identification and prioritization of areas introducing uncertainties, therefore, requiring further research efforts.

In order for performance-based methodologies to find wide application and utility a systematic international cooperation is needed. The following generic issues should be addressed:

- assessment of risk analysis methodologies: current state of the art on major hazard analysis, estimation of uncertainty, comparison of methods and procedures, assessment of advantages and limitations of each approach.
- state of the art of available data bases.
- reexamination and evaluation of specification-based prescriptive codes from a performance-based perspective.
- identification of needs supporting implementation of performance-based standards, e.g., bench mark studies, reliability certification of protection and control systems, reliability/maintainability/supportability design.

The same methodology can be applied for material flammability assessment.

References

1. Building Regulation Review "Microeconomic Reform: Fire Regulating," Prepared by Mr.Claude Eaton (BOMA & NBFSS Project Coordinator), Australia, May 1991.
2. Magnusson, S. Erik, "Performance Based Codes," Interflam 93, Interscience Communication Ltd., London, England, p. 413, 1993.
3. Bukowski, R.W., "A Review of International Fire Risk Prediction Methods," Interflam 93, Interscience Communication Ltd., London, England, p. 437, 1993.
4. Karydas, D.M., "A Probabilistic Methodology for the Fire and Smoke Hazard Analysis of Electronic Equipment," Interflam 93, Interscience Communication Ltd., London, England, p. 509, 1993.
5. Snell, T., Babrauskas, V., Fowell, A.D., "Elements of a Framework for Fire Safety Engineering," Interflam 93, Interscience Communication Ltd., London, England, p. 447, 1993.
6. Stavrianidis, P. and Karydas, D.M., "Methodology for the Reliability Evaluation of an Electronic Gauging System Used for Safety in Power Boilers," presented and published in the International Conference on Reliability, Availability, Maintainability and Quality Control (Inter-RAMQ), Philadelphia, PA, 1992.
7. Stavrianidis, P., "Reliability and Uncertainty Analysis of Hardware Failures of a Programmable Electronic System," Journal of Reliability Engineering and System Safety, Elsevier Science Publications, England, Vol. 39, 1992.

PROGRAM FOR THE STUDY OF FIRE PATTERNS

PATRICK M. KENNEDY
NATIONAL ASSOCIATION OF FIRE INVESTIGATORS

JAMES H. SHANLEY, JR., PE
JOHN A. KENNEDY & ASSOCIATES, INC.

ABSTRACT

Fire and arson investigators often rely on fire patterns to determine the origin of fires. Fire patterns are visible manifestations of the heat and smoke produced by the fire which remain on room interior surfaces and furnishings after the fire is extinguished. This program covers a series of full-scale compartment (room) fire tests that are designed to evaluate the fire characteristics of room fires under actual fire conditions and the effect those conditions have on fire pattern formation. Particular inquiry and analysis is to be made into the unique and distinguishing characteristics of fire patterns on ceilings, walls, and floors caused by accelerated (i.e. arson) verses non-accelerated fires.

There is no known or current fire research to evaluate the fire patterns which fire investigators and analysts are commonly using to assess fire origins and fuels. This program sets forward a protocol for a series of initial tests which will set a standard of background research which the professional fire investigation community can use to asses the propriety of their fire pattern opinions.

The production of this program for the study of fire patterns involves the specification of the test room, ignition source, test fire(s), instrumentation, test procedures, safety, observations and data gathering, analysis and reporting of results.

The full-scale laboratory testing will utilize two baseline runs where the test room will not be furnished. Eight pattern analysis tests will follow where the test room will be furnished. It is anticipated that as a separate effort full-scale fire tests will be done in actual residential or other structures as a follow up and comparison to these laboratory tests.

BACKGROUND

The investigation and analysis of fires and the accurate determination of fire causes is an integral and essential element in the overall effective fire protection and prevention system in the United States.

Without an accurate listing of fire causes a number of elements of the total fire protection system cannot function to their fullest values. These include such fundamental elements as: code promulgation and enforcement, fire suppression and training, hazard and risk analysis, life safety codes, and many other similar areas of interest.

In a system model of the total fire protection establishment, produced by one of the authors[1], Fire Analysis is listed as of equal importance with such other fields at Fire Protection Engineering, Fire Suppression, and Codes and Standards.

Fire investigation and analysis has been a professional discipline since the late 1940's. It has been a subject of academic study on the post-secondary level since the 1950's. The first accredited baccalaureate degree program in fire investigation was instituted by the Eastern Kentucky University's Fire and Safety Engineering Technology Department in 1986. But fire investigation and analysis has only been the subject of serious scientific study, evaluation, and judgment since the mid- to late- 1980's.

The recent issuance of the 1992 National Fire Code, NFPA 921, *The Guide for Fire and Explosion Investigations*[2] has highlighted this new scientific interest in the principles of fire investigation.

TEST PLAN

The pattern tests will be conducted in a test room which has been instrumented to provide temperature, heat release rate, mass loss rate, and radiant energy data. The test plan has been put together to satisfy both the needs of scientific data collection data and the production of usable and representative fire patterns. The goals of the testing include being able to relate compartment fire dynamics with the production, appearance, and persistence of fire patterns.

The design, construction, and furnishing of the test room will be done to give reproducible results and to closely represent typical residential rooms. This room will be 12 ft by 12 ft, with an 8 ft high ceiling. It will have a standard size door opening and a 3 ft by 3 ft glass window 42 in. above the floor. It will be constructed in a manner to closely simulate common residential construction. The room will be provided with bedroom type furnishings.

Instrumentation of the tests will include a room calorimeter with associated fire product species concentration monitoring, thermocouples, load cell(s), and radiometers. All data will be gathered electronically at regular intervals of no less than 20 seconds.

Photographic records of the tests will include video cameras at view ports in the door, in the wall with the window, and in the opposite wall where the fires will originate. Still photography will be utilized to record fire conditions in the room, and to fully document the patterns which are created on all surfaces of the room and on the furnishings. Additional analysis will be conducted to evaluate accelerant evidence collection procedures and chemical analysis.

The test plan calls for a total of ten tests. The first two will be done as baseline tests where just the effect of the ignition sources will be evaluated without any furnishings. The two ignition sources will be either a wood crib or gasoline. In some of the tests the gasoline will be poured on the floor from the interior of the room towards the door. In eight of the ten tests the fire will be started in the center of a wall, and the remaining two will be ignited in a corner.

REFERENCE

1. Kennedy, Patrick, M., "A Model of the Fire Protection System", Monograph presented to the National Fire Protection Association, Fall Meeting 1991.

2. NFPA 921, *The Guide for Fire and Explosion Investigation,* National Fire Protection Association, Quincy, MA. (1992)

NEW YORK STATE FIRE GAS TOXICITY FILING PROGRAM

William P. Chien, Ph.D.

Hazardous Materials Bureau
Office of Fire Prevention and Control
New York State Department of State
Albany, New York 12231

In the early 1980's, New York State initiated fire safety legislation in response to a significant concern regarding the combustion toxicity hazards of materials used in the modern building construction environment [1, 2]. By December 1986, New York had become the first state in the nation to require that combustion toxicity data on specified building materials and finishes be registered and made publicly accessible.

The covered building products include electrical conduit, electrical wire insulation, pipe, duct, thermal insulation, interior finishes and interior floor finishes. A covered product may be registered as a single product, as a product within a class, or as a component product. Under each option, marketing information is linked to test results obtained from accepted testing organizations using the University of Pittsburgh (UP) Toxicity Test protocol [3]. The approved filed product is assigned a Department of State (DOS) registry number, which is used by code enforcement officials to ensure that required construction materials have been filed and registered.

By May 1994, the database included 27,900 products filed (DOS numbers issued) which are linked to 161,000 market names and over a million end-use products. Approximately, 97 percent of these products are filed under one of the 169 approved product classes. The remaining 3 percent of the products are filed with supporting University of Pittsburgh toxicity test data. A total of approximately 1,150 individual UP sets of test data on varied covered products are currently available in the data bank. An inter-laboratory round robin testing program (involving seven laboratories) has been conducted and the standard deviation of LC_{50} was within 28 percent of the mean value.

Some efforts are being directed to the areas of data analysis, program evaluation, and enforcement. Preliminary data analyses are presented, which include both the distribution of all filed products and a grouping scheme of all products as a function of LC_{50} values (Fig. 1, Table 1). A recent toxicity method developed by Southwest Research Institute and National Institute of Standards and Technology (the SwRI/NIST Method) is cited [4, 5] and commented. The huge data base of New York Program is frequently queried, data searches performed, and reports generated. Local code enforcement officials use the system daily to ensure compliance with the New York State Uniform Fire Prevention and Building Code.

Many indications suggest that the New York program and the associated database can be useful in evaluating available building materials and finishes to control and improve the combustion toxicity risks inherent in the building construction environment. New York State stands ready to work with all concerned parties on this extremely important safety issue.

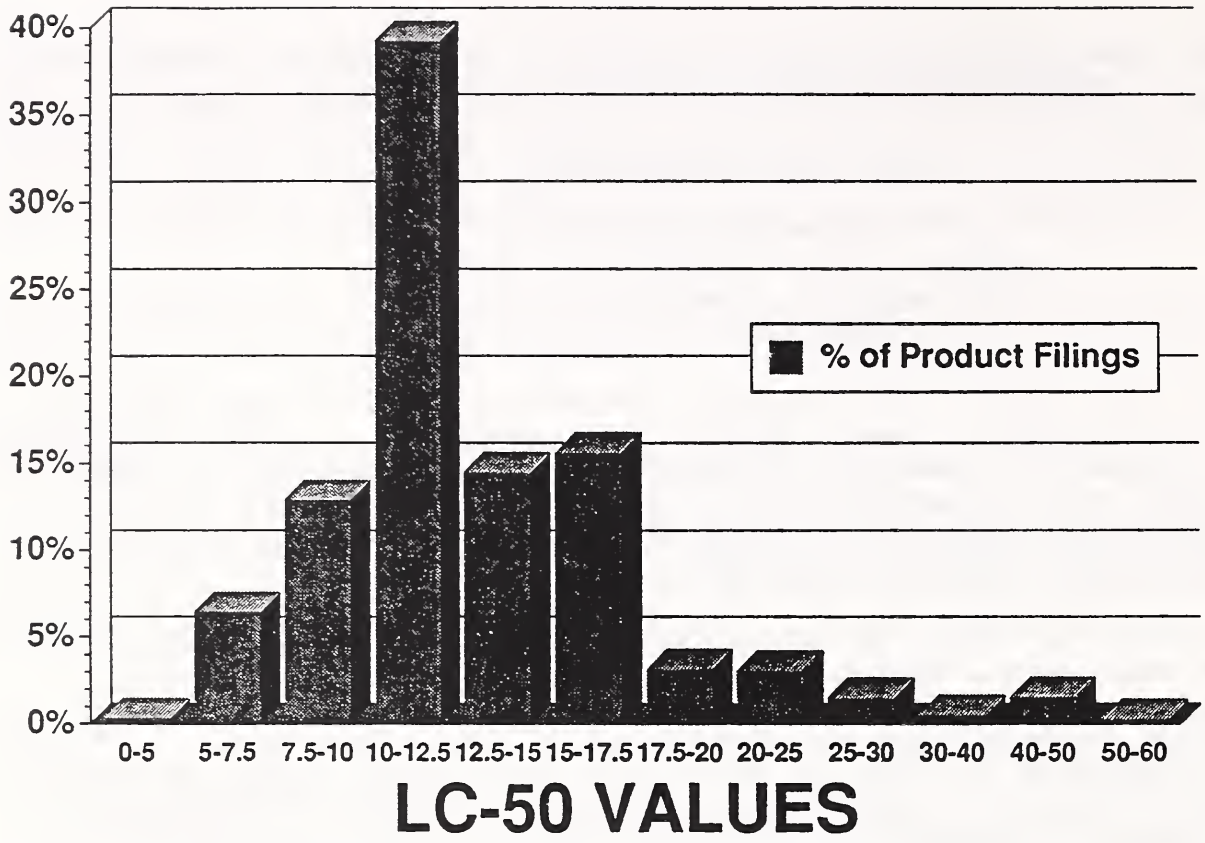

FIGURE 1. % OF PRODUCT FILINGS VS. LC-50 VALUES

TABLE 1. FIRE GAS TOXICITY PRODUCTS GROUPING BASED ON LC_{50} VALUES

	Group 1	Group 2	Group 3	Group 4	Group 5
LC_{50} Range	0 - 5	5 - 12.5	12.5-28.1	28.1-63.3	>63.3
No. Prd. Filing	85	14662	9396	649	226
Percent Total Filing	0.34	58.6	37.6	2.59	0.90

REFERENCES

1. "Adequacy of Existing Fire Codes and Recommendations for their Improvement," Special Fire Safety Task Force Report to Governor H. L. Carey, February 1981.
2. Anderson, R. C., P. A. Croce, and J. D. Sakura "Study to Assess the Feasibility of Incorporating Combustion Toxicity Requirements into Building Material and Finishing Codes of New York State," A. D. Little Inc. Report, May 1983.
3. Alarie, Y. and R. C. Anderson, "Toxicological Classification of Thermal Decomposition Products of Synthetic and Natural Polymers," Toxicol. Appl. Pharmacol., 57:181-188 (1981).
4. Babrauskas V., R. H. Harris, Jr., E. Braun, B. Levin, M. Paabo, and R. G. Gann, "The Role of Bench-Scale Test Data in Assessing Real-Scale Fire Toxicity", NIST Technical Note 1284, January 1991.
5. Babrauskas V., B. C. Levin, R. G. Gann, M. Paabo, R. H. Harris,Jr., R. D. Peacock, S. Yusa, "Toxic Potency Measurement for Fire Hazard Analysis", NIST Special Publication 827, December 1991.

COMPARTMENT FIRE EXHAUST GAS TRANSPORT AND OXIDATION

Brian Y. Lattimer, David S. Ewens and Uri Vandsburger
Virginia Polytechnic Institute and State University
Blacksburg, Virginia
and
Richard J. Roby
Hughes Associates
Columbia, Maryland

Introduction

Exhaust gas inhalation accounts for approximately two-thirds of all deaths in fires[1]. Many of these fatalities occur at enclosed locations which are remote from the burning compartment [2]. Carbon monoxide (CO), an odorless and colorless gas, is a major component within the exhaust gases which are transported through burning buildings and into locations remote from the actual fire. Studies have also indicated that (CO) is the most significant toxic exhaust gas for a wide range of fuels [3].

The focus of the experiments reported herein was to determine the phenomena which control the oxidation of the exhaust gases during sustained external burning, which is known to reduce CO levels [4], within a hallway. This was done by varying the global equivalence ratio (GER, defined as the mass ratio of fuel to air inside the compartment nondimensionalized by the stochiometric mass fuel to air ratio) and the fluid dynamics within the hallway.

Experimental

The experiments were performed at the VPI&SU Compartment Fire Dynamics facility which is discussed in detail elsewhere [5]. The GER was experimentally determined by measuring the fuel vaporization rate and the air into the fire,. The fluid dynamics inside the hallway were varied by adjusting the soffit heights from 0 to 20 cm at both the entrance and the exit of the hallway. The concentrations of CO, CO_2, O_2, and total unburned hydrocarbons (THC) within the exhaust gases were sampled at different locations along the length of the hallway and in the fume hood duct which was downstream of the hallway. The vertical temperature profile at the sampled locations within the hallway was determined using a rake of nine aspirated thermocouples spaced 6.4 cm apart. Each test was video taped to provide permanent visual record of the experiment. The recorded data was then averaged over the "quasi" steady state period which was during sustained external burning.

Results and Discussion

The post-hallway sampled tests provided information on the overall oxidation efficiency of the exhaust gases while the in-hallway experiments showed the evolution of the exhaust gases as they were transported and oxidized down the hallway All compartment fires were sufficiently underventilated to ensure sustained external burning within the hallway.

The overall oxidation efficiency of combustion gases which were transported from a burning compartment down a hallway having different soffit combinations is documented in Table I for a GER ranging from 1.5 to 3.5. These values are compared to the experimental results of the unconstrained fire jet from a compartment tests [4].

Figure 1 shows a detailed mapping of the normalized species concentrations along the length of the hallway which was generated from the results of the in-hallway experiments with no soffits at the inlet and exit of the hallway. The poor oxidation of the CO within the hallway was attributed to the inefficient mixing of the exhaust gases with the air in the hallway, the presence of the hydrocarbons and the thermal quenching of the exhaust gases. When a 20 cm soffit was attached to the exit of the hallway, the oxidation of CO, THCs and soot became even less efficient, as seen in Table I. These reductions in oxidation were attributed to the upper layer becoming much thicker which further decreases the mixing of ambient air into the layer.

A detailed mapping of the normalized species within the exhaust gases as they are transported down the length of the hallway with a 20 cm inlet and 0 cm exit soffit is shown in Figure 2. The hallway inlet soffit made

the constrained fire plume exiting the compartment during sustained external burning more jet like in structure causing the oxidation of CO to be as efficient as an unconstrained fire jet when fuel vaporization rates are less than 0.010 kg/s. The THC levels reduction levels were only slightly dependent on the fuel vaporization while the soot level reduction efficiency was in between CO and THC oxidation. When a 20 cm soffit was placed at the exit of the hallway, the reduction in species yields was still as efficient as the unconstrained jet experiments when fuel vaporization rates were less than 0.009 kg/s.

Conclusions

Poor oxidation of the exhaust gases was present when there was no soffit at the hallway inlet. The addition of a 20 cm soffit at the hallway exit decreased the oxidation of the exhaust gases when no soffit was present at the hallway entrance. With a 20 cm soffit at the inlet of the hallway, the oxidation of the exhaust gases was as efficient as the open jet experiments when the vaporization rate is less than 0.010 kg/s with no exit soffit, or less than 0.009 kg/s with a 20 cm exit soffit.

References

1. Hardwood, B. and Hall, J.R., 1989, "What Kills in Fires: Smoke Inhalation or Burns?," *Fire Journal*,Vol. 83, pp. 29-34.
2. Nelson, H.E., 1988, "An Engineering Analysis of Fire Development in the Hospice of Southern Michigan, December 15, 1985," *Fire Safety Science*, Proceedings of the Second International Symposium, pp. 927-938.
3. Morikawa, T., Yanai, E., Okada, T., and Sato, K., 1993, "Toxicity of the Atmosphere in an Upstairs Room Caused by Inflow of Fire Effluent Gases Rising from a Burning Room," *Journal of Fire Sciences*, Vol. 11, pp. 195-209.
4. Gottuk, D.T. and Roby R.J., 1992, "A Study of Carbon Monoxide and Smoke Yields from Compartment Fires with External Burning," *Twenty-Fourth Symposium (International) on Combustion, The Combustion Institute*, Pittsburgh, PA, pp. 1729-1735.
5. Ewens, D.S., Vandsburger, U., and Roby, R.J., 1993, "Oxidation of Exhaust Gases from a Burning Compartment in a Remote Location,", *Chemical and Physical Processes in Combustion*, Eastern States Section of The Combustion Institute, Paper No. 69.

Table I. Post-compartment exhaust gas oxidation with the GER ranging from 1.5-3.5.

Species	Unconstrained Jet Experiments [5]	Soffits: 0 cm inlet 0 cm exit	Soffits: 0 cm inlet 20 cm exit	Soffits: 20 cm inlet 0 cm exit[1]	Soffit: 20 cm inlet 20 cm exit[2]
CO	75-90%	54-68%	22-42%	78-89% (45-55%)	71-91% (39-51%)
THC	N/A	83-93%	75-89%	92-97% (88-91%)	91-98% (86-93%)
Soot	50-100%	48-86%	22-57%	61-92% (42-56%)	56-88% (28-46%)

1 values in parenthesis are for fuel rates > 0.0010 kg/s

2 values in parenthesis are for fuel rates > 0.009 kg/s

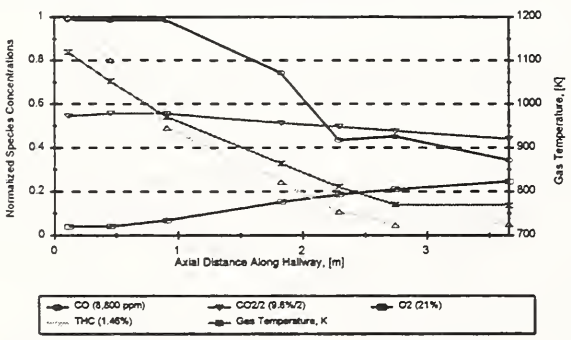

Fig. 1 0 cm inlet and 0 cm exit soffits.

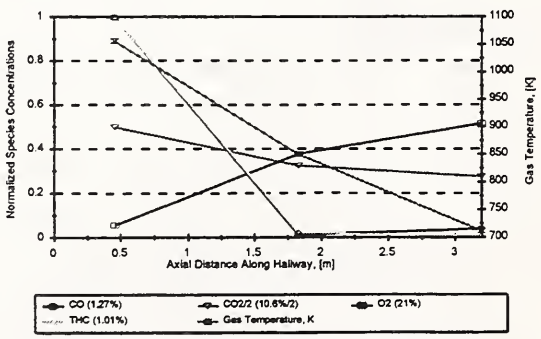

Fig. 2 20 cm inlet and 0 cm exit soffits.

AN ENGINEERING ALGORITHM FOR THE ESTIMATION OF CARBON MONOXIDE GENERATION IN ENCLOSURE FIRES

William M. Pitts

Building and Fire Research Laboratory
National Institute of Standards and Technology
Gaithersburg, MD 20899

Roughly two thirds of all deaths resulting from enclosure fires can be attributed to the presence of carbon monoxide (CO) [1],[2] which is the dominant toxicant in fire deaths [3]. A long-term program (Carbon Monoxide Production and Prediction Project) at the Building and Fire Research Laboratory is seeking to develop an understanding of and predictive capability for the generation of CO in enclosure fires [4].

During the past five years a great deal of research has been performed which forms the basis of an engineering approximation for estimating the generation of CO **within** a burning enclosure. A detailed summary of much of the work through 1993 is available [5].

It had previously been shown that the major products of combustion measured in hoods located above open fires in the laboratory are strongly correlated with the global equivalence ratio (GER, defined as the ratio of masses derived from fuel and air normalized by the ratio for stoichiometric burning) for the gases trapped in the hood [6],[7]. The existence of these correlations has been termed the GER concept [5]. Much of the recent research effort was focused on answering the question: Can the generation behavior of CO observed in hood experiments designed to model two-layer burning be extended to predict CO generation in actual enclosure fires? Unfortunately, tests in reduced-scale [8] and full-scale [9] enclosures have shown that the GER concept alone is insufficient to predict the observed CO concentrations. Actual concentrations are found to be higher than predicted by the GER concept [5].

The various investigations have identified four mechanisms for the generation of CO during enclosure fires:

1. **Quenching of a turbulent fire plume upon entering a rich upper layer.** This is the mechanism considered by the hood experiments [6],[7]. It should be noted that while the products of combustion correlate well with the GER in the hood experiments, the concentrations of products observed have been found to vary over a upper-layer temperature range of 700-900 K [5],[7].

2. **Mixing of oxygen directly into a rich, high-temperature upper layer.** Detailed kinetic modeling has shown that if oxygen is introduced directly into a rich upper layer having temperatures greater than 800 K, that reaction with fuel will generate primarily CO [5],[10],[11]. Evidence from fire tests in a reduced-scale enclosure [5],[8],[12] indicates that direct mixing of air into and subsequent reaction of rich upper-layer mixtures does occur leading to higher concentrations of CO than predicted by the GER concept.

3. **Approach to full-equilibrium combustion product concentrations in a rich, high-temperature upper layer.** Equilibrium concentrations of CO for rich upper layers and temperatures greater than 900 K approach 16% for a GER of 3. Normally, these concentrations are not observed because the mixtures are kinetically frozen. However, it has been shown that these rich mixtures do begin to react towards equilibrium concentrations for temperatures on the order 1400 K [11]. If these high temperatures occur for underventilated fires, the concentrations of CO can increase dramatically.

4. **Pyrolysis of wood in high-temperature, vitiated environments.** Experiments in the reduced-scale enclosure have shown that wood located in a high-temperature, highly vitiated upper layer undergoes pyrolysis which efficiently generates CO [13]. The majority of pyrolyzed wood carbon is lost as

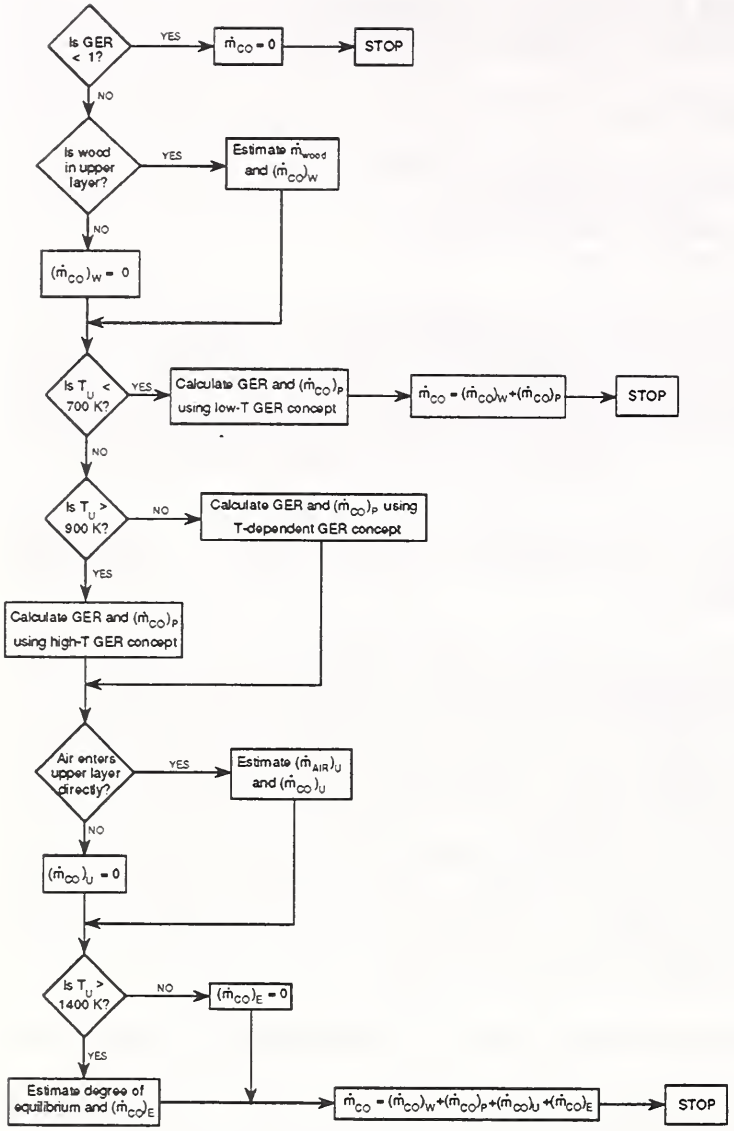

a roughly 1:1 mixture of CO and CO_2. Depending on the flow rate of the upper layer gases, the resulting increases in CO concentration can be quite large.

One should keep in mind that other pathways for the generation of CO may exist.

The algorithm shown at the left is based on these findings. It is designed to guide engineering calculations of CO generation rate in enclosure fires. The various symbols are defined as follows. $\dot{m}$ with a subscript are mass flow rates or reaction rates for the indicated species. The subscripts P, U, E, and W refer to generation of CO by processes 1-4 listed above, and T_U is a measure of the average upper-layer temperature.

Engineering estimates will be necessary for many of the parameters required to use this algorithm. Despite the uncertainty in such estimates, this approach should provide much improved predictions of CO generation in enclosures during underventilated burning than have been possible in the past.

Once generation rates are available within the enclosure, it will be necessary to model the reaction behavior and transport of the gases outside of the enclosure. This is the subject of ongoing research.

References

[1]. Harland, W. A.; Anderson, R. A. *Proceedings, Smoke and Toxic Gases from Burning Plastics*; pp. 15/1 to 15/19; Jan. 6-7, 1982, London, England.

[2]. B. Harwood and J. R. Hall, *Fire J.* **83** (1989) 29.

[3]. V. Babrauskas, B. C. Levin, R. G. Gann, M. Paabo, R. H. Harris, Jr., R. D. Peacock, S. Yusa, *NIST Special Publication 827* (1991).

[4]. W. M. Pitts, *NISTIR 89-4185* (1989).

[5]. W. M. Pitts, *NIST Monograph 179* (July, 1994).

[6]. C. L. Beyler, *Fire Safety J.* **10** (1986) 47.

[7]. E. E. Zukoski, J. H. Morehart, T. Kubota, S. J. Toner, *Combust. Flame* **83** (1991) 325.

[8]. N. Bryner, E. L. Johnsson, and W. M. Pitts, *National Institute of Standards and Technology Internal Report* (1994), to appear.

[9]. N. Bryner, E. L. Johnsson, and W. M. Pitts, unpublished results.

[10]. W. M. Pitts, *Twenty-Fourth Symposium (International) on Combustion*, (1992) 1737.

[11]. W. M. Pitts, *Fire Safety J.*, to appear.

[12]. W. D. Davis, *National Institute of Standards and Technology Internal Report* (1994), to appear.

[13]. W. M. Pitts, E. L. Johnsson, and N. P. Bryner, *Twenty-Fifth Symposium (International) on Combustion*, to appear.

Carbon Monoxide Production in Compartment Fires - Full-Scale Enclosure Burns

Nelson P. Bryner, Erik L. Johnsson, and William M. Pitts
Building and Fire Research Lab
National Institute of Standards and Technology
Gaithersburg, MD 20899 301-975-6868

Introduction

Recent studies attribute a large percentage of fire injuries and deaths to the generation of carbon monoxide (CO) [1-3] and indicate that in roughly two-thirds of the fire deaths the fire victims have fatal or incapacitating levels of carboxyhemoglobin in their blood. A series of natural-gas fires within reduced- and full-scale rooms have been designed to improve the understanding of and develop a predictive capability for CO formation in compartment fires. The findings will be used in realistic fire models and in the development of strategies for reducing the number of deaths attributed to carbon monoxide.

The full-scale room burns described by this paper extend the earlier work conducted in a reduced-scale (2/5ths) enclosure (RSE) [4]. The Full-Scale Enclosure (FSE) experiments were designed to examine whether the gas species and temperatures observed in the RSE could be used to predict the conditions in a FSE. While over 140 fires with heat release rates (HRRs) ranging from 7 to 650 kW were burned within the RSE, a more limited series of twelve fires ranging from 450 kW to 3500 kW were completed within a full-scale version of the standard room. Fires of greater than 200 kW and 1400 kW HRR created post-flashover conditions within the RSE and FSE, respectively. The RSE experiments had demonstrated that for flashed-over conditions, the upper layer was nonuniform in carbon monoxide and carbon dioxide concentrations as well as upper-layer temperature.

Experimental

The FSE is a standard room, 2.44 m wide by 2.44 m tall by 3.67 m deep with a 0.76 m wide by 2.03 m tall door centered at the bottom of the front wall as described by ISO/DIS 9705 [5]. The room consists of a sheet metal stud framework which is lined with three layers of 1.27 cm thick gypsum wallboard and a single layer of 1.27 cm thick calcium-silicate board. The FSE was instrumented with thermocouple trees located in the front and rear of the enclosure. Cooled and uncooled probes were positioned at different locations to sample the upper combustion layer, lower layer, and outside the doorway. The FSE was located under a large instrumented exhaust hood which allowed oxygen calorimetry and gas analysis to be performed on the exhaust gases from the enclosure. Doorway mass flows were measured through the door in two ways using a pressure probe and aspirated thermocouples located in the doorway. The burner was centered in the enclosure and each fire ranged from 15 to 20 minutes in duration.

Results and Discussion

Figure 1 shows a plot of CO concentrations versus time for the rear in the upper layer for several heat release rates. At 1400 kW HRR, the CO concentration begins to rise and peaks at about 0.5% in the front (not shown) and rear. As the HRR exceeds 2000 kW, the CO concentration quickly reaches 3 % and gradually peaks over 6 % in both the front and rear of the upper layer. CO concentrations are slightly higher in the front than in the rear of the enclosure. Figure 2 shows O_2 concentrations for the fires ranging from 450 kW to 3500 kW. The O_2 concentration drops to near zero at 1200 kW and remains near zero for all higher HRR. Typically the depletion of oxygen occurred more quickly in the rear of upper layer than the front portion.

Since temperatures in the upper layer exceeded the range of chromel-alumel thermocouples, a pair of platinum-rhodium thermocouples were installed for a 2300 and 3500 kW fires. In the 3500 kW fire, front and rear temperatures peaked at 1200 C and 950 C, respectively. Slightly higher temperatures were observed in the front and rear, 1300 C and 1000 C, respectively, for a 2300 kW fire. As was observed in the reduced-scale work, the front portion of the upper layer in the FSE was typically hotter than the rear. The reduced-scale study hypothesized that an interaction between the plume and upper layer was causing additional air to be injected directly into the upper layer. This additional oxygen reacted with unburned fuel in the upper

layer to form additional CO while releasing energy which increased the temperature in the front portion of the upper layer.

Different scaling parameters including plume entrainment, fuel mass flow rate, ceiling jet, volume, surface area, and ventilation rate were used to scale-up the fire size from the reduced-scale work. Using a ventilation rate parameter, $Ah^{1/2}$ [6], seemed to produce the best results.

Conclusions

The FSE burns generated significantly higher upper-layer carbon monoxide concentrations than observed in the RSE burns. The upper layer was more uniform in terms of gas species concentrations than in the RSE. The front and rear of the upper layer was quickly depleted of O2 for HRR > 1200 kW. Carbon monoxide concentrations of about 6 % were measured in the front and rear of the FSE during higher HRR fires. These CO levels are two times higher than the concentrations observed in the reduced-scale enclosure burns [4] and about three times higher than reported by previous researchers conducting idealized hood experiments [7-9]. Temperatures in the upper layer of the FSE appeared to be significantly higher than in the RSE, but the front portion of the upper layer in both the FSE and RSE was significantly higher than the rear. The physical and chemical mechanisms which produce the high concentrations of CO and high temperatures in the RSE also appear to be functioning in the FSE burns. Correlations and/or models need to be developed that include the production of carbon monoxide in high temperature vitiated regions of compartment fires.

REFERENCES

1. *World Almanac*, Editor Mark S. Hoffman, New York, NY: 1991. 850-851.
2. Harland, W.A and Anderson, R.A. Causes of death in fires. *Proceedings Smoke and Toxic Gases from Burning Plastics*; 15/1-15/19; Jan. 6-7, 1982; London, England.
3. Harwood, B. and Hall, J.R. What kills in fires:smoke inhalation or burns? *Fire J.* 83:29-34; 1989 May/June.
4. Bryner, N., Johnsson, E.L. and Pitts, W.M. Carbon Monoxide Production in Compartment Fires - Reduced-Scale Enclosure Test Facility. *NISTIR XXXX*; in WERB review.
5. Fire tests- Full scale room test for surface products. *Draft International Standard ISO/DIS 9705*. International Organization for Standardization. 1990; 41 p.
6. Quintiere, J.G. Scaling Applications in Fire Research. *Fire Safety Journal*; 15:3-29; 1989.
7. Beyler, C.L. Major Species Production by Diffusion Flames in a Two-layer Compartment Fire Environment. *Fire Safety Journal*, 10: 47-56, 1986 January.
8. Toner, S.J.; Zukoski, E.E.; Kubota, T. Entrainment, Chemistry, and Structure of Fire Plumes. *NBS-GCR-87 -528*; 1987 April; 200 p.
9. Morehart, J.H.; Zukoski, E.E.; Kubota, T. Species Produced in Fires Burning in Two-layered and Homoge neous Vitiated Environments. *NIST-GCR-90-585*; 1990 August; 259 p.

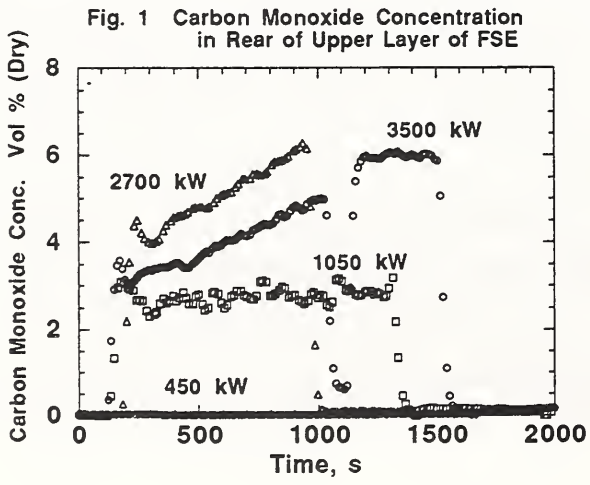

Fig. 1 Carbon Monoxide Concentration in Rear of Upper Layer of FSE

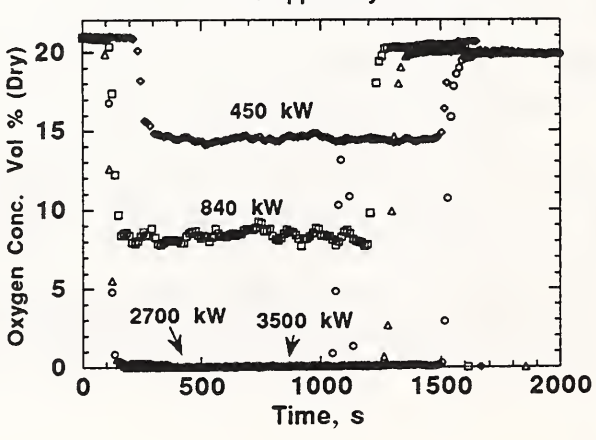

Fig. 2 Oxygen Concentration in Rear of Upper Layer of FSE

Flash Points of Hydrocarbon Solutions

David M. Finnegan
Robert G. Zalosh
Center for Firesafety Studies
Worcester Polytechnic Institute

Background

There have been several explosions involving hydrocarbon liquids with very high flash points. Some of these explosions occurred in storage tanks and others on tanker ships and barges. The liquids involved include asphalt, Number 6 fuel oil, and other commercial hydrocarbons. One suspected cause of the explosions is the contamination of these high flash point hydrocarbons with much lower flash point hydrocarbons. The pertinent question regarding this hypothesized explanation is: "how much contaminant is needed to lower the flash point to the tank temperature?" which is often about 66°C and 150°C to facilitate transfer of Number 6 fuel oil and asphalt, respectively.

In the case of simple multicomponent alkane solutions, Affens and McLaren (1) showed that their solution flash point reduction data could be predicted theoretically from the vapor pressures and flammability limits of the individual components. However, the compositions of asphalt and residual fuel oils are much more complex and probably do not satisfy the same simple ideal solution and ideal gas mixture relations as used by Affens and McLaren. No. 6 fuel oil and petroleum based asphalt are residues of the distillation of crude oil. These residual oils are comprised mostly of aromatic hydrocarbons with some paraffin and napthene hydrocarbons. The exact compositions are not usually available from either the supplier or the shipper, let alone the end user. Samples for testing described here were obtained from independent suppliers in Massachusetts.

The contaminants chosen for testing were heptane and No. 2 fuel oil. Heptane (closed cup flash point = -4°C) is a light paraffin hydrocarbon that is present in many residual oils and can be released during cargo heating as well as by a contaminant. No. 2 fuel oil (closed cup flash point = 58°C) can be used as a tank cleaning agent and is normally transported/stored in the same ships/tanks that carry/store No. 6 fuel oil.

Test Procedure.

The sample hydrocarbon liquids were tested at WPI in a Pensky-Martens closed cup tester. The test procedure used was the Pensky-Martens Closed Cup Flash Point ASTM D 93-IP 34 (2). This test method covers the determination of flash point by Pensky-Martens closed cup tester for fuel oils, lubricating oils, suspensions of solids, and other liquids of similar viscosities. This test method provides the only closed cup flash point test procedures for temperatures to 370°C. Open cup flash point measurements for the given samples were provided by an independent test lab.

Contaminants were measured in a graduated cylinder and added to the test sample. The sample and contaminant were then mixed inside the test cup for 10 minutes with the cover attached and shutter closed. The sample was then slowly heated according to (2) and flash points taken. Several tests were conducted with different amounts of contaminant in order to develop a graphical representation of the effects of contamination on complex hydrocarbon solutions to at least 5°C below the Grade E minimum flash point of 66°C.

Test Results.

Experimental results for heptane contamination of No. 6 fuel oil, asphalt, and lubricating oil are shown in Figure 1. The No. 6 fuel oil sample had an open cup flash point of 101°C and a closed cup flash point of 95°C. Only a 1% by volume contamination of heptane was necessary to lower the flash point of No. 6 fuel oil below 66°C. Experimental results for the sample of asphalt (closed cup flash point of 197°C) showed approximately 3.4% by volume contamination of heptane lowered the flash point below 66°C. In all three cases, the flash point reduction with heptane addition is quite steep for heptane concentrations less than about 3 volume %. Experimental results for lubricating oil (closed cup flash point of 166°C) showed a 1.7% by volume contamination of heptane lowered the flash point below 66°C.

Figure 2 shows results for contamination by No. 2 fuel oil. A 30% by volume contamination of No. 2 fuel oil was necessary to lower the flash point of No. 6 fuel oil below 66°C. A 73% by volume contamination of No. 2 fuel oil was necessary to lower the flash point of lubricating oil below 66°C. A 33% by volume contamination of No. 2 fuel oil was necessary to lower the flash point of asphalt below 66°C. Thus, contamination of high flash point hydrocarbons with small concentrations of heptane and similar alkanes (pentane and hexane) can significantly reduce the flash point of these commercial hydrocarbons, whereas small concentration contamination with Number 2 fuel oil or similar medium flash point commercial hydrocarbons does not produce the kind of flash point reductions required to produce flammable tank atmospheres at normal handling temperatures.

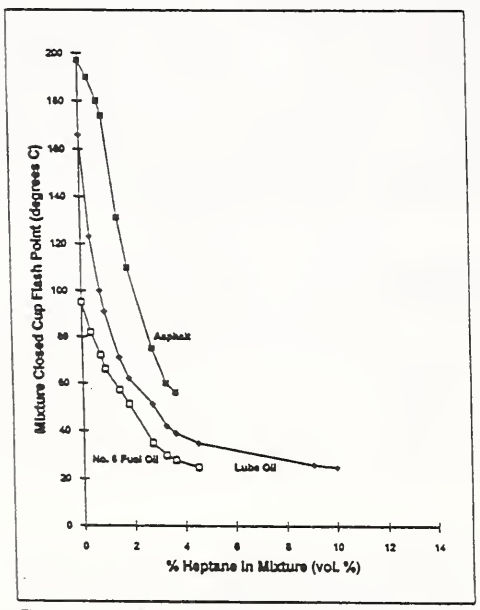

Figure 1. Effect of Heptane Contamination on Flash Points of Hydrocarbon Liquids

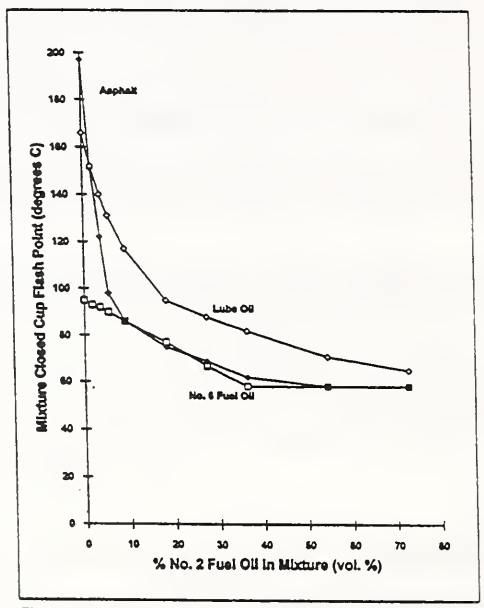

Figure 2. Effect of No. 2 Fuel Oil Contamination on Flash Points of Hydrocarbon Liquids

Acknowledgement

This work was conducted as part of a WPI study performed for the U.S. Coast Guard under Contract No. DTCG39-92-D-E38K37, D.O. 93-F-E00571. The authors are grateful for this support.

References.

1. Affens, W.A., and McLaren, G.W., "Flammability Properties of Hydrocarbon Solutions in Air," Journal of Chemical and Engineering Data, vol 17, No. 4, 1972.

2. ASTM D 93-90, "Test Method for Flash Point by Pensky-Martens Closed Tester", 1993 Annual Book of ASTM Standards, Vol 05.01, Petroleum Products, Lubricants and Fossil Fuels, American Society for Testing and Materials, Philadelphia, PA., 1993.

Halon Replacement Intermediate Scale Fire Testing at NRL

Ronald S. Sheinson[a], Harold G. Eaton[b], Bruce Black[c], Roger Brown, Howard Burchell, Alexander Maranghides[c], Clark Mitchell[c], Glen Salmon[d], and Walter D. Smith.

NAVAL RESEARCH LABORATORY
Navy Technology Center for Safety and Survivability
Code 6180, Washington, DC 20375-5342 USA
(202) 404-8101, Fax (202) 767-1716

An extensive series of halon in-kind replacement evaluations was performed at the Naval Research Laboratory's (NRL) 56 m^3 (2000 ft^3) test compartment located at the Chesapeake Bay Detachment (CBD) facility. Heptane pool fires were used to evaluate CF_3H (FE-13), C_3F_7H (FM-200), and C_4F_{10} (PFC-410), as total flooding halon replacement agents. Heptane spray reignition attempts assured extinguishment was not due to concentration transients. Such transient temporal and spatial behavior can be pronounced, especially in smaller compartments. Successful fire extinguishment with a specific nozzle, chamber geometry and fire placement may **not** accurately predict extinguishment in a different configuration or circumstances due to agent dispersal idiosyncracies.

These tests quantified the effects of agent design concentration and discharge time on fire out time and decomposition product formation. The agent concentration-time profiles at the base of the fire were always determined from discharge initiation on through successful extinguishment. Shorter discharge times yielded shorter fire out times (Table 1) as well as lower HF values (Table 2) for similar design concentrations. Higher design concentrations yielded shorter fire out times and reduced decomposition products for similar discharge times (Table 3). Increased fire size reduced oxygen concentration and increased temperatures in the compartment, which decreased fire out time and reduced the required extinguishing agent design concentration. An increase in fire size (from 0.23 m^2 to 1.1 m^2) increased HF production by a factor of three to five. An agent design concentration adequate to rapidly extinguish flammable liquid fires may not be adequate to minimize corrosive and toxic HF production. For example, for a 0.23 m^2 heptane pool fire, FM-200 at 7% design concentration, 11 seconds discharge produced over 1% HF; FE-13 at 14.4%, 5 seconds discharge produced 0.8% HF.

A comparison of NRL fire extinguishment times and acid production with tests by NMERI (18 m^3, 645 ft^3 compartment) and Hughes Associates, Inc. (28 m^3, 1000 ft^3 compartment) shows a compartment of 28 m^3 or larger should be employed to minimize wall effects and obtain proper scaling factor results for large fire scenarios.

Supported by the U.S. Naval Sea Systems Command.

a. Author to whom correspondence should be addressed.
b. Currently at Office of Naval Research.
c. GEO-CENTERS, Inc., Fort Washington, MD.
d. Hughes Associates, Inc., Columbia, MD.

Table 1
FM-200: Effect of Discharge Time on Fire Out Time

Discharge Time (sec)	Design Concentration %	Fire Out Time (sec)
5.1	8.3 (CB + 26%)	11
15.7	8.6 (CB + 30%)	19
5.7	9.7 (CB + 47%)	6
17.5	9.7 (CB + 47%)	17

Table 2
FM-200: Effect of Discharge Time and Design Concentration on HF Production
(Fire Out > = Discharge Time)

Discharge Time (sec)	Design Concentration %	HF_{max} (ppmv)
10.5	10.8 (CB + 64%)	2800
5.5	9.8 (CB + 48%)	2500
19.2	9.7 (CB + 47%)	6000
5.1	8.3 (CB + 26%)	5100
15.7	8.6 (CB + 30%)	12000

Table 3
FM-200: Effect of Design Concentration on HF Production
(Discharge Times: ~5 seconds)

Design Concentration %	Fire Out Time (sec)	HF_{max} (ppmv)
8 (CB + 21%)	12	8000
8.2 (CB + 24%)	12	6300
8.3 (CB + 26%)	11	5100
9.8 (CB + 48%)	7	2500

CF_3I - Halon 1301 Total Flooding Fire Extinguishment Comparison

Ronald S. Sheinson[a], Bruce Black[b], Roger Brown, Howard Burchell, Alexander Maranghides[b], Clark Mitchell[b], Glen Salmon[c], and Walter D. Smith.

NAVAL RESEARCH LABORATORY, Navy Technology Center for Safety and Survivability
Code 6180, Washington, DC 20375-5342 USA, (202) 404-8101, Fax (202) 767-1716

Halon 1301 (CF_3Br) is an extremely effective flame suppressant. The current commercialized and EPA approved in-kind clean replacements are much less effective. At least twice the agent liquid volume or weight is required for equal protection. Trifluoroiodomethane (CF_3I), has been the only current contender for a "drop-in" replacement. CF_3I was identified in the classic Army Purdue report of 1956 as being very efficient in flame burette tests. Russian patents in the early 1970s advocated this compound for specific fuel fires. NRL cup burner tests[1] published in 1978 showed this iodine analog of brominated halon 1301 was almost as effective (based on mole percent) in extinguishing heptane fuel fires. NRL cup burner studies with synthetic air mixtures and agent blends[2] using halon 1301 and CF_3I showed similar non-linear concentration dependent efficiencies (Figure 1). Our 1989 prediction[3] that CF_3I would have a low ozone depleting potential (ODP) was verified by measurements and calculations in conjunction with Dr. Molina of MIT. Stability and toxicity concerns remain.

Results of tank engine compartment fire extinguishment tests performed for the Army at NMERI showed that agent distribution was a very significant factor. Later tests at NMERI in their 18 m^3 (645 ft^3) compartment gave further evidence of transients as average extinguishment concentrations were very low compared to cup burner requirements. A halon 1301 - CF_3I comparison test at 5 percent design concentration at the Naval Research Laboratory's (NRL) highly instrumented 56 m^3 test compartment facility with 0.23 m^2 heptane pool fires and identical discharge times showed that CF_3I extinguished the fire in 6 seconds, compared to 8 seconds for CF_3Br. Halide acid values were comparable; both much less than generated from HFC and PFC candidates. Concentration-time profiles during the discharge interval showed CF_3I concentrations at the fire were temporarily slightly higher than CF_3Br levels before reaching identical equilibrium values (Figure 2). This small distribution difference was responsible for the increased relative effectiveness of CF_3I, not an innate higher effectiveness. The difference in vaporization rates causes different flow and distribution dynamics. Extensive pipe flow and fire extinguishment test series are needed. The recently determined cardiotoxicity LOAEL value of 0.4% for onset of cardiac arrythmia under epinephrine challenge means CF_3I is **not** a candidate for occupied space usage. Thus for many applications there still is no halon-like drop-in.

Supported by the U.S. Naval Sea Systems Command.
CF_3I donated by Pacific Scientific and West Florida Ordinance.

a. Author to whom correspondence should be addressed.
b. GEO-CENTERS, Inc., Fort Washington, MD.
c. Hughes Associates, Inc., Columbia, MD.

1. Sheinson, R.S., Gellene, G.I., Williams, F.W., and Hahn, J.E. Quantification of Fire Suppressant Action on Liquid Pool Fires. Paper 18, 1978 Combustion Institute, Eastern Section Meeting, Proceedings. Miami Beach, FL, November 29 - December 1, 1978.
2. Sheinson, R.S., and Driscoll, D.C. Fire Suppressant Concentration Requirements: Agent Mixtures and Depleted/Enriched Oxygen Concentrations. 23rd International Symposium on Combustion, Abstracts Book, Orleans, France, The Combustion Institute, July 1990, p. 204
3. Sheinson, R.S., and Driscoll, D.C., Fire Suppression Mechanisms: Agent Testing by Cup Burner. Proceedings, International Conf. on CFC & Halon Alternatives, Washington, DC, October 10-11, 1989.

CHEMICAL SUPPRESSION EFFICIENCY

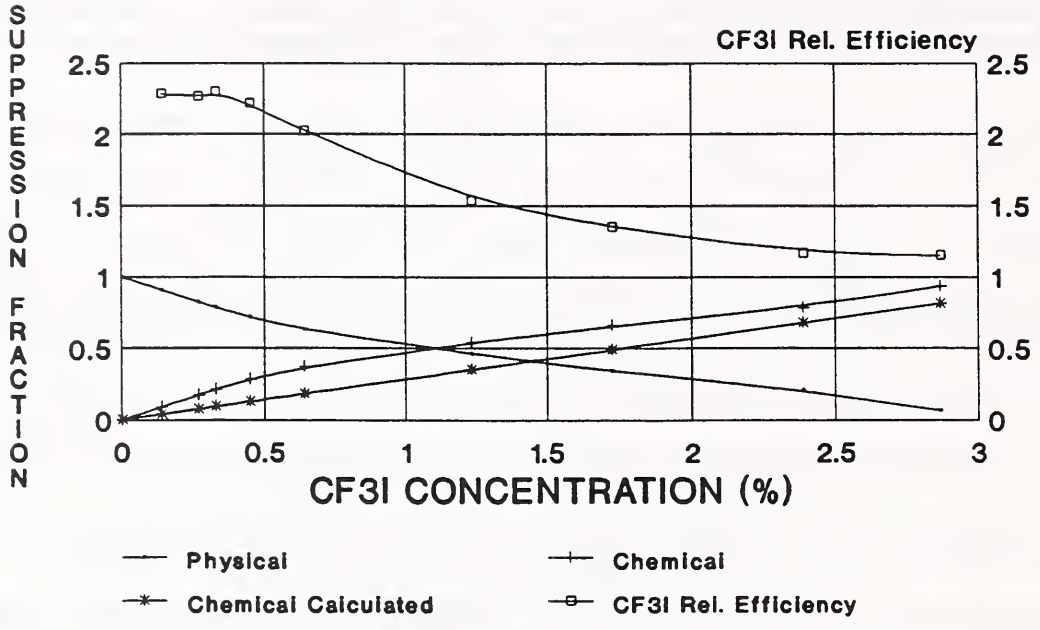

CF_3Br (5.09%) & CF_3I (5.03%)

2.5 ft^2 n-Heptane Pan Fire

3/16" Navy Nozzle

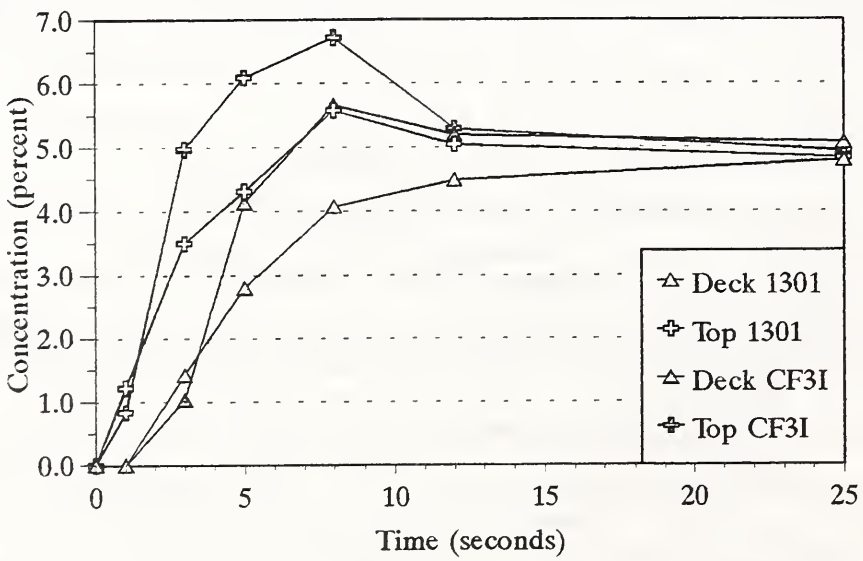

Conducting Shipboard Total Flooding Fire Testing with Halon 1301 Replacements

Ronald S. Sheinson[a], Alexander Maranghides[b], Doug Barylski[c], Bruce H. Black[b], Roger Brown, Peter Byrne[d], Tom J. Friderichs[e], Michelle Peatross[f], Walter D. Smith, and Frederick W. Williams.

NAVAL RESEARCH LABORATORY
Navy Technology Center for Safety and Survivability
Code 6180, Washington, DC 20375-5342 USA
(202) 404-8101, Fax (202) 767-1716

Total flooding halon replacement agents are being evaluated for extinguishing heptane and diesel pool and spray fires in a real scale 840 m^3 (29,700 ft^3) compartment. The tests are being conducted aboard the Ex-USS SHADWELL located in Mobile Bay, Alabama. The compartment is being equipped with engine and ventilation mockups (Figure 1) in order to realistically simulate the machinery spaces of US Navy current and planned ships. The purpose of these tests is to determine how these Halon 1301 replacement agents function in a realistic environment. Agent design concentration and discharge time effects on fire out time and decomposition product formation, as well as agent pipe flow and distribution in a large compartment will be determined. A multiple level, 9 nozzle discharge system is being used; FM-200 will be nitrogen charged at high pressure (4.1 MPa, 600 psi, and higher). Agent distribution data in no-fire discharges are being obtained from thermal conductivity detectors. Extensive, multiple location, continuous and discrete monitoring of agent, acids, CO, CO_2, and O_2 will be used to characterize the fire extinguishment environment. Compartment temperatures and pressures will be monitored. Optical density meters, radiometers and video cameras (visible and IR) will also be used. Fire threats will range from small telltale pools, 250 kW pools and sprays to 2 to 5 MW pool and spray fires. The fuel will usually be heptane, with diesel fuel also used for the larger fires. The fire threats are situated to present a difficult challenge to the extinguishing system.

Candidate replacement agents C_3F_7H (FM-200), CF_3H (FE-13), and to a lesser degree C_4F_{10} (CEA-410) are being evaluated aboard the Ex-USS SHADWELL. The same simulated shipboard machinery space test facility is being employed for fine water mist fire extinguishment as well as for pyrogenic fine solid aerosol and other candidate evaluation in the future. Many additional employees and contractors are involved in this major effort. The detailed test plan contains the specific sensor and sampling point locations, fire threats, test conditions, agent concentrations and discharge intervals, as well as test protocols. This presentation will describe the facility and its extensive capabilities.

Supported by the U.S. Naval Sea Systems Command.

a. Author to whom correspondence should be addressed.
b. GEO-CENTERS, Inc. Fort Washington, MD.
c. NAVSEA 03G2, Crystal City, VA.
d. University of South Alabama, Mobile, AL.
e. MPR Associates, Inc., Alexandria, VA.
f. Hughes Associates, Inc. Columbia, MD.

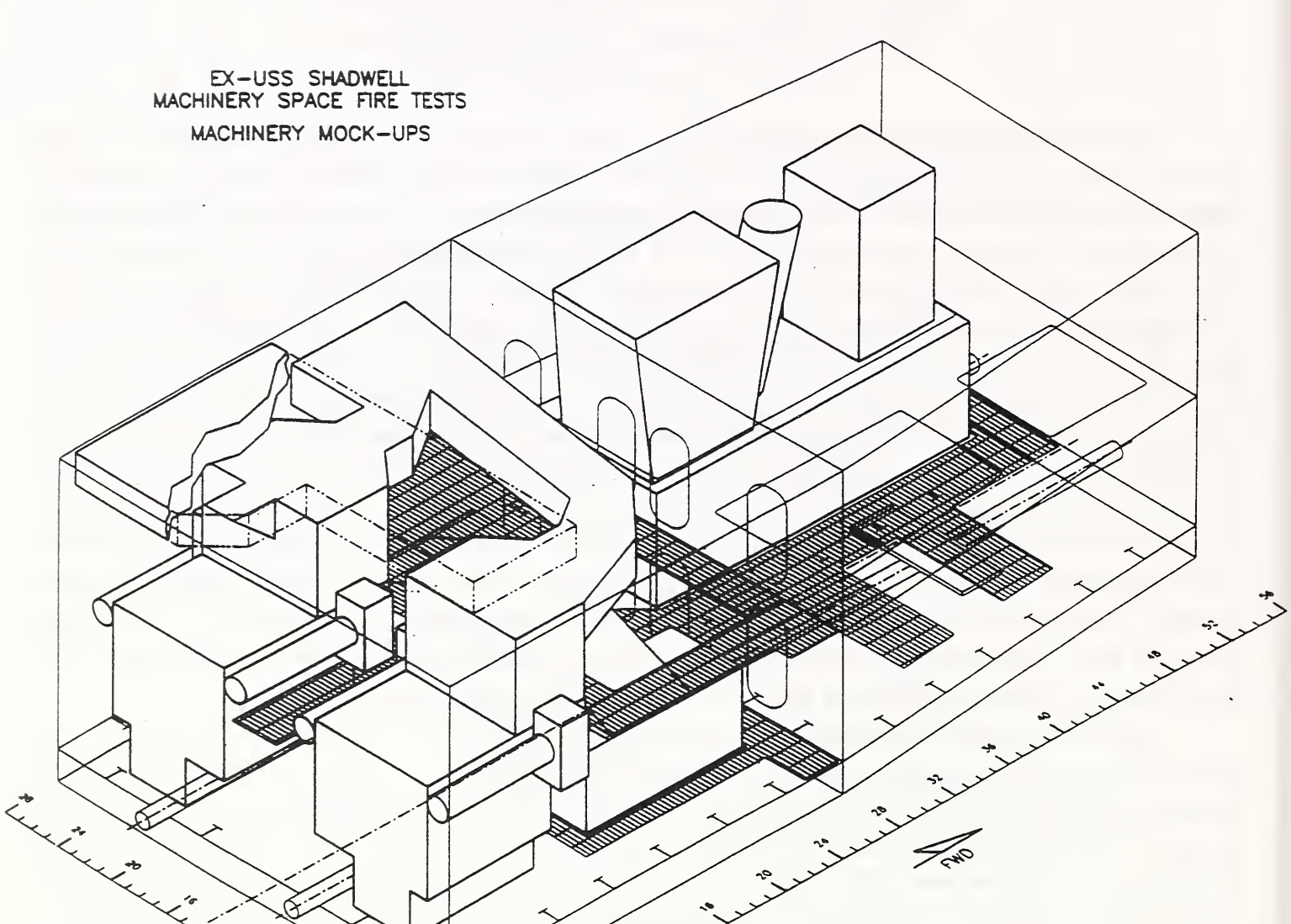
EX-USS SHADWELL
MACHINERY SPACE FIRE TESTS
MACHINERY MOCK-UPS
FWD

Shipboard Total Flooding Fire Testing with Halon 1301 Replacements: Test Results

Ronald S. Sheinson[a], Bruce H. Black[b], Roger Brown, Scott Heyworth[c], Alexander Maranghides[b], Michelle Peatross[d], Glen Salmon[d], Walter D. Smith, and Frederick W. Williams.

NAVAL RESEARCH LABORATORY
Navy Technology Center for Safety and Survivability
Code 6180, Washington, DC 20375-5342 USA
(202) 404-8101, Fax (202) 767-1716

The total flooding halon replacement agents C_3F_7H (FM-200), CF_3H (FE-13), and to a lesser degree C_4F_{10} (CEA-410), are being evaluated for extinguishing heptane and diesel pool and spray fires in the 840 m^3 (29,700 ft^3) compartment aboard the Ex-USS SHADWELL described in another paper at this conference. A series of background fires have been studied to characterize the space. Oxygen depletion does occur with the larger fires. While the extent is not sufficient to quickly self-extinguish the fires, it will have effects on agent requirements, extinguishment times, and acid production.

The discharge equipment utilizes Navy type halon 1301 hardware including 9 nozzles in an unbalanced complex system. The nozzles are made with 3.8 cm (1.5 in) pipe fittings as the standard Navy 2.5 cm (1 in) pipe size nozzles are inadequate for the larger volume flows required with the less efficient replacement candidates. "Cold" discharges of FM-200 have verified discharge system design. The figures show preliminary pressure measurements at 11 points in the piping, and agent concentration at one point. The test compartment is being fitted with engine and ventilation mockup obstructions simulating machinery spaces of US Navy ships.

Fire extinguishment times and hydrogen fluoride acid concentrations, as well as agent pipe flows and compartment distributions, will be determined as functions of agent design concentration, discharge time, and fire size in a realistic shipboard compartment environment. A large number of employees and contractors are involved in this major effort. Results of this ongoing highly instrumented evaluation program will be presented.

Supported by the U.S. Naval Sea Systems Command.

a. Author to whom correspondence should be addressed.

b. GEO-CENTERS, Inc., Fort Washington, MD.

c. Center for Firesafety Studies, WPI, Worcester, MA.

d. Hughes Associates, Inc., Columbia, MD.

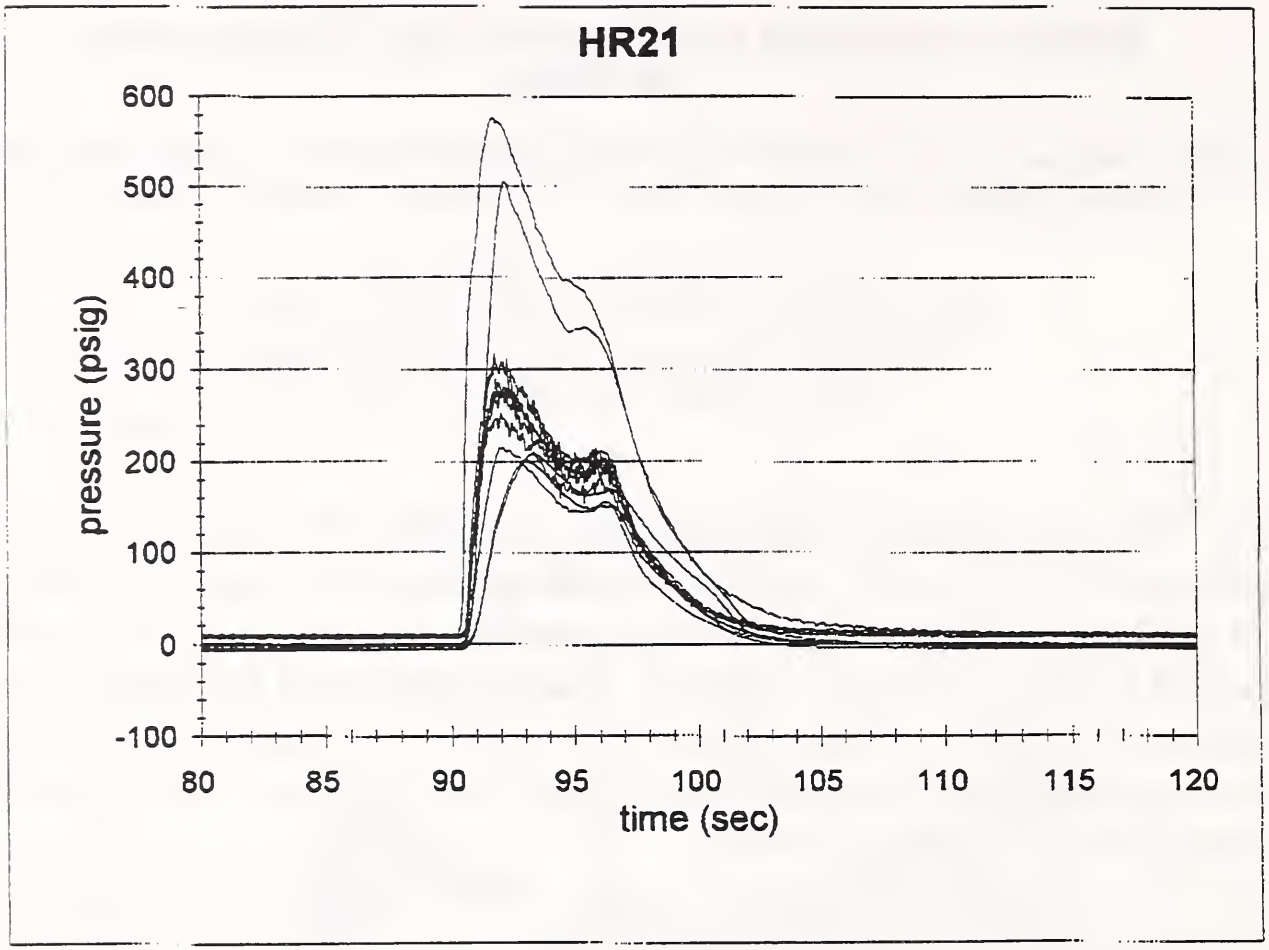
HR21
600
500
400
300
200
100
0
-100
pressure (psig)
80
85
90
95
100
105
110
115
120
time (sec)

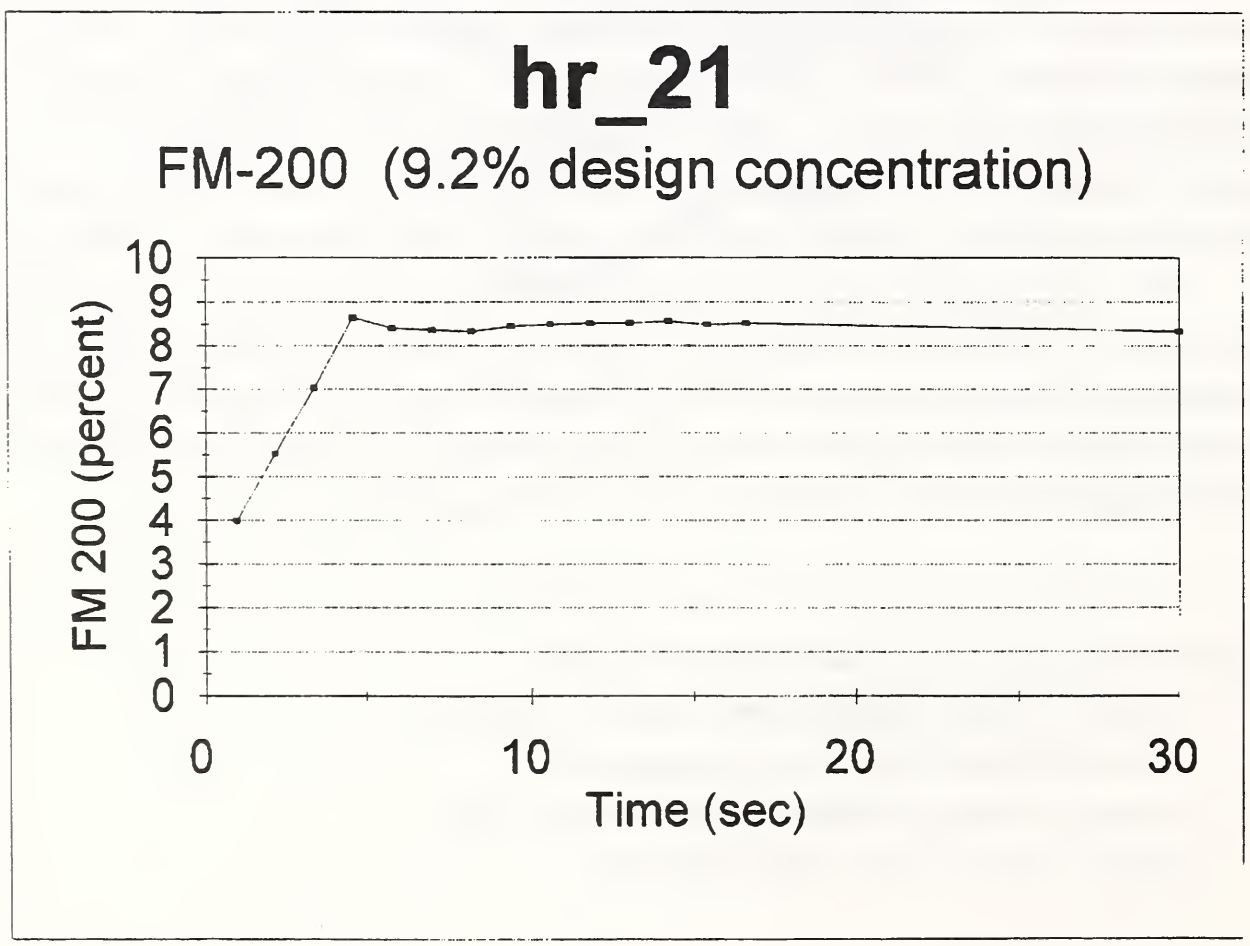
hr_21
FM-200 (9.2% design concentration)
10
9
8
7
6
5
4
3
2
1
0
FM 200 (percent)
0
10
20
30
Time (sec)

NEXT GENERATION FIRE SUPPRESSION TECHNOLOGY: A RESEARCH STRATEGY AND PLAN

Richard G. Gann
Fire Science Division
Building and Fire Research Laboratory
National Institute of Standards and Technology
Gaithersburg, MD 20899

Halon 1301, CF_3Br, has been used extensively to protect vital Department of Defense systems and facilities from unwanted fires often caused by enemy attack. The fire protection for most current weapons systems has been, in fact, designed around its excellent capabilities. Because of the chemical's high suppression efficiency, there has been minimal engineering for optimal distribution and design concentration.

Unfortunately, halon 1301 has now been found to contribute significantly to stratospheric ozone depletion, and commercial production has ceased by law as of January 1, 1994. Government agencies and private firms have created "banks" of new or recycled halon 1301 as a temporary means of continuing protection. Near-term replacement of this suppressant has become a high priority. There has been some examination of commercially available "drop-in" replacements (generally aliphatic halocarbons), and the best of these will soon be identified.

The use of different technologies or dissimilar fluids is not a near-term possibility for protecting current weapons systems. Significant re-engineering of the multiple and diverse hardware requires time and billions of dollars, while increasing production of a chemical from laboratory to meeting commercial demands can take years. Thus, there is little ongoing systematic research on new approaches.

The Office of Advanced Technology under the Director of Defense Research and Engineering is concerned that there be effective and efficient fire protection for future systems. They have requested the development of a research plan to create and develop next-generation fire suppression technologies appropriate for Department of Defense needs that match the effectiveness of halon 1301 without its associated environmental penalties. This plan has been developed with the collaboration of experts in fire science, the contributing disciplines, instrumentation, and testing. It is intended to commence during FY 1995 and reach completion in 8 years.

Experience has shown that the development and examination of new fire suppressant technologies is not likely to be brief or easy. First, a quick survey of fires for which the DoD currently uses halon 1301 showed an extremely broad range of fire locations, fuels burning modes, and required times for suppression (10^{-2} - 10 seconds). The hazards to be avoided include harm to people, thermal damage to equipment, post-fire corrosion, loss of visibility, overpressure. Second, successful suppressants must possess a wide variety of desirable properties. Third, a number of the more obvious chemicals have already been tested and found wanting. Fourth, the environmental demands on the agents will likely change during the course of the program.

To address this broad spectrum of applications and constraints, the strategy is to conduct a program comprising six technical thrusts:

- Fire Suppression Principles: conception and examination of the mechanisms of flame extinguishment.

- New Suppression Concepts: generation of new ideas.

- Emerging Technology Identification and Improvement: finding approaches that are already under development and accelerating their maturation. This will likely involve partnering with commercial firms.

- Suppression Optimization: developing the knowledge to obtain the highest efficiency of each candidate technology.

- Laboratory Testing: developing/adapting and implementing lab-scale methods for evaluating the key properties for suppressants and suppression system components.

- Real-Scale Validation: ascertaining the performance of candidates at real scale. This will make use of appropriately-enhanced existing DoD (etc.) facilities.

Elements of these will be performed concurrently and synergistically. New ideas generated, for instance, during validation tests will then be examined further. New instrumentation developed during laboratory testing may be adapted for real-scale tests. This approach will result in the establishment of a broad understanding of the suppression process and a diversity of tested approaches. This will enable the prompt development of further technology should future requirements change.

Each element of the program will make use of existing facilities and will coordinate with other on-going programs. The research will be performed by experts in the critical technical areas and focussed on the plan objective. The research will involve the best technical experts, making extensive use of capabilities within the Federal laboratories.

The research plan will begin with:

- An in-depth survey to identify the characteristics and environment of the fire types for which halons are currently deployed.

- A workshop to hear about the realm of technologies currently under development.

- Studies to establish the mechanistic basis for fire suppression.

- Completion of development of laboratory methods for measuring and characterizing the benefits and drawbacks of candidate technologies.

As designed, this program should quickly begin producing a steady flow of ideas for further development and examination. Those ideas showing promise will be pursued to the point of practical demonstration. To the extent that a given approach is appealing to a business, partnership arrangements will be arranged to enable commercialization. All information on chemicals and systems and their test results will be in the public domain.

We are highly confident that this program will succeed in providing demonstrated and documented alternatives that are sufficiently effective that the DoD users will have real options. We believe that this output will have broad applicability to non-defense fire protection as well.

AN EXPERIMENTAL AND THEORETICAL STUDY OF MECHANISMS OF FIRE SUPPRESSION BY WATER

ARVIND ATREYA, TODD CROMPTON AND JAEIL SUH
Combustion and Heat Transfer Laboratory
Department of Mechanical Engineering and Applied Mechanics
The University of Michigan, Ann Arbor, MI 48109-2125

(Supported by NIST)

This paper attempts to provide a quantitative understanding of the chemical and physical mechanisms of fire suppression by water through an integrated approach of small-scale experiments and theoretical models. Water is known to have two physical effects: (i) cooling of the burning solid by water evaporation, and (ii) smothering caused by dilution of the oxidizer and/or the fuel by water vapor. In addition to these two well known effects, there are three more effects, namely: (iii) enhanced radiative heat loss due to increased water concentration, (iv) enhanced mixing as a result of volumetric expansion caused by water evaporation, and (v) a little known but significant chemical enhancement effect which reduces the soot concentration and decreases the luminous flame radiation. Our experiments show that the last two effects considerably increase the combustion efficiency and reduce the suppression effectiveness of water (defined as: decrease in the heat release rate per unit mass application rate of the suppression agent). Since, the physical cooling effect of water [i.e. (i)] has been extensively studied earlier, the objective of this work is to quantify the gas-phase effects [i.e. (ii) through (v)] and model them. Understanding of these gas-phase effects is important for water mist suppression.

Experiments were conducted for different O_2 concentrations (to change the soot volume fraction) and for different constant water application rates (applied both as liquid water and as water vapor). Methane and ethylene were used as fuels, and fuel and oxidizer flow rates were held constant. The overall transient species composition measurements in the exhaust of the stagnation-point flow apparatus were used to calculate the effect of water on the overall heat release rate. An increase in the CO_2 production rate and the O_2 depletion rate corresponds to an increase in the burning rate and vice versa. Also, detailed flame structure measurements in the presence of water vapor were made in the steady counterflow diffusion flame and numerical calculations were performed to help interpret the data and understand the suppression mechanisms. The dilution effect of H_2O is compared with the dilution by N_2 & CO_2, enhanced radiative heat loss is calculated via a model and mixing and chemical enhancement effects are investigated experimentally and theoretically. A brief summary of the experimental results is presented below.

SUPPRESSION EXPERIMENTS WITH LIQUID WATER: These experiments began with liquid water applied to the surface of a burning PMMA sample. However, to eliminate the physical cooling effect of the solid, an uncooled porous ceramic methane burner was used and liquid water was gently applied to the surface of this burner with a constant methane flow rate. It was found that: (i) For a blue methane flame, fuel dilution due to water evaporation decreased the CO_2 & CO production rates and the O_2 depletion rate. Less hydrocarbons were burned and the hydrocarbon percentage increased until extinguishment was obtained. Thus, chemical enhancement was not observed. (ii) However, for a sooty methane flame, the O_2 depletion rate and the CO_2 production rate was observed to increase as the water application rate was increased. This implies an increase in the heat release rate (i.e. more efficient combustion). With further increase in the water application rate, dilution effects become dominant and the flame gets extinguished.

The above results seem to contradict some previous work which claims that water simply acts as a diluent. Thus, to further eliminate the *possibility* of enhanced mixing due to flow disruptions that *may* be caused by volumetric expansion of liquid water (although not observed visibly in the experiments), these experiments were repeated with water vapor. Both stagnation-point flow and the steady counterflow diffusion flame apparatuses were used. The flame structure was measured and calculated with the help of a theoretical model which incorporates the SANDIA CHEMKIN code.

SUPPRESSION EXPERIMENTS WITH WATER VAPOR: In the experimental results presented below, different amounts of water vapor was added to the air side. The experiments were conducted both in the stagnation-point flow apparatus (to measure the cumulative transient effects and compare them with the previous results) and in the steady counterflow diffusion flame (to measure the flame structure and compare them with theoretical calculations).

Transient Experiments: Table 1 summarizes the measured mass flow rates in the exhaust both with and without water vapor application. In all these experiments the O_2 concentration was held constant at 15% and different amounts of water was added to the air stream as replacement of N_2 on a volumetric basis (cold air stream flow rate: 12 lpm). The fuel stream was pure CH_4 (cold fuel flow rate: 1.5 lpm). Thus, the oxidizer flow with 30% water vapor contained 15% O_2, 30%

H_2O and rest N_2. Normalized measured mass flow rates of CO_2 and CO in the exhaust are plotted in figures 1 & 2 and measured boundary and peak temperatures are listed in Table I. There is a slight reduction in the peak flame temperature as water replaces N_2 (~20°C; Table I) but an increase in temperature elsewhere. Measured temperature profiles show that the reaction zone becomes wider upon water vapor addition. The temperatures at the fuel and oxidizer inlet also increase upon water vapor addition (see Table I). Visually, the flame becomes less bright and sooty as N_2 is replaced by water vapor.

Figures 1 & 2 respectively show the excess CO_2 produced & CO consumed when water vapor was added to the oxidizer flow of a counterflow diffusion flame. These experiments were conducted by the following procedure: First, a steady diffusion flame was established with N_2 in the air stream and then a predetermined amount of N_2 flow rate was substituted with an equal molar flow rate of water vapor. Water vapor was turned off after about 900 seconds and an equal molar flow rate of N_2 was re-substituted. While this procedure ensures that the initial and final flame conditions remain the same, it causes large fluctuations during changes. Thus, the useful data is at the two steady state conditions: one without water and one with prescribed amount of water. This comparison is also shown in Table I. Note that for each experiment the initial steady state condition with N_2 is nearly the same, indicating excellent repeatability.

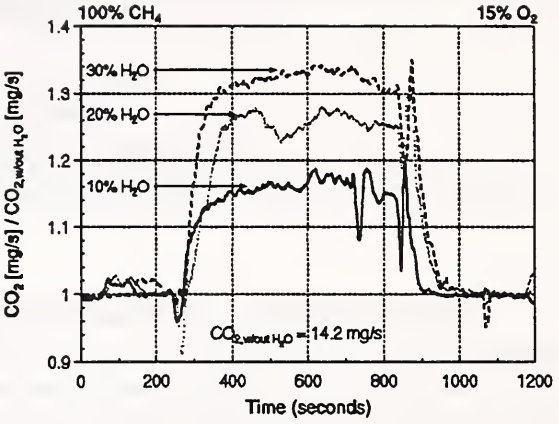

Fig. 1: Normalized CO_2 Production Rate Showing Excess CO_2.

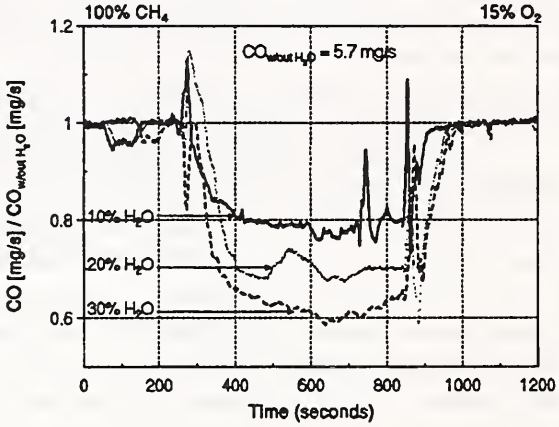

Fig. 2: Normalized CO production rate showing reduction in CO

These results clearly show that more CO_2 was produced as the concentration of water vapor was increased. This CO_2 came from oxidation of CO, additional consumption of unburned hydrocarbons, and some additional consumption of O_2. Thus, the combustion efficiency was increased upon addition of water vapor. A corresponding increase in the flame temperature (except at the peak) was also observed despite a 25% larger ρC_p for water. These results are qualitatively consistent with previous experiments where water was applied in a liquid form. Quantitative comparisons show that they are somewhat lower - indicating enhancement due to mixing.

These results are also consistent with the experiments conducted in sooty (fuel-rich) methane counterflow diffusion flames. Here detailed flame structure measurements were made. It was found that by reducing the O_2 concentration while maintaining the flame temperature by preheating the reactants (thus reducing the H_2O concentration in the reaction zone) led to an early soot inception and increased soot volume fraction. However, direct addition of only 3.6% H_2O (while holding all other conditions constant) resulted in delayed soot nucleation and a significant reduction in the soot volume fraction. These observations can be consistently explained by the mechanism of *OH* interference with soot inception. An increase in the H_2O concentration (brought about either by an increase in the O_2 concentration or by direct addition) results in an increase in the *OH* concentration provided the flame temperature is high enough. This reduces the *PAH* and C_2H_2 concentrations (the corresponding reduction in total hydrocarbons and *CO* was observed in the stagnation-point flow diffusion flame) and delays soot inception. This substantially decreases the ultimate soot loading and increases the combustion efficiency and hence the burning rate.

Table I - Measured Exhaust Mass Flow Rates for experiments where Water Vapor Replaces Nitrogen in the Air Stream.

%H_2O → Species↓	0% -----10%	0% -----20%	0%-----30%
THC	8.4 ------- 8.1	8.4 ------- 7.9	8.4 ------- 8.0
CO (mg/sec)	5.7 ------- 4.4	5.7 -------- 4.0	5.7 ------- 3.5
CO_2 (mg/sec)	14.3 ----- 16.8	14.2 ----- 17.9	14.2----- 19.0
O_2 (mg/sec)	33.6 ---- 34.1	33.6 --- 34.2	34.2 -- 34.6
O_2Temp. (K)	751 ----- 754	751 ------- 760	750 ---- 764
FuelTemp(K)	684 ----- 688	690 ----- 700	690 --- 707
MaxTemp(K)	1622 --- 1607	1623 --- 1605	1625 -- 1596

MULTI-DROPLET EVAPORATIVE COOLING

S. Tinker, M. di Marzo
Mechanical Engineering Department
University of Maryland - College Park, MD 20742

The modeling of the cooling effect of a sparse spray impinging on a low thermal conductivity semi-infinite solid is proposed. The results of the single droplet evaporative cooling model for the case of radiant heat input from above the surface are used to modify a closed form solution available in the literature.

The sparse spray used by Dawson [1] is characterized by a distribution function which can be expressed as a polynomial of the sixth order. This distribution function represents very closely the measured droplet distribution. The arguments to derived this distribution are based on physical measurements and on the kinematic analysis of the droplet generator positioner. The droplets are equal in size and are delivered with similar kinetic energy to the surface.

The study of the effect of the droplet transient geometrical configuration revealed that a simple model based on a segment of a sphere approximation with the proper consideration for the receding angle condition provided good agreement with the data.

The multi droplet model is based on the closed form solution previously described which is used in the close field (i.e. for distances up to 5 radii from the droplet deposition location). In the far field, the droplet is represented by an instantaneous point sink which is time-delayed by 60 percent of the evaporation time [2].

The results of the computations are qualitatively compared with the data in Fig. 1. Great care is taken in selecting a computational field that matches the same portion of the data collection field. The two top contour plots are obtained via infrared thermography, while the two bottom plots are the results of the code computations. The droplet deposition sites are random-generated in accordance with the distribution function previously discussed. Note the similar extent of the isothermal at 129 °C and at 130 °C in the snapshots at 600 seconds and the similar correlation for the 116 °C and 120 °C isothermals at 50 seconds.

In Fig. 2 the overall transient is represented for all the data available [1]. The temperatures are normalized with respect to the initial solid surface temperature, Tso, and with respect to the steady state temperature Tss. The steady state temperatures are obtained from the code computations after validation against the data. Note that the experimental data and the results of the computations are in good agreement and that all the points are within ±20 percent of the steady state value. The data set for Tso = 162 °C and for a water mass flux G = 0.5 g/m^2-s is not within this bound since the initial portion of the transient happens to be in nucleate boiling.

The most notable result is that the temperature normalization is able to collapse the data and the computations. Note that the water mass flux is used to compute the steady state solid surface temperature. The time constant of the process yields a characteristic length of about one centimeter (i.e. penetration depth). This is comparable with the radius influence associated with the cooling effect of the single droplet [3].

Acknowledgements The authors are indebted to Dr. H. Baum for his guidance in the development of the single and multi-droplet codes and to Dr. D. Evans for his continuous support and advice.

References

1. H. Dawson, M. diMarzo, *AIChE Symp. Ser.*, 89, 295, pp. 26-35 (1993)
2. P. Tartarini, Y. Liao, M. diMarzo, *Heat & Tech.*, 11, 1-2, pp. 98-106 (1993)
3. M. diMarzo, P. Tartarini, Y. Liao, D. Evans, H. Baum, *Int. J. Heat Mass Transfer*, 36, 17, pp. 4133-4139 (1993)

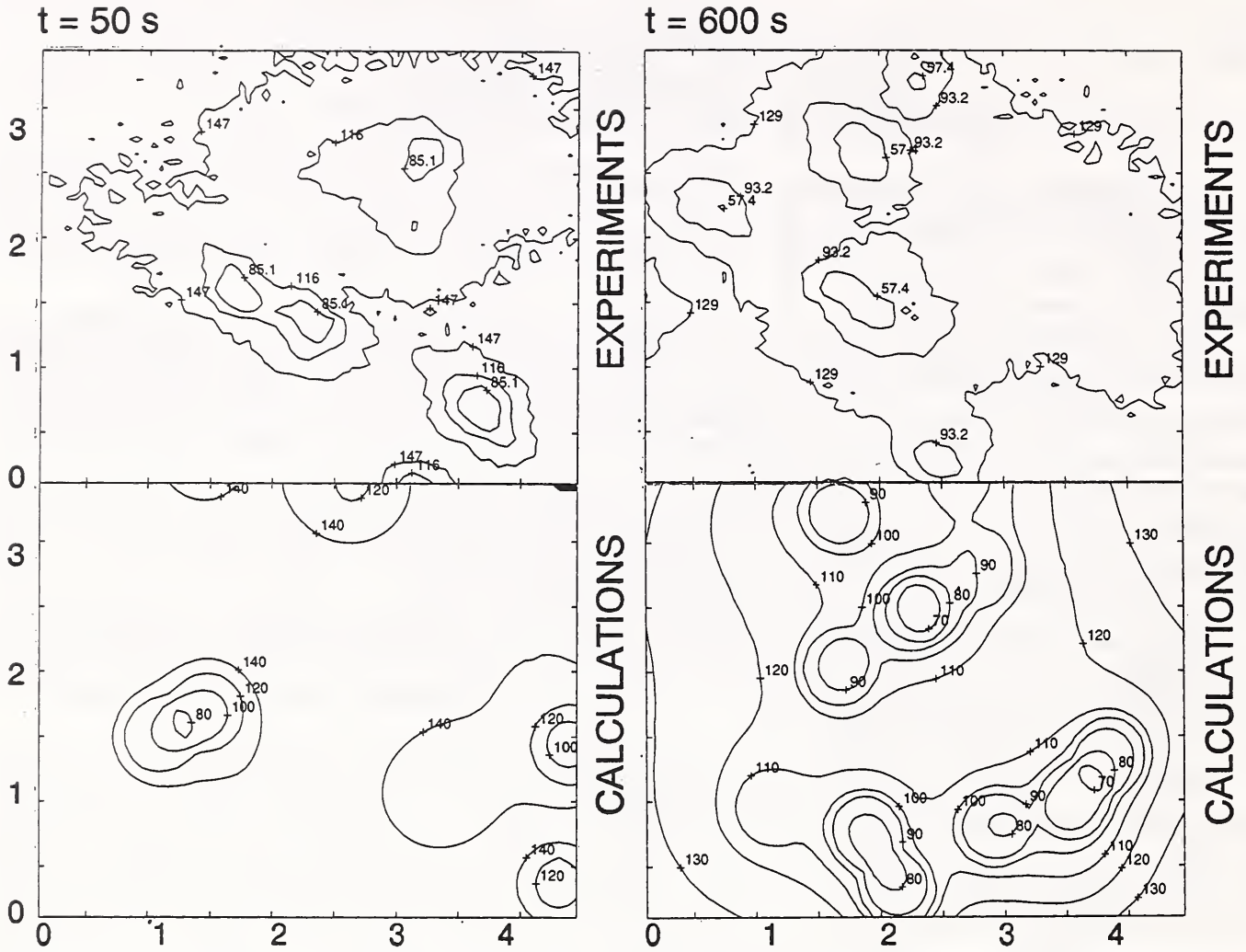

Figure 1 - Typical transient surface temperature distributions (mass flux G = 0.96 g/m^2 s; initial surface temperature Tso = 151 °C; distances in centimeters on both axis)

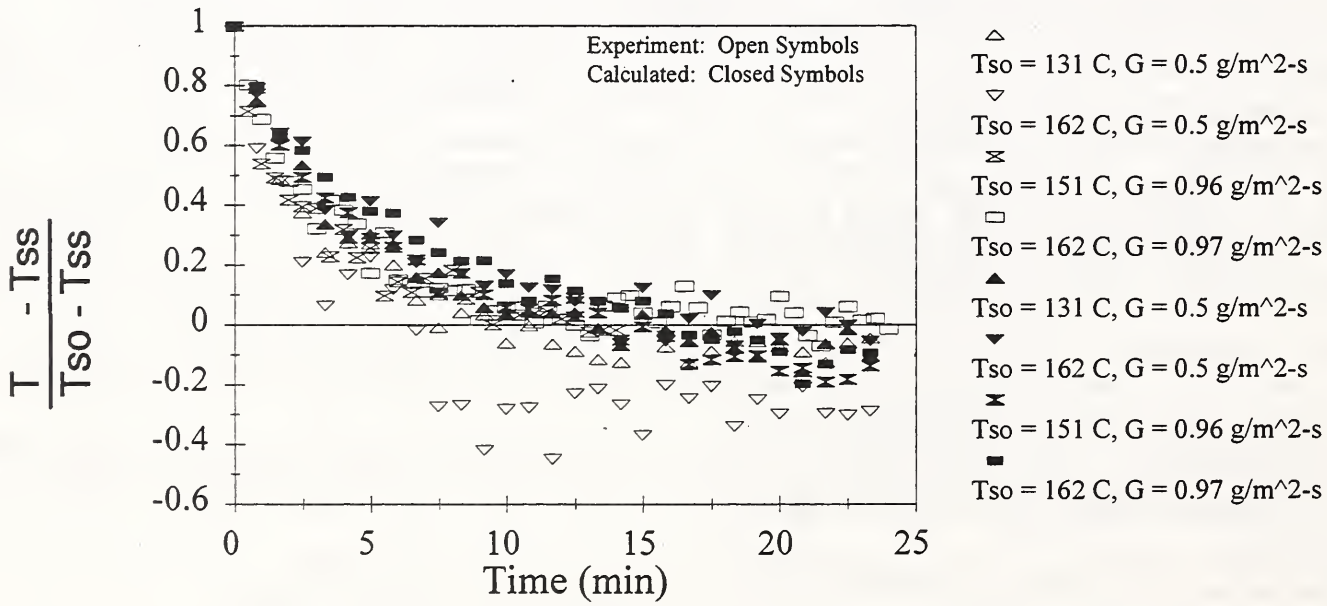

Figure 2 - Summary of results: calculations versus experiments (note: Tss is the final steady state surface temperature)

CFD Modelling of Liquid Pool Fire Suppression Using Fine Watersprays

George Hadjisophocleous
National Fire Laboratory
National Research Council
Ottawa, Ontario, Canada K1A 0R6
and
Kevin Knill
Advanced Scientific Computing, Ltd.
554 Parkside Drive, Unit 4
Waterloo, Ontario, Canada N2L 5Z4

In the search for extinguishing agents to replace Halon, many researchers have devoted their efforts, during the past few years, to the development of water mist systems for the suppression of liquid-fuel fires in compartments. Most of these efforts have focused on full-scale experimentation with the objective of investigating the effectiveness of such systems in extinguishing fires, as well as in understanding the mechanism of extinguishment. These experiments have shown that water mist systems are effective in extinguishing fires in some situations but not in others, indicating that suppression using water mist systems is case-dependent and that the design has to be custom-made for each specific application. Although the experiments have led to some explanations about the extinguishment mechanisms, there is no clear indication as to which of these mechanisms dominates during the extinguishment process. These difficulties are due partly to the complexity of the problem and partly to the poor visualization capabilities during the experiments.

To assist in the research effort in this area, the National Fire Laboratory (NFL) of the Institute for Research in Construction, National Research Council of Canada and Advanced Scientific Computing Limited (ASC) are collaborating on the development and validation of computer models for simulating liquid-fuel pool fires and fine watersprays using ASC's CFD code TASCflow. Although TASCflow has many of the basic modelling capabilities needed for these simulations, the present collaboration has added new or has improved existing submodels for fuel evaporation, spray injection, transient droplet tracking, water droplet evaporation, and the flow of water droplets through porous media.

The computer code is used to simulate experiments done in a 6x6x4 m mock-up room, shown in Figure 1, constructed at the NFL to represent a machinery room in a ship. The room has obstacles representing the ship's engines (sand-filled barrels), porous media representing the various piping systems, as well as a ventilation duct that provides fresh air to the compartment and an opening to the outside. The liquid fuel used for these simulations is heptane, which is contained in pans below perforated deck plates that represent the floor on the ship. The objectives of these simulations were to validate the model, and to provide some insight into the flow characteristics in the room and the dominant extinguishment mechanisms.

The simulation starts by first running the code with the ventilation system on and without combustion to create the cold flow pattern in the room that exists prior to ignition. Following that, the fire is ignited in the pans and then the transient calculation continues for 90 s. At this time, the waterspray is activated and the code tracks the flow of water droplets in the room and the interaction between the gas and the droplets in terms of mass, momentum and heat transfer.

The results of the simulations demonstrate the development of the fire in the compartment and the fire-induced flows, which are quite complex, due to the incoming fresh air and the various obstructions in the room. Figure 2 shows a constant temperature surface of 1100 K at 90 s. The figure shows that the hot gases create a plume over the pans and then move toward the corner opposite to the ventilation inlet duct. At the time that the nozzles are activated, there is rapid cooling of the hot gases near the room ceiling, causing a sudden drop in pressure to the point that air is rapidly sucked into the compartment from the opening. Figure 3 shows that the 1100 K surface has been pushed back due to the waterspray and the flow of incoming air. With the help of this flow, the water droplets are able to penetrate the fire plume. The size of the fire plume is reduced quickly due to the water evaporation and, in about 5 s, the fire is reduced to flaming just above the pans. At 8.5, s the fire is extinguished. These results are in close agreement with the observations from the tests.

These predictions show that, for this case, oxygen depletion is not the main cause of extinguishment as there is still enough oxygen in the room to sustain combustion. Extinguishment is achieved by the cooling of the fire plume and the flow of cool gases over the pans. This demonstrates the strong dependence of the extinguishing process on the flow characteristics in the room which, in turn, depend mainly on parameters such as the location of the fire, the obstacles present, the location and size of the openings, the flow rate of water and the incoming ventilation air.

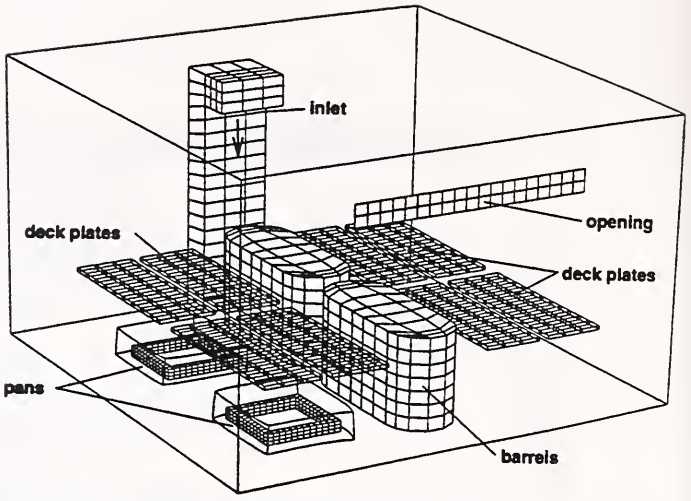

Figure 1. Elements of computational domain.

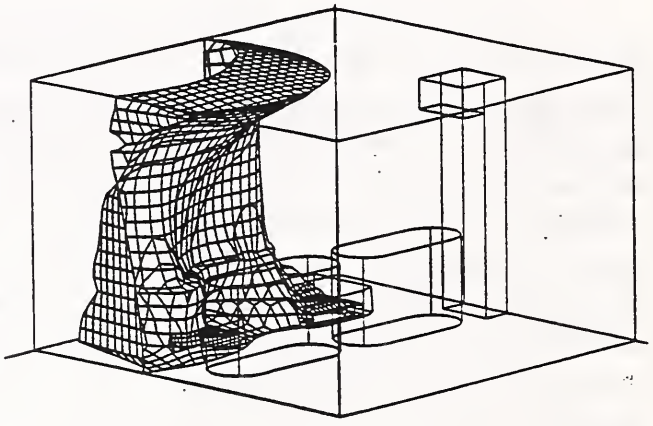

Figure 2. Constant temperature surface of 1100 K just prior to nozzle activation

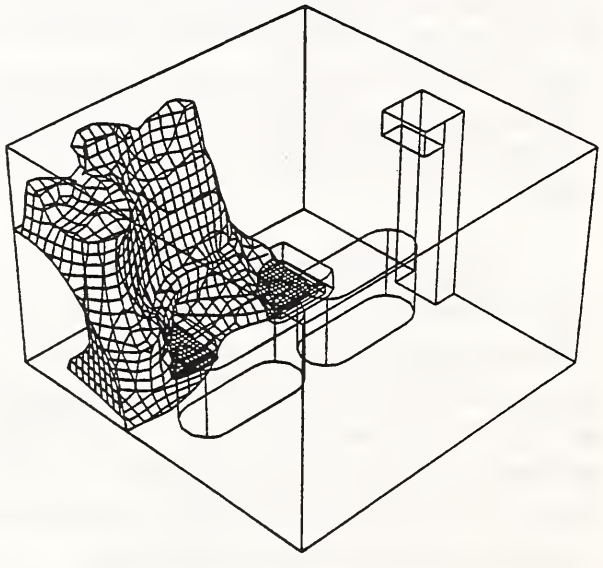

Figure 3. Constant temperature surface of 1100 K at 0.5 s after nozzle activation

INTERACTION OF A LOW THRUST WATER MIST WITH A BUOYANT DIFFUSION FLAME

Bruce Downie*, and C. E. Polymeropoulos
Department of Mechanical and Aerospace Engineering
Rutgers University, Piscataway, N. J. 08901

G. Gogos
Department of Mechanical Engineering
University of Nebraska, P.O. Box 880656, Lincoln, NE 68588-0656

ABSTRACT

This work describes some observations and measurements from the interaction of the spray produced by a 90° hollow cone nozzle, with purely buoyant diffusion flames from a 25x25 cm natural gas ceramic plate burner located directly underneath the nozzle. The nozzle was operated at its rated pressure and flow rate (380 kPa, 0.013 kg/sec) and the heat release from the fires was varied to a maximum of 53 kW. Previous work with this nozzle has shown that the mean droplet size generated 27cm beneath the nozzle ranged from approximately 25 μm at the centerline to 145 μm near the spray edge. This type of nozzle has been used in testing fire suppression systems in aircraft cabin fires.

The experimentation was carried out in a 2x2x2 m glass enclosed test chamber, (Fig. 1) and for the majority of the tests the burner was located 2 m beneath the nozzle. The chamber was open at the top, and partial exhaust was provided using an extraction hood located above the chamber. A 0.13 cm high opening along the bottom of the chamber allowed room air to be drawn into the fire. The ceramic burner plate was 3 cm thick and the 25x25 cm square burner area consisted of a uniformly distributed hole pattern with 449 holes 0.8 mm in diameter each. The burner plate was instrumented with thermocouples cemented on its top and bottom surfaces to assess the influence of the spray. A set of thermocouples was also used to measure centerline temperatures above the burner plate. An imaging system was used to record the presence of droplets near the burner surface, and a narrow angle total radiation detector was used to measure changes in flame radiation.

For the conditions tested the plume to spray thrust ratio was large, resulting in negligible direct penetration of the droplets into the fire region. This is clearly shown in video records of the process and also in fig. 2 which is a 1/30 sec exposure of the nozzle discharging into a 53 kW flame. A consequence of the low spray thrust was an almost droplet free region above the flame. Interaction between the flame and the spray appeared to occur from droplet entrainment into the flame and from cooling of the ceramic burner surface. The latter effect was due to decreased radiant emission from the flame as well as direct droplet impaction. Figure 3 is an example of a measured decrease in burner temperature with spray application, and fig. 4 is a radiometer record of the relative energy received from a position corresponding to the end of the flame region of a 53 kW flame. Application of the spray resulted in a more transparent flame suggesting decreased soot radiation. Entrainment of droplets onto the burner plate was observed from trajectory angles obtained using the imaging system.

Centerline flame temperatures did not change significantly upon application of the spray, at least within the error limits of thermocouple measurements. A limited number of measurements of

---

* Now at General Dynamics Inc. Groton CT

O_2 and CO concentrations around the flame tip region showed a significant decrease on O_2 and an increase in CO upon application of the spray.

Although this has not yet been carried out, an energy balance on the ceramic plate surface using the measured temperature histories promises to yield an estimate of water deposition rates on the base of the flame region.

This work was supported by the Fire Safety Branch of the FAA Tech Center, Atlantic City Airport, N. J.

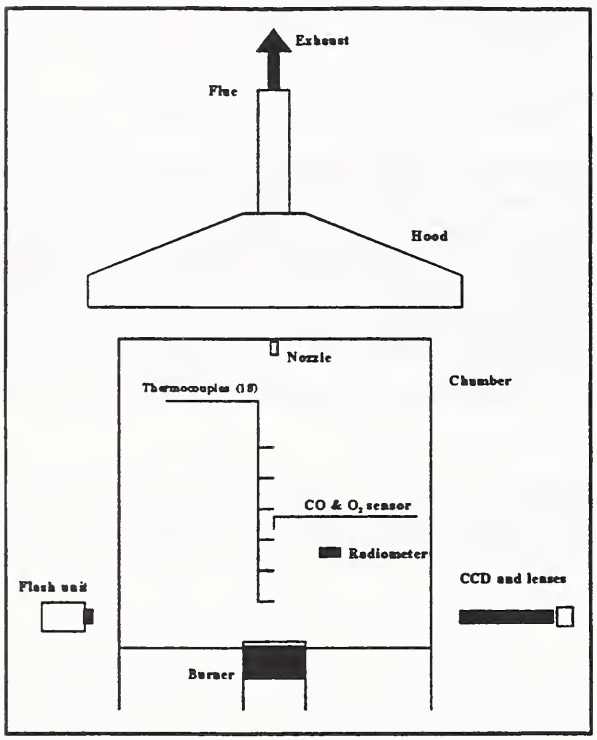

Fig. 1 Schematic of test chamber

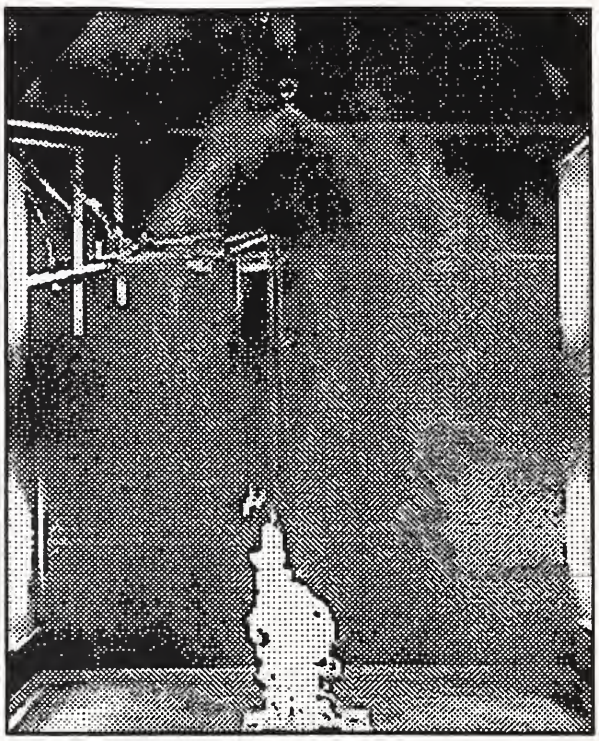

Fig. 2 Spray/fire interaction, 53 kW

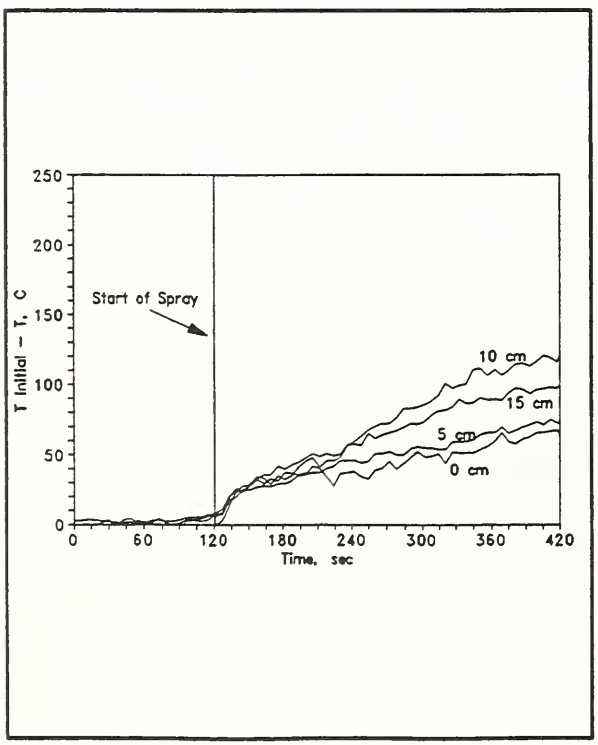

Fig. 3 Plate temperatures, 53 kW

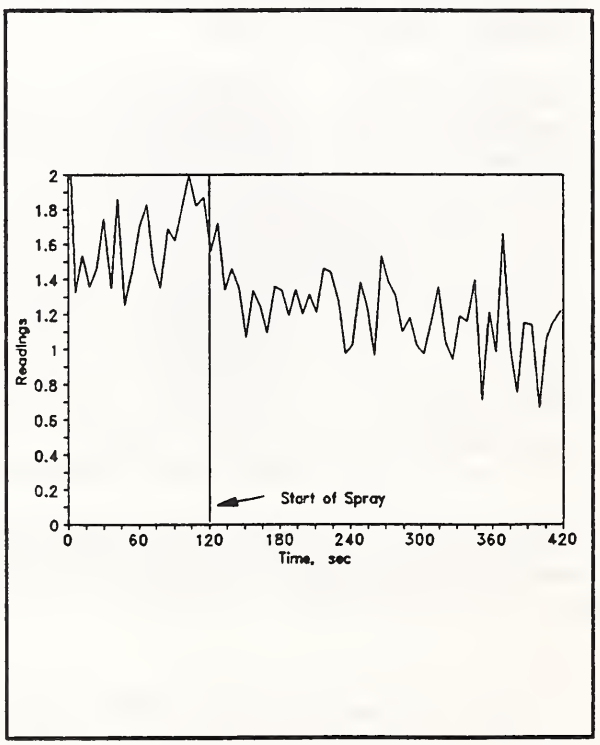

Fig. 4 Radiometer readings, 53 kW

SUPPRESSION WITHIN A SIMULATED COMPUTER CABINET USING AN EXTERNAL WATER SPRAY*

William Grosshandler, Darren Lowe,
Kathy Notarianni and William Rinkinen
Building and Fire Research Laboratory
National Institute of Standards and Technology
Gaithersburg, MD 20899

A total ban on halon production has created a vacuum in the fire protection industry which is likely to be filled by more than one suitable replacement. A water-based system is an attractive replacement candidate because water, in addition to being an effective fire suppressant, is non-toxic, environmentally friendly and competitively priced. The latest generation of spray systems requires much less water than traditional sprinklers, and is being considered for applications heretofore limited to non-condensing agents such as halon 1301.

There are two fundamental differences between halon and water mist that make the direct substitution of one for the other problematic: (1) the dynamics controlling the transport of the liquid water droplets are completely different from the dynamics of vaporized 1301, and (2) water is a good conductor of electricity where 1301 is not. This project is looking at the applicability of mist systems for extinguishing fires in an environment containing data processing equipment; the issue of electrical conductivity is not addressed.

The first task was to define a representative electronics cabinet and room geometry, fuel load, and ignition source. This was done after reviewing the literature and having conversations with those familiar with the application. A scaled-down, mock electronics package was designed and a chamber built to contain the spray to emulate the physical system of interest. The test chamber is 1.68 m wide, 0.91 m deep, and 2.13 m high, with an exhaust fan at the center of the top to remove products of combustion after each test has been run. Two walls are glass to allow visual observation of the entire process.

The mock electronics cabinet is 0.5 m wide by 0.2 m deep and 0.4 m high, and is shown in Figure 1. The fuel is a 3 mm thick plate of polymethylmethacrylate (PMMA), placed vertically in an aluminum frame centered among a number of aluminum "circuit boards" spaced every 25 or 50 mm. Three fans are located near the bottom of the cabinet to simulate the flow of cooling air. Ignition is by a small natural gas line burner.

The influence on extinguishing efficiency of the nozzle geometry, location relative to the fire, water application rate, and the depth to which the fire is buried within the simulated cabinet are all parameters which have been examined. A phase-Doppler particle analyzer (PDPA) is used to determine the droplet size distribution and two components of velocity at locations internally near the fire in the circuit board and external to the cabinet. These data are key to relating the extinguishment event to conditions adjacent to the fire, and indicate the fate of the droplets as a function of different initial conditions in the spray.

A baseline study was performed to determine the amount of a gaseous agent (CF_3H) necessary to extinguish fires as a function of the extent to which the fire is buried within the simulated electronics cabinet. Trifluoromethane was used rather than halon 1301 because it is a proposed gaseous alternative total flooding agent, and is significantly less effective than halon 1301.

A minimum enclosure situation corresponds to a PMMA circuit board totally exposed to the air and water spray. This arrangement is the easiest to extinguish, and identifies the locations within the test chamber where there is the greatest likelihood of suppression. Figures 2 and 3 indicate the time required to suppress the PMMA sample following a 30 second preburn time as a function of position below the pressure jet nozzle. The pressure in Figure 2 is 2.1 MPa and the flow rate is 2.1 l/min. The pressure in Figure 3 is double that amount, and the corresponding flow is 2.9 l/min. The affect of pressure is to greatly expand the region in which extinguishment is possible in under 60 s. This is due partly to the greater flux of water and partly due to the increased momentum of the water spray.

---

*This work was supported by the U.S. Fire Administration, under the direction of Mr. Larry Maruskin

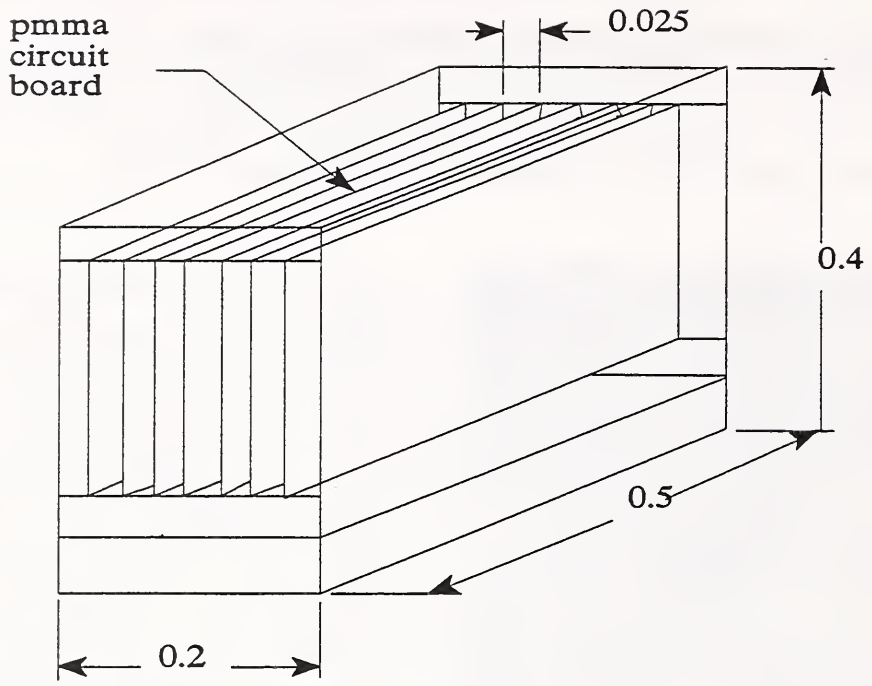

Figure 1. Schematic of mock electronics cabinet

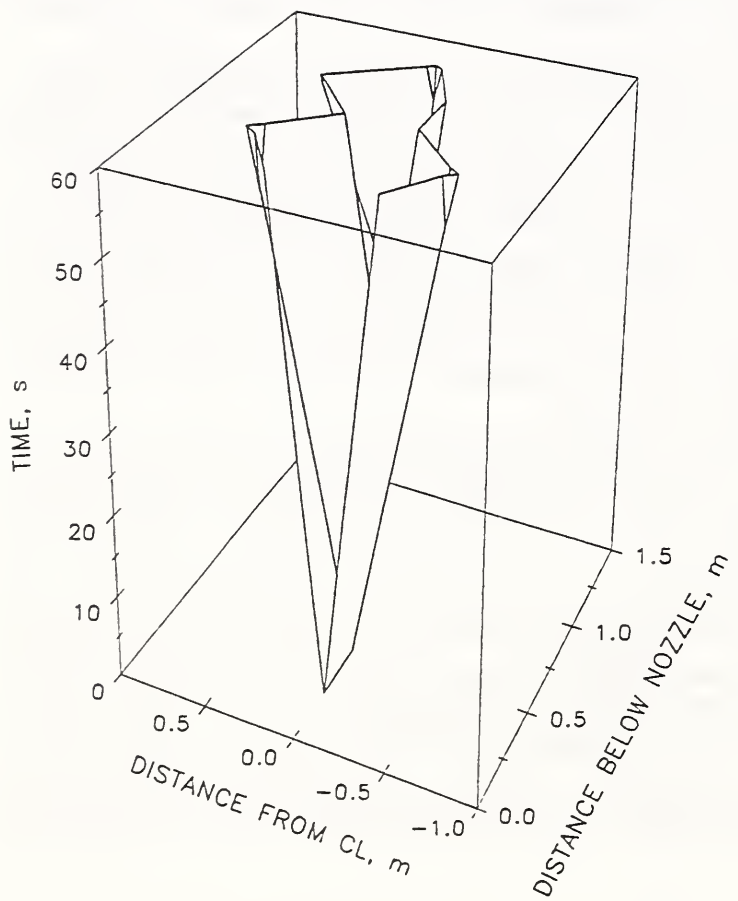

Figure 2. Time to extinction of flame (water pressure is 2.1 MPa)

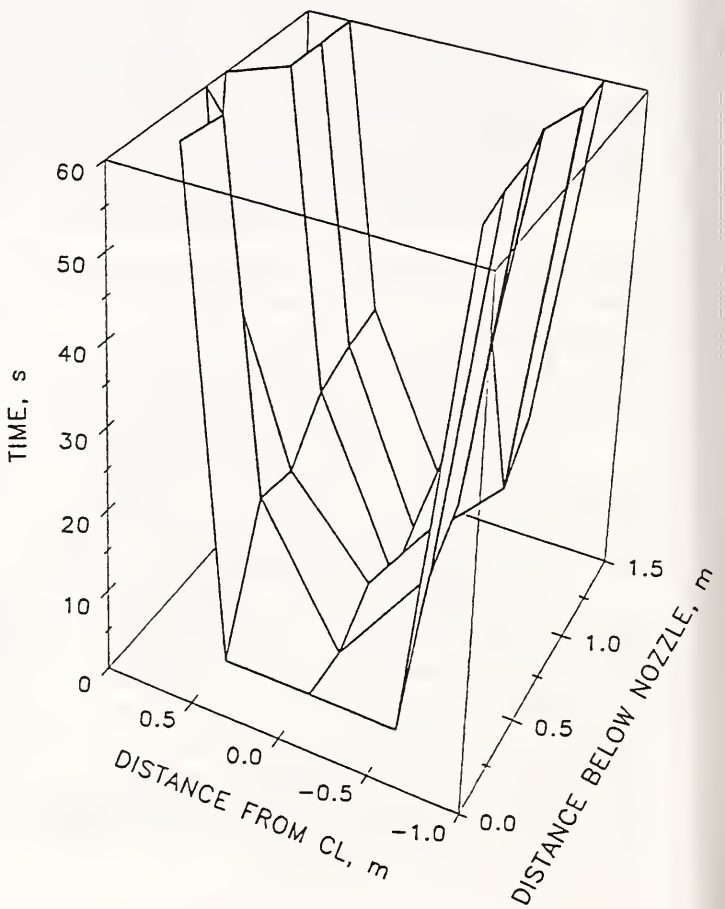

Figure 3. Time to extinction of flame (water pressure is 4.1 MPa)

POOL BURNING OF SILICONE FLUIDS

R. Buch[1], A. Hamins, J. Shields, P. Borthwick, T. Baum, M. Nyden, and T. Kashiwagi

Building and Fire Research Laboratory, NIST
Gaithersburg, MD 20899

Siloxane fluids have a number of industrial applications including use as transformer fluids. The objective of the present study was to improve our understanding of the burning of siloxane fluids. The fluids studied are octamethylcyclotetra siloxane, $[(CH_3)_2SiO]_4$ which is known as D4, and trimethylsily end-blocked polydimethyl siloxane, $[(CH_3)_3Si\text{-}O[\text{-}Si(CH_3)_2\text{-}O]_n\text{-}Si(CH_3)_3]$, where n indicates the polymer chain length and the number of silicon atoms in the molecule. These fluids are ranked by viscosity which is related to the average polymer chain length as shown in Table 1.

Measurement of the burning rate and the radiative heat loss fraction (χ_r) for siloxanes with different average polymer chain lengths was determined for pool fires with diameters of 10, 30, and 60 cm. Flame ignition for the longer chain length fluids could only be accomplished after heating to more than 100 °C. Ash was observed both in the gas phase and on the surface of the liquid pool, where it collected and with time submerged. The apparent mass burning rate was corrected accordingly, based upon assays of the ash in the unburnt fuel at the conclusion of the experiment. The rate of ash deposition was largest for the slow burning long chain length fluids. The collected ash was analyzed for carbon, silicon, and hydrogen content and found to be predominantly silicon dioxide (silica). Because of capillary effects, deposition of silica on the fuel surface led to fuel dripping over the burner rim. The silica attached to the rim was moved with a stirring rod, preventing fuel leakage. The fuel level in the burner was maintained at a constant level using a number of systems including an overflow and a thermocouple controlled feedback device. The measured burning rate was found to be a strong function of chain length.

Silicon dioxide was apparent in the emission spectra of the siloxane flames as determined using an open-path FTIR spectrometer. Differences in the emission spectra between heptane and siloxane flames were related to broad band emission in the 8-10 μm region of the siloxane flame which was attributed to silica. Radiative emission was measured at multiple locations on the surface of a cylindrical control surface surrounding the fire after a nearly steady-state mass burning rate was achieved. Results showed that for the shorter chain length siloxanes, χ_r increased from ≈0.3 to 0.5 as the burner diameter increased from 10 to 60 cm. For the longer length siloxanes, however, χ_r remained nearly constant or decreased with pool diameter.

Measurements are currently underway to determine the rate of gasification of siloxanes using the BFRL Radiative Gasification Apparatus. The measured gasification rate was found to be a strong function of chain length.

Table 1 Average viscosity and chain length

Viscosity (cS, 298 K)	n
0.65	0
1.0	1
1.5	2
2.0	3
10	≈15
20	≈27
50	≈57

1 Guest Researcher, Dow Corning Corporation, 2200 W. Salzburg Rd, Midland, MI 48686

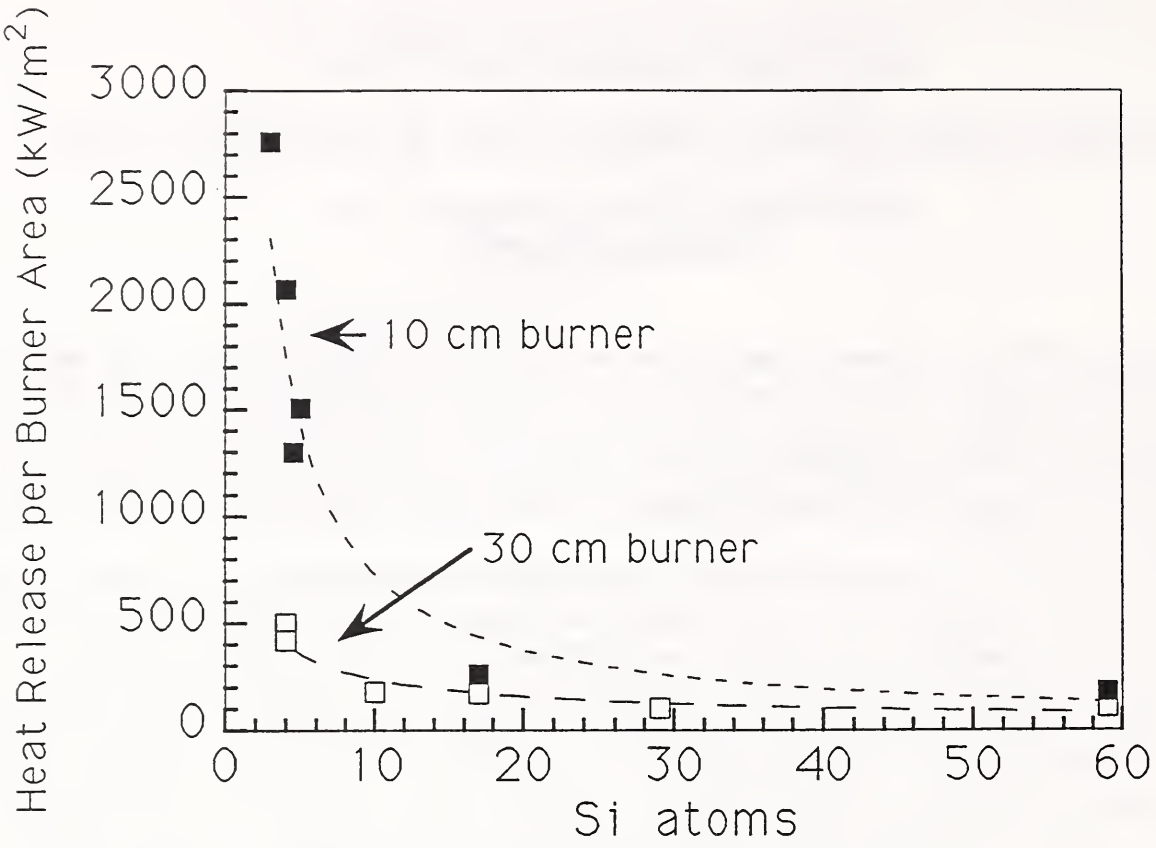

Figure 1 Heat release rate per unit area of pool surface in 10 and 30 cm burners as a function of siloxane chain length (number of siloxane units).

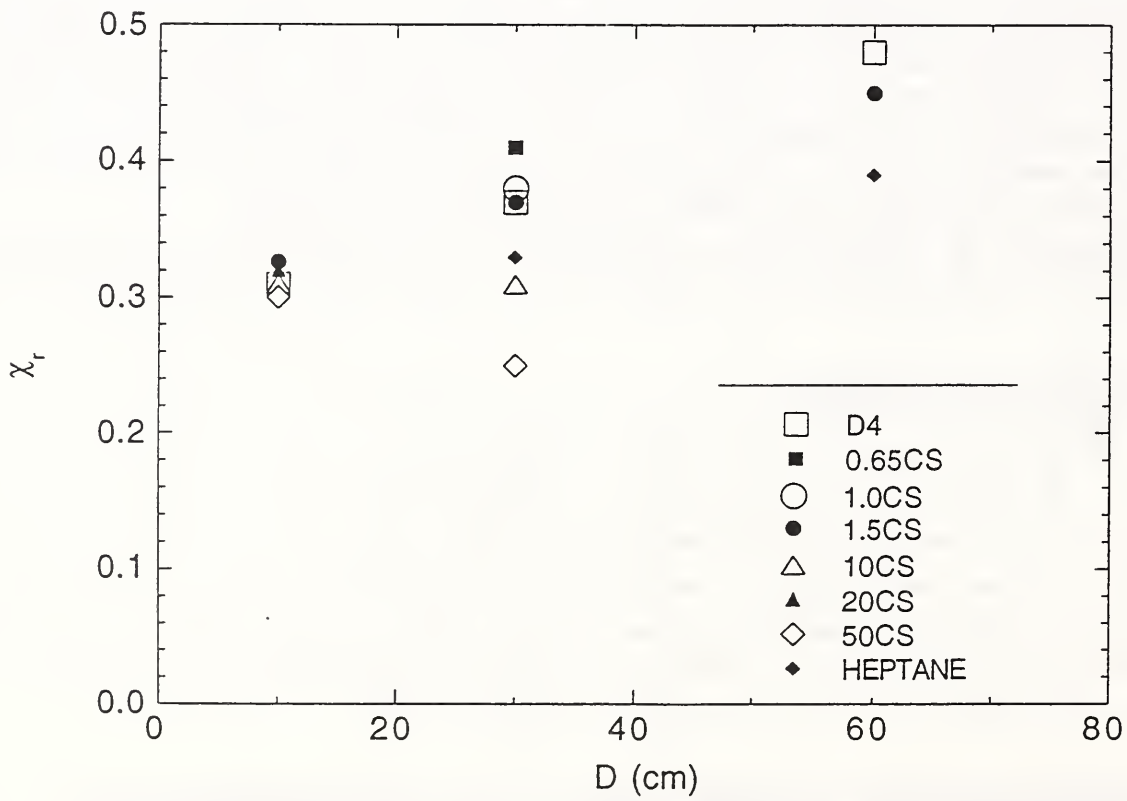

Figure 2 Radiative heat loss fraction as a function of pool diameter for siloxane fluids and heptane.

Fire Near Field Entrainment Measurements

by
N.A. Dembsey
P.J. Pagni and R.B. Williamson
University of California, Berkeley

To obtain information on the entrainment rates of "full" scale compartment fires twenty experiments were conducted using a 0.61m by 1.22m porous surface propane burner with rates of heat release ranging from 330kW to 980kW. These experiments were conducted in a ceramic fiber board lined fire test compartment which is 2.44m by 3.66m in plan and 2.44m in height. The compartment has a single doorway, 0.76m wide by 2.03m high. The burner was placed in the compartment at two locations, compartment center and compartment side-wall. The burner porous surface was 0.61m above the floor of the compartment.

The entrainment rates (plume mass flow rates) of the fires were determined by measuring a compartment gas vertical temperature profile (corner), the doorway gas centerline vertical temperature profile and a compartment wall surface vertical temperature profile (corner). These measurements allowed the entrainment rate of each fire to be determined from the doorway vent flow, the doorway mixing and the wall flows. For these experiments the mass flow rate of the propane is considered negligible.

It is found in these experiments that the fire entrainment rates increase, at a decreasing rate, with increasing fire rate of heat release and range from 0.74kg/s to 0.98kg/s with an error of ±20%. The position of the burner did not affect the entrainment rates.

Entrainment data[1,2,3,4,5,6,7,8] from the literature was compiled to form a data set of buoyancy driven gas burner and pool fires that range in size from: Diameter (or area equivalent) 0.10m to 0.97m and rate of heat release 3kW to 980kW. Entrainment measurements for this data set where taken at various elevations above the burner/pool surface from near 0% of the mean flame height to just over 500% of the mean flame height. It was found that this data set could be correlated using the far field entrainment model (with virtual origin) of Cetegen et al.[1] A curve fit of the data was developed and is shown below. It should be noted that 75% of the data points used in the curve fit are from Cetegen et al.[1] Cetegen's et al.[1] gas burner fire sizes were: Diameter 0.10m to 0.50m and rate of heat release 3kW to 158kW.

$$m = \beta m_{Far}$$

$$(1) \qquad \beta = 1, \quad \frac{Z_e}{Z_{fl}} \geq 2; \qquad \beta = \exp\left(0.50 - 0.25\frac{Z_e}{Z_{fl}}\right), \quad 0.6 \leq \frac{Z_e}{Z_{fl}} \leq 2;$$

$$\beta = 1.4\exp\left(3.1 - 5.2\frac{Z_e}{Z_{fl}}\right), \quad 0.3 \leq \frac{Z_e}{Z_{fl}} \leq 0.6$$

m = plume mass flow rate, m_{Far} = Cetegen et al.[1] far field model (with virtual origin), Z_e = entrainment height, Z_{fl} = mean flame height.

The factor β equal to unity for Z_e greater than $2.0Z_{fl}$ is expected since the far field solution should be valid at $2.0Z_{fl}$. The range of Z_e from $2.0Z_{fl}$ down to $0.6Z_{fl}$ shows β increasing nearly linearly

to a value of 1.4. Below $0.6Z_{fl}$, β increases much more quickly. Below $0.3Z_{fl}$, the data scatter significantly and were not included in the curve fit. It is interesting that the rapid increase in β beyond 1.4 corresponds to the 100% intermittency flame height ($0.6Z_{fl}$) for the experiments conducted here and for Cetegen's et al.[1] 0.50m diameter burner data.

The data used in the curve fit corresponding to Z_e less than $0.6Z_{fl}$ show there is some divergence between the data for diameters less than or equal to 0.50m and greater than 0.50m. To either improve the curve fit or show that the divergence is really due to a diameter effect, much more data is needed for diameters greater than 0.50m. Only 6% of the data points used for the curve fit are for diameters greater than 0.50m.

When the models/correlations of Baum and McCaffrey[9], Cetegen et al.[1], Delichatsios[10] and Heskestad[11] are compared to the data from the 20 experiments conducted here it is found that Baum and McCaffrey[9] matches the data best coming to within -20% of the data on average. The near field modification, equation (1), matches the data as closely as does Baum and McCaffrey[9] for fires less than 500kW coming to within -20%, but overestimates the data for fires greater than 600kW coming to within only +50% of the data on average. The change in accuracy of equation (1) occurs because the less than 500kW fire data were taken at Z_e greater than $0.6Z_{fl}$, while the greater than 600kW fire data were taken at Z_e less than $0.6Z_{fl}$ where the possible diameter effect occurs.

The data set compiled was also compared to the near field entrainment model of Thomas[12]. It was found that an offset to Z_e was required to match the data. For diameters less than 0.50m the offset was found to be of the order of the diameter and not a function of $Q^*(D)$. Where as the offset for diameters greater than or equal to 0.50m was found to be a liner function of $Q^*(D)$ ranging up to the order of the diameter. Where $Q^*(D) = Q/(1110D^{2.5})$, Q = rate of heat release [kW] and D = diameter [m].

---

[1] Cetegen, B.M., Zukoski, E.E., Kubota, T., Entrainment in the Near and Far Field of Plumes, *Combustion Science and Technology*, 39 (1984) 305-331.

[2] Lim, C.S., Mixing in Doorway Flows and Entrainment in Fire Plumes, Thesis, California Institute of Technology, Pasadena, CA (1984).

[3] Toner, S.J., Zukoski, E.E., Kubota, T., Entrainment, Chemistry and Structure of Fire Plumes, California Institute of Technology, Pasadena, CA, Grant Number 60NANB6D0638, U.S. Department of Commerce, National Bureau of Standards, Center for Fire Research (1986).

[4] Morehart, J.H., Zukoski, E.E., Kubota, T., Species Produced in Fires Burning in Two-Layered and Homogeneous Vitiated Environments, California Institute of Technology, Pasadena, CA, Grant Number 60NANBD90958, U.S. Department of Commerce, National Institute of Standards and Technology, Center for Fire Research (1990).

[5] Tokunaga, T., et al., Mass Flow Rate Formula for the Upward Current Above Diffusion Flames, *Fire Science and Technology*, 2:2 (1982) 117-125.

[6] Yumoto, T., Koseki, H., Gross Structure of Heptane Pool Fire: Some Experimental Results, *Fire Science and Technology*, 2:2 (1982) 91-97.

[7] Thomas, P.H., et al., Buoyant Diffusion Flames: Some Measurements of Air Entrainment, Heat Transfer and Flame Merging, in *10th Symposium (International) on Combustion*, The Combustion Institute, Pittsburgh, PA (1965) 983-996.

[8] Steckler, K.D., Quintiere, J.G., Rinkinen, W.J., Flow Induced by Fire in a Compartment, in *19th Symposium (International) on Combustion*, The Combustion Institute, Pittsburgh, PA (1982) 913-920.

[9] Baum, H.R., McCaffrey, B.J., Fire Induced Flow Field -- Theory and Experiment, in *Fire Safety Science -- Proceedings of the Second International Symposium*, Hemisphere Publishing Co., New York (1989) 129-148.

[10] Delichatsios, M.A., Procedure for Calculating the Air Entrainment into Turbulent Pool and Jet Fires, *Journal of Fire Protection Engineering*, 2:3 (1990) 93-98.

[11] Heskestad, G., Fire Plume Air Entrainment According to Two Competing Assumptions, in *21st Symposium (International) on Combustion*, The Combustion Institute, Pittsburgh, PA (1986) 111-120.

[12] Hinkley, P.L., Rates of 'Production' of Hot Gases in Roof Venting Experiments, *Fire Safety Journal* 10 (1986) 57-65.

Effects of a Floor on the Entrainment Flow Field Induced by a Pool Fire

X. C. Zhou and J. P. Gore
School of Mechanical Engineering, Purdue University, West Lafayette, IN 47907

The entrainment flow field of a 7.1 cm toluene fire with a 51 cm floor has been recently (Zhou and Gore 1994a, b) studied using a laser Doppler velocimeter (LDV) and a particle imaging velocimeter (PIV). The results of these studies showed that the fire induced flow field in the presence of a floor is highly transient with root mean square (RMS) entrainment velocities having the same order of magnitude as the mean entrainment velocities. Thus instantaneous outflow (extrainment) from the visible fire surface as well as motion of the air in a direction parallel to the axis of the fire was observed. The mean velocity field showed a net inflow of ambient air into the fire surface corresponding to the air needed for the combustion process. However, the mean velocity field had no resemblance to any of the instantaneous fields. It was shown that the rate at which the ambient air is set in motion by the fire is much larger than the rate at which air enters the visible flame surface which was found to correspond closely to a location at which the vorticity increased significantly. It was found that the entrainment rate depends significantly on the definition of the size of the fire induced flow field. It was also conjectured that many of the past measurements of entrainment rate depended on the unknown definition of the flow field boundary caused by the measurement hardware such as a collection hood.

In the present work, the PIV technique was used to measure the differences between the entrainment flow field of a 7.1 cm toluene fire with and without the 51 cm diameter floor. The results show dramatic differences between the two cases. The instantaneous flow patterns surrounding the fire with the floor are shown in Fig 1a-c while those surrounding the fire without the floor are shown in Fig. 2a-c. The flow patterns without the floor show very distinct instantaneous features. Figure 1a shows strong entrainment upstream and downstream of a visible flame bulge with unique features of the flow several labeled A-E. Figure 1b shows a phase during which the air moves in a vertical direction but involves many features labeled A-D. Figure 1c shows the instantaneous extrainment phase in which the air moves away from the visible flame interface and consists a few flow features labeled A-B.

Contrary to the above, the flow field around the fire with identical burning rates and ambient conditions but without the floor is restricted to the region near the pool edge as shown in Figs. 2a-c. The flow field does not show large variations and appears to have a consistent upward and radially inward direction. The dramatic differences in the flow fields with and without the floor translate into significant differences in the entrainment rate above the fuel surface. However the overall entrainment is reduced below that of the case with floor only at axial distances above one diameter due to the entrainment occurring from below the pool surface in case of the fire without the floor.

The reasons for the dramatic instabilities caused by the floor deserve attention from both fundamental and practical view points. Fundamental questions relate to the processes driving the radial instabilities in the presence of the floor. The practical questions relate to whether the knowledge of the fire induced flow can be used in safer design of furniture size and layout.

Acknowledgment: NIST Grant No. 60NANB2D1291, Drs. Hamins and Kashiwagi.

References

Zhou X. C. and Gore J. P., 1994a, Air Entrainment Flow Field Induced by a Pool Fire, Twenty Fifth Symposium (International) on Combustion, The Combustion Institute, Pittsburgh, PA, special issue of *Combustion and Flame,* in press.

Zhou X. C. and Gore J. P., 1994b, Particle Imaging Velocimetry of the Flow Field Induced by a Small Toluene Pool Fire, Proceedings of the ASME Winter Annual Meeting, Chicago, IL, 1994, in press.

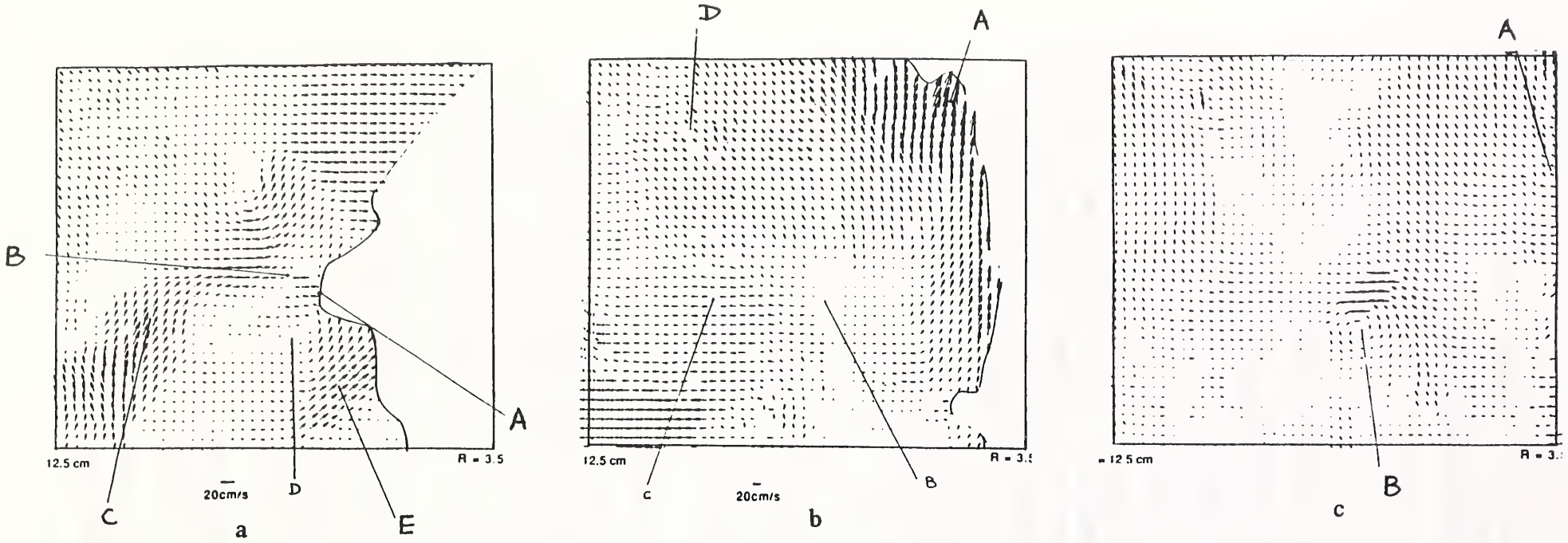

Figure 1: Flow patterns around a 7.1 cm toluene pool fire with a 51 cm floor.

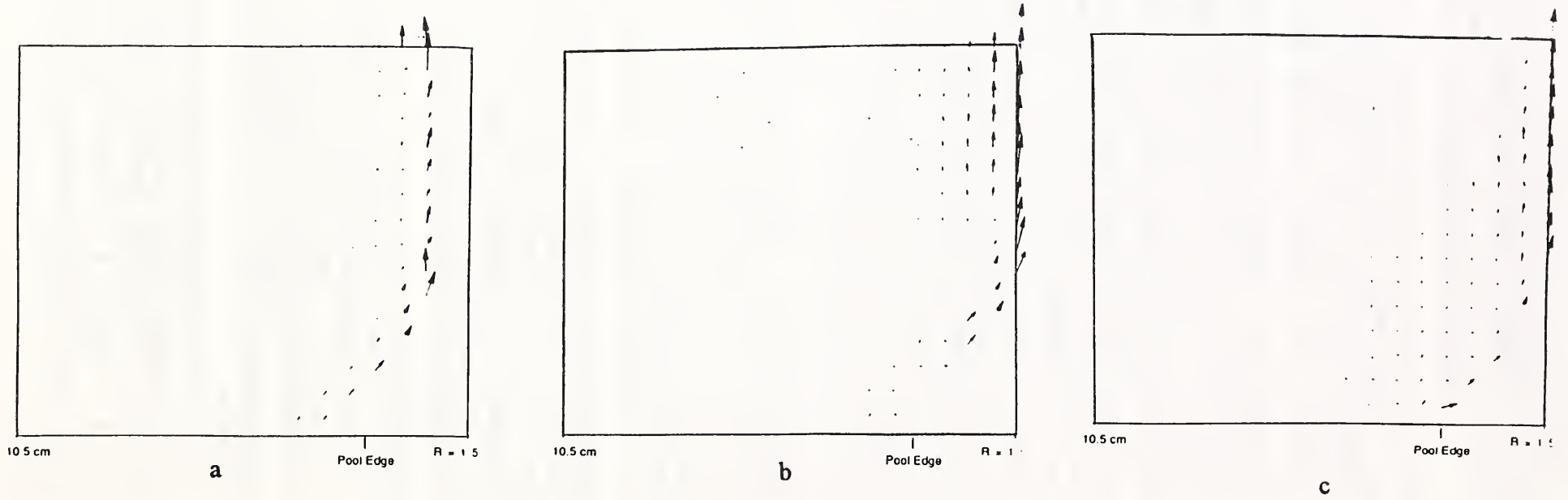

Figure 2: Flow patterns around a 7.1 cm toluene pool fire without a floor.

Proposed for Presentation at
The Annual Conference on Fire Research
Gaithersburg. MD, October 17-20, 1994
SAND94-1900A

Large-Scale Vortical Structures and Flame Shapes in Large Open Pool Fires[1]

Vernon F. Nicolette, Sheldon R. Tieszen, Louis A. Gritzo, and Jaime L. Moya
Thermal and Fluid Engineering Department 1513
Sandia National Laboratories
Albuquerque, NM

Gil Cornell
Code C27C
Naval Air Warfare Center
China Lake, California

A phenomenological and numerical investigation of flame shape and large-scale vortical structures in open pool fires is under way as Sandia National Laboratories. The goal of this work is to determine the underlying physical phenomena that produce the flame shape and large vortical structures, and the ability of time-averaged k-ε turbulence models to predict their existence.

Based on observation of large, open pool fires, we have developed hypotheses concerning the development of vortical structures in the fire. The fire tests were conducted at the Naval Air Warfare Center at China Lake California with JP-4 fuel in a 18.9 m diameter pool. Tests were conducted with different wind speeds ranging from 0 to 7.3 m/s. Several types of large, coherent rotational structures were observed. For dead calm conditions, large, unsteady ring vortices were formed that are associated with the puffing motion found in smaller fires [1,2]. For slightly disturbed conditions, coherent rings were not found but ring arcs or segments were observed. For winds above a couple of meters per second, steady, large counter-rotating, columnar vortices were observed on the leeward side of the fire. On the windward side of the fire unsteady ring arcs were also present.

Based on these observations and analogy to plume flows, we postulate that there are two key physical mechanisms that are responsible for the formation of these large structures. The first is baroclinic vorticity generation. Baroclinic vorticity generation results from the misalignment of the gradients in the pressure field and gradients in the density field. A pressure gradient always exists in fires. In the absence of a dynamic flow induced gradient, there is always a hydrostatic pressure gradient. The density gradient is between the hot gas generated by the fire and the relatively cold ambient. It is postulated that the rotational motion in the fires is principally a result of this baroclinic vorticity generation mechanism. The second key physical mechanism is amalgamation. We observe from the fire tests that the scale of the rotational structures grows with increasing distance from the toe of the fire. This is similar to both jets

1. This work was performed at Sandia National Laboratories, Albuquerque, NM, managed by Martin Marietta Corp. for the U.S Department of Energy under Contract DE-AC04-94AL85000.

and plumes which show structures of increasing scale downstream of the injection point. In this sense, a fire may be thought of as a near source, very low velocity, thermal plume in which the buoyancy is increasing due to heat release faster than it is decreasing due to mixing with ambient air.

Numerical simulations of these fires have been performed using a fire field model under joint development at Sandia and SINTEF. This model is based on the KAMELEON Fire Model [3]. Modifications have recently been made to the combustion model to allow for incomplete combustion effects in the fuel-rich regions of the flame. The formation of intermediate species (such as CO and H_2) is now included in the model. Incorporation of these modifications has resulted in a 200-300 K decrease in flame temperatures compared to previous calculations which only modeled 'complete' combustion [4]. The calculated flame temperatures are now in excellent agreement with thermocouple data from large-scale pool fires.

Calculations have also been performed for direct comparison to the large-scale pool fire tests discussed above. The numerical results show excellent agreement with the test results, in terms of: flame height, flame angle (due to wind), and rear flame-zone lift-off (in high winds). These results conclusively demonstrate the ability of the numerical model to predict such parameters for large pool fires. They also represent the initial stages of validation for the numerical model for fires of this type.

In the present model, a standard k-ε turbulence model is employed. This essentially time-averages the time-dependent turbulence in the flow. As a result, the model will not capture *transient* large-scale vortex motions (unless these motions result from a transient mean flow). Also there is some doubt as to the ability of such a model to capture the *steady* vortices seen in large pool fire tests with wind. However, in spite of the limitations inherent in the k-ε model, the numerical results successfully predict the formation of the *steady*, large counter-rotating vortices observed on the leeward side of the fire when the wind is present. These somewhat surprising results serve to further elucidate the strengths and weaknesses of the k-ε model for fire applications.

References

1. Hamins, A., Yang, J. C., and Kashiwagi, T. "An Experimental Investigation of the Pulsation Frequency of Flames," Twenty-Fourth Symposium (International) on Combustion, The Combustion Institute, 1992, pp. 1695-1702.

2. Cetegen, B. M. and Ahmed, T. A., "Experiments on the Periodic Instability of Buoyant Plumes and Pool Fires," Combustion and Flame 93:157-184. (1993).

3. Holen, J., Brostrom, M., and Magnussen, B. F., "Finite Difference Calculations of Pool Fires," Twenty-Third Symposium (International) on Combustion, The Combustion Institute, 1990, pp. 1677-1683.

4. Nicolette, V. F., "Comparison of Kameleon Fire Model to Experimental Data," presentation at the annual NIST Conference on Fire Research, October, 1993.

Proposed for Presentation at
The Annual Conference on Fire Research
Rockville. MD, October 17-20, 1994
SAND 94-1897A

Continuous Flame Zone Measurements and Analysis from Large, Open, JP-4 Pool Fires Including the Effects of Wind*

Louis A. Gritzo, Edward G. Muzio, Sheldon R. Tieszen, Jaime L. Moya
Thermal and Fluid Engineering, Department 1513
Sandia National Laboratories, P. O. Box 5800
Albuquerque, NM 87185-0835

Gill Cornell
Code C27C
Naval Air Weapons Center
China Lake, CA 93555

Numerical simulation of a large pool fire which occurs, for example, as a result of a facility fire or transportation accident requires that many coupled, nonlinear, physical phenomena be represented. Fire field models which are capable of predicting the fire environment based on a "first principles" approach are presently under development by numerous research organizations, including a collaborative effort established between Sandia National Laboratories (SNL) and the Norwegian Institute of Technology (NTH)/SINTEF. Code validation using high fidelity experimental data is an essential component of the model development process. Comparing model predictions with experimental results also helps to direct research efforts towards the appropriate areas.

Data from large-scale pool fires is required for calibration of the SNL Risk Assessment Compatible Fire Models (RACFMs). These models are simplified, deterministic fire models recently developed at SNL which apply first principles to the dominant physical phenomena (radiative and advective transport) and rely on empirically determined parameters to represent the remaining physics [1]. Using this approach, RACFM run times are reduced to a level acceptable for probabilistic safety assessments. Since RACFMs are partially empirical, the acquisition and analysis of experimental data are essential parts of the model development process.

In support of these model development efforts, a series of 62' diameter JP-4 pool fire tests were recently performed at the Naval Air Weapons Center (NAWC). The objectives of these tests are to; 1) gain a better understanding of fire phenomenology, 2) provide empirical input parameter estimates for RACFMs, 3) assist in continuing fire field model code validation and development, and 4) enhance the data base of fire temperature distributions that has been acquired for spill fires [2], i.e. fires in which liquid fuel is spilled onto a solid, impermeable substrate where it spreads as it burns. The first three test objectives will be addressed here.

Tests were performed over a variety of wind conditions ranging from still air to 15 m.p.h. crosswinds. Winds were often sustained at a steady speed and direction for a period of several minutes. During these periods, and after the initial transient behavior of the fire, the fire was assumed to reach a steady-state condition and time-averaged temperatures, heat fluxes, and RMS temperatures within the continuous flame zone were calculated. In the interior of the plume and near the pool surface, low mean and low RMS temperatures were noted for low wind conditions which tend to indicate the presence of an oxygen-starved (i.e. vapor dome) region. Using mean and RMS temperature distributions from the data obtained in these tests, the spatial extent of the vapor dome was estimated for a range of wind conditions. Conclusions reached from the temperature data were consistent with observations from the video record. Characterization of the vapor dome region is an important aspect of fire phenomenology since; 1) the physical extent of the vapor dome will strongly influence the radi-

*This work was performed at Sandia National Laboratories, Albuquerque, NM, managed by Martin Marietta Corp. for the U.S. Department of Energy under Contract DE-AC04-94AL85000

ative feedback to the pool which, in turn, influences the burning rate, 2) it is expected that large quantities of soot are formed in the vapor dome due to fuel pyrolysis, and 3) heat fluxes to objects located in the vapor dome will be significantly reduced.

The results obtained here indicate that occasional combustion does occur within regions which otherwise appear to be predominately oxygen-starved. However, a sharp increase in the frequency of combustion, as indicated by an increase in the RMS temperature, occurs with increasing distance from the plume interior. Therefore, the physical extent of the vapor dome is not strictly defined but rather is interpreted by comparison of the RMS temperatures to those observed in regions where active combustion is known to occur.

The size and location of the vapor dome is strongly influenced by wind. Under low wind conditions, the vapor dome extends to approximately 4' in elevation and 12' in radius. A significant decrease in the overall vertical extent is observed with increasing wind.

Input parameter estimates for SNL RACFMs were also obtained using data from these tests. To remain consistent with the straightforward geometry addressed by the original[3], and subsequent object response-coupled [4] models, a large (7'X15') flat plate calorimeter was placed at the leeward edge of the pool for three of the tests. Given temperature measurements along the center line of the plate, and a matrix of thermocouple and heat flux measurements within the fire environment, RACFMs were employed to perform an inverse calculation of the effective gas absorption coefficient, a, and the effective volumetric energy generation rate, S'''. Using temperature and hemispherical heat flux measurements for each zone within the matrix, the effective absorption coefficient was determined using an inverse solution of the two-flux radiative transfer approximation. Temperature and heat flux measurements also allowed the effective volumetric energy generation rate within each zone to be determined using an energy balance. The presence of several periods of steady-state behavior allowed input parameters to be obtained for different wind conditions. Parameters obtained from model calibration, in conjunction with scoping analyses performed using a validated fire field model, are expected to yield trends throughout the parameter space of fire conditions. The model can be expected to yield reasonable results for conditions other than those of the specific tests since the influence of the changing conditions is accounted for by modeling the dominant heat transfer mechanisms.

Data from these tests are also being used for qualitative comparisons of fire phenomenology with fire field model predictions. The spatial extent of the vapor dome and the optical thickness (as approximated by the effective absorption coefficient) within the continuous flame zone are compared to ensure consistency with trends predicted by fire field models.

References

1. Gritzo, L. A., Moya, J. L., and Nicolette, V. F "Use of Simplified Deterministic Fire Models to Estimate Object Response for Probabilistic Fire Safety Assessments," presented at The Annual NIST Conference on Fire Research, Rockville. MD., October 18-22, 1993.
2. Johnson, H. T., Linley, L. J., and Mansfield, J. A.,"Measurement of the Spatial Dependence of Temperature and Gas and Soot Concentrations Within Large Open Hydrocarbon Fuel Fires," NASA Tech. Memo. 58230, March 1982.
3. Nicolette, V. F. and Larson, D. W. "The Influence of Large Cold Objects on Engulfing Fire Environments," Heat and Mass Transfer in Fires. J. G. Quintiere and L. Y. Cooper (eds), ASME HTD Vol. 141, Heat and Mass Transfer in Fires, 1990, pp. 63-70.
4. Gritzo, L. A. and Nicolette, V. F. "Coupled Object Response of Objects and Participating Media in Fires and Large Combustion Systems," ASME HTD Vol. 250, Heat Transfer in Fires and Combustion Systems, 1993, pp. 161-172

Fire-Induced Mass Flow into a Reduced-Scale Enclosure

Erik L. Johnsson, Nelson P. Bryner, and William M. Pitts
Building and Fire Research Laboratory
National Institute of Standards and Technology
Gaithersburg, MD 20899 301-975-3083

Introduction

Enclosure fires are of great interest because of the resulting loss of life and property, yet the fluid dynamic and chemical behaviors of fires within enclosures are still not well understood. In recent decades, it has become clear that burning rates, fire growth and spread, production of toxic gases, and depletion of oxygen in room fires are very dependent on air supply and entrainment rates.

A recently developed procedure for calculating the mass flow rate into and out of a room has been applied to a reduced-scale enclosure having a single doorway. Both overventilated (preflashover) and underventilated (flashover) conditions have been studied for a series of natural-gas-fueled, quasi-steady-state fires. The new computational approach employs mass conservation to locate the neutral-plane height, z_N. Results using the new method are compared to results using an earlier method for estimating z_N based on a single static pressure measurement. Concentration measurements within the upper layer of the enclosure provided reliable estimates of the actual equivalence ratio within the enclosure which were related to the mass flow rates into and out of the doorway.

Background

Fire-induced flows through a doorway may be monitored using a grid of velocity probes and thermocouples to measure the velocities and estimate the densities necessary for calculating mass flow. While accurate, these measurements are expensive, tedious, and intrusive. Simpler approaches employing less instrumentation are clearly desirable.

A simple computation of flows models the vent such that a pressure gradient draws cool air into the enclosure through the lower region of the vent and hot, expanded combustion products exhaust through the upper region. At the vent, the boundary between the outgoing and incoming flows is referred to as the neutral plane and is required in order to determine mass flow rates through the vent. The equations necessary to calculate mass flow rates from quantities measured in an enclosure fire were derived beginning with Bernoulli's equation and assuming orifice flow. The instrumentation required for the practical use of the equations in experiments includes a thermocouple tree just inside the doorway of the enclosure, a thermocouple tree in the vent, and an ambient temperature measurement outside the enclosure.

Janssens and Tran[1] reviewed the necessary equations and gave descriptions of various approaches for locating z_N. To the same fires they applied and compared the z_N results for the single-pressure-probe approach, a mass-balance approach suggested by Nakaya et al.[2], and interpolation between multiple pressure probes. The mass-balance approach when applied to overventilated, full-scale enclosure fires was shown to be more accurate and consistent than that using a single pressure probe. The z_N location is obtained by solving the mass flow and mass balance equations iteratively. The mass flow rates into and out of the enclosure, $\dot{m}_i$ and $\dot{m}_o$, are then calculated by substituting the z_N height back into the mass flow expressions.

Experimental Apparatus and Procedure

Two vent-flow computation approaches, that using mass-balance by Janssens and Tran[1] and that using a single pressure probe, were applied to a series of fire tests performed at the National Institute of Standards and Technology. The experiments were conducted in the Reduced Scale Enclosure (RSE) test facility in the Fire Test Facility at NIST. A detailed description of the RSE and the experimental procedure will soon be available.[3] The RSE was instrumented with the required thermocouples and a pressure probe as well as front and rear combustion layer sampling probes for CO, CO_2, and O_2 concentration measurements. The front probe also supplied gases to an instrument referred to as a "phi-meter"[4], developed at NIST to measure the local equivalence ratio, ϕ_ℓ. A subroutine, "mass-flow-2", in the data reduction software RAPID[5] was modified to apply the new approach.

Results and Discussion

Figure 1 shows plots of z_N normalized by doorway height, $\dot{m}_i$, and $\dot{m}_o$ determined using the mass-balance

approach as a function of heat release rate (HRR). The z_N values calculated using the mass-balance approach agree with visual observations of layer interface height and are generally located near the center of the doorway. z_N decreases somewhat as fire size increases and levels off for underventilated fires. The $\dot{m}_i$ rise sharply with increasing HRR until approximately 120 kW, at which point a maximum is reached. For HRRs > 160 kW there is only a slight decrease in $\dot{m}_i$ with increasing HRR.

The global equivalence ratio is the ratio of upper layer gases derived from fuel to those derived from air and normalized by the stoichiometric ratio. The phi-meter was used to measure values of ϕ_ℓ at the front probe location of the RSE. Figure 2 shows ϕ_ℓ plotted versus the calculated ϕ_g. The two equivalence ratios are in excellent agreement. The behaviors of upper-layer concentrations were also found to be consistent with the calculated gas flows when using the mass-balance approach. Values of mass flow rates derived using a single pressure probe gave poor estimates for z_N, did not obey mass balance, and were in poor agreement with the observed upper-layer concentrations.

Conclusions

A new approach for calculating the z_N in an enclosure with a vertical opening using mass balance has been applied to a series of reduced-scale enclosure fires for a wide range of natural-gas fire sizes. The z_N results and calculated $\dot{m}_i$ values are validated by measurements of upper-layer chemical species and local equivalence ratios.

The mass-balance approach has been shown to be valid for a wide range of fire regimes including underventilated burning and flashover conditions. The mass balance approach of Janssens and Tran[1] is recommended for the whole range of fire conditions as a method for calculating z_N, $\dot{m}_i$, and $\dot{m}_o$ in vertical vents of enclosures. The approach is easily implemented and is considerably more accurate than a previously used single-pressure-probe approach.

References

1. Janssens, M. & Tran, H., Data Reduction of Room Tests for Zone Model Validation. *Journal of Fire Sciences*, **10**: (1992) 528-555.
2. Nakaya, I., Tanaka, T., Yoshida, M., & Steckler, K. D., Doorway Flow Induced by a Propane Fire. *Fire Safety Journal*, **10** (1986) 185-195.
3. Bryner, N. P., Johnsson, E. L., & Pitts, W. M., *Carbon Monoxide Production in Compartment Fires - Reduced-Scale Test Facility*, National Institute of Standards and Technology, Internal Report to appear.
4. Babrauskas, V., Parker, W. J., Mulholland, G. W., & Twilley, W. H., *The Phi-meter: A Simple, Fuel-independent Instrument for Monitoring Combustion Equivalence Ratio*, to appear in Reviews of Scientific Instruments.
5. Peacock, R. D., Breese, J. N., & Forney, C. L., *A User's Guide for RAPID, Reduction Algorithms for the Presentation of Incremental Fire Data V.2.3.* National Bureau of Standards, Gaithersburg, MD, 1991, Special Publication 798, 112 p.

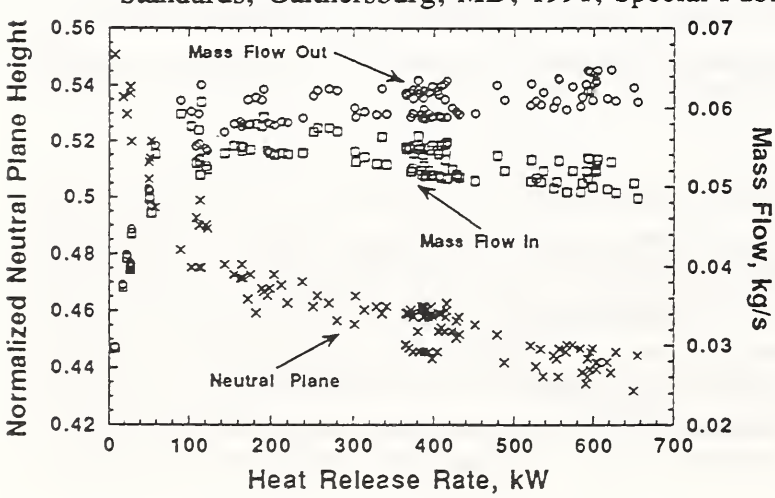

Figure 1: Neutral plane height normalized by doorway height and mass flow rates plotted versus heat release rate, Janssens and Tran approach.

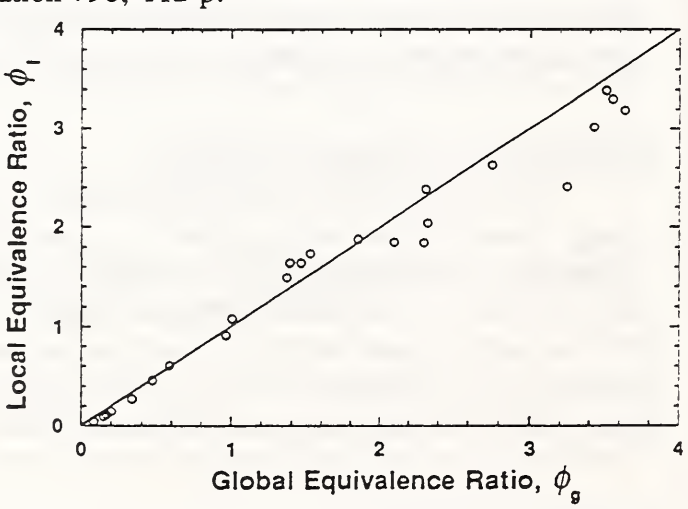

Figure 2: Local equivalence ratio plotted versus global equivalence ratio calculated using the Janssens and Tran approach

Steady State Temperature Profiles under a Beamed Ceiling

Zheng P. Yuan and Vahid Motevalli
Worcester Polytechnic Institute
Worcester, MA 01609

Introduction

Temperature and velocity profiles for beamed ceiling jet flows have been found to be a function of the fire size and geometric variables associated with beams and ceilings[1]. These geometric variables include the beam width, w, beam depth, d, beam spacing, $2l_b$, and ceiling height, H, see Figure 1. It is important to define key regions of the flow in this arrangement. The primary bay, or channel, is the region between two ceiling beams where the fire plume impinges. The secondary bay is the adjacent bay to the primary bay, see Figure 1.

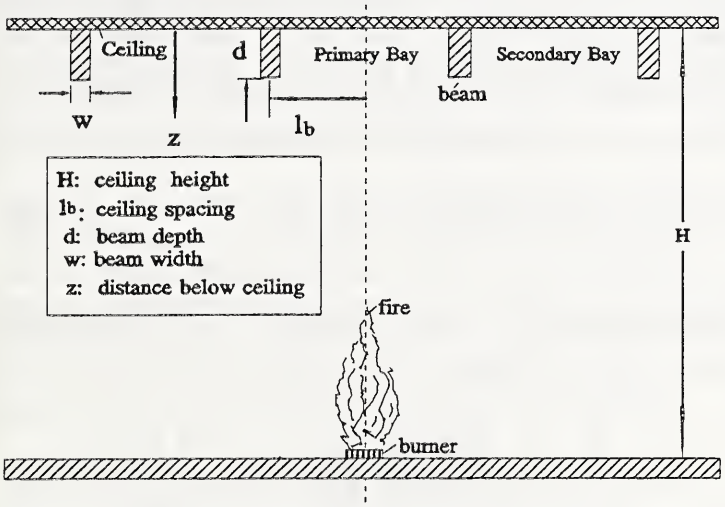

Figure 1 Beamed Ceiling Jet Simulation Schematic

Currently, the NFPA standards[2,3] do not contain the necessary detailed engineering information to address these problems. Furthermore, very little work has been done in this area to justify modification of the NFPA standards. The most recent research[4] was launched by Building and Fire Research Laboratory at NIST. Some of the issues[1,5,6,7,8] have also been addressed by other researchers. The complexity of this problem has limited the applicability of the results to a limited number of ceiling configurations. Particularly, no correlations for the beamed ceiling jet temperature and velocity on the midline within the secondary channel have been developed. In this work, the beamed ceiling jet temperature was investigated for multiple beam spacings, and at positions along the midline of secondary bay. The ultimate product has been easy-to-use correlations to quantify the effect of geometric variables associated with an obstructed ceiling on the temperatures of unconfined ceiling jet flow within the secondary channel.

Theory and Approach

The temperature correlations of the smooth ceiling jet can be developed and expressed as a function of ceiling configuration, i.e. height, distant from plume axis and convective heat release rate. By analogy, the temperature correlation of beamed ceiling jet also can be expressed as a function relating to geometric variables of beamed ceiling, such as beam depth, width and spacing. Using dimensional analysis, the maximum temperature of the unconfined beamed ceiling jet flow within a secondary channel can be described by:

$$\Delta T(r,\alpha)_{max,b}=F(\frac{X}{H},\frac{Y}{H},\frac{w}{H},\frac{d}{H},Q^*) \quad (1)$$

Where subscript, b, refers to the beamed ceiling. Since $X=2l_b$ and $Y=2l_b/\tan(\alpha)$, Equation 1 can be also rewritten as follow:

$$\Delta T(r,\alpha)_{max,b}=F(\frac{l_b}{H},\frac{w}{H},\frac{d}{H},\frac{\alpha}{90},Q^*) \quad (2)$$

where α is a function of X and Y (see Figure 2).

The beamed ceiling jet maximum temperature can be related to the smooth ceiling jet in the following normalization[1]:

$$\theta_{max}=\frac{\Delta T^*_{max,b}}{\Delta T^*_{max,s}} \quad (3)$$

Experiment

The experiments were designed to cover a large range of Q^*(0.0024-0.0351), w/d(0.267-0.889), l_b/H(0.2 -0.4), d/H(0.03-0.25) and α/90(0.389-1.0). In each experiment, temperature profile measurements were obtained at five different locations parallel to the beams and at the mid-plane of the secondary channel (α= 90, 75, 60, 45, and 35) for a steady state fire source and ceiling conditions.

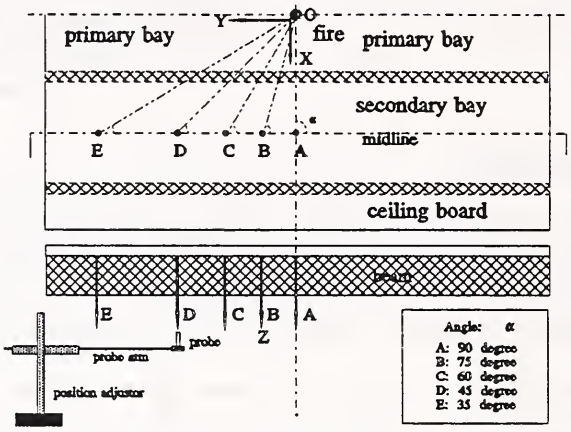

Figure 2 Top View of Beamed Ceiling Configuration

Results and Analysis

Temperature profiles on the midline within the secondary channel have been measured with a variety of multiple beam spacings, beam widths, beam depths, ceiling heights, and fire sizes. Results reveal that the effect of beam width and beam spacing on beamed ceiling jet temperatures are very slight and can be reasonably neglected in the analysis under the condition of general beamed ceiling configuration. The correlation for the maximum ceiling jet temperature within can be expressed as follows:

$$\theta_{max}=[0.42-4.15(\frac{d}{H})+23.49(\frac{d}{H})^2-51.72(\frac{d}{H})^3][3.90-3.02(\frac{\alpha}{90})+1.38(\frac{\alpha}{90})^2] \quad (4)$$

The constants in the above correlation have been obtained by using a modified Levenbery-Marquardt algorithm and a finite-difference Jacobia to solve this nonlinear least square's problem. This correlation has a 0.995 correlation coefficient, is plotted in Figure 3 and seems to fit the experimental data very well within $0.03 \le d/H \le 0.25$.

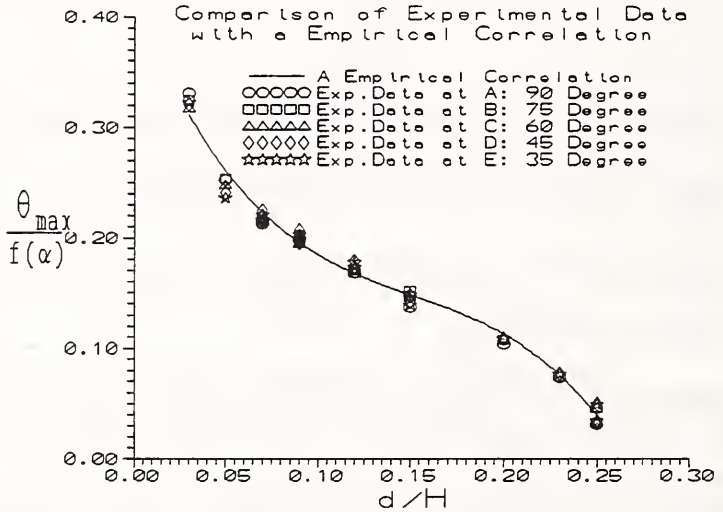

Figure 3 Experimental Data and Correlation

Conclusions

The correlation for beamed ceiling jet maximum temperature within the secondary channel has been established to be a function relating to the ratio of beam depth to ceiling height and the position along the secondary bay axis. It is obvious that after d/H>20%, the non-dimensional maximum temperature decreases dramatically, and the flow within the bay approaches a corridor's flow. There is on the average a 15% to 90% reductions in the temperature of ceiling jet within secondary channels for the beam depth equal to 3% and 25% of ceiling height, respectively, when compared with the smooth unconfined case.

References

1. Koslowski, C. and Motevalli, V., Journal of Fire Protection Engineering, Vol. 5, No. 3, 1993.
2. NFPA 13, "Installation of Sprinkler Systems", National Fire Protection Association, (1991).
3. NFPA 72, "Standard on Automatic Fire Detectors", National Fire Protection Association, (1990).
4. Forney, G.P., Davis, W.D., Klote, J.H., NISTIR 4994, NIST, Dec., 1992
5. Heskestad, G., "Model Study of ESFR Sprinkler Response Under Beamed Ceilings", Technical Report, FMRC J.I.0N0E3.RU, July, 1987.
6. Bill, R.G. Jr., Kung, H-C, Brown, W.R., Hill, E.E., 3rd Int'l Symp. on Fire Safety Sci., pp. 643, Elsevier Pub., 1988.
7. Heskestad, G. and Delichatsios, M., "Environment of Fire Detectors Phase II:Effect of Ceiling Configuration", FMRC, No. 22584, 1978.
8. Delichatsios, M., "The Flow of Fire Gases Under a Beamed Ceiling", Combustion and Flame, Vol.43, 1981.

FIRE-INDUCED FLOW OF SMOKE AND HOT GASES IN OPEN VERTICAL SHAFTS

G.P. Mercier, Y. Jaluria and G.L. Wu
Mechanical and Aerospace Engineering Department
Rutgers University, New Brunswick, NJ 08903

Introduction

The flow in vertical shafts is very important in the accurate modeling of fire growth in multi-leveled buildings since a considerable amount of flow and thermal transport occurs in the shaft. This transport mechanism must be included for predicting the spread of smoke, hot gases and other combustion products, particularly toxic ingredients. Despite the importance of vertical shafts in the spread of fire in multi-leveled buildings, very little work has been directed at this problem. This effort was initiated to provide both a better understanding of the flow in vertical shafts as well as to obtain quantitative inputs which may be used in the modeling of building fires.

Among the most important investigations on this problem are those by Marshall [1,2], who studied stairwells and vertical shafts experimentally using a 1/5 scale model of a relatively short shaft. The mixing and entrainment in the shaft were studied. The flow gave rise to a wall plume which was modeled. The natural convective flow pattern in vertical shafts has also been analytically modeled [3]. Brine solution and dense gas-air experiments were also carried out to validate the models. Work has been done on smoke movement and control [4-7], using analytical and experimental approaches, in order to predict the development of hazardous conditions in buildings.

Experimental Arrangement and Results

Over the last year, substantial work has been done on the flow in vertical shafts with natural ventilation. A fairly versatile experimental system has been designed and fabricated. A sketch of the experimental arrangement is shown in Fig. 1. Smoke or hot gases are injected into the shaft at the lower opening and the downstream flow is monitored by means of thermocouples, hot-wire anemometers, visualization and optical sensors. The inlet temperature of the hot gases can be varied up to around 80 °C. Both natural and forced ventilation can be investigated in the shaft. The opening dimensions can be varied up to around 0.2 m. The shaft is about 2.0 m in height and has an aspect (height/width) ratio A of about 3.0. The conditions at the outlet are also monitored to determine the effects of entrainment into the flow and heat transfer to the walls. Wide ranges of all the physical variables in the problem are obtainable, allowing the simulation of flow due to fire in multi-leveled buildings with vertical open shafts. Typical values of the operating conditions have been investigated, ranging from high buoyancy levels, for which the flow stays close to the vertical wall of the shaft, to much lower levels, at which the flow enters the shaft with a significant flow velocity and spreads outward very quickly.

Shadowgraph pictures of the thermal field in the neighborhood of the inlet channel were obtained. Such visualization allows one to study the different flow patterns and regimes that arise in the shaft, as obtained in earlier studies [8]. Fig. 2 indicates the time taken for smoke injected at the lower opening to reach the top opening as a function of the inlet temperature. With increasing temperature at the inlet, the buoyancy effect is larger resulting in higher velocities and shorter time to reach the top. This time is an important quantity since it indicates the speed with which smoke and other combustion products reach into the higher levels of the building. The effect of the inlet mass flow rate is found to be smaller, with a larger flow rate resulting in smaller time. The temperature at the outlet depends on heat transfer to the walls as well as on the flow velocity and is measured.

Detailed measurements of the velocity and temperature fields have also been taken. Figure 3 shows typical isotherms resulting from these experiments, obtained for a range of Reynolds and Grashof numbers, Re and Gr, respectively, where these parameters are based on the inlet conditions. The local velocity V and temperature T in the shaft are nondimensionalized in terms of the inlet conditions. The vertical distance x

and horizontal distance y are measured from the inlet and are normalized by the inlet channel height D or the width of the shaft W. It must be noted here that the results obtained on the naturally vented, relatively short, vertical shaft considered so far indicate that the flow and temperature are not uniform across a horizontal plane in the shaft. A wall plume is generated which conveys the hot fluid rapidly along the shaft wall from the inlet to the outlet. A recirculating flow arises away from this wall and this flow affects the heat transfer and flow in the wall plume. This, in turn, affects the entrainment into the flow, decay of the temperature field and rate of downstream movement. The flow pattern is similar to those observed in [1-3]. Therefore, horizontally uniform conditions can not be assumed here, as employed in several studies such as [6] for tall shafts. The wall plume has to be modeled in this case, considering the entrainment into the boundary layer flow and the effect of the recirculating flow on the temperature field. Quantitative relationships are obtained so that these may be incorporated in the modeling of building fires. The basic characteristics of the flow are also determined. Therefore, the conditions under which the model has to be based on wall plume analysis and under which horizontally uniform conditions can be assumed are determined. This is an important input for the modeling of flow in vertical shafts.

Acknowledgments

The authors acknowledge the financial support provided by the National Institute of Standards and Technology, under Grant No. 60NANB1H1171, and the several discussions with Dr. Leonard Y. Cooper.

References

1. M.R. Marshall, Fire Safety J., 9, 245- 255, 1985.
2. M.R.Marshall, Fire Safety J., 10, 37-46, 1986.
3. J.B. Cannon and E.E. Zukoski, Turbulent Mixing in Vertical Shafts Under Conditions Applicable to Fires in High Rise Buildings, Tech. Rep. 1, NSF Grant GI-31892-X, Jan. 1986.
4. T. Wakamatsu, Fire Stds. Safety, ASTM STP 614, Am. Soc. Test. Mat., 168-193, 1977.
5. G.T. Tamura and C.Y. Shaw, ASHRAE Trans., 83, 179, 1976, and 86, 54, 1978.
6. J.H. Klote, SFPE Handbook of Fire Protection Engg., SFPE, Boston, MA, Ch. 3-9, 1988.
7. G.T. Tamura and J.H. Klote, Elevator World, 37, 80, 1989.
8. S.H.-K. Lee, W.K.-S. Chiu and Y. Jaluria, Proc. Fall Tech. Meet., Eastern Sect. Combust. Inst., Princeton, NJ, 327-330, 1993.

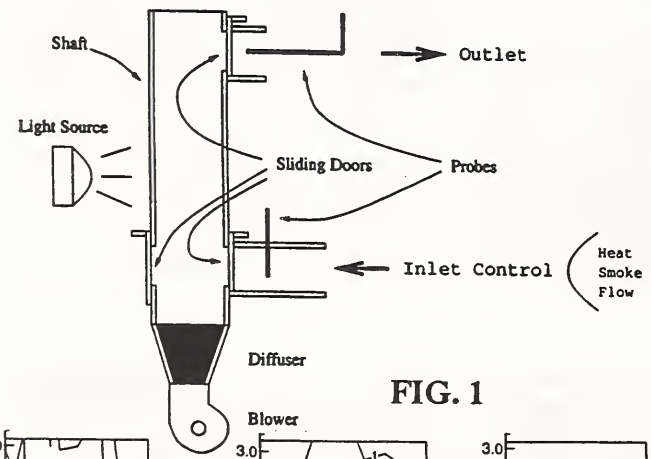

FIG. 1

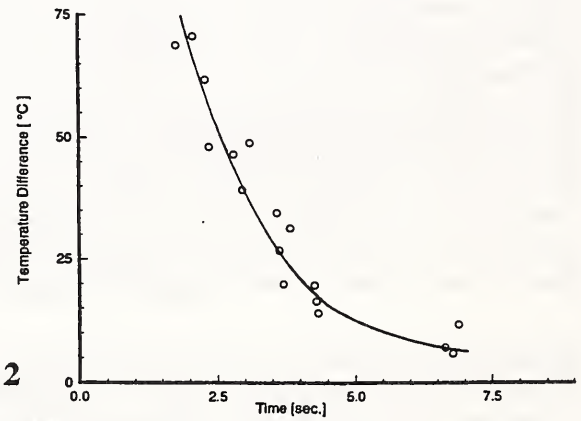

FIG. 2

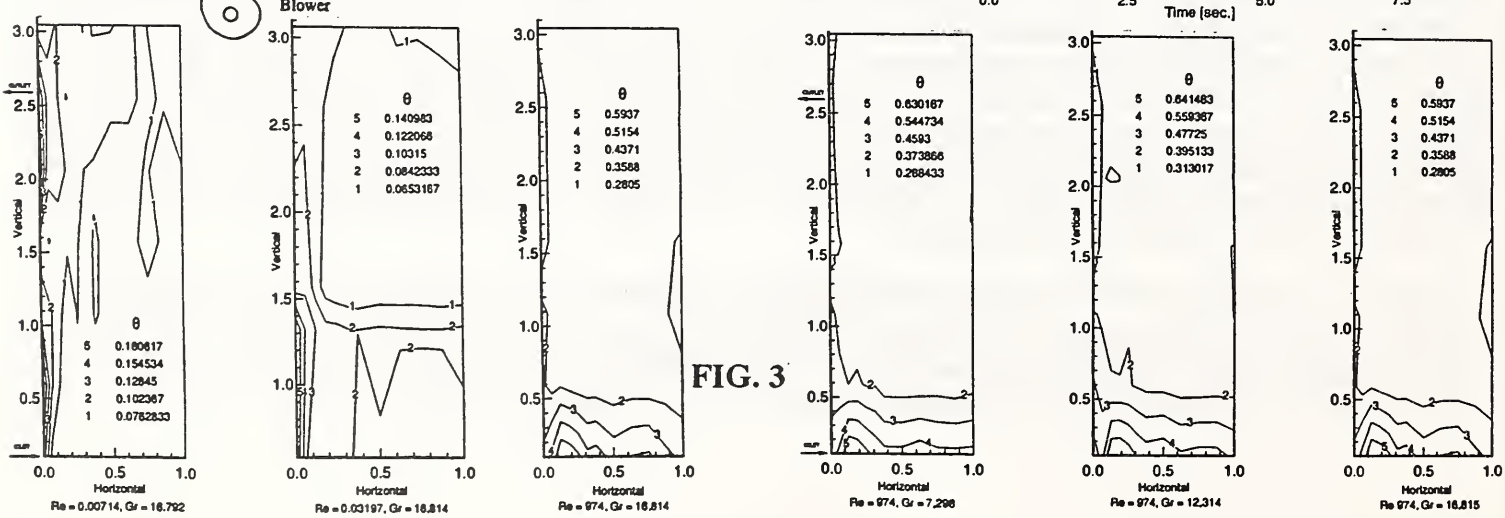

FIG. 3

OVERVIEW OF A THEORY FOR SIMULATING SMOKE MOVEMENT THROUGH LONG VERTICAL SHAFTS IN ZONE-TYPE FIRE MODELS

Leonard Y. Cooper
Building and Fire Research Laboratory
National Institute of Standards and Technology, Gaithersburg, MD 20899

INTRODUCTION

A Limitation of the Two-Layer Quasi-Steady-Buoyant-Plume Approach to Modeling Compartment Fires. The modeling strategy which uses the concepts of one-to-two uniform layers per room, room-to-room mass exchanges by vent flows, and layer-to-layer mass exchange by quasi-steady buoyant plumes has proven to be very robust. However, there are important practical room configurations and associated fire scenarios where these basic concepts are inadequate. If the basic concepts are not applicable to a particular room configuration, then, to the extent that room plays a significant role in the spread of fire and smoke throughout the facility (e.g., the room is the connecting flow path between the room of fire origin and a threatened space), the inadequacy of the simulation in that room can render inadequate the entire simulation.

Let L and d, be the height and horizontal span, respectively, of a room configuration. Then, for rooms with $L/d >> 1$ it is not reasonable to expect a two-layer, zone-type, modeling approach to lead to a successful simulation of fire environments if such spaces are described and treated in the manner of a standard, two-layer, room element, with plumes, etc. For such room configurations, some of the previously mentioned basic modeling assumptions become invalid, e.g. as the plume rises and spreads, its volume eventually becomes significant and it starts to fill a large fraction of the section of the shaft/duct; it is not reasonable to expect that characteristic times of mixing in the shaft will generally be small compared to times of interest; and there is no basis for support for a uniform, two-layer approximation to the density/temperature distribution. An illustration of a generic problematic facility and room configuration is presented in Fig. 1. In this facility, traditional modeling concepts would typically be applicable in the small-L/d room of fire origin, the upper floors, etc., but they would not be applicable in the large-L/d shaft.

A Strategy for Modeling Flow Through Shaft-Like Spaces in Zone-Type Compartment Fire Models; Objective of This Work. For the traditional two-layer, etc., zone-type modeling approach to be valid, large-L/d spaces in a multi-room facility need to be treated as a special class of room configuration. Fire-generated environments there need to be simulated with a method of analysis that 1) uses a valid intra-room fire dynamics modeling approach and 2) can be implemented in the compartment fire model to study fire scenarios in facilities which include other "standard," i.e., small-to-moderate-L/d, room elements.

Once a method of analyzing large-L/d spaces is developed and validated, it would be incorporated into an existing multi-room fire model. The revised model would then be capable of describing smoke movement through shaft-like spaces in a particular facility of interest. The strategy for carrying out simulations with the revised fire model would require the user of the model to characterize each room of a modeled facility as either a small-to-moderate-L/d space or a large-L/d space. When carrying out a simulation the model equations would invoke the traditional, two-layer, isolated-plume, etc. model equations for the small-to-moderate-L/d spaces and the new model equations for large-L/d spaces.

In carrying out the above strategy, a reasonable rule for distinguishing between the two types of spaces is to designate spaces as small-to-moderate-L/d when $L/d \leq 5$ and as large-L/d when $L/d > 5$. Note that an even more advanced strategy might eventually consider an additional, third class of facility space, designated as a "moderate-L/d" space. The analysis of the fire environment in the "moderate-L/d" space would be designed to bridge the gap between small- and large-L/d spaces by including important modeling features of both.

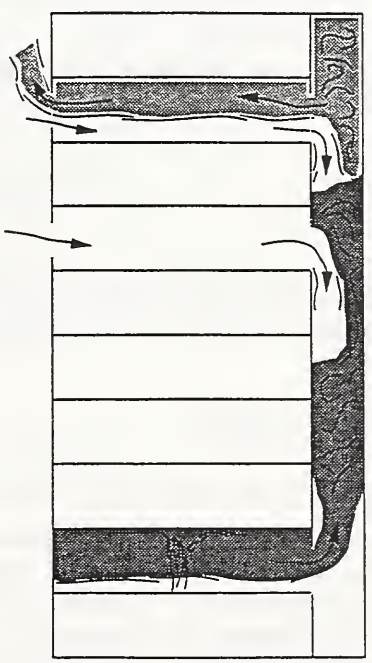

Fig. 1. Sketch of a facility where traditional, two-layer, zone-type, modeling concepts are not uniformly applicable.

COMBINED BUOYANCY- AND VENTILATION-DRIVEN FLOW THROUGH A LONG VERTICAL SHAFT; TURBULENT FLUCTUATIONS IN THE SHAFT FLOW

The Turbulence Equations. Consider perfect gas flow through a shaft of length L, and characteristic section dimension, d. Consider long shafts ($L/d >> 1$), where ρ and T, the gas density and temperature averaged across the section, vary along the shaft. In general, the shaft is ventilated; gas inflow or outflow can occur at vents in the shaft walls, or at its ends. Inflowing gas has specified density and temperature, ρ_{VENT} and T_{VENT}, which can vary along the shaft. Outflowing gas has density and temperature, ρ and T. The rate of

mass addition due to ventilation is $\dot{m}'''_{VENT}$ (rate of mass added to the shaft per unit volume). Heat is transferred to the gas from the shaft surface at the rate $\dot{q}'''_{HT}$ (rate of heat transfer to the gas per unit volume). Assume that the only significant component of flow is along z, the shaft axis, with average velocity, V_z, across a section. Also, account for possible turbulent shaft flow fluctuations by introducing time-averaged ("barred") and fluctuating ("primed") components of the variables, e.g., $\rho = \bar{\rho} + \rho'$. Then, in was found in [1] that conservation of mass and energy, and the equation of state, with Reynolds averaging and neglect of heat conduction through the gas, and other assumptions outlined in [1] lead to the following equation set:

$$\partial\bar{\rho}/\partial t + \bar{V}_z\partial\bar{\rho}/\partial z + \partial(\overline{V_z'\rho'})/\partial z = \dot{m}'''_{VENT}(1 - \bar{\rho}/\rho_{VENT}) - (\bar{\rho}/\rho_{AMB})\dot{q}'''_{HT}/(T_{AMB}C_p);$$
$$\partial\bar{V}_z/\partial z = (C_pT_{VENT}\dot{m}'''_{VENT} + \dot{q}'''_{HT})/(\rho_{AMB}T_{AMB}C_p); \quad \bar{\rho}\bar{T} = \rho_{AMB}T_{AMB} = constant \qquad (1)$$

where C_p is the specific heat at constant pressure, and ρ_{AMB} and T_{AMB} are the density and temperature at an ambient reference state.

Turbulent fluctuations leading to significant values of $\overline{V_z'\rho'}$ will occur along the shaft where there are buoyancy-generated instabilities in the vertical density distribution, i.e., where, locally, the density is increasing with elevation, $\partial\bar{\rho}/\partial z > 0$. Indeed, such instabilities are the driving force for the turbulent-like mixing phenomenon which is of particular interest here. Also, shaft flow scenarios of present interest are such that $\bar{V}_z$ is small enough as never to lead to turbulent fluctuation enhancements that would significantly affect the value of $\overline{V_z'\rho'}$. For example, at elevations along the shaft where the gas is stably stratified, i.e., where $\partial\bar{\rho}/\partial z \le 0$, there will be no buoyancy-driven turbulence and it is reasonable to assume that $\partial(\overline{V_z'\rho'})/\partial z$ can be neglected completely.

Solutions to Eqs. (1) with initial and boundary conditions would provide a description of the fire environment that develops in ventilated, shaft-like, room configurations. However, to actually implement Eqs. (1) it is necessary to develop supplementary model equations to represent $\overline{V_z'\rho'}$ and the source terms, $\dot{m}'''_{VENT}$ and $\dot{q}'''_{HT}$. ($\dot{m}'''_{VENT}$ can be established from known vent-flow considerations.)

The task of establishing a representation for $\overline{V_z'\rho'}$ was a major result of [1]. Following ideas in [2], [3], and [4], the following representation was adopted in [1]

$$\overline{V_z'\rho'} = -D\partial\bar{\rho}/\partial z; \quad D = \begin{cases} Kd^2[(g/\bar{\rho})\partial\bar{\rho}/\partial z]^{1/2} & \text{if } \partial\bar{\rho}/\partial z > 0 \\ 0 & \text{if } \partial\bar{\rho}/\partial z \le 0 \end{cases} \qquad (2)$$

Then, it was determined in [1], that solutions to Eqs. (1) and (2) correlate well with all relevant data from the experiments of [2] (unsteady vertical-tube experiments with both salt-water/fresh-water and heavy-gas/light-gas systems) when $K = 0.44$.

CONCLUSIONS

Eqs. (1) and (2), with $K = 0.44$, should be used to describe time-dependent fire environments in ventilated, shaft-like, room configurations. This requires development of general representations for the $\dot{m}'''_{VENT}$ and $\dot{q}'''_{HT}$ terms of Eqs. (1). Also, confidence in the equations will be subject to validation with data from experiments on hot-air/cold-air systems involving gas-to-surface heat transfer exchanges. Finally, it is noted that the proposed equation set can be used to advance traditional, zone-type compartment fire models. This will require development of an efficient and robust method for solving the new equation set together with (i.e., coupled to) an existing, multi-room, zone-type model equation set. The advance would result in a compartment fire modeling capability that does not now exist; namely, the capability to simulate with confidence fire scenarios in facilities with shaft-like compartment elements.

REFERENCES

[1] Cooper, L.Y., Simulating Smoke Movement Through Long Vertical Shafts in Zone-Type Fire Models, to appear as NISTIR, National Institute of Standards and Technology, Gaithersburg.

[2] Cannon, J.B. and Zukoski, E.E, Turbulent Mixing in Vertical Shafts Under Conditions Applicable to Fires In High Rise Buildings, Tech. Report 1 of California Institute of Technology under NSF Grant GI31892X, Jan. 1976.

[3] Baird, M.H.I. and Rice, R.G., Axial Dispersion in Large Unbaffled Columns, Chem. Eng., Vol. 9, pp. 171-174, 1975.

[4] Gardner, G.C., Motion of Miscible and Immiscible Fluids in Closed Horizontal and Vertical Ducts, International Journal of Multiphase Flow, Vol. 3, pp. 305-318, 1977.

The Distribution of Fire Gases Throughout a Multiconnected Building

Howard W. Emmons
Harvard University (Retired)

A fire produces a large volume of product gases which after cooling results in a volume about twice that of the air consumed. This excess volume causes a mean flow throughout the building toward all exits or leaks to the atmosphere and slightly raises the internal pressure. As a first approximation, this flow is solved in steady state for a constant density gas.

The flow rate is set by the fire, while the pressure distribution is set by the resistance to flow of doors, corridors, rooms, etc. The pressure drop-flow relation is $\Delta p = Rm^2$. The building is replaced by a resistance network. This network is simplified by use of the series and parallel resistance formulas. The flow throughout the resultant reduced network is solved by noting that the net mass flow at each node is zero.

To solve the resultant nonlinear node equations, the bisection method used iteratively seems ideal since it is always stable and there is for each node one and only one root bracketed above and below by the pressures at the surrounding nodes. Figure 1 shows the two cases solved; the 7 node test case and the 10 node irreducible Beverly Hills fire case.

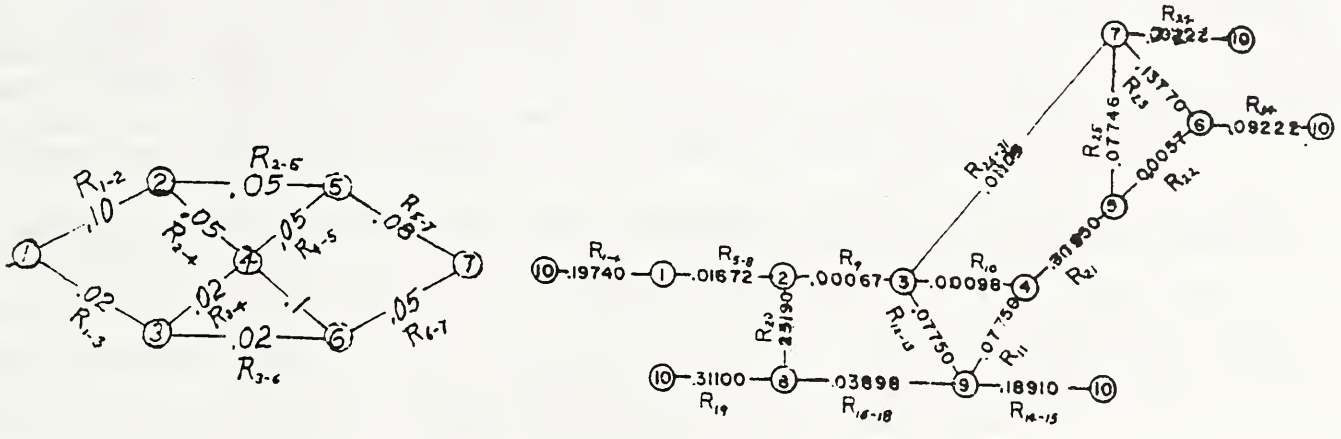

Figure 1

Note that by solving any node, the solution for all connecting nodes are changed. Thus time spent getting high precision early in the process is time wasted. If the pressure in the fire room is set as 1 and the atmospheric pressure is set at 0, the best solution time occurs for an initial accuracy of 1 with a .8 time improvement at each iteration.

The Newton - Raphson solution method is known to be much faster except that there are several disastrous loop traps. If these are avoided by bisection steps, the best time occurs using the final desired precision from the beginning.

The ten node building took 50 times longer to solve than the 7 node case. A 20 node building would take an undesirably long time even on the fastest present P. C. s.

Multi-story buildings will have a resistance network on each floor. These will be connected by holes, stair wells, elevator shafts, etc. These passages can again be represented by resistances. In addition, however, the pressure between floors will change by the hydrostatic pressure change thru the hole at the lower floor gas density plus the hydrostatic pressure change on the upper floor at the upper floor gas density. The plume on the upper floor changes the gas smoke concentration and temperature but not the pressure. If the density on

the lower floor is different at several different holes, a loop circulation will occur.

The pressure drop across exits (or leaks) will vary from floor to floor by the external pressure set by the external density as well as by the effect of the local wind.

As soon as the local pressures at all nodes are found, the flow rates and velocities are known throughout the building. This permits the first approximate calculation of the smoke concentration throughout the building as a function of time. The smoke at any node may arrive at different times and at different rates by different routes. Thus the smoke concentration will change with time by mixing.

Table 1 gives the pressure at each node required to maintain the flow from the fire, node 1, to the atmosphere node 10. The table also gives the time smoke arrives at each node sometimes by several different paths. The time t is in minutes from the smoke start at the fire room. The composition is the fractional concentration relative to that in the fire room, Y = C/C1.

Table 1

Node	1	2	3	4	5	6	7	8	9	10
Pressure [Pa]	1	.4186	.3998	.3977	.2790	.2707	.3060	.3312	.3382	0
Time t	0	.5880	.7590	1.661	2.951	3.613	1.050	1.917	.7590	Varies
Concentration Y	1	1	1	1	.512	.7047	1	.5916	1 hot layer	with Exit
Time t					4	4		41	41	
Concentration Y					1	1		1	1 to floor	

HELIUM-BASED SIMULATOR TO MODEL SMOKE SPREAD DUE TO FIRE IN ENCLOSED SPACES

M.R. Phipps and Y. Jaluria
Mechanical and Aerospace Engineering Department
Rutgers University, New Brunswick, NJ 08903
and
T. Eklund
FAA Technical Center
Atlantic City, NJ 08405

Introduction

This study was undertaken to investigate experimentally the helium smoke simulator which has been used for simulating smoke spread in aircraft cabins during inflight tests. The smoke from cabin fires is buoyant due to the higher temperatures involved, compared to the surroundings. However, the smoke from commercially available smoke generators is nonbuoyant and an addition of helium is employed to make it buoyant so that the actual circumstance is closely represented. The dependence of buoyancy on the amount of helium and the accuracy of the approximation are important questions that need to be answered. The focus of the study is on the Helium Smoke Simulator developed by the Fire Safety Group at the FAA Technical Center. In this technique, helium is added to smoke from a commercially available smoke generator in order to provide the buoyancy in the flow due to the lower density of helium [1]. By introducing this buoyancy component in the smoke, the technique can be used to simulate the flow of smoke and toxic gases in the cabin of an aircraft without resorting to heated air to approximate these gases. Since buoyancy plays a very important role in the flow and spread of smoke and hot gases [2-4], it is important that the simulation include this effect in order to closely represent the actual flow .

The buoyancy level in the smoke can be varied by changing the helium to air ratio. This is given in terms of the apparent temperature T_{app} of the smoke, which indicates the temperature at which the same buoyancy level is achieved. The apparent temperature is given by $T_{app} = 1.16\, T_{amb} / (1.16 - \chi)$, where T_{amb} is the ambient temperature in Kelvin and χ is the volume fraction of helium in the smoke mixture. The helium to air ratio may be adjusted obtaining an apparent smoke temperature of about 250 °C at a 50/50 setting. This setting has been used in smoke spread tests because earlier work has shown that this is an approximate temperature of smoke from a typical fire source on an airplane.

Experimental Arrangement and Results

In this study, earlier work done on the spread of smoke and hot gases in buildings is used to provide a basis for quantifying the use of the simulator [5-8]. The simulation of smoke spread using the Helium Smoke Simulator is investigated for the flow of hot gases in ceiling jets and in corner and wall flows [7]. Heated air is discharged adjacent to an isothermal or adiabatic horizontal boundary representing the ceiling of a room. The flow near a corner and the downward flow over a vertical boundary representing the wall are investigated. The buoyancy force is upward and this results in a negatively buoyant situation, which causes the flow to come to stagnation and reverse. Buoyancy plays a very important role in such flows which are, thus, ideally suited for the use of the Helium Smoke Simulator.

The experimental system used is shown in Fig. 1. A mixing chamber is used to form a mixture of helium, air and smoke before it enters the main flow region. A blower is used for the air flow. The volumetric flow rate is varied by means of a variac attached to the blower. The flow rates are measured by using flow meters and by measuring the velocity [5]. Thus, the flow rates of helium, smoke and air are adjusted and measured. The oxygen concentration in the flow is measured by means of a Teledyne oxygen analyzer. This indicates how the oxygen concentration changes as the smoke flows along the ceiling and the wall of the chamber. Velocity measurements are undertaken by means of a hot-wire anemometer, both along the ceiling and the vertical wall, in order to determine the effect of buoyancy on the resulting flow. A traversing mechanism is used for accurate positioning of the velocity probes.

Some typical results are shown in Fig. 2 in terms of the helium concentration profiles at various horizontal distances x away from the inlet. It is seen that the profiles are fairly uniform over much of the flow region, sharply dropping to zero at y/D of around 15, where y is the vertical coordinate distance from the ceiling and D is the inlet height. This uniformity is largely due to diffusion of the species, as seen earlier for the thermal field in heated ceiling flows. However, instead of decreasing temperatures obtained as one approaches the wall due to heat loss, an essentially zero slope is observed here. The velocity profiles, shown in Fig. 3, indicate the ceiling boundary layer flow and the outward flow arising from the negatively buoyant wall flow. These results can be used to determine the penetration depth δ_p for different inlet conditions, given in terms of the Grashof and Reynolds numbers, Gr and Re, respectively. The basic trends were found to be quite similar, as seen in Fig. 4 from the concentration results, and the penetration to be of the same order of magnitude, lending support to this approach of simulating smoke spread in enclosures.

Acknowledgments

The authors acknowledge the financial support provided by the Federal Aviation Administration Technical Center, under Grant No. 93-G-041, for this work and the support for the first author under the FAA Fellowship Program.

References

1. Eklund, T., FAA Tech. Rep. DOT/FAA/CT-90/9, Sept. 1990.
2. Maylor, E., FAA Tech. Rep. DOT/FAA/CT-89/9, March 1989.
3. Maylor, E., FAA Tech. Rep. DOT/FAA/CT-88/22, July 1988.
4. Abramowitz, A., Neese, W. and Slusher, G., FAA Tech. Rep. DOT/FAA/CT-89/31, Nov. 1990.
5. Jaluria, Y. and Kapoor, K., Combust. Sci. Tech., Vol. 59, pp. 355-369, 1988.
6. Jaluria, Y. and Cooper, L. Y. Prog. Energy Combust. Sci., Vol. 15, pp. 159-182, 1989.
7. Jaluria, Y. and Kapoor, K., Combust. Sci. Tech., Vol. 86, pp. 311-326, 1992.
8. Kapoor, K. and Jaluria, Y., Int. J. Heat Mass Transfer, Vol. 36, pp. 155-167, 1993.

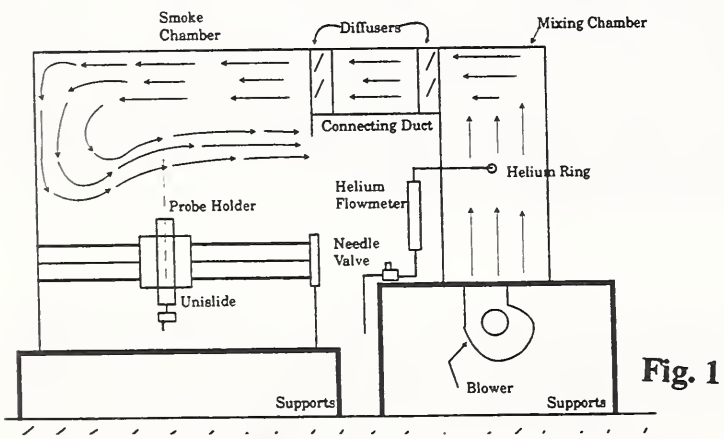

Fig. 1

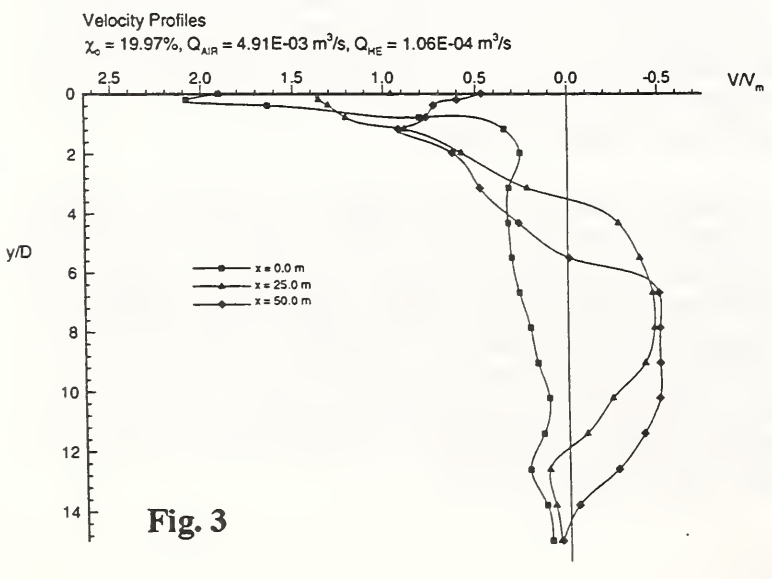

Fig. 3

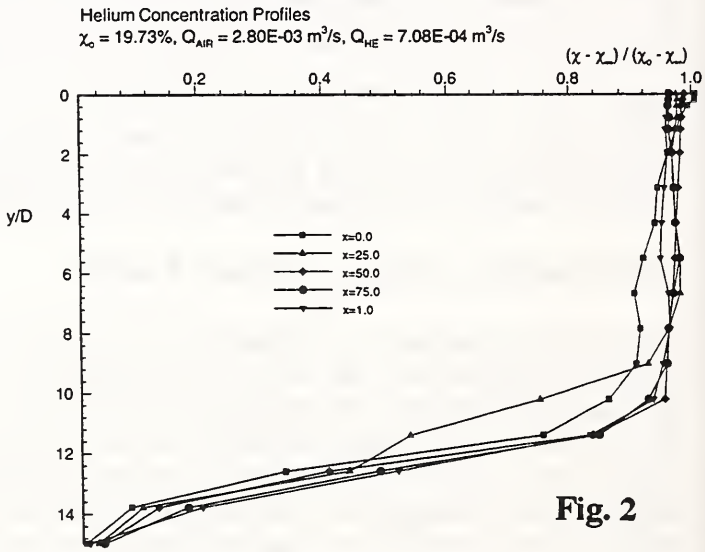

Fig. 2

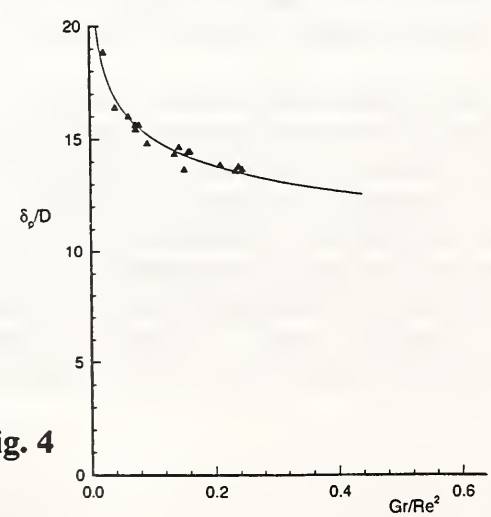

Fig. 4

Oakland Hills Fire Induced Winds

J. Trelles and P.J. Pagni, University of California, Berkeley

The 20 October 1991 Oakland Hills "Tunnel" Fire brought into sharp focus the devastation possible from a conflagration originating from an urban-wildland interface. As civilization continues to encroach on wilderness areas, the need for information regarding fire hazards in this new, boundary environment becomes critical. Under development is a modular urban/wildland interface fire growth model to meet this need. This model will incorporate the effects of distributed fire sources, ambient and convective column-induced winds, fire spread via various mechanisms (especially brands) and will treat the problem from the fire source to areas where fire-free structures are threatened by fire growth. The fire induced winds module is based on the Baum and McCaffrey [1] mass fire model. Of interest here is the information this module has provided regarding the early nature of the Oakland Hills Fire.

The flow field for a single, steady state, axisymmetric fire, based on the McCaffrey plume model [2], serves as the fundamental computational tool. The aerodynamic effects of a large scale, composite fire are then represented as a collection of distributed plumes. Flow field decomposition makes it possible to determine the complete, nondimensional velocity field. It is determined by solving two Poisson equations for the stream and potential functions. Once the nondimensional flow field for a single fire is known, the velocities induced by N fires may be determined by scaling, based on the each fire's strength, Q_i, and on ambient properties. The influences of all the fires are then simply summed to obtain the velocity at any desired observation point.

As is stipulated in Ref. [1], it is assumed that there are no overlapping plumes in the computational domain. However, at higher altitudes, the plumes will begin to merge. In order to make the model applicable, intersecting plumes need to be combined based on suitable criteria. Here the net effect of the fires is represented by partwise combinations of single, intersecting plumes. For velocity field patterns in the X-Y plane at different altitudes, Z, the criterion for conglomeration is based on the 1/e point in the vertical velocity profile, i.e., the plume spread radius, $R(Z)$. The total distance between two plume centerlines must be greater than the sum of their radii for the plumes to be considered independent. At a given altitude, perform this comparison to identify any plume pairs which do not satisfy this criterion. Combine the pair with the minimum separation into a single plume such that

$$Q_{NEW} = Q_1 + Q_2, \qquad X_{NEW} = (X_1 Q_1 + X_2 Q_2)/Q_{NEW}, \qquad Y_{NEW} = (Y_1 Q_1 + Y_2 Q_2)/Q_{NEW}. \tag{1}$$

After each combination, the new fire replaces its parents in the algorithm. This pairing technique is repeated until all the resultant plumes are independent. Once an overlap-free set of plumes is arrived at, apply the methodology detailed above to determine the flow field.

To test the model's abilities, use is made of the vast database collected from the Oakland Hills "Tunnel" Fire. The accompanying figures were generated using the noon data for the locations of structures assumed to be fully involved. Each cross represent a structure burning at an average Q = 50 MW. The increasing Y-direction is north and the increasing X-direction is east. The domain is divided up into 1000 ft square sectors corresponding to the California plane system. The wind at the center of the sector is represented by two component and one resultant vectors. In the upper left corner of each sector, the magnitude of the resultant vector is given in m.p.h. Below it is the angle, given in the meteorological convention, measured from the north direction to the *tail* of the resultant vector. Figure 1a gives contours of constant vertical velocity in the composite convection column. The rest of the figures indicate that the simple combination of a streaming atmospheric wind and the fire induced wind is characterized by an augmented flow towards the burning area from the upwind direction and a "suction" back into the fire zone just downwind of the conflagration. The ambient winds, as estimated by meteorology professor John Monteverdi, are presented in Figure 1b. In Figure 1c, it is evident that the fire's effect is to draw air in towards its fire-centroid. Comparing Fig. 1b with Fig. 1d demonstrates that the combined effect changes the direction of the purely ambient vectors and increases the magnitude for those vectors pointing in the general direction of the fire centroid. The opposite effect is naturally observed for vectors pointing away. It is believed that this phenomenon played a role in the rapid slowdown of the fire spread at noon [3], thereby demonstrating that, when a fire reaches conflagration proportions, its spread in the (atmospheric) windward direction is countered by the inflow into the flames and plume.

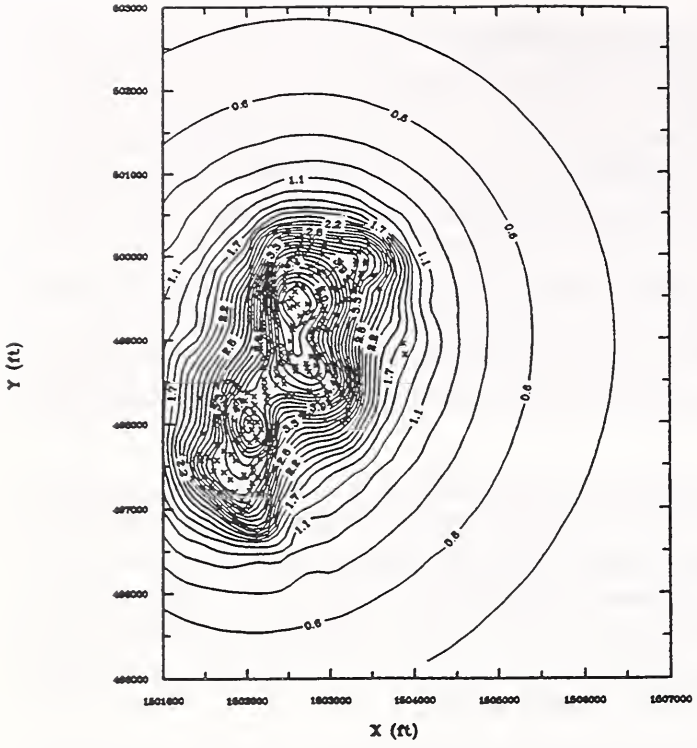

Figure 1a

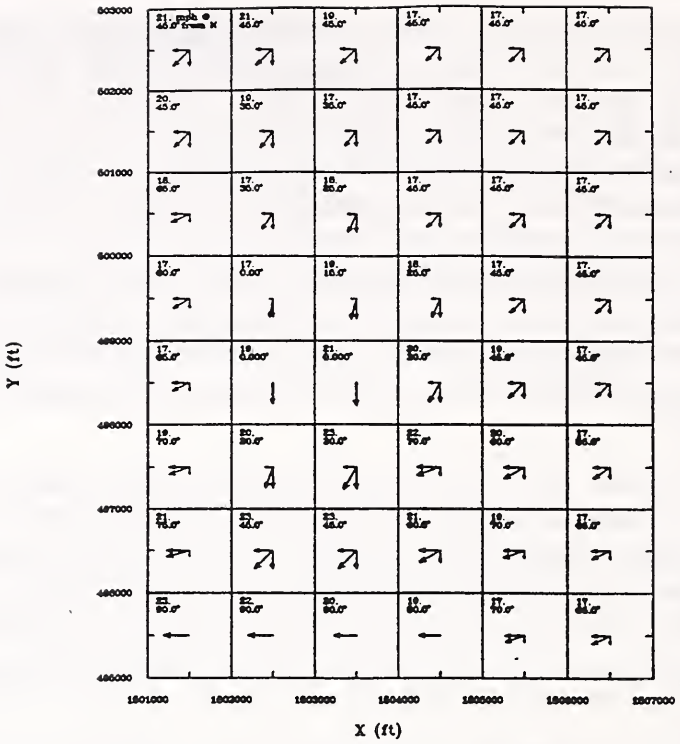

Figure 1b

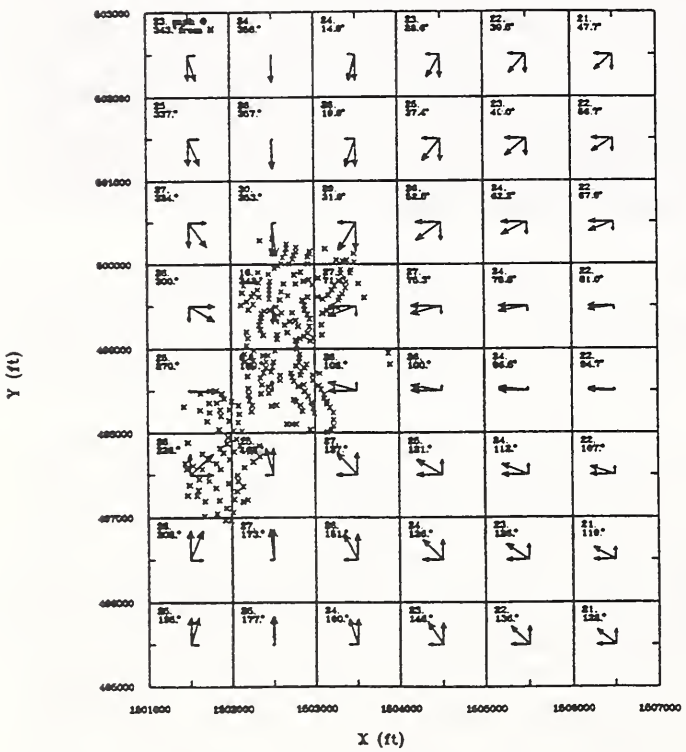

Figure 1c

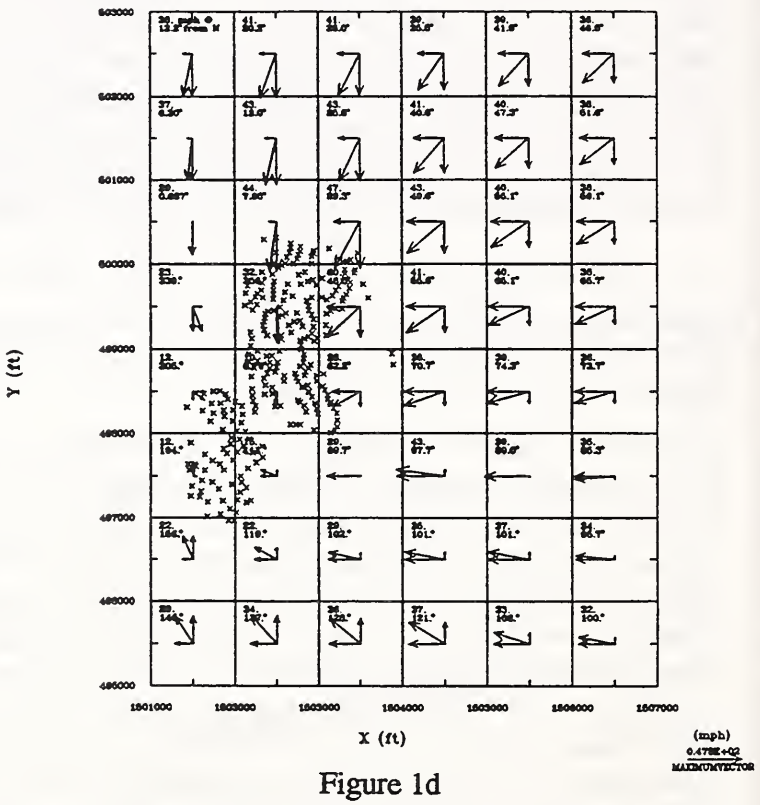

Figure 1d

Fig. 1a, contours of the vertical, fire-induced convection column winds only. Fig. 1b, vector components of the ambient winds only. Fig. 1c, vector components of the induced winds only. Fig. 1d, vectors for the combined winds.

1. Baum, H.R., and McCaffrey, B.J., "Fire-Induced Flow Field - Theory and Experiment," *Fire Safety Science - Proceedings of the Second International Symposium,* New York: Hemisphere, 129 - 148, 1989.

2. McCaffrey, B.J., "Momentum Implications for Buoyant Diffusion Flames," *Combustion and Flame* 52, 149 - 167, 1986.

3. Pagni, P.J., "Causes of the 20 October 1991 Oakland Hills Conflagration," *Fire Safety Journal*, 21, 331 - 339, 1993.

THERMAL DECOMPOSITION CHEMISTRY OF POLY(VINYL ALCOHOL): CHAR CHARACTERIZATION

Jeffrey W.Gilman[1] *, Takashi Kashiwagi[1] and David L. VanderHart[2]
1-Building and Fire Research Laboratory
2-Materials Science and Engineering Laboratory
National Institute of Standards and Technology
Gaithersburg, Maryland 20899-0001

Currently, due to concerns over the environmental effects of halogenated compounds, there is an international demand for the control of polymer flammability without the use of halogenated or metal based additives.[1,2] Our approach to this issue is first to characterize the fundamental condensed phase processes and structures which lead to char formation during polymer combustion and then, to use this information to design new strategies, that do not use halogenated additives, which increase char formation and therefore will reduce polymer flammability.[3,4]

The polymer we chose to investigate was poly(vinyl alcohol), PVA, because of its linear aliphatic structure, low char yield and commercial applications (paper, textile and adhesives). The thermal decomposition of PVA has been studied both in the gas and condensed phases, however, only limited characterization of PVA chars exists.[5,6,7] We prepared PVA chars in a flow pyrolysis apparatus with an inert atmosphere (N_2) at several temperatures. This experimental setup allows study of the condensed phase decomposition processes in the absence of gas phase oxidation.[8] Upon heating PVA above the decomposition temperature the polymer begins a rapid chain-stripping elimination of H_2O.[9,10] This process coupled with melting causes the material to foam or intumesce as it decomposes. As a result most of the chars are rigid foams. The physical appearance, hydrogen-to-carbon ratio and char yields are shown in Table 1.

Table 1. Material	Appearance	H/C Ratio	Char Yield (%)
PVA	white solid	2:1	NA
250 °C Char (30 min)	yellow-orange foam	1.9:1	60
300 °C Char (30 min)	tan rigid foam	1.4:1	47
350 °C Char (30 min)	dark brown foam	1.2:1	17
400 °C Char (30 min)	black powder	1:1	5

The chars were characterized using CP/MAS ^{13}C NMR. Figure 1 shows the PVA and char NMR spectra. The preliminary results suggest that during the well known chain-stripping elimination reaction of PVA a random chain scission reaction is also in progress. We also see evidence of formation of carbon-carbon bonds (non-protonated (substituted) olefinic/aromatic carbons) at all char temperatures. At temperatures up to 350 °C the polyene products from the elimination reaction are converted into aliphatic groups, possibly via Diels-Alder and/or radical reactions. Even in chars formed at 400 °C almost all of the aliphatic carbons are protonated. It appears that these chars retain a significant amount of hydrogen since the H:C ratio is as high as 1:1 at 400°C.

We plan to utilize FTIR, and other spectroscopic techniques to further characterize the decomposition of PVA and of PVA with char enhancing additives.

Figure 1.
^{13}C NMR (25 MHz)
1ms CP time
3 sec rep time
4 kHz MAS

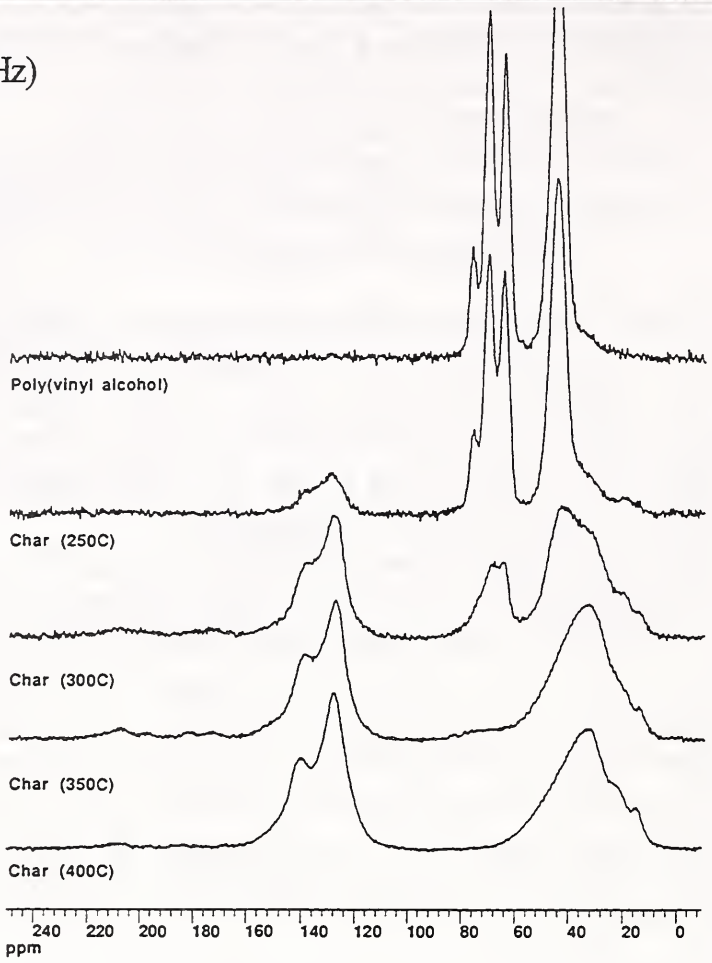

1. R. Dumler, D. Lenoir, H. Thoma and O. Hutzinger, *Journal of Analytical and Applied Pyrolysis*, 16, **1989**, 153-158.

2. K. F. Lindsay, *Modern Plastics*, February **1994**, 54.

3. D.W. van Krevelen, *Polymer*, **1975**, vol. 16, 615-620.

4. S. K. Brauman, *J. of Fire Retardant Chemistry*, Vol.6, November, **1979**, 248-265.

5. D.W. van Krevelen, *Polymer*, **1975**, vol. 16, 615-620.

6. S. K. Brauman, *J. of Fire Retardant Chemistry*, Vol.6, November, **1979**, 248-265.

7. X. Zhang, K. Takegoshi, K. Hikichi, *Polymer* **1992**, vol.33, no. 4, 718-724.

8. Previous studies have shown that the elemental composition, char yield and physical structure of polymer chars, in many systems, were independent of whether they were formed via pyrolysis in nitrogen, combustion in air, or burning. See: S. K. Brauman, *J. of Fire Retardant Chemistry*, Vol.6, November, **1979**, 266-275.

9. C.F. Cullis, M.M. Hirschler, *The Combustion of Organic Polymers*, Clarendon Press, Oxford, **1981**, 117-119.

10. H. Anders, and H. Zimmerman, *Polymer Degradation and Stability*, **1987**, 18, 111-122.

Effect of Gas Phase Oxygen on Chain Scission and Monomer Content in Bulk Poly(methyl methacrylate) Degraded by External Thermal Radiation

James E. Brown and Takashi Kashiwagi
Building and Fire Research Laboratory
National Institute of Standards and Technology
Gaithersburg, MD 20899

BACKGROUND

The effect of the atmosphere on the thermal degradation and gasification of bulk polymeric materials is not fully understood with respect to ignition and flame spread [1]. It is of interest to know whether molecular oxygen influences these aspects of polymer flammability through direct attack on the condensed phase.

Poly(methyl methacrylate), PMMA, is often used as a model to study thermoplastics decomposition in fire-like environments. PMMA has been well characterized with respect to its gasification behavior in inert atmospheres. The gasification can be initiated from weak links in the polymer chains at lower temperatures and from random scissions along the polymer chains at higher temperatures [see for example ref. 2]. In the presence of oxygen the initiation and gasification proceed at an intermediate temperature. These characterizations were made on very small samples without a significant temperature gradient in the polymer or composition gradient for the atmosphere in contact with the polymer [3]. In some fire environments a polymeric material undergoing gasification may be subjected to broad temperature gradients and atmospheres of widely different compositions.

OBJECTIVE

To investigate, at the molecular level, the effect of the concentration of atmospheric oxygen on the decomposition of bulk PMMA at different incident heat flux levels simulating radiative heating of the surface by fires.

APPROACH

The approach used to ascertain the effect of oxygen on PMMA degradation was to determine the number of chain scissions experienced by the residual polymer after a period of exposure to thermal radiation. Degradation was achieved by exposing 1 cm thick PMMA plates in atmospheres containing 0, 10, 21,and 43 % oxygen in nitrogen to black body radiation simulating the radiant energy flux of fire environments. Molecular weight measurements, from which the scission numbers are calculated, and residual monomer content were determined on successive thin layers about 0.1 mm thick cut from the exposed surface and at various deeper levels throughout the sample showing indications of decomposition by bubble formation. These determinations were made on solutions of PMMA in tetrahydrofuran. The analyses were made by gas chromatography and size exclusion chromatography for monomer content and molecular weights, respectively.

RESULTS

Figure 1 shows that at an irradiance of 17 kW/m^2 oxygen enhances the scission number of the degraded surface layer to a depth of about 1 mm or less, apparently, as a result oxygen entrapment in openings formed by bursting bubbles of escaping monomer vapor. Figure 2 illustrates a similar oxygen effect when the polymer was degraded at a higher irradiance, 30 kW/m^2, except that the effect is somewhat less pronounced when the scission number in nitrogen is compared to those in the presence of oxygen. The higher irradiance is expected to be sufficiently energetic to induce random scissions in the polymer chains but these scissions are evidently enhanced by the presence of oxygen.

The scission numbers calculated from the M_n values of the surface layers for each exposed sample are plotted against the mole fraction of oxygen in the surrounding atmosphere and shown in figure 3. The chain scissions appear to follow a linear relationship with oxygen concentration at both irradiance levels.

The monomer content of the near surface was found to be greater in the PMMA degraded at the lower flux, 17 kW/m^2, than at the higher flux, 30 kW/m^2, when oxygen is present. This is attributed to a lower temperature and a larger melt viscosity due to fewer chain scissions at the lower flux, both of which impede volatilization of the monomer. At the higher flux the sample temperature is also sufficiently elevated so as to increase evaporation of the monomer and to contribute to the lower melt viscosity by a greater number of random chain scissions. This is illustrated in figure 4 where the monomer content of the upper most surface layer (about 0.1 mm thick) is plotted against the oxygen mole fraction of the atmospheres in which the surfaces were irradiated.

REFERENCES

1. Kashiwagi, T. and Ohlemiller, T. J., Nineteenth Symposium (International.) on Combustion, The Combustion institute, Pittsburgh, 815, (1982).
2. MacCallum, J. R. Makromol. chem. 83, 137 (1965).
3. Kashiwagi T., Inaba, A., Brown, J. E., Hatada, K., Kitayama, T., and Matasuda, E., Macromolecules 19, 2160 (1986).

Figure 1. Chain Scission Number of the Surface of PMMA Radiatively Heated at 17 kW/sq. m for 420 s

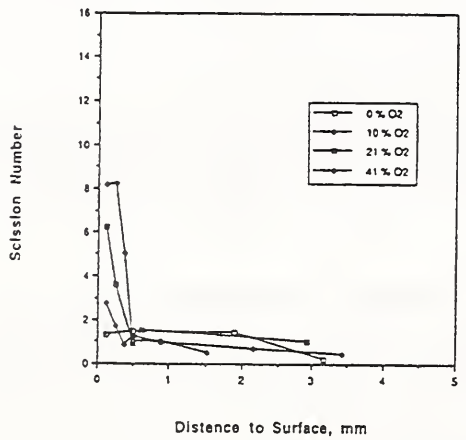

Figure 2. Chain Scissions near the Surface of PMMA Radiatively Heated at 30 kW/sq. m for 420 s

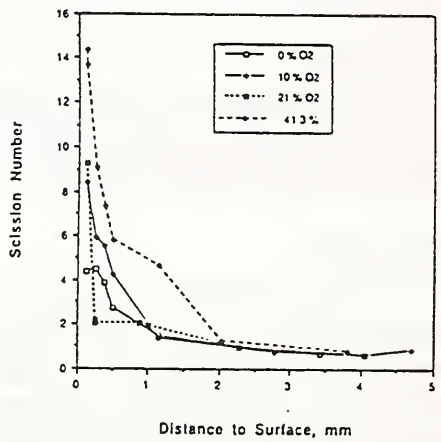

Figure 3. Comparison of the the Scission Number Dependence on Oxygen Concentration at Two Flux Levels

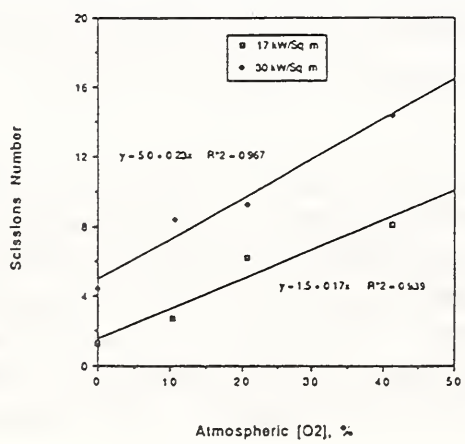

Figure 4. Comparison of the Monomer Content at the Surface layer of PMMA with Respect to Oxygen Concentration and External Flux

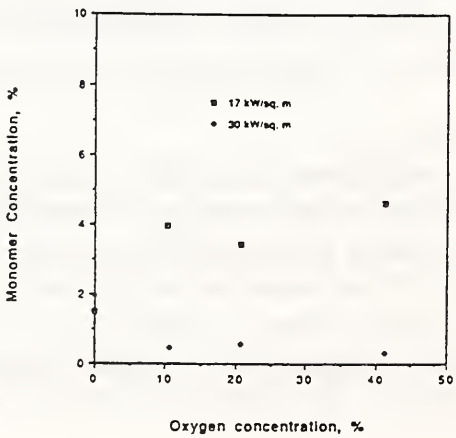

CORRELATIONS OF HYDROGEN CHLORIDE OR HYDROGEN CYANIDE EVOLVED DURING THE THERMAL DECOMPOSITION OF CHLORINE- OR NITROGEN- CONTAINING MATERIALS

By Maria I. De Rosa

ABSTRACT

The U.S. Bureau of Mines conducted experiments to determine if correlations exist between the percentage of chlorine or nitrogen contents of the original materials and the hydrogen chloride (HCl) or hydrogen cyanide (HCN) concentrations evolved during the thermal decomposition of these materials. Concentrations of carbon monoxide (CO) and submicrometer smoke particles were also determined.

The experiments were carried out in a 20-L furnace (Fig. 1) with 1-g samples; the furnace temperature, rising from ambient, was set at 1,000 C with an airflow through the furnace of 10-L/min.

The variables measured were the HCl, HCN, CO, and submicrometer smoke particle concentrations (treated as load values), the sample and furnace temperatures, and the sample weight loss.

Results show that there are significant correlations (Figs. 2, 3) between the percentage of chlorine or nitrogen contained in the materials and the HCl and HCN gas loads evolved during the thermal decomposition of these materials; the higher the contents, the higher are the load values.

For the chlorine-containing materials, the polyvinyl chloride samples (P1, B2), followed by the neoprene sample (N1), released the highest HCl gas loads because of the high chlorine content of the materials; the fiberglass brattice sample (F1), followed by the styrene butadiene rubber sample (S1), released the lowest HCl gas loads because of the low chlorine content of the materials (Fig. 2). Sample S1, however, released the highest concentrations of CO and submicrometer smoke particles.

For the nitrogen-containing materials, the wool sample (W1), followed by the nylon and polyurethane foam samples (Ny, Pr and Pn)), released the highest HCN gas loads because of the high nitrogen content of the materials; the cotton batting sample (Cb) released the lowest HCN gas load because of the low nitrogen content of the material (Fig. 3). Furthermore, samples Pr and Pn released very high concentrations of CO and submicrometer smoke particles, and decomposed earlier at faster rates.

The mass loss rates necessary to produce dangerous concentrations of HCl (100 ppm) or HCN (50 ppm) in a ventilated system were calculated from the data and shown in Figure 4.

These correlations and predictions may be used to evaluate the hazard of materials during fire. The measurements of CO and submicrometer smoke particles may also be used in the evaluation.

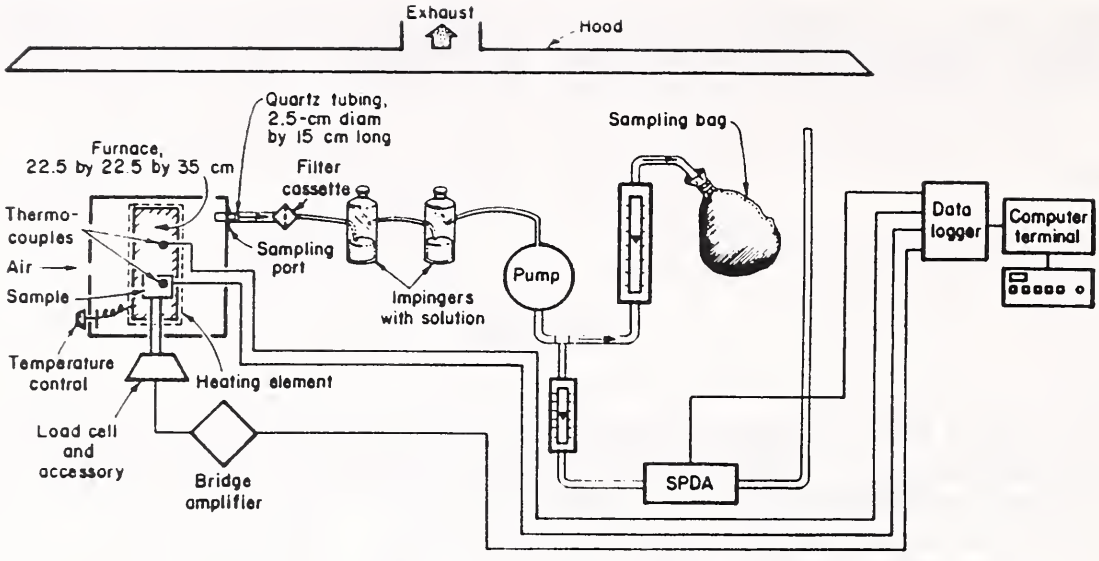

Figure 1.—Experimental system.

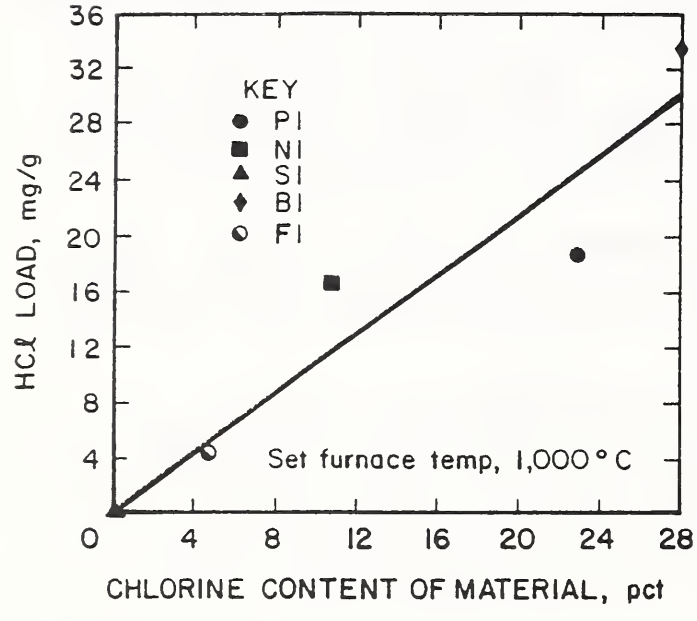

Figure 2.—Hydrogen chloride load versus the chlorine content of materials at 1,000° C set furnace temperature.

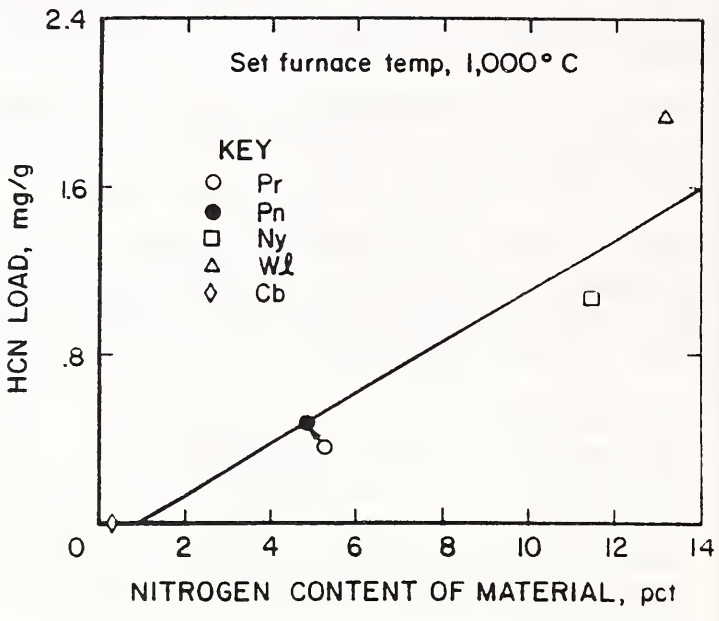

Figure 3.—Hydrogen cyanide load versus the nitrogen content of materials at 1,000° C set furnace temperature.

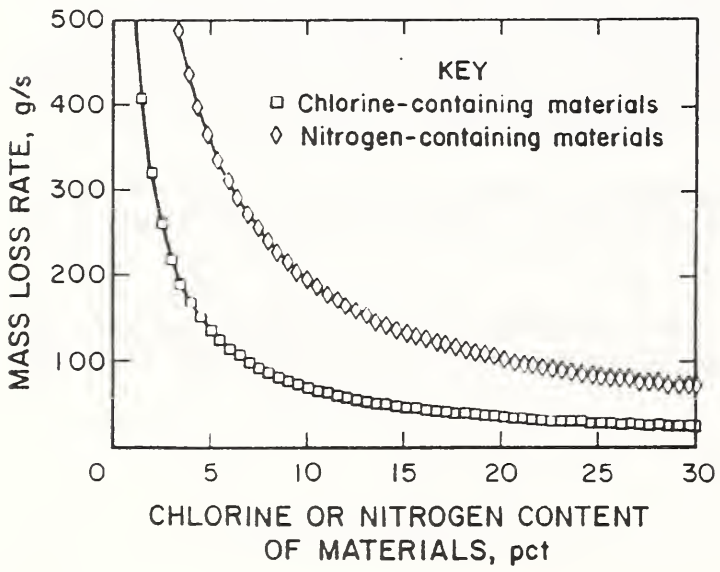

Figure 4.—Mass loss rates to produce 100 ppm of HCl or 50 ppm of HCN (IDLH levels) in a given ventilated system for chlorine- or nitrogen-containing materials.

THE BEHAVIOR OF CHARRING SOLIDS UNDER FIRE-LEVEL HEAT FLUXES

Ivan Milosavljevic and Eric M. Suuberg
Division of Engineering, Brown University
Providence, RI 02912
(Work Sponsored by the Building and Fire Research Laboratory-NIST, under grant 60NANB0D1042)

It has recently been argued in the fire research community that the ability to quantitatively describe flame spread over combustible solids has reached the point at which our understanding of the complexity of the solid phase processes is limiting. Often the processes occurring in the solid are modeled by simple thermal diffusion in a solid (with ill-defined thermal properties) together with a crude empirical decomposition rate law. A critically important parameter- release rate of combustibles into the vapor phase- often becomes little more than an adjustable parameter, as decomposition rates, products of pyrolysis and solids thermal properties under relevant conditions are only approximately known. This is particularly so in the practically important case of charring solids such as wood and other cellulosics. As a result, it is difficult to claim that a truly critical testing of combustion models for bulk, charring solids has ever been possible. This communication addresses some issues related to this problem.

Before attempting to model the behavior of more complex charring solids, we felt it important to better understand the solid phase behavior of one of the "simplest" charring solids- cellulose. What differentiated this study from many others on the same material were the careful attempts made to obtain kinetic and transport properties in experiments separate from those that simulate fire behavior, but with the latter experiments always being guided by the conditions found in fire situations. We further believe that the fire community would be well-served by focusing on "standard" easily-prepared materials of the kind studied here, so that there would be an ability to compare results between laboratories, as well as providing fire modelers a more reliable property data base than currently exists.

To simulate wood or other bulk cellulosic building materials, high purity alpha cellulose powder (Whatman CF-11) was dry-pressed in an ordinary laboratory press into pellets whose bulk densities bracketed those of real woods (0.4-1.0 g/cc). The intent here was *not* to simulate the full complexity of wood, but rather to obtain detailed data on a model charring material that is very wood-like in its behavior. The densities were reproducible from sample-to-sample to about 5%. An advantage of these samples is that they are relatively pure (0.009% ash) and contain none of the heterogeneity of real wood (i.e. no hemicellulose or lignin). This is important insofar as establishing the kinetics of pyrolysis is greatly simplified when potentially catalytic impurities are absent, and when there are not several distinct organic phases present. This allowed comparison with the large amount of data in the literature on cellulose decomposition, and also offered the possibility of reliable experimentation, on several scales, using several analytical techniques, to establish key properties.

The results of experiments on simulated woods and real woods are shown in Figure 1. The experiments were simulated fire experiments in which samples of 3.8 cm diameter and 1 cm thickness were irradiated on their front faces by a quartz lamp delivering 40 kW/m^2. The irradiation was chosen to simulate a fire level heat flux, but in this case the experiment was performed under inert gas, to avoid the further complexities introduced by actual combustion. Clearly the results show the ability to simulate

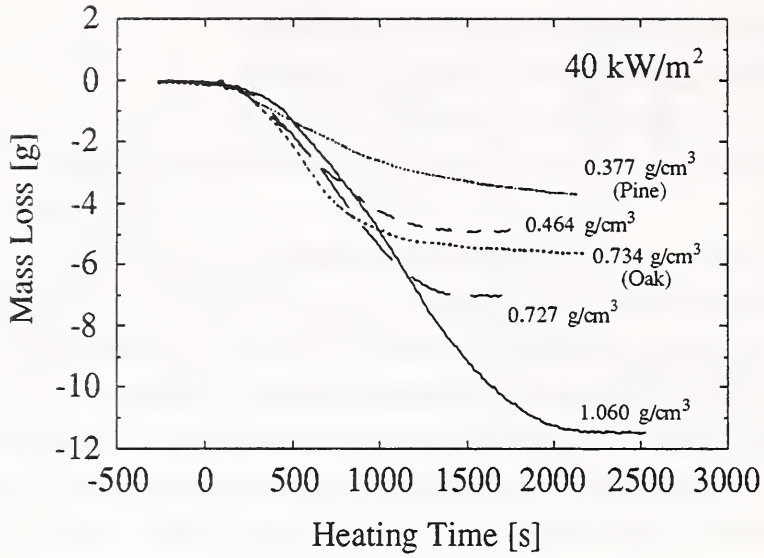

Figure 1. Mass loss as a function of time under simulated fire conditions for three different density cellulose samples and for two wood samples.

wood behavior, as far as combustibles release rates are concerned. The relatively constant pyrolysis front propagation velocity, implied by the nearly linear decrease in mass with time, is a consequence of the constant heat flux surface condition. A relatively constant temperature gradient between surface and pyrolysis front is maintained.

Attempts to model the observed simulated fire behavior led to a further battery of characterizattions of the cellulose powder, bulk cellulose and char samples by TGA, DSC, and other thermal analysis techniques. These tests led to several unexpected conclusions, including the following:

• *The kinetics of cellulose decomposition will probably not be fit by a simple single reaction rate law, in a fire spread situation. There is a shift in the apparent decomposition kinetics at near 600 K which is of importance in the range of heating rates of relevance to such problems.*

• *The surface absorptivity of a sample is a strong function of wavelength. It was found that in a relevant range of wavelengths, char absorptivity is far lower than had been earlier thought. (0.7-0.85).*

• *The values of char heat capacity are not well modeled by temperature-independent values. Also, values for cellulose and graphite are poor estimates for char properties.*

• *Thermal conductivity and diffusivity used in many previous modeling attempts have been at variance with the properties determined here.*

• *The heat of pyrolysis is a strong function of combustible volatiles yield, which is itself a strong function of mass transfer/heating rate conditions.*

This study has highlighted the critical importance of independent measurement of key solids thermal properties and chemical decomposition kinetics in developing quantitative descriptions of fire spread phenomena on charring materials. Many current models of the solids decomposition process can correctly predict key trends, but accurate quantitative prediction of combustibles release rates requires that much more careful attention be paid to solids properties than has historically been the case.

A THREE-DIMENSIONAL KINETIC MODEL FOR THE SWELLING OF INTUMESCENT MATERIALS

K.M. Butler, H.R. Baum and T. Kashiwagi
Building and Fire Research Laboratory
National Institute of Standards and Technology
Gaithersburg, Maryland 20899

An intumescent coating protects the underlying surface from fire by swelling into a thick insulating char. Design of intumescent materials has proceeded largely by systematic testing of a variety of formulations, since the mechanisms of physical, thermal and chemical behavior are not as yet well understood. Previous models of intumescent behavior [1]–[3] have treated the system as a one-dimensional heat transfer problem through a coating consisting of a char layer and a layer of virgin material separated by a thin pyrolysis zone. In this work, a fully three-dimensional, time-dependent numerical model combining the dynamics of the swelling process, the heat transfer through the coating, and the chemistry of gasification is described.

In the presence of fire, the intumescent material undergoes a series of chemical reactions that cause it to successively melt, generate a large volume of gas in a multitude of small bubbles, and eventually solidify as a multicellular insulating foam. To look at the swelling phenomenon, we first consider the dynamics of a single bubble as it expands and travels through the surrounding fluidized material. The viscosity of intumescent material is known to be a strong function of temperature, which varies considerably through the coating during exposure to fire. Under the influence of a viscosity gradient, an expanding bubble in a fluid of infinite extent feels a force in the direction of decreasing viscosity. Because the Reynolds number for the small bubbles of interest is small, the induced velocity field can be obtained analytically as a perturbation solution to the Stokes equation driven by the viscosity gradient force term. The bubble also feels a buoyancy force and pressure drag; the sum of all forces determines the net velocity of the bubble through the fluid.

Having determined the velocity field generated by a single bubble, we can now describe the swelling of the intumescent coating as the collective behavior of a large number of bubbles. Initially, the coating is represented by a rectangular volume of fluid with bubble nucleation sites randomly distributed throughout. The upper surface of the coating is exposed to a constant heat flux representing the fire source, and the temperature within the coating begins to rise. When the local temperature at a given bubble site exceeds a specified value, the bubble begins to expand. Its path through the fluid is determined by its own expansion rate, the local viscosity gradient, and the sum of the fields from all of the other bubbles, including a mirror image beneath the bottom surface to maintain the boundary condition of zero normal velocity at the rigid substrate. Bubble location and size are incremented in time according to a Runge-Kutta scheme. Merging of two overlapping bubbles is handled by replacing them with a single bubble of the combined volume located at the center of mass. The flexible upper surface of the intumescent material also feels the forces from all bubbles within the volume, and is pushed upward accordingly.

An early heat transfer model assumes simple conduction, with uniform conductivity

through the coating thickness. The detailed temperature field in the intumescent melt will eventually be solved using Lagrangian coordinates to take advantage of the simple initial geometry. The growth rate of each bubble is determined by the chemistry of gasification. An approximate expression for growth by diffusion in an oversaturated liquid-gas solution will be replaced by calculations that include the concentration of the blowing agent and local temperature and viscosity.

An example of the results from this three-dimensional model is shown in Figure 1. The upper surface is described by a grid, shown to the left, the location of whose nodes are incremented at each time step according to the instantaneous flow field. Note from the side view on the right that the bubbles near the bottom surface are much smaller than those near the top, since they have not had as much time to grow. At the time shown here, the temperature near the bottom surface is not yet hot enough to cause nucleation of the bubbles in this region.

This approach to the modeling of the dynamics and thermodynamics of an intumescent system has the attraction of providing a good physical picture of its behavior. Calculations for up to 10000 bubbles may easily be run on a workstation.

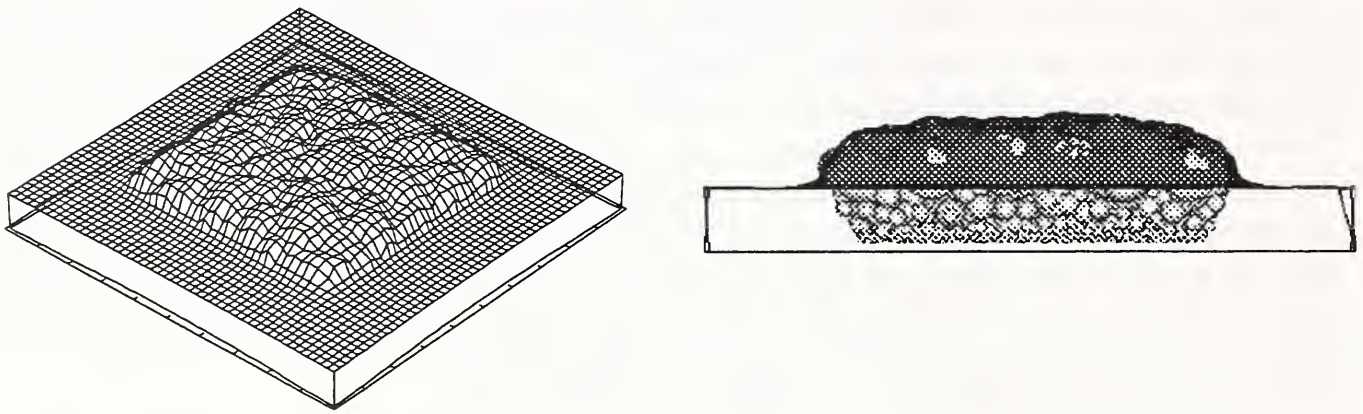

Figure 1: **Two views of an intumescent surface after development in time of 10000 bubble sites randomly distributed between (-3,3) in x and y directions in a 10×10×1 rectangular slab.**

References

[1] Cagliostro, D.E., Riccitiello, S.R., Clark, K.J. and Shimizu, A.B., "Intumescent Coating Modeling," *J. Fire & Flammability* 6:205–221 (1975).

[2] Anderson, C.E. and Wauters, D.K., "A Thermodynamic Heat Transfer Model for Intumescent Systems," *Intl. J. Engrg. Sci.* 22:881–889 (1984).

[3] Buckmaster, J., Anderson, C. and Nachman, A., "A Model for Intumescent Paints," *Int. J. Engng. Sci.* 24:263–276 (1986).

A MODEL FOR THE BURNING OF A HORIZONTAL SLAB OF WOOD: STATUS REPORT

K. Steckler, A. Hamins, and T. Kashiwagi
Building and Fire Research Laboratory
National Institute of Standards and Technology

We are in the process of developing a burning-rate model for char-forming materials. Currently, the combustion of a horizontal slab of wood, exposed to an external radiant source, is being modeled in terms of two coupled sub-models which simulate gas and solid (condensed) phase processes. Although there are still problems with the solid-phase model, the results to date are encouraging.

Gas Phase Model: The algorithm which is used to model the gas phase phenomena has been described previously (Hamins et al., 1992). It is a simple global model which predicts the mass burning flux for pool fires burning in a quiescent environment. The model assumes constant bulk properties such as flame temperature, soot volume fraction, and species concentrations. The computational procedure requires knowledge of the combustion properties of a fuel (the radiative heat loss fraction, the combustion efficiency, and a characteristic soot volume fraction in the flame) and fuel properties such as the stoichiometry, heat of vaporization, heat capacity, and boiling point. The combustion properties can be characterized by a single variable, the smoke point height of the fuel (Tewarson, 1988). The smoke point can also be correlated to a characteristic soot volume fraction for a pool fire.

For simplification, this model treats wood as a single component fuel, with the gas phase combustion properties invariant as a function of time after ignition.

An average component-weighted heat of combustion for Douglas Fir was found to be 12.6 kJ/g. This is in contrast to the bomb calorimeter results which yield values from 17 to 22 kJ/g for air-dried soft woods (Domalski et al., 1978). The bomb calorimeter heat of combustion results vary strongly with water content and can be as low as 5 kJ/g (Domalski et al., 1978). Cone calorimeter measurements (described below) gave a 12 kJ/g heat of combustion for the conditioned Douglas Fir sample. Thus, the combustion efficiency χ_a can be estimated as $\chi_a \approx 12/12.6 = 0.95$.

The radiative heat loss fraction χ_r and f_v were estimated using the relationship between the combustion properties and the smoke point (Tewarson, 1988). The smoke point height of wood (estimated as 16 cm) and χ_r were determined using Tewarson's correlations (1988) and f_v was estimated from pool fire results (Bard and Pagni, 1981) as a function of the fuel smoke point height. For simplicity and because few data exist regarding the effect of scale, the current gas phase model assumes that the combustion properties are invariant with scale over the range of interest.

Solid Phase Model: The model we are investigating (Atreya, 1983) treats the solid as an opaque, one-dimensional, locally reacting body, with finite thickness and density-dependent thermal properties. The local density is determined by a first order Arrhenius reaction. Gasification products from any location within the solid are assumed to be transported instantaneously to the exterior of the solid.

The governing equation is basically the heat conduction equation with the addition of the following source/sink term:

$$\frac{\partial \rho_s}{\partial t} \left[\Delta H_v - C(T - T_o) \right] \quad (1)$$

where ρ_s is the density of the solid, t is time, ΔH_v is the heat of pyrolysis, C is a constant comprising the specific heats and densities of the virgin, char, and volatile materials, T is the temperature of the solid, and T_o is the initial temperature of the solid. Note that the heat of pyrolysis term (the first term) in the bracket is an energy sink, whereas the second term is an energy source. Consequently, a net exothermic condition occurs when T reaches a certain level (about 400°C for the current calculations in which the heat of pyrolysis was 125 kJ/kg).

Figure 1 shows the results of gasification calculations made with this model. The solid curve was generated using a value of C = 0.37, which was determined from typical values of wood, char, and volatile properties. The second peak on this curve is larger and the time scale is shorter than expected from experiment. The dotted curve in the figure is closer to what is observed experimentally. The latter curve was generated by setting C = 0, which is equivalent to assuming that the enthalpy carried away by the volatiles is equal to that gained as a result of change from the solid to the char material. Although this is not a valid assumption, the results illustrate that the second peak is very sensitive to the physical properties of the components. Other calculations have shown that the second peak is sensitive to the rear-face boundary condition.

Currently we are assessing these and other sensitivities with the intent of reporting our findings as part of this presentation.

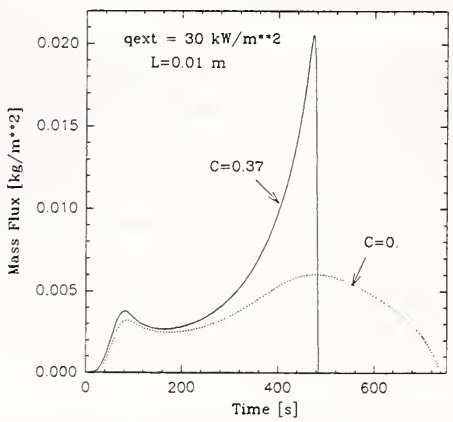

Figure 1. Calculated gasification rates

References

Atreya, A. (1983), "Pyrolysis, Ignition and Fire Spread on Horizontal Surface of Wood," Ph.D. Thesis, Harvard University, Cambridge, MA. Also published as National Bureau of Standards report, NBS-GCR-83-449, March 1984.

Bard, S. and Pagni, P.J., J. Heat Transfer, **103**, 357-62 (1981).

Domalski, E.S., Evans, W.H., and Jobe, T.L., "Thermodynamic Data for Waste Incineration," pp. 105-114, NBSIR 78-1479, US Department of Commerce, Washington, D.C., August, 1978.

Hamins, A., Steckler, K., and Kashiwagi, T., Burning Rate Project Progress Report, September, 1992.

Orloff, L., and De Ris, J., "Froude Modeling of Pool Fires," Factory Mutual Research Corp, Report No. RC81-BT-9, 1983.

Predicting The Burning Rate of Thermoplastic-like Materials in the Cone Colorimeter

D. Hopkins, B. Rhodes* and J. Quintiere

Department of Fire Protection Engineering
College of Engineering
University of Maryland College Park
College Park, MD 20742, USA

ABSTRACT

This study has sought to derive and utilize formulas to predict ignition and transient burning rate in the Cone Calorimeter. It is currently directed at thermoplastic-like materials that have been approximated to decompose from a solid to a vapor by simple surface phase change. Currently we have examined PMMA (cast), nylon 6/6, polyethylene, and polypropylene. The formulas developed have also been used to deduce material properties, as well as to predict the results of ignition and burning rate under various external radiant heat fluxes. It has been found that PMMA, burning in the Cone Calorimeter, experiences a nearly constant flame heat flux of 37 kW/m^2. The results for the other materials are as follows: Nylon - 30 kW/m^2; Polyethylene - 25 kW/m^2; Polypropylene - 14 kW/m^2.

The formula applied for ignition is given below:

$$t_{ig}=\frac{2}{3}(k\rho c)\frac{(T_{ig}-T_o)^2}{(\dot{q}'')^2} \quad (1)$$

It is an approximate result that departs somewhat from a more complete analysis by Abu-Zaid and Atreya [1]. Results for the materials examined are shown in figures 1 & 2.

The formula applied to predict burning rate is given as:

$$\dot{m}''\Delta H_v=\dot{q}''-\frac{2k}{\delta}(T_v-T_o) \quad (2)$$

and,

$$t-t_{ig}=\frac{\delta_s^2}{6\alpha}\frac{\Delta H_v}{L}\left[\frac{\delta_{ig}-\delta}{\delta_s}-\ln\left(\frac{\delta_s-\delta}{\delta_s-\delta_{ig}}\right)\right] \quad (3)$$

where,

$$\delta_s=\frac{2k}{c}\frac{L}{\dot{q}''},\ a\text{-}steady\text{-}value \quad (4)$$

and,

$$L=\Delta H_v+c(T_v-T_o),\ the\text{-}heat\text{-}of\text{-}gasification. \quad (5)$$

Examples of the predicted results are shown in figures 3 & 4.

* Current adress: Hughes Associates Inc, 6770 Oak Hall Lane, Columbia, MD 21045, USA.

REFERENCES

[1] Abu-Zaid, M. and Atreya, A., "Effect of Water on Piloted Ignition of Cellulosic Materials", National Institute of Standards and Technology, NIST-GCR-89-561, February, 1989.

[2] Rhodes, B.T., Burning Rate and Flame Heat Flux for PMMA in the Cone Calorimeter", University of Maryland College Park,May, 1994.

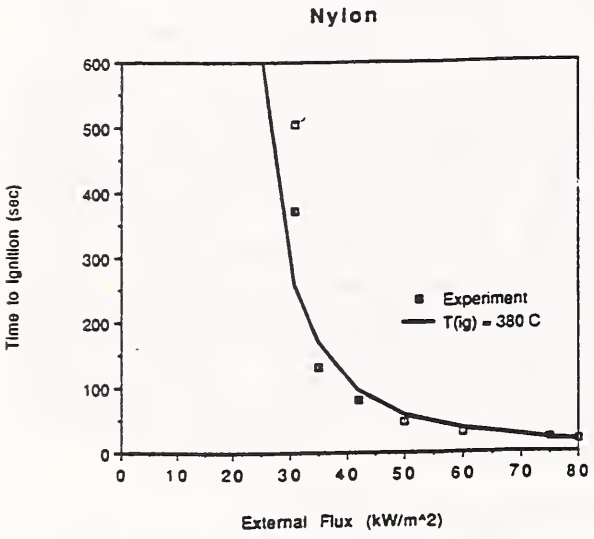

Figure 1: Calculated and measured ignition time of Nylon 6/6 as a function of external heat flux.

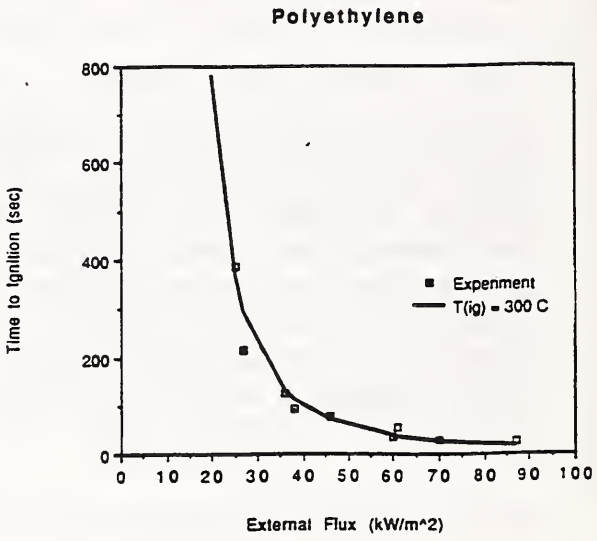

Figure 2: Calculated and measured ignition time of Polyethylene as a function of external heat flux.

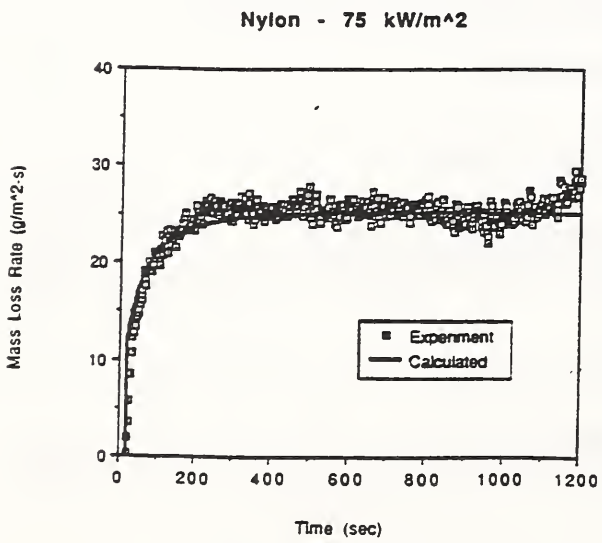

Figure 3: Calculated transient mass loss rate of Nylon with a 75 kW/m^2 external heat flux.

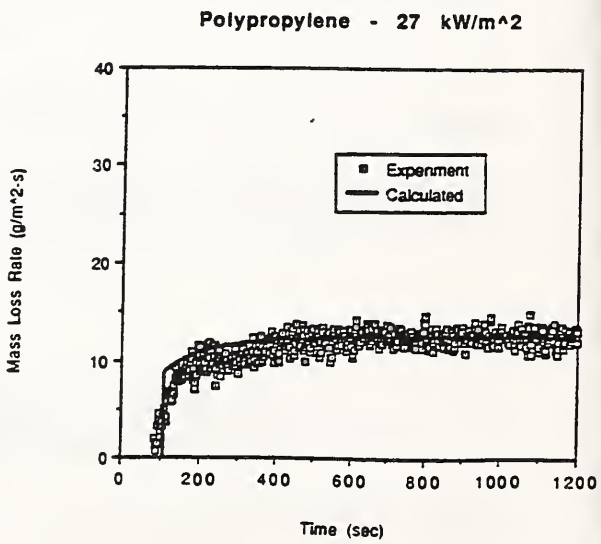

Figure 4: Calculated transient mass loss rate of Polypropylene with a 27 kW/m^2 external heat flux.

The Synthesis, Characterization, and Systematic Fire Safety Evaluation of High Volume and Specialty Hydrolytically Stable Phosphine Oxide Containing Polymeric Materials

J.E. McGrath, T.H. Yoon, D. Knauss, I.W. Yuan
Department of Chemistry
NSF Science and Technology Center: High Performance Polymeric Adhesives and Composites
Blacksburg, Virginia 24061-0344

Introduction: The research is attempting to determine whether or not chemically incorporated hydrolytically stable phosphorus systems can produce major improvements in fundamental fire resistant behavior. This chemically incorporated approach contrasts with the normal industrial method of physically adding fire retardants to the material systems. The disadvantage of the current approach includes the ideas that mechanical properties are impaired by the physical additives. Secondly, the additives may be extractable under conditions of use, possibly even producing unattractive, toxic byproducts. In contract, the chemically incorporated systems will not be extracted by detergents or subjected to environmental degradation by normal humidity in the air. Preliminary small scale burning tests and dynamic thermogravimetric analysis methods have been very encouraging. The NIST project is the first effort achieving a more fundamental understanding through the use of cone calorimetry methodologies, which permit determination of heat release rate, heats of combustion, smoke generation, and carbon monoxide generation.

Experimental and Discussion: During the past year it has been possible to synthesize a number of triphenyl phosphine oxide containing monomers, including the diamine, the dicarboxylic acid, the bisphenol, and the diglycidyl ether, and to use these monomers to prepare polyesters, polyamides, polycarbonates, and to generate epoxide networks. The structures of the most utilized monomers are provided below.

Polyamides have been generated which contained 10, 20, and 30 weight percent of the corresponding triphenyl phosphine oxide dicarboxylic acid. **The interest here was the possibility of making a semicrystalline high volume fiber forming material which would show inherent flame resistance.** Briefly, the heat release rate and heat of combustion were definitely decreased by the introduction of the phosphine oxide comonomer (Figure 1). Polycarbonates are also high volume engineering thermoplastics and it was of great interest to investigate whether the phosphine oxide bisphenol could be synthesized and copolymerized with the high volume bisphenol-A component. The initial results on copolymerization of the phosphine oxide bisphenol with bisphenol-A under commercial polycarbonate synthesis conditions have been quite promising. Tough, ductile, transparent materials have been obtained which are compression moldable. An increase in char yield as a function of phosphine oxide bisphenol has been realized. These samples are currently being prepared for evaluation by cone calorimetry. The efforts in these two areas are more thoroughly summarized in two papers which have been prepared for presentation at the American Chemical Society meeting on fire resistant materials in August of this year.

Epoxy diamine cured networks have also been investigated (Figure 2, Figure 3, and Table 1). These systems are more or less the backbone of aerospace matrix resin materials and fire resistance improvement is of great interest for aircraft interiors and also for marine applications. The characteristics of 30 mol percent BAPPO cured Epon resins were evaluated by an initial study by cone calorimetry. The resulting networks, even with only 30 percent of the curing agent containing phosphorus, were moderately encouraging and heat and combustion reduction for this system was demonstrated.

At this point it has been demonstrated that the phosphorus containing materials show a significantly higher char yield than their non-phosphorus conventional counterparts, as shown in Figure 3 below. Other phosphorus containing monomers with an increased concentration of phosphorus are being investigated in order to determine whether the increased phosphorus content and decreased aromatic structure will improve both heat release rate and at the same time diminish carbon monoxide generation.

Acknowledgments: This research was supported by the National Institute of Standards and Technology, Grant No. 70NANB3H1434, with T. Kashiwagi of the Building and Fire Research Laboratory serving as Scientific Officer.

References

Wan, I-Yuan, Kashiwagi, T., and McGrath, J. "Synthesis, Characterization and Flame Retardancy Behavior of Triaryl Phosphine Oxide Containing Nylon 6,6 Copolymers," *Polymeric Materials: Science and Engineering*, 71, 233, 1994.

Knauss, D., Kashiwagi, T. and McGrath J. "Copolycarbonates Containing Hydrolytically Stable Phosphine Oxide Comonomers," *Polymeric Materials: Science and Engineering*, 71, 229 1994.

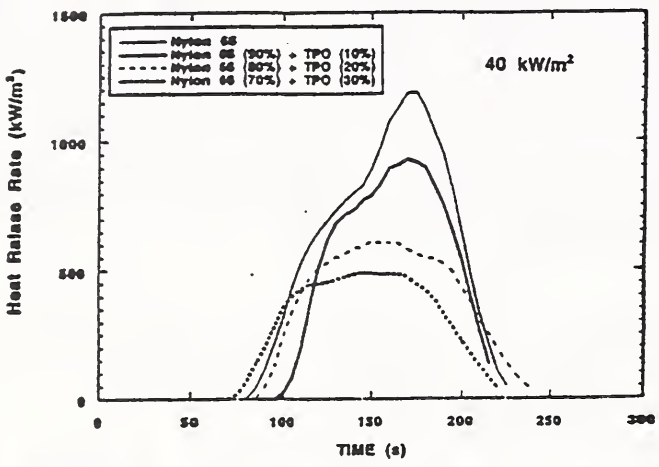

Figure 1: Heat Release Rate of Triaryl Phosphine Oxide Containing Nylon 6,6, Copolymers

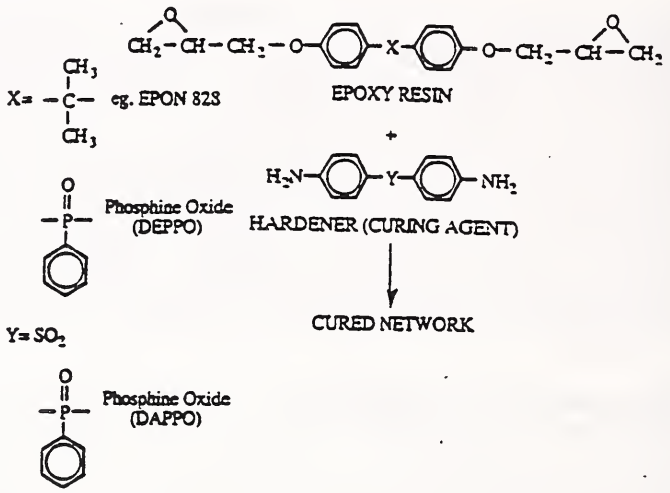

Figure 2: Development of Fire Resistant Cured Epoxy Networks Matrix and Adhesive Materials

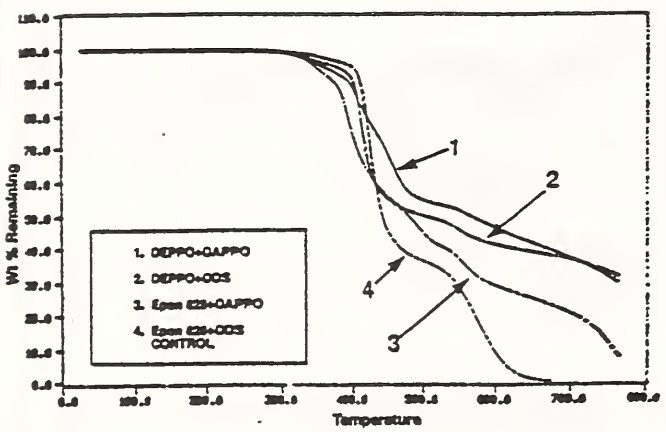

Figure 3: High Char Yields are Generated when New Epoxy Polymers are Degraded in Air

Epoxy Sample	Weight Remained		
	at 600°C	at 700°C	at 760°C
EPON 828=DDS	8.4%	0%	0%
EPON 828+DAPPO	29.0%	20.6%	8.25%
EPON 828+DAMPO	34.9%	26.1%	20.3%
EPON 828+BAPPO	37.5%	29.2%	21.6%
EPON 828+BAMPO	47.3%	38.6%	31.8%

Table 1: Thermal Stability of Epoxy Polymers 1

FIRE HARDENING OF COMPOSITE SYSTEMS

By
A.Tewarson
Factory Mutual Research Corporation, Norwood, MA.,
and
W. E.Haskell III
U.S. Army Research Laboratory,Watertown, MA

Composite systems consist of about 60 to 80 % of light weight high strength-high modulus reinforcing fibers and about 20 to 40 % of specialty resin systems. They have excellent mechanical properties and high strength-to weight ratio and are being used at an accelerated rate in aerospace, marine, aircraft, defense, automobile, and other industries. The resins release heat and various types of products during pyrolysis and combustion, there is thus a desire to fire harden the composite systems.

Fire hardening of materials increases the resistance to ignition and fire propagation with a reduction in the generation rates of heat, toxic and corrosive products and smoke. The resistance to ignition is determined from the relationship between the time to ignition (t_{ig}) and the external heat flux ($\dot{q}''_e$), such as the one for the thermally thick materials:

$$\sqrt{1/t_{ig}} = (\dot{q}''_e - \dot{q}''_{cr})/\Delta T_{ig}\sqrt{k\rho c_p} \quad . \qquad (1)$$

where $\dot{q}''_{cr}$ is the *Critical Heat Flux* (kW/m^2), ΔT_{ig} is the ignition temperature above ambient (K), **k** is the thermal conductivity (kW/m-K), ρ is the density (kg/m^3), and c_P is the specific heat (kJ/kg-K), t_{ig} is in sec and $\dot{q}''_e$ is in kW/m^2.

Fire hardening is achieved by increasing the values of $\dot{q}''_{cr}$ (*Critical Heat Flux*) and $\Delta T_{ig}\sqrt{k\rho c_p}$ (defined as the *Thermal Response Parameter, TRP*). Data for the composite systems, measured in our laboratory, are shown in Fig. 1. The TRP values increase with decrease in the resin fraction and increase in the fiber fraction. The TRP values are highest for the graphite fiber, intermediate for the glass fiber and lowest for the kevlar fiber based composite systems. Moderate variations in the measured ρ and ΔT_{ig} values for the composite systems with the different fiber fractions have small effect on the TRP values. The c_P values of the fibers do not show much variations either. Thus the value of k appears to have a dominant effect on the TRP value. The k values for graphite, glass and kevlar are 5.02, 1.03, and 0.200x10^{-3} kW/m-K respectively. Further fire hardening of composite systems could be achieved by using high k value fibers such as boron, beryllium, aluminum oxide (sapphire, 24 x 10^{-3}), boron carbide, silicon carbide (85x10^{-3}), and silicon nitride. The restraining factor for the use of these fibers would be their end-use compatibility and cost of the composite systems.

The increase in the resistance to fire propagation is determined by the flame spread rate beyond the ignition zone. For thermally thick materials, flame spread rate is proportional to the ratio of the flame heat flux transferred ahead of the pyrolysis front and the TRP value. The flame heat flux is expressed as a function of the heat release rate, such as the following expression, one of the several semi-empirical relationships for the flame spread rate:

$$\sqrt{u} \propto \{(\chi_{rad}/\chi_{ch})\,\dot{Q}'_{ch}\}^{1/3}/\Delta T_{ig}\sqrt{k\rho c_p} \qquad (2)$$

where u is the flame spread rate; $\dot{Q}'_{ch}$ is the chemical heat release rate in the actual combustion during fire propagation (kW/m), and χ_{ch} and χ_{rad} are the combustion efficiency and radiative component of the combustion efficiency respectively. Our experimental data show that for flames with high flame radiation and lower combustion efficiencies, typical of large-scale fires, $\chi_{rad}/\chi_{ch} \approx 0.40$. From Eq. 2, u is expected to be affected strongly by the first power TRP term than by the one-third power $\dot{Q}'_{ch}$ term. Small and large-scale flame spread experiments performed in our laboratory for variety of material systems show that flames do not propagate beyond the ignition zone for $\sqrt{u}\,x10^3 < 7$ (*defined as the*

non-propagating fire). For $\sqrt{u}\ x10^3 > 7$, flame spread is self-sustained beyond the ignition zone (*defined as the propagating fire*). The results for the propagating and non-propagating fires from our upward flame spread experiments are indicated by the numbers in Fig. 1. The results show that composite systems based on the kevlar and glass fibers (≥70% by weight) need modifications of the resins for fire hardening. Composite systems based on graphite fibers (≥ 60 % by weight) provide adequate fire hardening. Use of boron, beryllium, aluminum oxide (sapphire), boron carbide, silicon carbide and nitride would further enhance fire hardening.

Heat of combustion and yields of products and their ratios with the heat of gasification are used to assess the potential of a resin for thermal and nonthermal hazard. Data for the heat of combustion and yields of CO and smoke, measured in our study for the composite systems and ordinary combustibles, are listed in Table 1. The data for the ratios have been reported in various publications. As most of the composite systems examined in our study have some form of aromatic and halogenated ring structures, the data in Table 1 for the composite systems show that their combustion behavior is similar to the behavior of polymers with low combustion efficiency and high generation efficiencies of CO and smoke, i.e., aromatic (polystyrene) and halogenated (polyvinylchloride) polymers.

For composite systems with non-propagating fire behavior, the generation rates of heat and fire products are limited to the ignition zone, being significantly less than the rates for the systems with propagating fire behavior. We have quantified generation rates of heat and smoke, toxic (CO) and corrosive products for propagating and non-propagating fires of composite systems to support the concepts discussed here.

Table 1
Chemical Heat of Combustion and Yields of CO and Smoke

Composite system	ΔH_{ch} (MJ/kg)	y_{co} (kg/kg)	y_{smoke} (kg/kg)
Glass Fiber Based Composite Systems			
Polyester1-30%	17.9	0.055	0.070
Polyester2-30%	16.0	0.039	0.054
Polyester3-30%	9.3	0.102	0.068
Polyester4-35%	11.9	0.166	0.128
Epoxy1-35%	10.0	0.113	0.188
Epoxy2-35%	10.2	0.132	0.094
Epoxy3-24%	18.6	0.056	0.121
PPS-16%	17.0	0.133	0.098
Phenolic-20%	11.0	0.066	0.023
Kevlar Fiber Based Composite			
Phenolic-16%	14.8	0.025	0.041
Graphite Fiber Based Composite Systems			
Polycyanate-27%	18.9	0.058	0.102
Epoxy-29%	17.8	0.046	0.107
Ordinary Combustibles			
Wood (Red Oak)	12.4	0.004	0.015
Polyethylene	38.4	0.024	0.060
Polystyrene	27.0	0.060	0.164
Polyvinylchloride	5.7	0.063	0.172

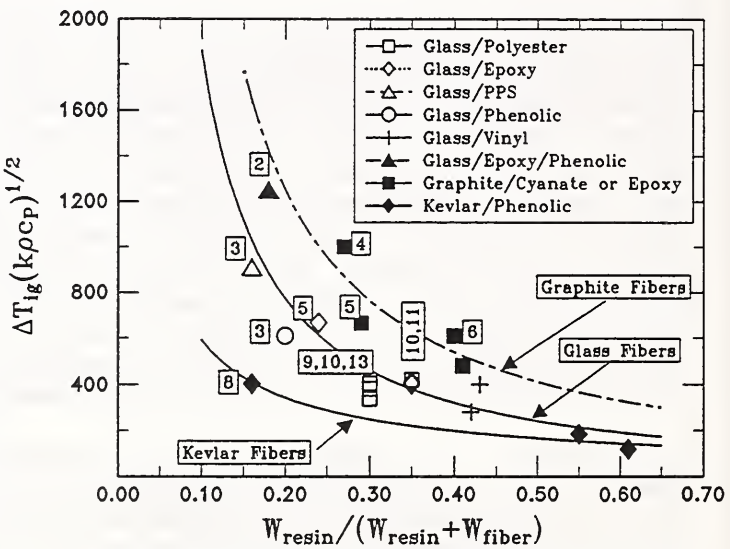

Figure 1. Ignition Resistance Versus Resin Fraction for Composite Systems. Numbers Less than 7 in the Figure Represent No Self-Sustained Flame Propagation. Numbers Greater than 7 Represent Self-Sustained Flame Propagation Beyond the Ignition Zone.

Furniture Mock-up Performance Under California Technical Bulletin 133 Test Conditions

T. Ohlemiller and J. Shields
Building and Fire Research Laboratory
National Institute of Standards and Technology

Introduction

Fires involving soft furnishings such as upholstered chairs and mattresses continue to play a prominent role in U. S. fire losses. This is a multi-faceted problem that has been addressed, over the years, from several directions with some significant success. Fire deaths and injuries involving these products show a substantial decline over the past 15 years. One of the more recent developments in this area is the increasing acceptance of a test protocol (CB 133) developed at the California Bureau of Home Furnishings, intended for upholstered chairs utilized in public occupancies (hotels, hospitals, etc.). The protocol imposes quite restrictive limits on the response of a chair (or equivalent mock-up) to an arson-like ignition source (an 18 kW gas burner). Of particular interest here is the rate of heat release response to burner exposure since this effectively measures the size and threat of the resulting fire.

Imposition of CB 133 requirements poses a substantial challenge to the furniture industry, given the enormous variety of fabrics and chair styles it employs. There is a strong interest in the potential use of small-scale tests, such as rate of heat release measurement in the Cone Calorimeter, as predictors of full-scale behavior. The relation, for a variety of material combinations, between behavior in the Cone Calorimeter and in full-scale chair mock-ups is one facet of the present study. A major approach employed by the industry in attempting to pass the CB 133 requirements involves the use of a barrier layer of material enclosing the polyurethane cushioning. These barriers are not always successful in limiting the size of the fire. An examination of the mode of failure of these barriers is another facet of the current work.

Experimental

Seven fabrics, four barriers and two polyurethane foams were examined in tests of 27 material combinations. Full-scale mock-ups having four cushions (seat, back, two arms) were tested in the NIST Furniture Calorimeter to ascertain the rate of heat release as a function of time, during and after the standard 80 second exposure to the gas burner in the seat area. Five of the tests were replicated. Extensive visual documentation was utilized. In addition, two heat flux gages were placed on the seat area to measure the local flux history involved in fire development.

Cone Calorimeter tests were run in triplicate on all of the material combinations at the nominally standard external flux of 35 kW/m^2. Heat release rate behavior as a function of incident radiant flux was measured for three of the material combinations and one barrier/foam combination without a fabric on top. Lateral flame spread behavior of some of the material combinations was available from a previous study.

Results and Discussion

The full-scale tests frequently resulted in two rate of heat release peaks. The first typically came near the end of the gas burner exposure; the second, when it was significant, followed much later and was often higher, signifying failure of the barrier to stop progression of the fire to the point of substantial involvement of the polyurethane in the cushions. The first peak appeared to be dominated by the fabric behavior but that behavior was often quite complex, involving macroscopic movements of appreciable quantities of fabric melt on the chair surfaces. The second peak appeared to be the result of a single failure mechanism which involved the development of a self-feeding, polyurethane melt fire at the bottom of one or more of the cushions. Sufficient heat was transferred from the upwardly buoyant flames, through the intact barrier, to the foam inside so as to cause a continual flow of fuel (polyurethane melt) to the flames. Such fires were sometimes able to grow and achieve heat output peaks of up to several hundred kilowatts, depending on the fabric and barrier.

Figure 1 shows a plot of the value of the first peak of heat release in the full-scale tests versus the averaged behavior for a period of 60 seconds after ignition in the Cone Calorimeter (at 35 kW/m^2). Note that the units on the two axes differ; the ordinate is not per unit area. The various symbols pertain to differing fabric and foam combinations; where the same symbol recurs, the only difference is the barrier. There clearly is a tendency for the full-scale behavior to follow the small-scale behavior. However, the uncertainty in the relationship is obviously large, making it doubtful that this relation has practical use. The sources of this variability are under study as is the possibility of other simple relationships between small-scale and full-scale behavior.

FIG. 1 CORRELATION BETWEEN CONE RHR AND FIRST FULL SCALE RHR PEAK

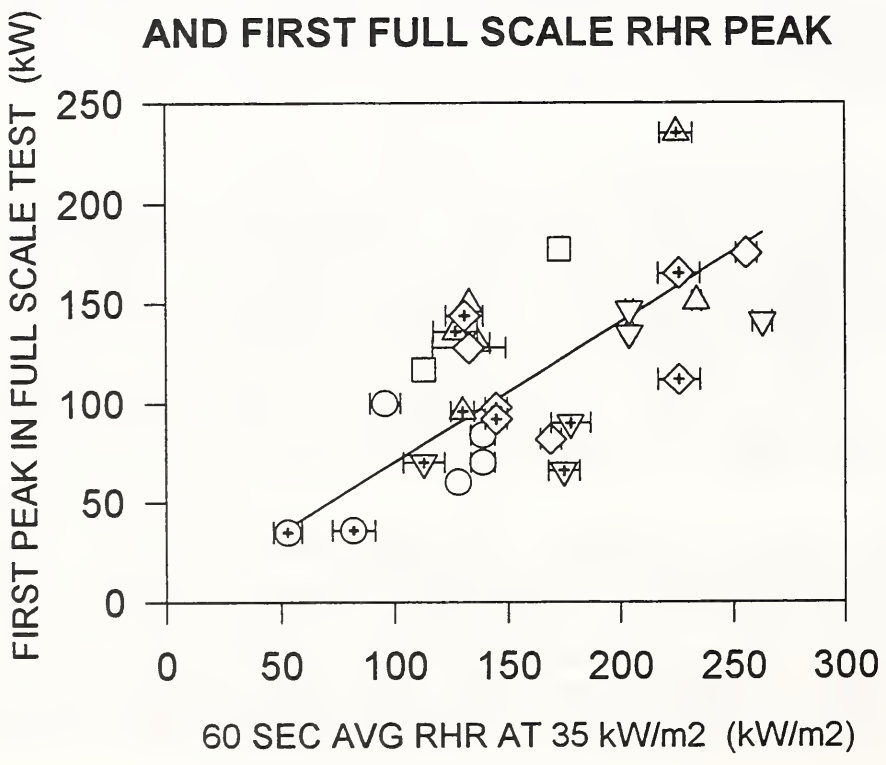

Effect of Ignition Location on Heat Release Rate of Burning Upholstered Furniture

Henri E. Mitler and King-Mon Tu

Building and Fire Research Laboratory
National Institute of Standards and Technology
Gaithersburg, MD 20899

Upholstered furniture has long been identified as the consumer product most frequently involved in home fires which result in personal injury or death. Hence an understanding of the way upholstered furniture performs when ignited, is desirable.

One aspect of furniture burning which has not received much attention is the possible dependence of the burning behavior on the location of the ignition. We selected four sites to investigate: (1) the center of the chair seat cushion, (2) lower center of the chair front, (3) lower center of the chair side, and (4) lower center of the chair back, as the four ignition locations for the current chair burn tests.

Based on previous furniture flammability studies, it has been found that the single most important characteristic, in terms of hazard, associated with upholstered furniture fires is the rate of heat release (RHR) history, especially the peak heat release rate.[1] We therefore concentrated on the rate of heat release history as a function of ignition location.

A series of twelve full scale chair burns were carried out inside the NIST full-scale fire test facility. Four kinds of full-size chairs were tested in our furniture calorimeter which, with its instrumented exhaust products collection system, can measure accurately fire heat release rates up to 700 kW.

The heat release rate was determined via oxygen consumption calorimetry. Other measured test data were CO concentrations, which is relevant to hazard from fires, mass loss rate from the weighing platform (needed to get the CO **yields**, and as a check on the RHR), and smoke production rates during the test period. A heat flux gauge was located 0.76 m from the chair front to monitor the radiative heat flux. The (flaming) ignition source was a propane gas tube burner of 10 kW capacity applied to the chair for sixty seconds.

The figure presents the heat release rate data, the peak heat release rate values and the times at which the peak heat release rate occurred for chairs of style C, with ignition at the four different locations. The heat release rate data were calculated based on the oxygen depletion and mass flow rate of exhaust gases through the exhaust duct.

The most striking effect on ignition-delay time is seen for chairs of style C, which used melamine-treated polyurethane foam. There the **shortest** delay before significant fire onset was about 10 minutes, generally enough time to alert occupants and permit extinguishment or escape. The rise to the peak RHR took another 4 minutes.

Ignition of the seat front (chair C4) almost failed to take place: although the fabric was ignited, the wood frame right under it acted as a heat sink, and failed to ignite at first. The burning then continued was largely smoldering but with a small sustaining flaming fire, and the transition to strong flaming only occurred after about 2200 seconds - i.e. about 36 minutes - when the cushion area was reached. The growth to the peak RHR was also somewhat slower here: it took another 5.3 minutes to reach the peak.

The principal conclusion of this study is that the location of the initial ignition can have a significant effect on the elapsed time to reach the peak heat release rate.

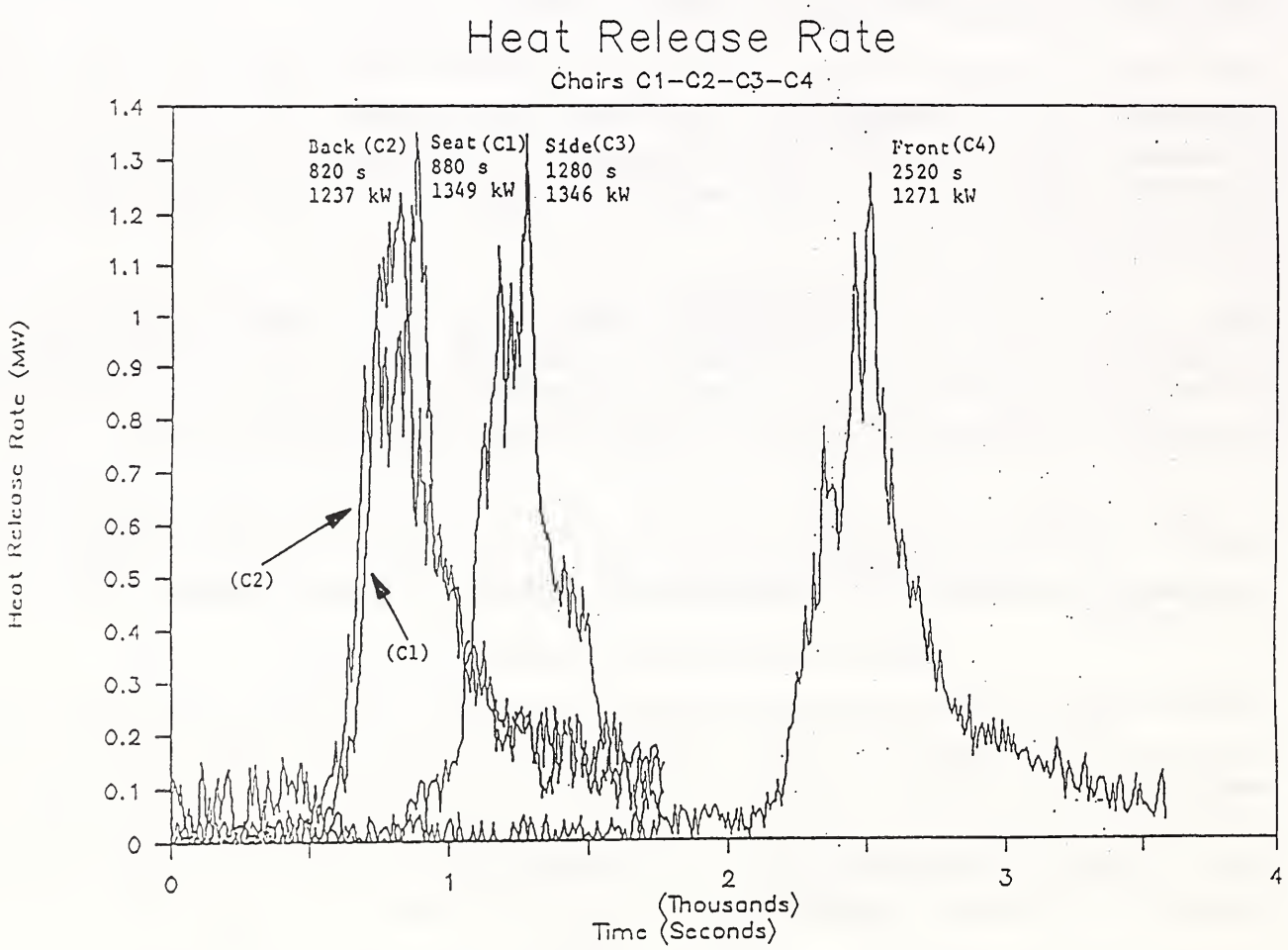

Figure 5. Heat Release Rate (Chairs C1, C2, C3 and C4)

References

1. V. Babrauskas and R.D. Peacock, "Heat Release Rate: The Single Most Important Variable in Fire Hazard," Fire Safety J. **18** (1992) 255-272

Experimental Study of the Optical Properties of Soot and Smoke

M. Y. Choi
Department of Mechanical Engineering
University of Illinois at Chicago
Chicago, IL 60607

G.W Mulholland, A. Hamins and T. Kashiwagi
Building and Fire Research Laboratory
National Institute of Standards and Technology
Gaithersburg, MD 20899

The accurate measurement of flame-generated particulates is a problem of current interest to researchers in the fire and combustion community. Within the flame, the soot concentration measurement is central to the study of soot growth [Santoro *et al.*, 1987; Harris and Weiner, 1983] and for radiant transport analysis [Choi *et al.*, 1994a]. In the post-flame region of large fires, particulate measurements are important in developing computational modeling of smoke plume movement [Evans et al, 1993; McGrattan, et al, 1993], in the detection of fires [Mulholland *et al.*, 1989], in assessing the reduction in visibility arising from a fire within a building [Mulholland, 1988; Peacock et al. 1993] and for estimating the health and environmental impacts [Benner *et al.*, 1990].

In the fire and combustion community, particulate concentrations are typically measured using light extinction techniques. However, it has been found that the accuracy of the measurements is sensitive to the choice of dimensionless extinction constant, K_e and the assumptions made regarding the light scattering behavior of particulates. The dimensionless extinction constant is calculated using reported values of refractive index along with the assumption of negligible scattering/absorption ratio. However, the reported refractive index can vary by a factor of two [Choi et al., 1994b] and the scattering to absorption ratio can be as high as 30% [Patterson et al., 1991]. These uncertainties can result in a factor of two variation in the calculated particulate concentrations. Thus, accurate measurement of the dimensionless extinction constant is necessary to improve the usefulness of the light extinction technique for determining concentrations of smoke-generated particulates.

Accurate determination of K_e is also important for improving current understanding of radiative and burning characteristics of large fires. Thermal radiation from the fire to the fuel surface is controlled by emissions from soot and product gases. Therefore, analysis of the burning characteristics of practical fires requires detailed information regarding the species and temperature distribution above the fuel surface.

The temperature measurements using ITWP technique is also very sensitive to the choice of dimensionless extinction constant and therefore suffers from the same degree of uncertainty as in the particulate concentration measurements. Compounding this is that all radiation heat transfer models use reported refractive index in determining the radiative characteristics of soot.

Thus, in order to improve the accuracy of the light extinction and ITWP techniques for use in combustion and fire applications, the dimensionless extinction constant must be determined accurately without relying on the available optical properties of soot. The focus of this study is on the development and the use of a new and innovative technique to measure K_e called Gravimetric-Sampling/Light-Extinction technique. This technique consists of isokinetically sampling the soot

at a known flow rate, measuring the mass of soot collected and determining the density of soot using helium pycnometry. The optical extinction measurements will be calibrated with the gravimetric soot volume fraction to calculate K_e. In this manner the magnitude and the spectral variation of K_e can be determined without relying on the refractive index of soot or making drastic assumptions regarding its scattering characteristics. Preliminary experiments demonstrated that K_e can be measured with an uncertainty less than 15% using the GSLE technique.

1. Benner, B.A., Bryner, N.P., Wise, S.A., and Mulholland,G.W., *Environmental Science and Technology*, **24**:1418 (1990).
2. Choi, M.Y., Hamins, A., Rushmeier, H. and Kashiwagi, T., "Simultaneous Optical Measurements of Soot Volume Fraction, Temperature and CO_2 in Heptane Pool Fire", Twenty-Fifth Symposium (Int'l) on Combustion, Accepted (1994a).
3. Choi, M.Y., Hamins, A., Mulholland, G.W. and Kashiwagi, T., "Simultaneous Optical Measurements of Soot Volume Fraction and Temperature", *Comb. Flame*, accepted (1994b).
4. Choi, M.Y., Mulholland, G.W., Hamins, A. and Kashiwagi, T., "Comparisons of Soot Volume Fraction Measurements Using Gravimetric and Light Extinction Techniques", *Comb. Flame*, submitted (1994c).
5. Evans, D.D., Walton, W.D., Baum, H.R., Rehm, R.G. and Teynnyson, E.J., "Smoke Plumes from In Situ Burning of Oil Spills", Proceedings of the Eighth Symposium on Coastal and Ocean Management, New Orleans, LA, p. 3409, 1993.
6. Harris, S.M. and Weiner, A.M., *Comb. Sci. Tech.*, **31**:156 (1983).
7. Klassen, M., Ph.D. Thesis, University of Maryland, Department of Mechanical Engineering (1992).
8. McGrattan, K.B., Baum, H.R. and Rehm, R.G., "Smoke Plume Trajectory Modeling", Annual Conference on Fire Research, p. 39, 1993.
9. Mulholland, G.W., "Soot Production and Properties", SFPE Handbook of Fire Protection Engineering (P.J. DiNenno, Ed.), p.368 (1988).
10 Mulholland, G.W., Henzel, V., and Babrauskas, V., "Proceedings of the Second International Symposium on Fire Safety Science", (T. Wakamatsu, Y. Hasemi, A. Sekizawa, P.G. Seeger, P.J. Pagni, and C.E. Grant, Eds) Hemisphere, N.Y., p.347 (1989).
11. Peacock, R.D., Jones, W.W., and Bukowski, R.W., "Verification of a Model of Fire and Smoke Transport", *Fire Safety Journal*, **21**, 89, 1993.
12. Santoro, R.J., Yeh, T.T., Horvath, J.J. and Semerjian, H.G., *Comb. Sci. Tech.*, **53**:89 (1987).

SOOT KINETICS/RADIATION INTERACTIONS IN METHANE/AIR DIFFUSION FLAMES

Y. R. Sivathanu and J. P. Gore
School of Mechanical Engineering
Purdue University
West Lafayette, IN 47907-1003

Introduction

Radiation heat transfer from flames depends on the instantaneous soot volume fractions and temperatures. The major obstacle to obtaining accurate soot volume fraction predictions in flames is the strong coupling between the finite rate kinetics of soot processes and radiation [1,2]. Detailed models of soot kinetics cannot be incorporated in turbulent flame studies due to the limitations of computer resources. Therefore, many studies have concentrated on simplified global kinetics models incorporating soot nucleation, growth and oxidation mechanisms[3,4]. The local temperatures needed for the soot kinetics calculations were obtained using simplified global radiation models. However, in strongly radiating flames it has been shown that the radiation and soot kinetics calculations need to be coupled to accurately predict observed soot volume fractions[2]. The degree of this coupling in weakly radiating flames, where radiation is predominantly from gas species molecules rather than soot, has not been studied. The objective of the present work is evaluate this coupling of radiation and soot kinetics in weakly radiating flames by using the simplified soot kinetics model of Ref. [4] along with a narrow-band radiation model [5].

Theoretical Methods

The parabolic boundary layer equations for an axisymmetric laminar reacting flow [6] are:

$$\frac{\partial}{\partial x}(\rho u \Phi) + \frac{1}{r}\frac{\partial}{\partial r}(r \rho v \Phi) = \frac{1}{r}\partial\frac{\partial}{\partial r}(r\frac{\mu}{\sigma_\Phi}\frac{\partial \Phi}{\partial r}) + S_\Phi \qquad (1)$$

where Φ represents velocity, mixture fraction, enthalpy, soot mass fraction and soot particle number density respectively. ρ is the density, μ is the viscosity, σ_Φ are the Prandtl/Schmidt numbers, and S_Φ are the source terms [2]. x and r are the streamwise and radial co-ordinates and u and v are the streamwise and radial velocities. The source term for the soot mass fraction equation includes soot oxidation due to O_2 [4] and OH [3]. The concentrations of major gas species are obtained from generalized state relationships and that of OH and C_2H_2 from Ref. [7]. The radiation source term was solved using a multi-ray method [2] in conjunction with the RADCAL program of Ref. [5].

Results and Discussion

The efficacy of the calculation procedure has been evaluated previously by application to strongly radiating acetylene/air diffusion flames[2]. The details of the coupling between radiation and finite rate soot kinetics in weakly radiation flames are highlighted in the present work. Figure 1 shows radial profiles at three representative axial locations in a methane/air laminar diffusion flame. The calculated stochiometric flame height was 170 mm. Close to the burner exit, at a height of 50 mm, soot formation from acetylene molecules takes place due to the rich stochiometry. This is close to the region of peak soot volume fractions and the local radiative fraction is around 8% at the center-line. Higher up, the soot oxidizes primarily due to reaction with the OH radicals and at a height of 100 mm, the soot levels are a factor of 10 lower. Radiative heat loss fraction, primarily due to contributions from the gas molecules has increased to around 10% and at an axial location of 160 mm, almost all the soot has oxidized with the radiative fraction reaching approximately 20% locally. Therefore, there is substantial variation in local radiative fractions and soot volume fractions over the entire flame.

Fig. 2. shows the effect of the variation in local radiative fraction on the soot volume fractions. The variation of peak soot volume fraction with axial distance is shown for four different calculations. The first calculation shown by the solid line is the fully coupled calculations including OH oxidation. The soot levels increase to about 0.07 ppm and then decrease rapidly to very low values due to OH oxidation at around two-thirds the flame height. The second calculations shown by the long dashed lines are fully coupled calculations neglecting OH oxidation. The soot levels rises to about 0.11 ppm and then decrease very slowly with soot being emitted from the tip of the flame contrary to experimental observations, highlighting the importance of OH oxidation. The last two calculations shown by the short dashed line and the dotted line assume a fixed radiation heat loss of 20% and 5% respectively. If a value of 20%, which has been observed experimentally, is used, the peak soot volume fraction reaches only about 0.03 ppm and oxidation is much slower. This is due to lower temperatures restricting both soot growth and oxidation. To match the peak observed in the fully coupled calculations an unrealistically low value of 5% radiative fraction has to be used. This causes oxidation to more rapid, and the lack of coupling makes the growth slower as seen in Fig. 2.

Fig 3 shows the development of mixture fraction and peak radial radiative fraction as a function of axial distance. Close to the burner, the radiative fraction is zero and increase to around 18% at the flame height. Thereafter, it remains roughly constant at around 19% which is the expected values for laminar methane/air diffusion flames. If oxidation of soot from OH is excluded, there is very little effect on this radiative fraction indicating that radiation is predominantly from gas molecules since the soot levels are vastly different for the two cases.

Conclusion

The coupling of gas band radiation with soot production and oxidation terms is important for correctly predicting soot levels in weakly radiating flames. OH oxidation is primarily responsible for the destruction of soot these flames.

Acknowledgment: This work is supported by the National Institute of Standards and Technology with Drs. Anthony Hamins and Kermit Smyth serving as NIST scientific officers.

References:

[1] Kent, J. H., and Wagner H. Gg., 1984, Combust. Sci. Technol., **41**, p. 245.
[2] Sivathanu, Y. R. and Gore, J. P., 1994, Combust. Flame, **97**, p.161.
[3] Villasenor, R. and Kennedy, I. M, 24th Symposium (International) on Combustion, p. 1023 (1992).
[4] Leung, K. M., Lindstedt, R. P., and Jones, W. P., 1991, Combust. Flame, **87**, p. 289.
[5] Grosshandler, W. L., 1980, Int. J. Heat Mass Transfer, **23**, p. 1447.
[6] Patankar, S. V., and Spalding, D. B., 1970, "Heat and Mass Transfer in Boundary Layers," Intertext Books, London.
[7] Miller, J. H., and Smyth, K. C., "Species Concentrations versus Equivalence Ratio in CH_4/Air Co-flowing Diffusion Flame," Personal Communications (1989).

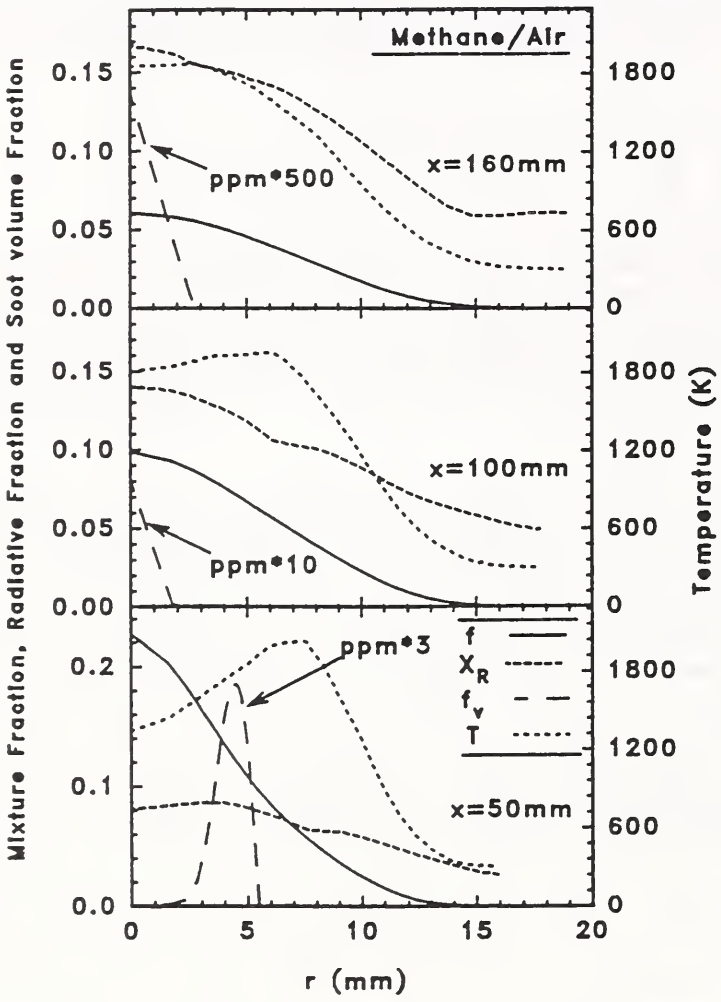

Fig. 1. Radial profiles of soot, mixture fraction, temperature and radiative fraction in a laminar methane/air diffusion flames

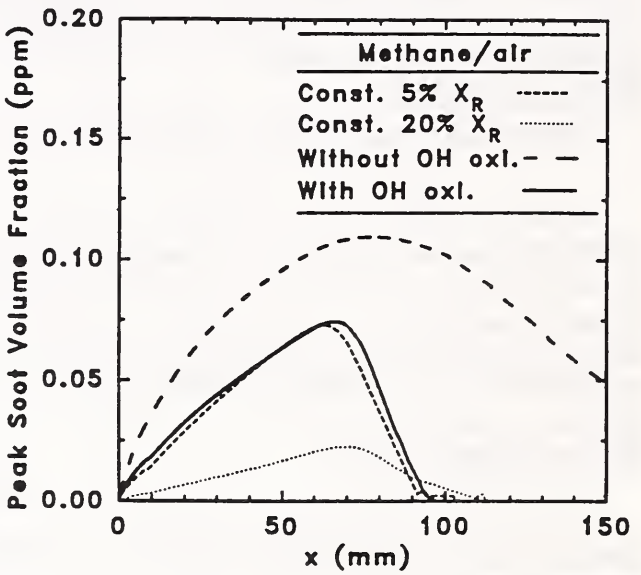

Fig. 2. Axial variation of peak soot volume fractions in a laminar methane/air diffusion flame.

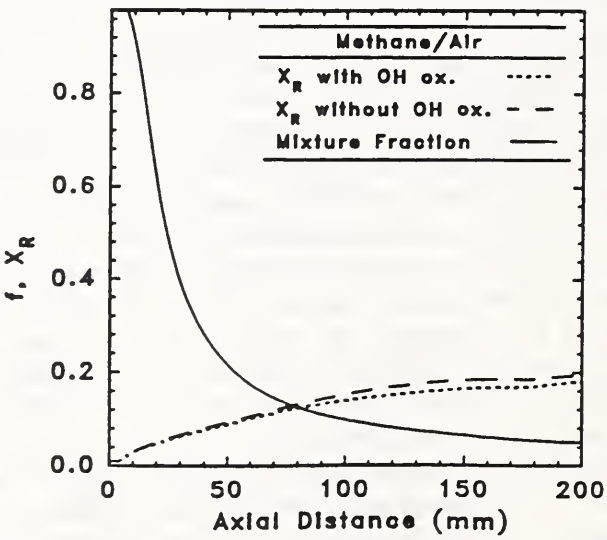

Fig. 3. Axial variation of mixture fraction and radiative fraction in a methane/air diffusion flame.

COMPUTATIONAL EVALUATION OF AN APPROXIMATE THEORY FOR THE OPTICAL PROPERTIES OF SOOT

Ü.Ö. Köylü and G.M. Faeth
Department of Aerospace Engineering
The University of Michigan
Ann Arbor, Michigan 48109-2118
and
T. L. Farias and M. G. Carvalho
Mechanical Engineering Department
Instituto Superior Técnico
1096 Lisbon, Portugal

Introduction. The absorption and scattering (optical) properties of soot are needed both to predict the continuum radiation properties of soot and to interpret nonintrusive optical measurements to find soot concentrations and structure. This is a challenging problem, however, because soot consists of small primary particles that combine into branched aggregates that exhibit neither simple Rayleigh nor Mie scattering behavior [1]. Nevertheless a potentially useful approximate theory for soot optical properties (denoted RDG-FA theory in the following) has been developed recently, based on the Rayleigh-Debye-Gans (RDG) scattering approximation while assuming that soot aggregates are mass-fractal objects [2-7]. In particular, recent measurements of both soot structure and scattering properties for soot aggregates found in flame environments have exhibited good agreement between RDG-FA predictions based on the structure measurements, and the scattering measurements [2,3]. Unfortunately, these soot populations involved relatively large soot aggregates so that it was not possible to adequately test RDG-FA theory in the small-angle (Guinier) regime where use of the RDG scattering approximation is least reliable. Thus, the objective of the present investigation was to undertake theoretical evaluation of RDG-FA theory, emphasizing the Guinier regime. The evaluation was based on computations using the ICP approach of Iskander et al. [8], which provides a more exact treatment of aggregate scattering in the Guinier regime than RDG-FA theory, by including effects of multiple and self-induced scattering. A full description of this study can be found in Farias et al. [9].

Theoretical Methods. Simplified RDG-FA predictions of soot optical properties were based on methods described in [2-7] but attention was focused on the approach of Köylü and Faeth [2] which extends the method of Dobbins and Megaridis [7] to provide an improved treatment of the large-angle (power law) regime.

The soot structure approximations of the RDG-FA and ICP calculations were the same. In addition, each primary particle constituted an ICP computational cell, which is satisfactory for primary particle optical size parameters $x_p \leq 0.4$ within the Guinier regime [9]. Present results were obtained as averages over various orientations of individual aggregates and populations of fractal aggregates of specified size (N primary particles), unless noted otherwise.

Aggregates were numerically simulated by cluster/cluster aggregation, following Jullien and Botet [10]. This involved starting with individual and pairs of primary particles, and attaching them to each other randomly. This procedure was used to form progressively larger aggregates but with the additional restriction that the aggregate fractal dimension, D_f, should be in the range 1.7-1.8 and the fractal prefactor, k_f, should be roughly 8 for $N > 8$ in order to match typical soot aggregate properties [1-3]. Some typical projected images of soot aggregates constructed in this manner are illustrated in Fig. 1 for N = 16, 64 and 256. The appearance of the aggregates varies considerably with direction of projection and from aggregate to aggregate within a population of given size; nevertheless, they are qualitatively similar to past observations and simulations of soot aggregates [1].

Results and Discussion. Discrepancies between RDG-FA and ICP predictions mainly increased with increasing x_p and scattering angle. Evaluation of ICP using Mie scattering predictions for compact spherical aggregates, and reasonably definitive experimental results for fractal aggregates in the power-law regime, however, indicated problems with ICP at large x_p and scattering angles due to truncation errors in the ICP algorithm. Thus, evaluations using ICP at large x_p were limited to the Guinier regime. Within this regime, discrepancies between RDG-FA and ICP were less than 10% for $x_p \leq 0.4$, indicating agreement within computational uncertainties.

Some typical normalized differential scattering patterns found from the RDG-FA and ICP theories are illustrated in Fig. 2, for the worst case condition, $x_p = 0.4$. The results are plotted as $k^2 C^a_{vv}(\theta)$, where k = wave number and $C^a_{vv}(\theta)$ = aggregate optical cross section at an angle θ, in order to highlight effects of aggregate size

on differential scattering patterns. The Guinier regime involves $\theta < 20°$, 40° and 90° for N = 256, 64 and 16, respectively; within this range of conditions the agreement between RDG-FA and ICP clearly is excellent. Combined with reasonable performance of RDG-FA predictions during recent experimental evaluations emphasizing the power law regime, these results suggest that RDG-FA theory is a reasonably effective way to treat the optical properties of soot for $x_p \leq 0.4$, which usually is the range of interest.

Acknowledgments. This research was supported by the United States Department of Commerce, National Institute of Standards and Technology, Grant No. 60NANB1D1175 with H. R. Baum of the Building and Fire Research Laboratory serving as Scientific Officer, the JNICT-CIENCIA BOLSAS program, NASA Grant No. NAG3-1245 and AGARD Support Project P-101.

References

1. Ü.Ö. Köylü and G.M. Faeth, J. Heat Trans. 115:409-417 (1993).
2. Ü.Ö. Köylü and G.M. Faeth, J. Heat Trans. 116:152-159 (1994).
3. Ü.Ö. Köylü and G.M. Faeth, J. Heat Trans., in press.
4. T. Freltoft, J.K. Kelms and S.K. Sinha, Phys. Rev. B 33:269-275 (1986).
5. J.E. Martin and A.J. Hurd, J. Appl. Cryst. 20:61-78 (1987).
6. M.Y. Lin et al., Proc. Roy. Soc. London A423:71-89 (1989).
7. R.A. Dobbins and C.M. Megaridis, Appl. Optics 30:4747-4754 (1991).
8. M.F. Iskander, H.Y. Chen and J.E. Penner, Appl. Optics 28:3083-3091 (1989).
9. T.L. Farias et al., J. Heat Trans., in press.
10. R. Jullien and R. Botet, *Aggregation and Fractal Aggregates*. World Scientific Publishing Co., Singapore, pp. 45-60, 1987.

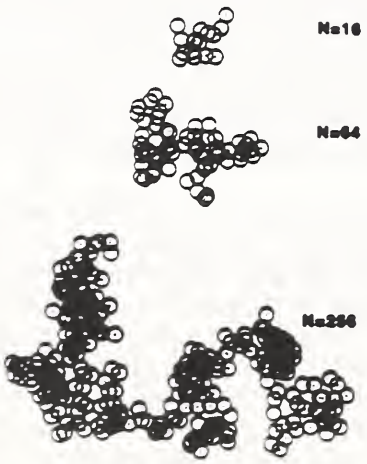

Fig. 1 Projected images of simulated soot aggregates.

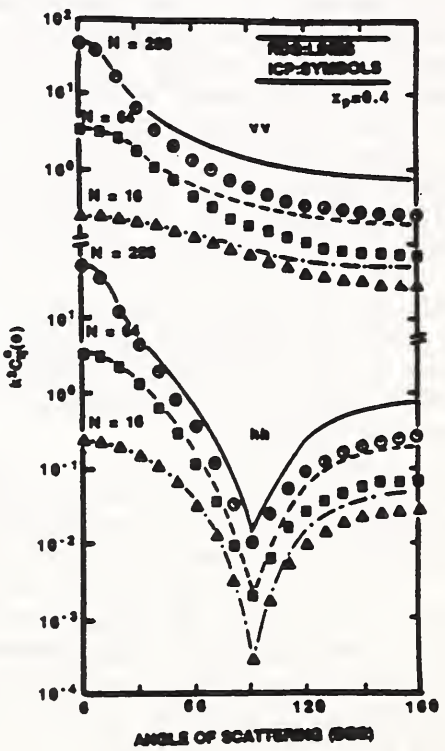

Fig. 2 RDG-FA and ICP predictions of normalized scattering patterns for soot aggregates of various size.

Light Scattering Studies of Fractal Soot Aggregates in Flames

C.M. Sorensen
Department of Physics
Kansas State University
Manhattan, KS 66506-2601

This paper presents an overview of our work concerning light scattering studies of soot in flames.[1-4] We have developed static light scattering (SLS) to an ability where a complete in situ characterization of soot cluster morphology can be obtained. The morphological parameters we can measure are soot cluster radius of gyration, Rg, fractal dimension, D_f, number of monomers per cluster, N, and monomer radius, a.[2] We have also developed an SLS technique to measure the width of the size distribution.

Our methods include an optical structure factor measurement[1] in which the scattered intensity is measured as a function of scattering angle, an example of which is given in Fig. 1. In Fig. 1 $q = 4\pi\lambda^{-1} \sin\theta/2$ where θ is the scattering angle. For small qRg, $I \sim 1 - q^2R_g^2/3$ hence Rg is easily measured. For large qRg, $I \sim q^{-Df}$ hence D_f can be easily measured if data are available in this regime. For general qRg, however, the detailed form of the structure factor depends on how the density of soot terminates at the cluster perimeter, the so-called cutoff function. This was previously poorly known but our recent work has refined our knowledge.[3,5]

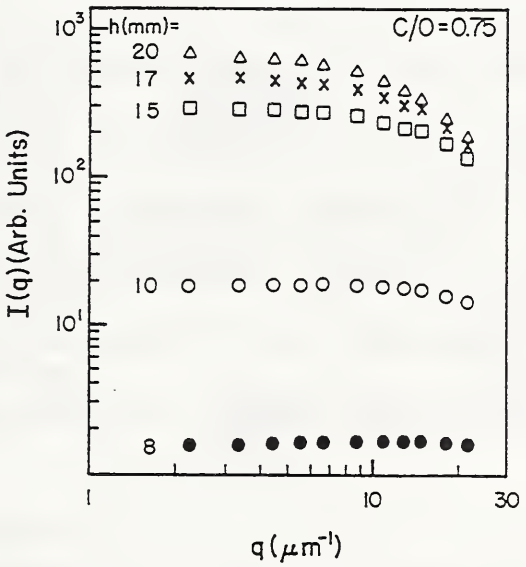

Fig. 1. Scattered light intensity $I(\mathbf{q})$ as a function of the scattering wave vector $\mathbf{q}$ for five different heights above burner h for the C/O = 0.75 flame.

A second measurement involves the classic scattering/extinction measurement. In this method an absolute measurement of the scattered intensity at small scattering angles is compared to the extinction of the light as it passes through the flame. This yields a volume equivalent sphere cluster size, the scattering/extinction radius R_{SE}, and cluster number density. We then use[2]

$$R_{SE} = aN^{1/3}$$

and

$$N = k_0 (R_g/a)^{Df}.$$

Given R_g and D_f from the optical structure factor measurement, and R_{SE} and the constant k_0, one can solve for N and a. Here again a heretofore poorly known

quantity, k_0, had to be determined[5] with reasonable accuracy before this synthesis of methods could yield viable results.

We will illustrate this method using data obtained from premixed flames. We also compare our light scattering measurements to TEM measurements successfully. This not only supports the viability of our method but also indicates the optical theories describing scattering and absorbtion from aggregates must be valid. Currently we are beginning to study laminar diffusion flames and we hope to have data by the meeting time.

These new abilities for cluster characterization have opened doors to other important measurements. For instance we have used dynamic light scattering to measure the diffusion coefficient of fractal soot clusters and, knowing their morphology via SLS, have determined how the diffusion coefficient depends on morphology.[6] This will be important for subsequent studies of aggregation kinetics. We have also studied depolarized light scattering, shown it is a result of intracluster scattering, and found its morphological dependence.[7] This may lead to in-situ optical constants measurements.

This work was supported by NIST and NSF through NSF Grant CTS 9024668.

References:

1. S. Gangopadhyay, I. Elminyawi, and C.M. Sorensen, Appl. Optics 30, 4859 (1991).

2. C.M. Sorensen, J. Cai, and N. Lu, Appl. Optics 31, 6547 (1992).

3. C.M. Sorensen, J. Cai, and N. Lu, Langmuir 8, 2064 (1992).

4. J. Cai, N. Lu, and C.M. Sorensen, Langmuir 9, 2861 (1993).

5. J. Cai, N. Lu, and C.M. Sorensen, submitted to J. Coll. Int. Sci.

6. J. Cai and C.M. Sorensen, Phys. Rev. E, in press.

7. N. Lu and C.M. Sorensen, Phys. Rev. E., in press.

Acetone and OH Imaging in a Acetone-seeded, Methane / Air Diffusion Flame

Michael A. T. Marro and J. Houston Miller
The George Washington University, Washington, DC 20052

Introduction

The correlation of species properties to scalar variables such as mixture fraction, ξ, or equivalence ratio, ϕ, has been an area of active research[1 a,b] and it has been shown that this approach works well for major combustion species[2]. Prior attempts at scalar tracking have utilized Mie[3], Raman[4], and Rayleigh[5] scattering, and LIF[6 a,b,c] techniques. Acetone fluorescence has been compared to various other fluorescence markers (both flame-seeded and flame-species) and has been shown to be a highly versatile flow field marker[7,8]. In this poster we present results for OH and acetone fluorescence observed in a methane/air flame supported on a Wolfhard-Parker burner[9] in which acetone has added to the fuel stream. These are the first images using acetone as a tracer in a hydrocarbon flame.

Experimental

A Lambda-Physik *Lextra 50* excimer laser was operated with XeCl to produce a 60 mJ, 10 ns pulse. The laser beam was attenuated and focused into the center of the burner. The final beam energy was measured to be 3.5 μJ (Figure 1).

The Wolfhard-Parker burner configuration has been studied extensively[9,10] and has been proven useful for LIF techniques. In these studies the burner could be moved laterally to profile fluorescence signals. The burner was mounted on four 1/4-20 threaded posts to allow for height adjustment and a x-axis positioning stage (50 mm travel) to position the burner laterally.

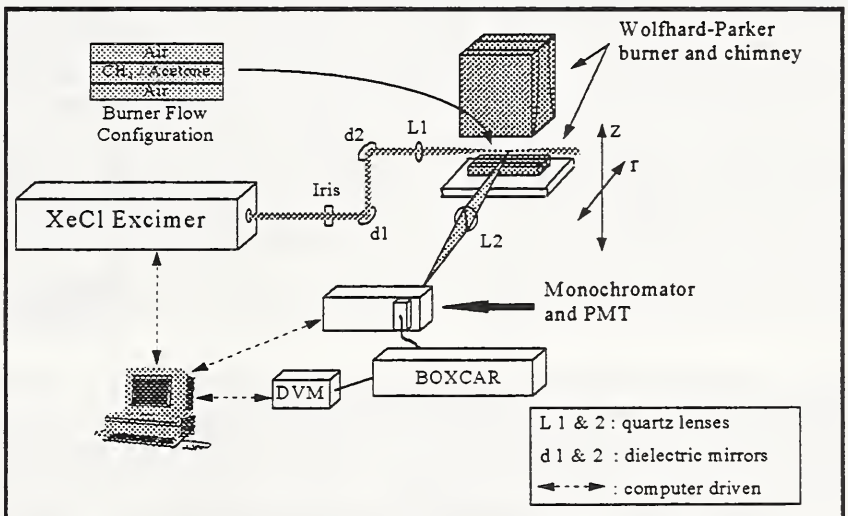

Figure 1: Experimental configuration for imaging experiments.

Fluorescence was collected through a 50 mm diameter, 10 cm focal length quartz lens and focused on to the entrance slit of a 0.35 meter grating monochromator equipped with a 1P-28 Hammamastu PMT. A slit width of 500 μm was used resulting in a 1 nm bandwidth. The PMT signal was processed with a boxcar amplifier and the resulting voltage monitored by a HP 3478A Multimeter interfaced to a 486 DX 33 Mhz computer.

The fuel, either methane or a 8.5% acetone / CH_4 mixture, was introduced to the burner's central fuel slot at 11 cm s^{-1} and was surrounded by 13.7 cm s^{-1} of co-flowing air to stabilize the flame. Acetone, when used, was introduced *via* a bubbler submersed in an ice bath at 0.5°C to produce the desired concentration.

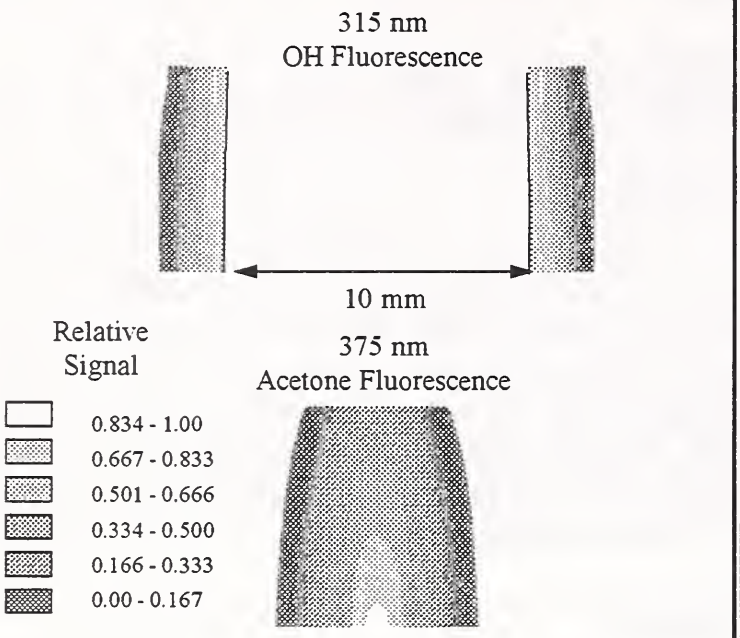

Figure 2: OH and Acetone images.

Data Analysis and Results

Images of OH (emission monitored at 315 nm) and acetone (375 nm) fluorescence are shown in Figure 2. The latter emission wavelength was chosen to minimize interference from PAH fluorescence. Figure 3 compares the correlations of mass-spectral CH_4 data and acetone to ξ. Although there is a slightly lower signal to noise ratio in the acetone signal, the fluorescence is well correlated with mixture fraction and may prove to be a valuable flow field marker in hydrocarbon, non-premixed flames.

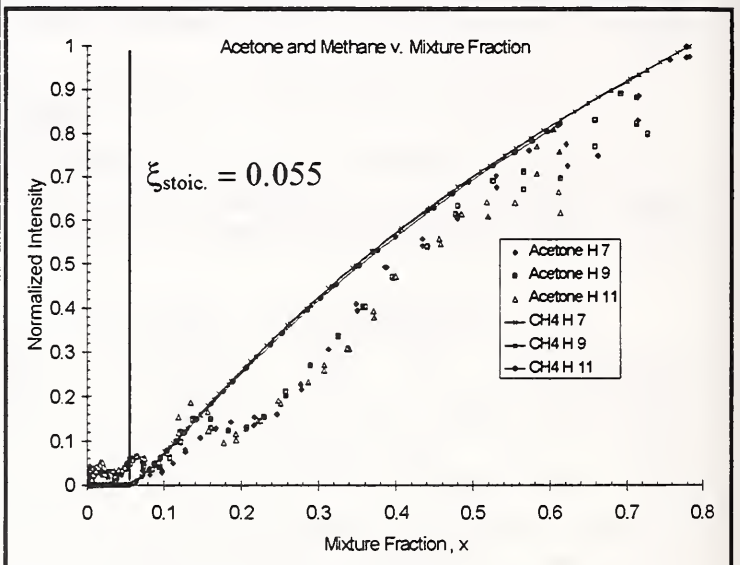

Figure 3: Acetone and Methane v. ξ

[1] [a]Bilger, R. W., *Combustion and Flame* 30:277 (1977).
[b]Sivanthanu, Y. R., and Faeth, G. M., *Combustion and Flame* 82:211 (1990).

[2] Marro, M. A. T., Miller, J. H., and Smooke, M. D., "*Validation of Conserved Scalar Relationships in Laminar CH_4 - Air Diffusion Flames*" , Technical Meeting of the Eastern States Section of the Combustion Institute Princeton University, Princeton, NJ October (1993).

[3] Long, M. B., Chu, B. T., and Chang, R. K., *AIAA Journal* , 19:1157 (1981).

[4] Dibble, R. W., Kollmann, E., and Schefer, R. W., *Combustion and Flame* 55:307 (1984).

[5] Driscoll, J. F., Schefer, R. W., and Dibble, R. W., *Nineteenth Symposium (International) on Combustion* , The Combustion Institute, p. 477 (1983).

[6] [a]Alden, M., Edner, H., Holmstedt, G., Svanberg, S., and Hogberg, T., *Applied Optics* , 21:8:1236 (1982).
[b]Kychakoff, G., Howe, R. D., and Hanson, R. K., *Applied Optics* , 23:5:704 (1984).
[c]Long, M. B., Stårner, S. T., and Bilger, R. W., *Combustion Science and Technology* , 92:209 (1993).

[7] Lozano, A., Smith, S. H., Mungal, M. G., and Hanson, R. K., *AIAA Journal* 32:1:218 (1994).

[8] Lozano, A., Yip, B., and Hanson, R. K., *Experiments in Fluids* , 13:369 (1992).

[9] Norton, T. S., Smyth, K. C., Miller, J. H., and Smooke, M. D., *Combustion Science and Technology* 89:1 (1993).

[10] Smyth, K. C., Tjossem, P. J. H., Hamins, A., and Miller, J. H., *Combustion and Flame* 79:366 (1990).

SOOT PRODUCTION IN FLICKERING METHANE, PROPANE, AND ETHYLENE DIFFUSION FLAMES

Christopher R. Shaddix and Kermit C. Smyth
Building and Fire Research Laboratory
National Institute of Standards and Technology
Gaithersburg, MD 20899

Diffusion flames originating from gaseous jets, liquid pools, or even solid materials frequently exhibit a periodic flickering behavior, whose effect on the chemical fields within the flame is not understood. In particular, the slow rates of soot particle inception chemistry and of carbon monoxide oxidation might be expected to result in strong sensitivity of soot and CO production to the complex, time-varying flowfields present in flickering flames; this would have important consequences for flame radiation and the emission of smoke and CO. Indeed in an earlier study of OH• laser-induced fluorescence and elastic scattering from soot in steady and time-varying methane/air flames, it was found that the soot scattering intensity in flickering flames was significantly greater than that observed for the steady (i.e., unforced) flame with the same mean fuel and air flow rates [1]. Measurements of the soot volume fraction fields in the steady and a moderately flickering flame reveal a factor of 5 enhancement in the peak soot volume fraction and a factor of 4 increase in the time-averaged, volume-integrated soot volume fraction in the flickering flame [2]. Mie analysis of the soot volume fraction and vertically polarized scattering measurements suggests that in the flickering methane/air flame soot particle number densities generally are comparable to steady flame values, whereas mean particle sizes are as much as 50% larger. Since diffusion flame soot chemistry is highly sensitive to fuel type [3] and methane is the weakest sooting hydrocarbon fuel, the trends in soot production observed for flickering methane flames may not hold for other hydrocarbon fuels. Therefore, measurements of soot scattering and soot volume fraction, as well as visible flame luminosity, have been made on steady and flickering propane/air and ethylene/air diffusion flames.

The burner and phase-locked imaging setup for studying time-varying diffusion flames have been described in detail previously [1]. In brief, unconfined laminar diffusion flames were stabilized on a coannular burner with a loudspeaker attached to the plenum below a 1.1 cm diameter fuel tube. The mean fuel flowrates were normalized to the methane flame fuel flowrate (7.7 cc/s) on a carbon atom basis, giving visible flame heights of ~ 85 mm and 88 mm for the propane/air and ethylene/air steady flames, respectively, compared to 79 mm for the methane/air flame. Measurements were performed on these steady flames and on moderately and strongly flickering flames produced by applying sine waves of magnitude 0.75 V and 1.5 V (pk-to-pk) to the plenum loudspeaker. Figure 1 shows previously measured OH• radical fluorescence and soot scattering for the two flickering methane flames. The flickering propane and ethylene flames show similar dynamics but are somewhat thinner than the methane flames, consistent with the decreased effect of buoyant expansion for these more heavily sooting fuels [4].

Figure 2 shows the optical arrangement for measuring polarization-specific soot scattering at visible wavelengths. An intensified CCD camera, with attached glass or dielectric filters, was used to record planar images at 90° to the direction of propagation of the laser light. For the scattering measurement, an attenuated reflection of the incident laser sheet was directed to the side of the CCD pixel array, allowing shot-to-shot correction of the measured signals for laser energy in the vertical plane. Comparisons of laser extinction derived soot volume fraction profiles and laser-induced incandescence (LII) signals in the steady methane flame have shown good agreement [2], lending support to the interpretation of properly calibrated LII as soot volume fraction. In this study soot volume fraction was measured by removing the sheet-forming lenses and polarization optics from the scattering setup and focusing the laser beam at the burner centerline to produce energy-saturated incandescence, which was recorded as a line image on the CCD. Visible flame luminosity was measured simply by turning off the lasers and using a short-pass filter (415-550 nm) in front of the camera.

The peak values of soot scattering and soot volume fraction measured in the different flames are shown in Table I and reveal some interesting trends. For moderately flickering conditions, the propane and ethylene flames both show an enhancement in the peak soot volume fraction of approximately 60% and in soot scattering of 170–200% in comparison to their corresponding steady flames. These increases in soot concentration and soot scattering are substantially less than the factors of 5.3 and 37 observed in the methane flame, but result in visible emission of smoke from the flickering propane and ethylene flames. For all three fuels investigated, there is no further increase in the peak soot scattering or soot volume fraction as the flickering intensity is changed from moderate to strong. Table I also shows the peak luminosity signals in the different flames, relative to the peak

intensity in the steady methane flame. The flickering methane flames exhibit substantially larger relative increases in peak luminosity than the propane and ethylene flames, as might be expected based on the soot volume fraction results. Otherwise, the trends in the peak soot volume fraction noted above are not well followed by the luminosity, presumably due to the strong dependence of soot radiation on the local temperature and thus the local dynamics of the flowfield.

REFERENCES

1. Smyth, K. C., Harrington, J. E., Johnsson, E. L., and Pitts, W. M., *Combust. Flame* 95:229-239 (1993).
2. Shaddix, C. R., Harrington, J. E., and Smyth, K. C., 25th Symp. (Intl) on Comb. (1994), in press.
3. Glassman, I., 22nd Symp. (Intl) on Comb., The Combustion Institute, Pittsburgh, 1988, pp. 295-311 and references therein.
4. Kaplan, C. R., Baek, S. W., Oran, E. S., and Ellzey, J. L., *Combust. Flame* 96:1-21 (1994).

TABLE I

Fuel	Peak scattering at 560 nm $Q_{vv,90°}$ (10^{-5}/cm-sr)			Peak soot volume fraction f_v (ppm)			Peak visible luminosity (relative to steady CH_4)		
	steady flame	0.75 V flame	1.5 V flame	steady flame	0.75 V flame	1.5 V flame	steady flame	0.75 V flame	1.5 V flame
methane	7.6	280	310	0.30	1.6	1.7	1.0	2.6	3.6
propane	650	1300	1300	5.2	8.2	6.6	5.1	5.5	8.4
ethylene	1400	2400	2200	8.0	12	14	5.6	9.3	11

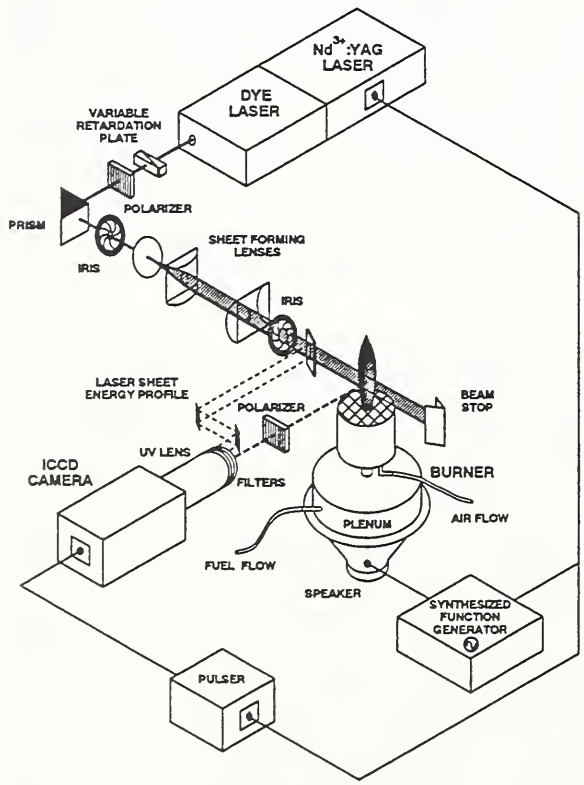

Figure 1. Experimental set-up for 1-D or 2-D imaging of axisymmetric diffusion flames which are acoustically excited and phase-locked to the pulsed dye laser system operating at 10 Hz. Images are recorded using an intensified charge-coupled device (ICCD) camera.

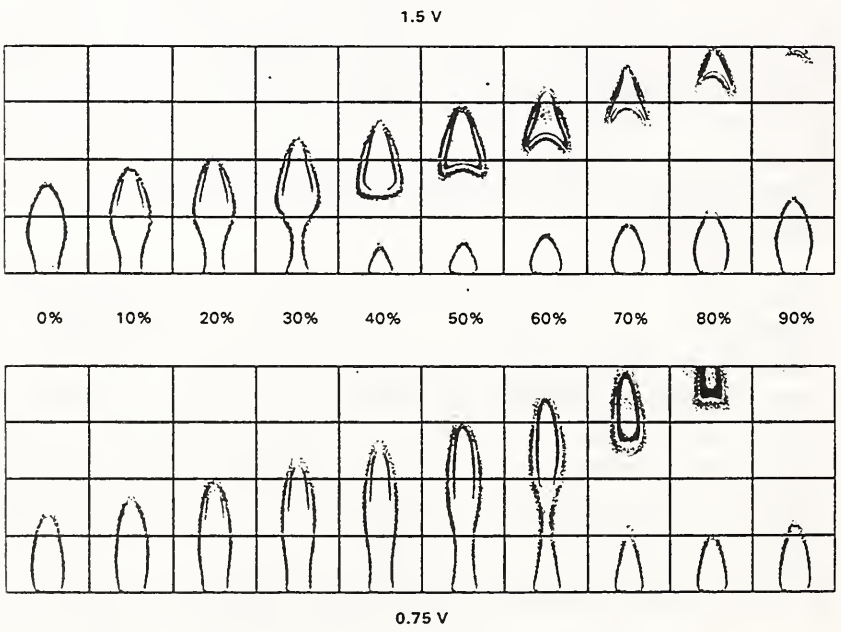

Figure 2. Soot scattering and OH• laser-induced fluorescence in flickering methane/air diffusion flames using horizontally polarized light at 283.55 nm. The OH• fluorescence signals surround intense scattering from the soot particles. Ten phases (arbitrary zero) are shown at two excitation voltages, corresponding to time intervals of 10 ms.

Measurement of Soot Oxidation in Post Flame Gases

M.P. Tolocka and J.H. Miller
the George Washington University
Washington DC 20052

Introduction

In fires, the concentrations of soot and carbon monoxide are found to be strongly correlated [1] and a significant fraction of the CO emitted from fires is believed to originate from soot particle oxidation. There have been a number of studies of particle oxidation within flames [2,3,4,5]. and in shock tubes [6,7], but little work on post-flame oxidation [8]. We have recently initiated a study of the transformation of post-flame smoke with an emphasis on the chemical transformation of surface-adsorbed polynuclear aromatic hydrocarbons and the subsequent formation of gas phase molecular oxidation products. Some preliminary results from these studies are described below.

Experimental

Figure 1 shows the configuration of the apparatus used in these studies. The burner consists of a central fuel tube that is 1/4 inch diameter surrounded by a ~3/4 inch diameter air co-flow tube to stabilize the flame. This burner is fitted into a 1 inch diameter sleeve which allows for vertical movement of up to 3.5 inches. There is a six way cross above the burner region which allows for optical and/or probe sampling of either the flame or immediate post-flame gases. A 1 inch diameter, 25 inch long quartz tube is enclosed by a tube furnace which operates at 400 - 1500 degrees Celsius. Above this is another six way diagnostics cross.

We have used two fuels for the preliminary studies. The first flame studied was an acetylene/air diffusion flame, desirable because of its low sooting height [9]. Extinction measurements were taken during heavily sooting conditions in the upper cross using a 1 mW HeNe laser operating at 632.8 nm while the tube furnace was adjusted to between ambient temperature and 700 °C. The beam was chopped at approximately 86 Hz and was monitored by photodiodes before and after the upper sampling region. Each signal was processed through an amplifier and a oscilloscope. The flow of soot through the sampling region was generally laminar but tended to drift during the course of the optical measurements.

In the second flame, a mixture of toluene in methane was used as the fuel. In the initial studies, the air flow was varied so that the global equivalence ratio in the burner varied between 0.5 and 1.2. The over-ventilated flame was non-smoking. However, as the overall stoichiometry became rich, the flame emitted smoke which could be detected via scattering and extinction of the HeNe laser beam.

Preliminary Results and Future Work

Figure 2 shows the results of the extinction measurements of the soot particles after the furnace region in the acetylene/air flame. The measurements show little reduction in smoke yield until the furnace temperature exceeds 500 °C. After this temperature, soot yield decreases rapidly with increasing temperature.

In addition to a more complete characterization of the light scattering and extinction measurements, we will perform a number of other diagnostic tests in this system. These will include

- particulate sampling and analysis of adsorbed Polycyclic Aromatic Hydrocarbons (PAH) using GC/MS
- particle morphology using scanning tunnelling microscopy (STM) and/or atomic force microscopy (AFM)
- tunable diode laser absorption spectroscopy (TDLAS) of CO and CO_2 which will provide quantitative information on soot oxidation rates.

Acknowledgements

The authors gratefully acknowledge support of this research from the National Institute of Standards and Technology and the George Washington University.

References

1. Koylu, and Faeth, G.M., "Soot Emission from Liquid Fueled Buoyant Turbulent Diffusion Flames," *Combustion and Flame* **87**, 61-76 (1991).
2. Puri, R., Santoro, R.J. and Smyth, K.C., "The Oxidation of Soot and Carbon Monoxide in Hydrocarbon Diffusion Flames," *Combustion and Flame* **97**, 125-144 (1994).
3. Skaggs, R.R. and Miller, J.H., "A Study of carbon Monoxide in a Series of Laminar Ethylene/Air Diffusion Flames Using Tunable Diode Laser Absorption Spectroscopy," *Twenty Fifth Symposium (International) on Combustion, The Combustion Institute, in press.*
4. Santoro, R.J., Yeh, T.T., Horvath, J.J. and Semerjian, H.G., "The Transport and Growth of Soot Particles in Laminar Diffusion Flames," *Combustion Sci and Tech.* **53**, 89-115 (1987).
5. Megardis, C.M. and Dobbins, R.A., "Comparison of Soot Growth and Oxidation in Smoking and Non-Smoking Ethylene Diffusion Flames," *Combustion Science and Tech.* **66**, 1-16 (1989).
6. Park, C. and Appleton, J.P., "Shock-Tube Measurements of Soot Oxidation Rates," *Combustion and Flame* **20**, 369-79 (1973).
7. Roth, P., Brandt, O. and Von Gersum, S., "High Temperature Oxidation of Suspended Soot Particles Verified by CO and CO_2 Measurements," *Twenty Third Symposium (International) on Combustion, The Combustion Institute,* 1485-1491 (1990).
8. Noirot, R., Gilot, P., Gadiou, R., and Prado, G., "Control of Soot Emission by Filtration and Post-Combustion. A Laboratory Study of the Regeneration of an Organic Particulate Trap Assisted by Hydrocarbon Injection," *Combustion Science and Tech.* **95**, 139-160 (1994).
9. Schug, K.P., Manheimer-Timnat, Yaccarino, P. and Glassman, I., "Sooting Behavior of Gaseous Hydrocarbon Diffusion Flames and the Influence of Additives," *Combustion Sci and Tech.*, **22**, 235-50 (1980).

FIGURE 1

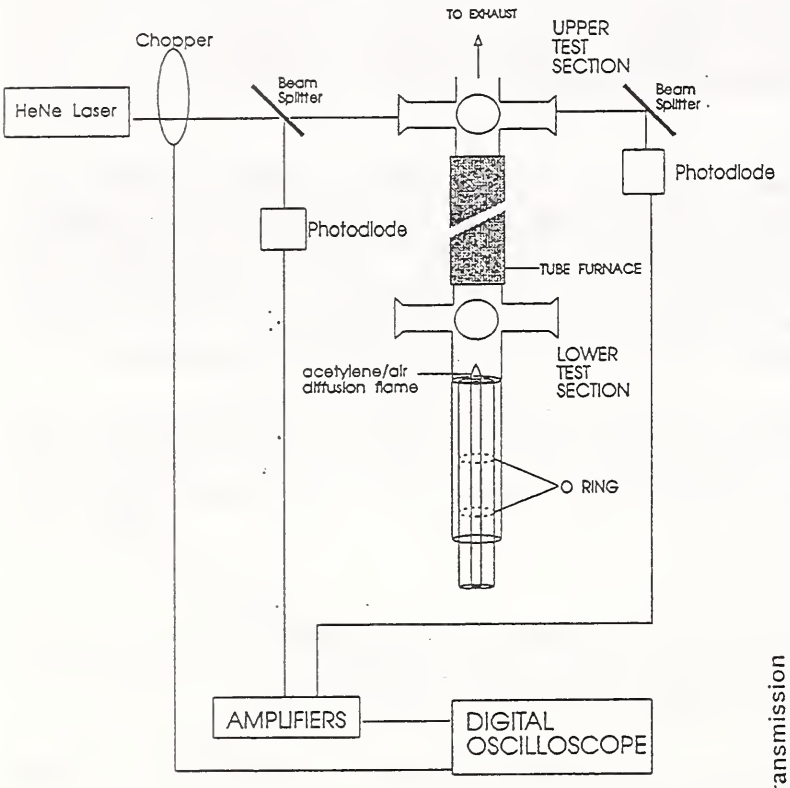

FIGURE 2

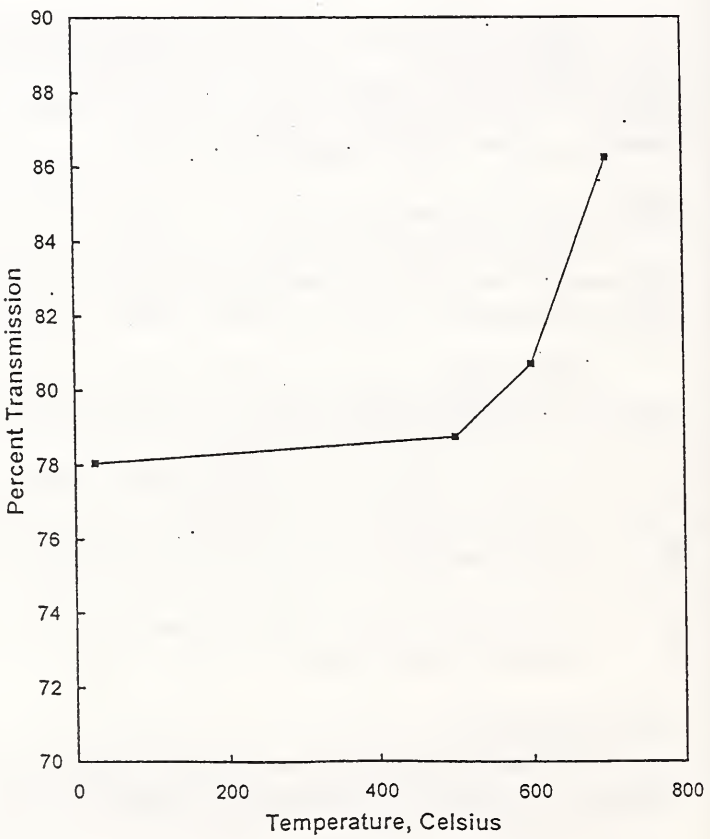

A REVIEW OF MEASUREMENTS AND CANDIDATE SIGNATURES FOR EARLY FIRE DETECTION

William Grosshandler
Building and Fire Research Laboratory
National Institute of Standards and Technology
Gaithersburg, MD 20899

The current generation of fire detection systems is designed to respond to the smoke, heat, or the electromagnetic radiation generated during smoldering and flaming combustion. Smoke is sensed either by measuring, with a photodetector, the light which is scattered from a controlled light source, or by the change in current created by charged particles passing through an ionizing radiation field. Heat can be easily sensed by a number of conventional devices, such as compensated thermocouples and thermistors. Both the absolute temperature and rate of temperature rise are used to define alarm conditions. The ultraviolet and infrared portions of the electromagnetic spectrum are typically detected with vacuum tube and solid state photodiodes, photoconductive and photovoltaic cells, thermopiles and pyroelectric cells [1].

Future developments in early warning fire detection are incumbent upon knowing what is unique about a fire as well as the means to measure those characteristics. The concept of a "fire signature" was defined by Custer and Bright [2] in their in description of the state of fire detection in the early 1970s. Advances in sensing and signal processing have been many over the last two decades, but relatively little new information on what occurs early in a fire has been revealed. The purpose of this paper is to reexamine the physical and chemical transformations associated with a burgeoning fire, to summarize the results of past experimental measurements of these transformations, to identify holes in the data which need to be filled, and to suggest a means by which these data can be used for developing new detection systems and evaluating their performance under realistic and unbiased conditions.

The literature has been reviewed to determine the extent to which fires have been characterized in their early phase (smaller than 100 kW). In particular, measurements of CO, CO_2, H_2O, H_2, O_2, smoke and temperature have been examined from tests performed by other laboratories simulating the UL and EN test protocols. Figure 1 is a plot of CO concentration measured in the six standard European fires (TF1 through TF6), a UL test, and a test performed with a transformer fire (CERB) [3,4]. Not surprisingly, the variation in magnitude and rate of growth vary dramatically with fuel type and geometry. The variation is also large between repeat runs of the same tests (TF1, TF2 and TF3). When scaled by estimated mass consumed of fuel (Figure 2), the different standard fires can be seen to group a bit more systematically. The measuring location for one series of TF1, TF2 and TF3 fires was three meters off the centerline, while the others were made directly above the center of the fuel. Additional measurements of species, temperature and velocity just above the flame are ongoing to get a more complete footprint of each fire type. Similar measurements of non-fire nuisance sources are required in order to discriminate between a fire and non-threatening situation with a high degree of certainty.

The concept of a universal fire emulator/detector evaluator (FE/DE) is being developed to supplement existing UL and EN standards involving prescribed full-scale room fires or smoke-flow boxes, and to develop an environmental chamber in which velocity, individual gas species, particulate matter and temperature can be controlled as a function of time. A detector would be placed inside the chamber and the desired environmental program would be selected to emulate either a fire or interfering signal. The objective is to have a facility in which alternative systems can be compared and new concepts evaluated on a level playing field. It will eliminate the run-to-run variation which is unavoidable in full-scale tests and allow more well controlled environments with realistic multiple stimuli. Computational fluid dynamics could be used to insert the fire source into the space being protected to guide detector placement and to predict system performance. Support for such a facility and the general approach is sought from the fire protection industry and regulating organizations.

[1] Cholin, J.M., *Industrial Fire Safety* 2, No. 5, p. 22, September/October 1993.
[2] Custer, L.P., and Bright, R.G., *Fire Detection: The State of the Art*, NBS TN 839, June 1974.
[3] Jackson, M.A., and Robins, I., "Gas Sensing for Fire Detection: Measurements of CO, CO_2, H_2,

O_2, and Smoke Density in European Standard Fire Tests," *Fire Safety Journal 22*, 181-205 (1994).

[4] Pfister, G., "Detection of Smoke Gases by Solid State Sensors - A Focus on Research Activities," *Fire Safety Journal 6*, 265-174 (1983).

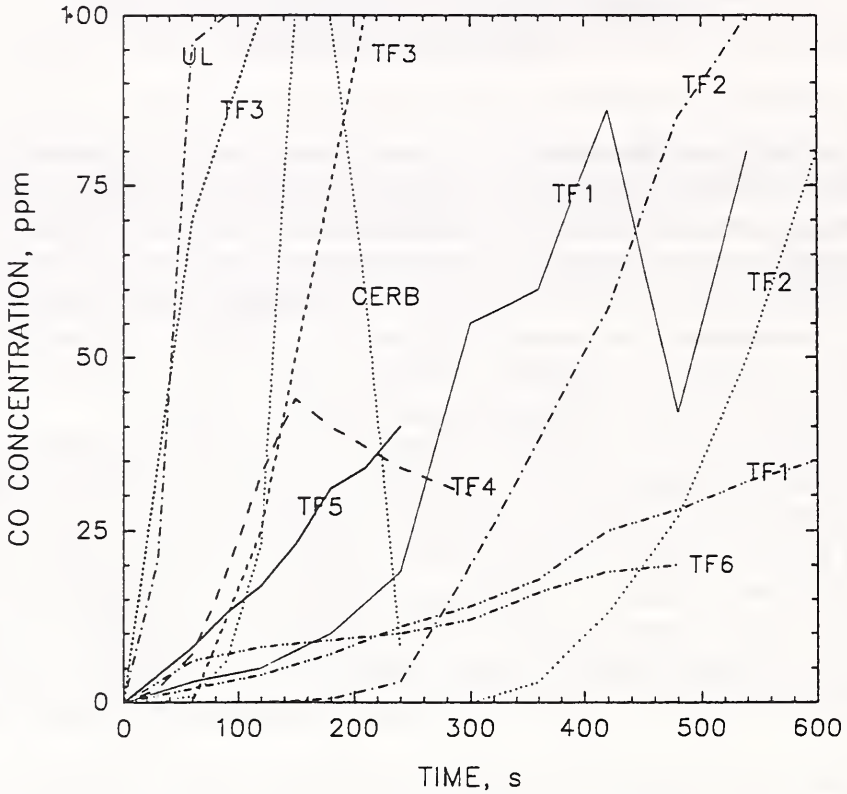

Figure 1. CO concentrations vs time in standard fire tests [3,4]

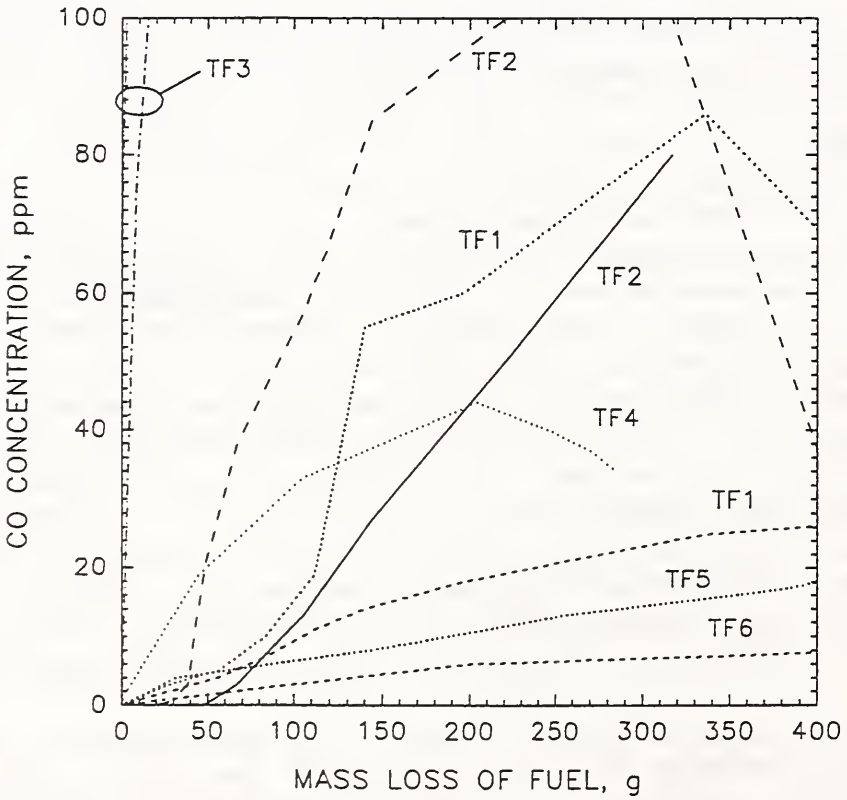

Figure 2. CO concentration vs mass loss in standard fire tests [3,4]

AN FT-IR BASED SYSTEM FOR FIRE DETECTION

Michael A. Serio†, Anthony S. Bonanno†, Kim S. Knight†, and Jeffrey S. Newman*

†Advanced Fuel Research, Inc.
87 Church Street
East Hartford, CT 06108

* Factory-Mutual Research Corp.
1151 Boston-Providence Turnpike
Norwood, MA 02062

ABSTRACT

A major advance in fire safety technology during the past two decades is the availability of low cost smoke detectors based on either ionization or photoelectric detectors. However, these detectors have some drawbacks because of the high frequency of false alarms and maintenance problems. Other types of detector technologies have been developed for specific gases, such as CO_2, CO, or O_2, based on metal oxide semiconductors, electrochemical sensors, or optical sensors. However, all single parameter methods are hindered by the lack of generality for several types of fires and a lack of "intelligence," i.e., not always being able to discriminate against false signals (1-3). It has long been recognized that multi-parameter detectors which can measure, for example, heat, smoke and CO gas are more reliable indicators of a real fire. In the case of buildings with high value contents, such as telephone central exchanges, clean rooms, banks, military installations, etc., the reliability and sensitivity of the fire detection technology are the most important criteria in selecting a detection system.

There are three recent events which together provide an opportunity to develop a new generation of fire detection systems, 1) the availability of low cost, high speed computation in the form of personal computers; 2) the availability of software packages involving data analysis techniques such as neural networks or fuzzy logic; 3) the availability of advanced sensor technology which can dramatically increase, at relatively low cost, the amount of information upon which an alarm condition can be established. One of the most significant recent advances in sensor technology is the development of portable, low cost FT-IR spectrometers which are operated by personal computers.

These are three basic approaches to implementation of an FT-IR based fire detection system. The first is to make short path measurements in a ventilation duct that removes air from a room or a combination of rooms, as shown in Fig. 1a. This is one of the simplest and least expensive solutions to implement. The major drawbacks are lower sensitivity due to the short path and dilution of the combustion products. This technique does not indicate the exact location of a fire in a room, although this may not be important if the room is relatively small.

The second approach is to make long path measurements across a room at the ceiling level, as shown in Fig. 1b. While this technique is inherently more sensitive, it also requires transport of the combustion products to the beam path. The path must also be arranged so that there are no obstructions between the source and detector and multiple beam paths may be required to properly cover a room. This can be accomplished with specially designed optics or multiple spectrometers.

A third approach is to integrate an FT-IR spectrometer equipped with a multi-pass gas cell into an extractive system, thus replacing the more conventional smoke detector. Such an implementation is shown schematically in Fig. 1c. Since the costs of installing the tubing network is estimated at $\$1/ft^2$, the cost of the detector technology becomes incidental for a large facility (>200,000 ft^2). An example of the type of data that would be obtained by this method is shown in Fig. 2. A piece of PVC insulation was heated in air at 10°C/min in a

TGA/FT-IR system. The combustion products in this instrument automatically flow into a multi-pass cell. The spectra include both pyrolysis and combustion products.

The paper will discuss the infrared spectral signatures observed during fire events, data analysis strategies for discriminating fire events from non-fire conditions, and the practicality of implementing an FT-IR based fire detection system for various applications. The combustion of a standard set of flammable materials, such as heptane, polystyrene, PMMA, and PVC is being studied. A comparison will be made to existing multi-parameter methods for fire detection developed by Newman and coworkers (4-6).

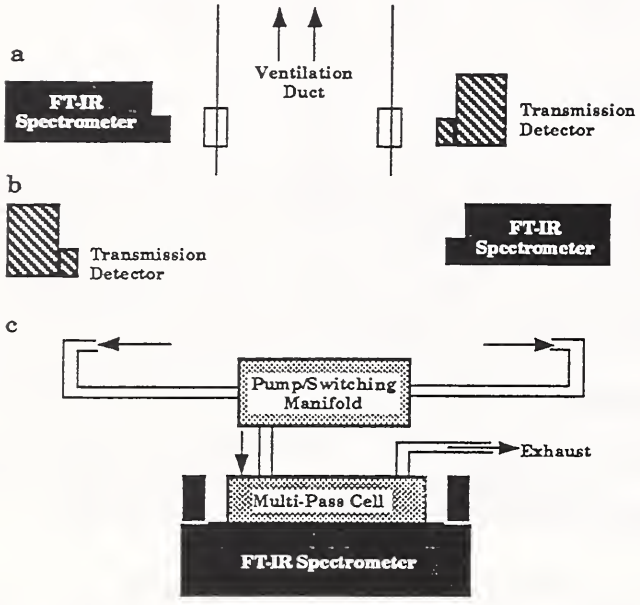

Figure 1. Possible Fire Detection Systems Involving FT-IR Spectroscopy. a) Short-Path Duct Measurements; b) Long-Path Room Measurements; c) Extractive Measurements in Multi-Pass Cell.

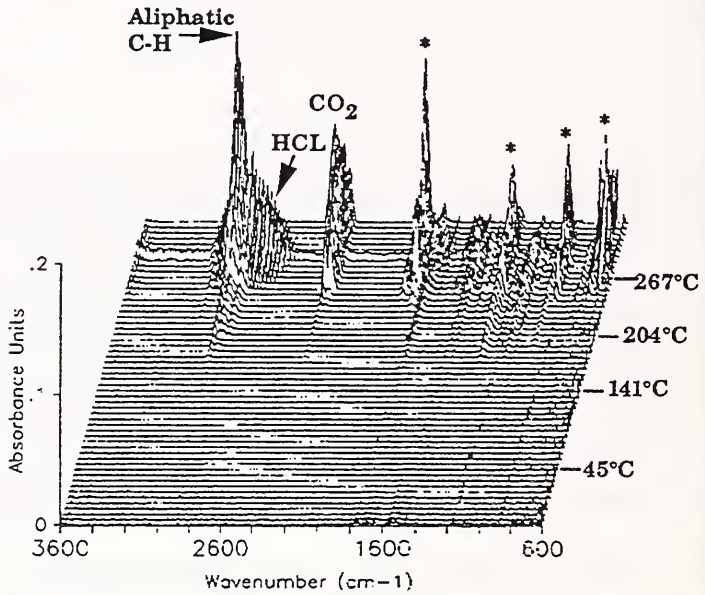

Figure 2. FT-IR Analysis of Combustion Products from PVC Insulation. Asterisks Indicate Spectra from Volatile Organics.

ACKNOWLEDGEMENTS

The authors would like to acknowledge the support of this work under the Department of Commerce Small Business Innovative Research program (Contract No. 50-DKNA-4-00096). The project managers are Dr. Norman Taylor and Dr. William Grosshandler of NIST.

REFERENCES

1. Grosshandler, W., Smith, R.L., Nyden, M., Harris, Jr., R., Jackson, M., "Advanced Fire Detection Sytems," Summaries of BFRL Fire Research In-House Projects and Grants, (1992).
2. Grosshandler, W., Nyden, M., Brown, E., "Detection and Monitoring of Fires with Open-Path FT-IR," Summaries of BFRL Fire Research In-House Projects and Grants (1993).
3. Grosshandler, W., "An Assessment of Technologies for Advanced Fire Detection," ASME Winter Annual Meeting, (1992).
4. Heskestad, G., Newman, J.S., FMRC J.I. 0R0R8.RU, 129 (1990).
5. Newman, J.S., "Principals for Fire Detection," Fire Technology, (May 1988).
6. Newman, J.S., "Prediction of Fire Detector Response," Fire Safety Journal, **12**, 205-211 (1987).

DESIGN OF A PROTOTYPE VIDEO-BASED FIRE DETECTION SYSTEM

A.W. Bakkom, R.F. Richards, and O.A. Plumb
Department of Mechanical & Materials Engineering
Washington State University
Pullman, WA 99165

ABSTRACT

A video-based fire detection system currently under development at Washington State University is presented. The prototype system is intended to be a practical solution to the need for fire protection in industrial settings, such as in warehouses and on factory floors, or in situations in which a black and white video camera is already in use (e.g. for surveillance).

The system utilizes a video camera to monitor temperature and species sensitive sensors that change color at a prescribed temperature or carbon monoxide concentration. When the sensors change color in response to an accidental fire, the color change is detected by the video camera and the digitized image passed on to a personal computer via a frame grabber. The personal computer subsequently determines the location of the sensor and the time of the color change. The times and locations of sensors changing color are used as data for an inverse problem solution algorithm, based on LAVENT [1], which signals the detection of a fire, and then determines the location and size of the fire.

Previous work reported by Munk et al. [2] dealt with the development of FORTRAN code to implement the inverse problem solution algorithm used for the determination of the fire location and size. Limits on the accuracy with which the inversion algorithm could locate and size fires were assessed using computer synthesized data from simulated compartment fires. The present work involves the design, fabrication, and testing of a working prototype of the video-based fire detection system. Development of both hardware and software are addressed.

The prototype system consists of a 486 personal computer, a PULNEX TM-7CN black and white video camera, a SCENTECH IV-P24 frame grabber, and an array of color-changing sensors. Both temperature-sensitive sensors such as reversible thermochromic liquid crystal sensors, and irreversible polyamide sensors, and carbon monoxide-sensitive sensors (commercially available) have been tested in conjunction with the video-detection system.

Particular attention has been paid to issues concerned with sensor design, since the ability of the video camera to detect a change in the color sensitive sensors is critical for the system operation. Basic design considerations related to the sensor geometry (size, shape, and layout), are of interest. For example, practical design considerations related to realistic operating conditions such as the number of sensors required, sensor array distribution, sensor color change characteristics, and the effect of lighting and camera-to-sensor distances on sensor visibility have been considered.

Figure 1 shows the number of pixels counted in the images of 10 x 10 cm square, white and black targets. The number of pixels, plotted versus target-to-camera distance shows the expected r^{-2} dependence. Of interest here is the relatively large number of pixels in the images of targets which are representative of the sizes planned for the color-changing sensors. Even at fairly large distances, ~20 feet, the number of pixels, ~100 pixels, is sufficient to average out electronic noise and sensor edge effects.

The magnitude of color change produced by triggering a TLC sensor which is visible to a black-and-white video camera can be seen in Fig. 2. The figure shows pixel values averaged over the entire images of unactivated TLC sensors (black), activated TLC sensors (gray), and white targets where the sensors and targets were 10 x 10 cm, and located 12 feet from the video camera. Pixel values have been normalized to vary between 0 (pure black) and 10 (pure white) and plotted versus intensity of illumination in units of lux. The increase in pixel value in the image of the TLC sensor upon activation is

not great, about one-sixth of the change visible if the sensor changed from black to white. However, for spaces where the sensors would receive illumination greater than 80 lux the increase in pixel value is sufficient to clearly distinguish activated from unactivated sensors. Marks' Mechanical Engineers' Handbook gives 60 lux as the minimum level of illumination recommended for corridors and stairways [3].

Recent work has focused on developing software to gather the time-versus-temperature information required by the inversion algorithm, from the distributed color-changing sensor array. Specifically, PC-based software able to reliably determine the activation of any sensor in an array, and then to relay the room location of the sensor and the time of activation to the inversion algorithm is being coded.

In the presentation, the operation of the prototype fire detection system, including color-changing sensors, will be demonstrated. An overall evaluation of the system will be presented, based on the criteria of quick fire detection, accurate fire location, accurate fire sizing, simplicity of set up, simplicity of operation, system versatility and cost.

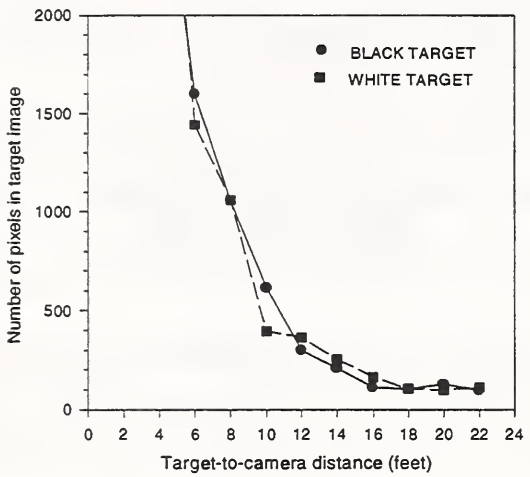

Fig. 1 Number of pixels in image of 10 x 10 cm target versus target-to-camera distance.

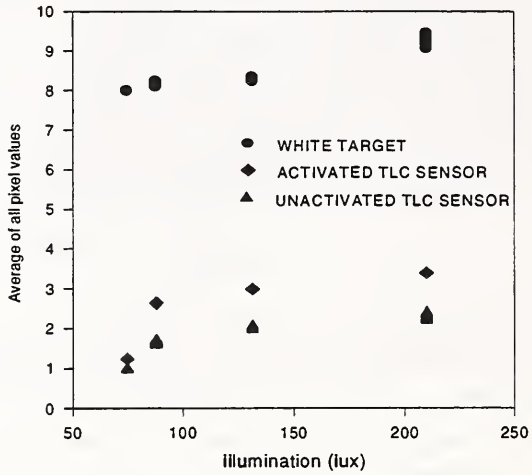

Fig. 2 Average pixel values of unactivated TLC sensors, activated TLC sensors, and white targets under varying illumination.

References

1. Davis, W.D. and Cooper, L.Y., Fire Technology 27:113-127 (1991).
2. Munk, B.N., Richards, R.F., and Plumb, O.A. Annual Conference on Fire Research: Book of Abstracts, NISTIR 5280, 87-88 (1993).
3. Marks, L.S., Mechanical Engineers' Handbook, Fifth Edition, McGraw-Hill, New York (1951).

Acknowledgement

This work is supported by NIST Grant 60NANB2D1290 with Dr. W.L. Grosshandler serving as Scientific Officer

AN INVERSE RADIATION SOLUTION FOR FIRE DETECTION

K. Padakannaya, R.F. Richards, & O.A. Plumb
Department of Mechanical and Materials Engineering
Washington State University
Pullman, Washington 99164-2920

An accidental fire in an enclosure can be detected by measuring the radiation emitted from the fire plume or from the layer of hot combustion gases that collect near the ceiling. The location and size of the fire can be determined by an inverse radiation solution from radiative heat flux measurements along the ceiling and walls. The advantages of fire detection by radiation over convection include the speed of radiative transport, and the fact that radiative heat transfer is not affected by air currents.

A two-dimensional cylindrical (r,z) geometry is used to model the fire plume as it grows vertically and the hot gas layer which expands radially from the point of impingement of the fire plume on the ceiling. In the analysis, we assume that the fire plume, as well as the layer of hot combustion gases, is a hot homogeneous isothermal region surrounded by much cooler diathermanous room air. The forward problem in the case of accidental fire is the solution of the radiative transfer equation obtaining an intensity distribution, from which the net radiative heat flux or incident radiation is calculated. Exact solutions for the radiative transfer equation can be very complicated and are not available for many multi-dimensional geometries. The Discrete Ordinates (S-N) method has been used extensively to numerically model the radiative transfer equation for a variety of geometries and medium properties. A detailed description of the discrete ordinates method is given by Lewis and Miller [1].

A FORTRAN code for discrete ordinates scheme in cylindrical geometry with a participating gray medium is presented. The method is verified with existing benchmark solutions for simple one and two-dimensional cases. The code is compared with one and two-dimensional exact solutions presented by Dua and Cheng [2] for a non-scattering medium in a cold black enclosure, and with exact solutions in one-dimension for isotropically scattering media developed by Siewert and Thomas [3]. Results are obtained by varying the number of control volumes for the S-2, S-4, and S-6 approximations, for different optical thicknesses and scattering coefficients. The results show that sufficient accuracy for the forward problem solution is obtained with the S-6 approximation and 20 control volumes in each direction. Figure 1 compares S-N approximations with the exact solution in one-dimension given by Siewert and Thomas [3]. The radial distribution of incident radiation is shown for a medium of optical thickness τ of 1.0 and scattering coefficient σ of 0.7, and with unit diffuse incident radiation at the bounding walls.

The inverse problem of interest is the retrieval of the temperature, absorption and scattering coefficients from the radiative heat flux measurements. Very accurate inverse solutions can be obtained with measurements (from heat flux sensors) at every control volume location. However, for practical reasons sensors are placed on the ceiling and the walls (the bounding surfaces of the medium) and only at a few locations between control volumes. Figure 2 shows the net radiative heat flux calculated from the temperature and absorption coefficient retrieved from 21, 11, and 5 sensor measurements respectively. The measurements are obtained from the one-dimensional forward problem solution for a medium at 400 K with absorption coefficient α of 1.0. The retrieved temperatures and absorption coefficients for each case are given in the table below.

	exact	21 sensors	11 sensors	5 sensors
Temperature (K)	400.0	398.0	407.9	413.8
Absorption coefficient	1.0	1.020	0.921	0.862

A major concern is the stability and uniqueness of the inverse solution. At present the number of unknowns is being limited to a minimum of three (T, α, and σ) by assuming a homogeneous, isothermal medium. Determining these unknowns is called *parameter estimation* and is found by solving a system of overdetermined equations by the *least-squares minimization* method [4]. Although this method has been traditionally used with

inverse heat conduction problems [4], the same principles are applied to our inverse radiation problem. The least-squares approach has been used by Ho and Ozisik [5] to determine optical thickness and single-scattering albedo from measured radiation intensities for a plane-parallel medium. More recently, several inverse radiative methods for non-scattering axisymmetric medium were presented by Sakami and Lallemand [6].

The presentation focuses on how many sensors placed on the ceiling and walls would be necessary to ensure stability and convergence to the correct solution for a simplified two-dimensional cylindrical geometry. In addition, the sensitivity of measurements and initial parameter estimates to the stability of the solution are presented.

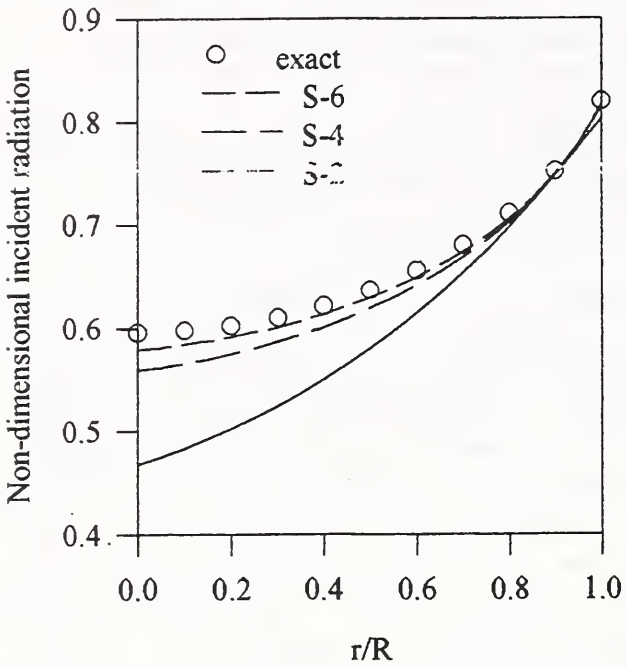

Figure 1. The forward problem: discrete ordinates approximations compared to exact solutions for an infinite cylinder [3]

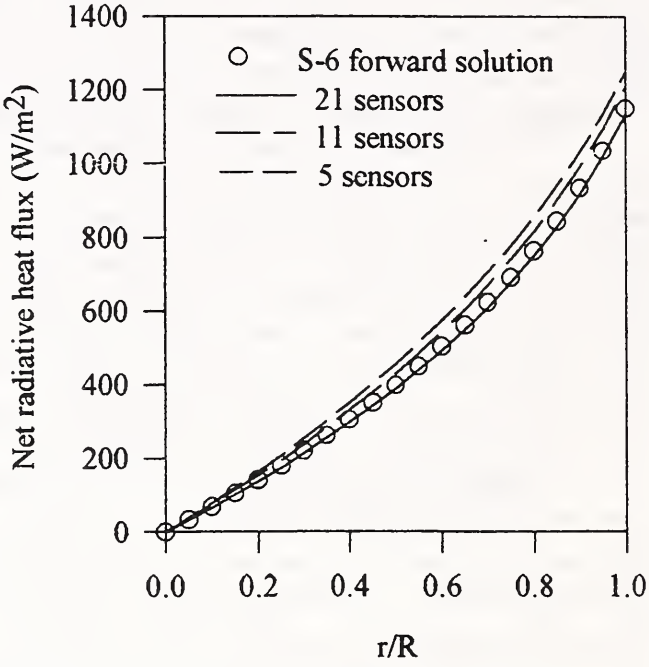

Figure 2. The inverse problem: reconstruction of net heat flux from temperature and absorption coefficient estimation

References

1. Lewis, E.E. and Miller, W.F., Jr. Computational Methods of Neutron Transport. John Wiley & Sons. New York, 1984.
2. Dua, Shyam S. and Cheng, Ping. Multi-dimensional radiative transfer in non-isothermal cylindrical media with non-isothermal bounding walls. International Journal of Heat and Mass Transfer, Vol. 18, 1975, pp. 245-259.
3. Siewert, C.E. and Thomas, J.R. Jr. Radiative transfer calculations in spheres and cylinders. Journal of Quantitative Spectroscopic, Radiative Transfer. Vol. 34, No. 1, 1985, pp. 59-64.
4. Ozisik, M.N. Heat Conduction. John Wiley & Sons. New York, 1993.
5. Ho, C.H. and Ozisik, M.N. Inverse radiation problems in inhomogeneous media. Journal of Quantitative Spectroscopic, Radiative Transfer. Vol. 40, No. 5, 1988, pp. 553-560.
6. Sakami, M. and Lallemand M. Retrieval of absorption and temperature profiles in axisymmetric and non-axisymmetric emitting-absorbing media by inverse radiation methods. Presented at the first conference on Inverse Problems in Engineering, Palm Coast, Florida, June 1993. Published by ASME, 1993.

Large-Scale Experiments of Fire Signatures to Develop a Discriminating Fire Detector

James A. Milke and Bjarne C. Hagen
Department of Fire Protection Engineering

Thomas J. McAvoy and D. Pan
Department of Chemical Engineering

University of Maryland at College Park
College Park, MD 20742

Incorporating intelligence into a fire detector can provide the capability to promptly react to smoke while discriminating between smoke from fire and non-fire sources. The primary purpose of this study was to investigate the patterns of signatures associated with fire and environmental signatures via experiments. During the most recent phase of research, work is being conducted to supplement the small-scale experimental effort reported previously [1]. The research is being conducted at the University of Maryland by teams in the Departments of Fire Protection Engineering and Chemical Engineering. The fire protection engineering team is concentrating on identifying signatures from fire and non-fire sources. The chemical engineering team is investigating the applicability of neural networks to discriminate between fire signatures.

Initially, small-scale tests were conducted to characterize the signatures from fire and non-fire sources. The experiments were designed to be conceptually similar to those by Okayama [2], with modifications incorporated to provide a greater range of measurements for describing the signature.

The small-scale experimental apparatus was a simplified tunnel which included a means for generating odors, measurement equipment and sensors. Measurements of light obscuration, temperature, and gas species concentrations (CO, CO_2 and O_2) and presence of any oxidizable gas are provided. The presence of oxidizable gases was measured by a Taguchi metal oxide sensor. Sources of the smoke or odor were placed under a hood at the inlet end of the apparatus. Smoke and odors were produced from a wide range of conditions: samples with flaming and pyrolyzing combustion, heated samples and samples maintained at ambient conditions where the odor was introduced into the box via an atomizer. The specific fuels and environmental sources were intended to be representative of a residential environment.

The following patterns in the small-scale experimental data were evident: the maximum CO_2 concentrations for flaming fires were at least 1500 ppm, while the maximum CO_2 concentration for the non-flaming fires (pyrolzing fires, heated liquids and environmental odors) were all less than 1500 ppm. The non-flaming sources can be distinguished based on the CO and metal oxide sensor peak

measurements. All but three of the pyrolzing solids had peak CO concentrations of at least 28 ppm and a signal of less than 6 V from the Taguchi detector. Based on these observations, an elementary expert system appears to be capable of identifying the source of the odor.

The level of success attained from the small-scale experimental program indicated the feasibility of the concept presented by Okayama. However, the success of the expert system only relates to the limited range of fuel sources investigated and the small-scale test apparatus. A large-scale experimental program is being conducted to determine whether the trends identified in the small-scale experimental effort also can be observed in large-scale environments. The large-scale experiments being conducted at the University of Maryland are conceptually similar to the small-scale experiments. Signatures from fires and environmental sources involving a wide variety of fuel sources are monitored. As in the small-scale study, patterns are being sought, with the applicability of an expert system or neural network investigated.

The large-scale experiments are being conducted in a 12 x 12 ft room with a height of 8 ft. Measurements include temperature, mass loss of the fire sources, CO, CO_2 and O_2 concentrations and the voltage output from three different metal oxide sensors. The three metal oxide sensors respond to the presence of CO, oxidizable gas and environmental odors respectively.

In addition to the large-scale experiments being conducted, results from a wide variety of large-scale experiments conducted at international research institutions including NIST, VTT, SP, SINTEF and DIFT are being analyzed to describe early fire signatures. This data is useful to describe signatures only from flaming and non-flaming fuel sources, excluding signatures from environmental sources.

This work is ongoing. Analysis of experimental data and application of neural network will be reported.

This work is supported by the Building and Fire Research Laboratory at the National Institute of Standards and Technology. The technical monitor is Dr. William Grosshandler.

Selected References

[1] Milke, J.A., Denny, S.A, McAvoy, T.J. and Pan, D., "Initial Application of Neural Networks to Discriminate Between Fire and Non-fire Odors," presented at the Annual Conference on Fire Research, Rockville, MD, October 19, 1993.

[2] Okayama, Y., "Approach to Detection of Fires in Their Very Early Stage by Odor Sensors and Neural Net", Proceedings of the Third International Symposium of Fire Safety Science, 1991, p. 955-964.

Simulating the Effect of Sloped Beamed Ceilings on Detector and Sprinkler Response

by

William D. Davis, Glenn P. Forney, and Richard W. Bukowski
Building and Fire Research Laboratory
National Institute of Standards and Technology

The rapid activation of fire detection and suppression systems in response to a growing fire is one of the important factors required to provide for life safety and property protection. Rapid activation requires that sensors be located at optimal distances both beneath the ceiling and radially from the fire. Ceiling obstructions, such as beams and joists, and ceiling slope can significantly modify the flow of smoke along the ceiling and must be taken into consideration when a particular detection system is designed. At present, the standards used to guide the design of these systems contain very little quantitative information concerning the impact of beamed, sloped ceilings on detector placement.

A multiyear, International Fire Detection Research Project sponsored by the National Fire Protection Research Foundation (NFPRF) was initiated to provide quantitative information on the impact of beams, ceiling slope, and forced ventilation on the movement of smoke and response of smoke and heat detectors. During the first year of the project, numerical modeling was validated and additional simulations of smoke and heat detectors in level, beamed ceiling geometries for slow, medium, and fast growing fires of 100 kW and 1 MW were completed [1]. Beamed ceilings with beam spacings of 1.2 m (4 ft), 1.5 m (5 ft), 1.8 m (6 ft), 2.1 m (7 ft) or 2.4 m (8 ft) and beam depths of 0.1 m (4 in), 0.2 m (8 in), 0.3 (12 in) and 0.6 m (24 in) were modelled. The ceiling heights modelled included 3.3 m (11 ft), 4.6 m (15 ft), 5.8 m (19 ft), 6.7 m (22 ft), 7.6 m (25 ft) and 8.5 m (28 ft). Smoke detectors were assumed to activate when the temperature reached 13 ^{o}C above ambient. Heat detectors were simulated using the model of Heskestad and Smith [2] and were assumed to activate when the temperature reached 57 ^{o}C above ambient. It was found that conditions under beams may be equivalent in some cases to conditions in the channels between the beams at an equivalent depth beneath the beam or ceiling. Also, depending on detectable fire size, beam depth and beam spacing, smoke detectors or quick response fusible link may not be required for each beam channel. Recommendations for detector placement were made for the geometries studied.

This presentation describes the results of the second year of the project. During the second year, numerical simulations of smoke movement in response to sloped, beamed ceilings were studied using the computational fluid dynamics model HARWELL-FLOW3D. Sloped ceilings of 10, 25, and 50 degrees were studied for beams running along the ceiling slope. Beam spacings of 1.2 m (4 ft) and 2.4 m (8 ft) with beam depths of 0.1 m (4 in), 0.2 m (8 in), 0.3 m (12 in) and 0.6 m (24 in) were modelled. Medium growth fires of 100 kW and 1 MW were used in the study and ceiling heights above the plume were restricted to 3.3 m (11 ft) and 4.6 m (15 ft). It was found that increasing ceiling slope allowed the parallel beams to channel the smoke more effectively in the upslope direction. Downslope flow decreased substantially as ceiling slope was increased. When smoke flowed into an adjacent beam channel, the conditions under the beam separating the two beam channels were suitable for detector placement. Slow response detectors (RTI 300 $(m\ s)^{1/2}$) require substantially denser placement requirements in order to produce satisfactory detection compared with fast response detectors (RTI 50 $(m\ s)^{1/2}$) or smoke detectors.

Numerical simulations for beams perpendicular to the ceiling were done for ceiling slopes of 10 and 25 degrees. Beam spacing of 2.4 m (8 ft) and beam depths of 0.15 m (6 in), 0.30 m (12 in) and 0.46 m (18 in) were used with the medium growth fires of 100 kW and 1.0 MW. Ceiling heights were chosen to be 3.3 m (11 ft). It was found that increasing the ceiling slope caused the beams to be less effective at slowing the smoke flow up the ceiling. There was also substantially less smoke flow over beams located beneath the plume center on the downslope side of the ceiling. The perpendicular beams produced substantial flow along the beams. For the 0.46 m (18 in) beams, upslope flow tended to occur where the beam meet a side wall rather than occurring directly upslope from the plume.

Special cases of beams with gaps between the top of the beam and the ceiling were also studied. For beams parallel to the ceiling, a ceiling slope of 50 degrees was used for beams separated by 1.2 m (4 ft) on center with a beam gap of 0.08m (3 in) for 0.6 m (24 in) beams. It was found that this gap did increase the smoke flow into adjacent channels.

For beams perpendicular to the ceiling, a ceiling slope of 25 degrees was used for beams separated by 2.4 m (8 ft) on center with a beam gap of 0.13m (5 in) for 0.46 m (18 in) beams. While the beams did provide some resistance to the flow of smoke up the ceiling, the gap provided a substantial increase in the flow rate up the ceiling.

Recommendations for the placement of smoke detectors and heat detectors with RTI ratings of 50, 100, and 300 $(m\ s)^{1/2}$ are made for both parallel and perpendicular beam geometries for the detection of 100 kW and 1 MW fires.

1. Glenn P. Forney, Richard W. Bukowski, and William D. Davis, Field Modeling: Effects of Flat Beamed Ceilings on Detector and Sprinkler Response, National Fire Protection Research Foundation, Batterymarch Park, Quincy, Mass, USA. 1993.

2. Gunnar Heskestad and Herbert F. Smith. Investigation of a New Sprinkler Sensitivity Approval Test: The Plunge Test. Technical Report Serial No. 22485 2937, Factory Mutual research Corporation, Norwood, MA, 1976. RC 76-T-50

ON SOLID FUEL IGNITION AND FLAME SPREAD

A. Carlos Fernandez-Pello
Department of Mechanical Engineering
University of California at Berkeley
Berkeley, CA 94720, USA

ABSTRACT

The gas phase ignition of a solid and the subsequent spread of flames over its surface, are important processes in the combustion of solid fuels. In addition to the need of understanding theses processes fundamentally, there is a need for the development of predictive formulas for the ignition delay and flame spread rate that can used in practical applications, such as models of fire development and hybrid rocket fuel combustion. Those are the objectives of this work. Based on the available information on these processes, it is proposed to analyze the flame spread as a solid ignition problem where the flame acts both as the source of solid heating and gasification, and of ignition of the gas phase reaction (pilot). The flame spread rate is then given by the ratio of a solid heating length to the ignition time. An analysis of solid fuel ignition is developed that provides explicit expressions for the ignition delay, which is then used to obtain an explicit expression for the flame spread rate. This expression predicts well the available experimental flame spread rate data, including the fast and slow chemistry regimes, and the blow-off and surface heat losses extinction (no spread) limits.

IGNITION: The gas phase ignition of a solid fuel is generally the combined result of an externally applied heat flux that causes the gasification of the solid, and the presence of thermochemical conditions that will lead to the onset of a sustained combustion reaction between the vaporized fuel and the oxidizer gas. Considerable work has been conducted on the ignition of solid fuels (Vilyunov and Zarko, 1989). Particularly relevant for the present work is the experimental studies of Kashiwagi et al. (1971), and Niioka et al. (1981) of the spontaneous ignition of several polymers in a high temperature oxidizing gas flow. The former experiments were conducted in a flat plate flow and the latter in a stagnation point flow. They suggest that two primary, competing mechanisms control the solid ignition process. One is the heating and gasification of the solid, and the other is the onset of the gas phase chemical reaction. The former one gives way to the definition of a "solid pyrolysis" time that decreases as the heat flux (stretch rate) is increased, and that is represented by the descending branch in the ignition curves. The later one gives way to the definition of a gas phase "induction" time that increases as the stretch rate increases (convective cooling), and that is represented by the ascending branch in the ignition curves. Explicit formulas for both times can be developed from analyses of the solid heating problem and the gas phase ignition problem (Niioka, 1981, August and Fernandez-Pello, 1993).

FLAME SPREAD: For a flame to spread over the surface of a combustible material, enough heat must be transferred from the flame to the unburnt material ahead of the flame to pyrolyze it. The vaporized fuel is then diffused and convected away from the surface, mixing with the oxidizer and generating a flammable mixture ahead of the flame leading edge, which is then ignited by the flame. The rate of flame spread is therefore determined by the ability of the flame to transfer the necessary heat to pyrolyze the solid and to ignite the combustible mixture ahead of it. Considerable work has also been conducted on the spread of flames over a solid combustible surface (Fernandez-Pello and Hirano, 1983, Wichman 1992). Particularly relevant to the present work are the results of the experimental measurements of Fernandez-Pello et al. (1980), of the rate of flame spread over the surface of thick PMMA sheets as a function of the velocity and oxygen concentration of a gas flowing parallel to the solid surface in the

opposite direction of flame propagation. The results show that for high oxygen concentrations, as the flow velocity is increased the spread rate first increases, reaches a maximum, and then starts to decrease. For low oxygen concentrations, the spread rate decreases as the gas velocity is increased until the flame can no longer propagate against the opposed gas flow.

Through phenomenological arguments, the above authors postulated that the flame spread rate was controlled by the interaction between processes dominated by heat transfer from the flame to the solid and by gas phase chemical kinetics, and proposed correlating the flame spread rate data in terms of two non-dimensional parameters. One, a non-dimensional flame spread rate derived from a heat transfer flame spread analysis, and the other the Damkohler number.

THE RELATIONSHIP BETWEEN IGNITION AND FLAME SPREAD: An interesting aspect of the above studies is the similarity between the mechanisms controlling the ignition of the solid and the spread of the flames over its surface. In fact, by simply comparing the ignition data, and the flame spread data, it can be inferred that there is an inverse relationship between the ignition delay and the flame spread rate. This observation leads to the concept that the spread of the flame can be viewed as a solid ignition process where the flame acts both as a source of solid heating and as a pilot for gas phase induction. Furthermore, it is possible to develop a simplified model of flame spread that is based on the analyses developed for the solid ignition.

To develop the analysis, it is convenient to describe the sequence of events that lead to the spread of the flame over the solid surface as those that a solid element, initially at the forward edge of the solid region heated by the flame, would undergo to its ignition. Since the time for the solid element to ignite is the same as for the flame to propagate to the solid element location, the flame spread rate would be given by the ratio of the length of the solid heated region ahead of the pyrolysis front to the solid ignition time. Thus, for a specific flame spread problem, the analysis would consist of two sub-analyses; one that would give the solid ignition time, and another that would give the length of the solid region ahead of the flame (or pyrolysis) front. The flame spread rate would then be given by the ratio of the latter to the former values.

Such an analysis has been developed for the case of flame spread in an opposed forced flow, and used to correlate the data from Fernandez-Pello et al. (1980). The results of the correlation are quite good except at low oxygen concentrations, where chemical kinetic effects are important and the ignition model falters somewhat due to the used simplified chemistry. Similar types of analyses can also be developed to predict flame spread under other flow conditions, i.e., downward and upward spread in natural convection, forward forced flow, etc.

REFERENCES

August. M, and Fernandez-Pello, A.C.: *14th Int. Coll. Dyn. Exp. and React. Syst.*, Coimbra, Portugal, August 1993.

Fernandez-Pello, A.C., Ray, S.R., and Glassman, I., *18th Symp. (Int.) Combust.*, 1980, 579.

Fernandez-Pello, A.C., and Hirano, T., *Combust. Sci. Technol.*, 1983, **32**, 1.

Fernandez-Pello, A.C., "The Solid Phase," *Combustion Treatise on Fire*, G. Cox, editor, Pergamon Press, (in press), 1994.

Kashiwagi, T. MacDonald, B.W., Isoda, H., and Summerfield, M.,: *13th Symp. (Int.) Combust.*,1971,1071

Niiioka, T., *18th Symp. (Int.) Combust.*, 1981, 1087.

Niioka, T., Takahashi, M., and Izumikawa, M., *18th Symp. (Int.) Combust.*, 1981, 741.

Vilyunov, V.N., and Aarko, V.E., *Ignition of Solids*, Elsevier, 1989.

Wichman, I.S., *Prog. Energy Combust. Sci.*, 1992, **18**, 6, 553.

FLAME-SURFACE HEAT FLUX MEASUREMENTS IMPROVE HORIZONTAL CONCURRENT FIRE SPREAD PREDICTIONS

V.B. APTE and A.R. GREEN
Londonderry Occupational Safety Centre
132 Londonderry Road, Londonderry, NSW 2753, Australia

ABSTRACT

Horizontal wind assisted fire spread is driven by the flame-surface heat flux. **The present paper aims at improving our earlier [1] flame spread predictions by measuring the flame to surface heat flux.**

A 50 m long section of a 5.4 m wide x 2.4 m high tunnel was used for the tests. 0.5, 1.0, 1.5, 2.0 and 2.5 m long clear PMMA sheets (6mm thick, 0.654 m wide) were used to create pool fires simulating successive stages of fire spread. The PMMA sheet was supported on a weighing platform. Heat flux gauges were arranged downwind of the pool fire to measure the flame-unburned surface heat flux. A mixture of PMMA shavings, paraffin oil and octane was used to uniformly ignite the entire PMMA sheet thus creating a pool fire. The fuel mass, heat flux and air flow data was logged on a computer. Experiments were conducted at wind speeds of 1.0, 1.5, 2.0 and 2.5 m/s in the tunnel.

Equation 1, [2] is used to predict the flame spread velocity V_p.

$$V_p = \frac{dX_p}{dt} = \frac{(X_f - X_p)\ (\dot{q}''_f)^2}{\frac{\pi}{4}\ k\rho c\ (T_{ig} - T_\infty)^2} \qquad (1)$$

The previous [1] X_f (flame length) and X_p (pyrolysis length) data are used. To estimate the surface heat flux $\dot{q}''_f$ in Eq. 1, a correlation of $\dot{q}''_f$ vs. mass loss flux $\dot{m}''$ (Fig. 1) obtained using the present data for all the sheet lengths and wind speeds is used. $\dot{q}''_f$ corresponds to the surface location immediately after the end of the pyrolysis front. Data only during the fire growth are considered. These data are represented as :

$$\dot{q}''_f = 16.44 + 3180.82\ \dot{m}'', \qquad \dot{m}'' < 0.0136 \qquad (2)$$

$$\dot{q}''_f = 44.48 + 1148.83\ \dot{m}'', \qquad \dot{m}'' > 0.0136 \qquad (3)$$

The intercept and the slope of Eqs. 2 and 3 represent $\dot{q}''_{r,r}$ (heat flux re-radiating from the PMMA surface) and L (heat of vaporisation) which includes the transient conduction loss into PMMA respectively. Equation 2 corresponds to the early heat-up period when $\dot{q}''_{r,r}$ is small and L is large as it accounts for the transient heat conduction into PMMA. As the sheet heats up (Eq. 3), $\dot{q}''_{r,r}$ increases and L decreases due to reduced conduction losses. Using Eqs. 2 and 3 for the earlier $\dot{m}''$ data [1], the revised surface heat flux $\dot{q}''_f$ values to be used in Eq. 1 are calculated.

Using piloted ignition data for PMMA exposed to radiant heat fluxes in the range of 20-75 $kW.m^{-2}$ in a cone calorimeter and methods reported in literature [1,2], T_{ig}= 600 K and $k\rho c$=0.8 $kW^2.m^{-4}.K^{-2}.s$.

Figure 2 compares measured [1] and predicted (using Eq. 1) spread velocities at a wind speed of 2 m/s. The revised prediction (curve 4) is better than the earlier predictions [1] corresponding to curves 2 and 3 because the $\dot{q}''_f$ values based on measurements (using Eqs. 1 and 2) are used for curve 4. The predictions begin to deviate rapidly from the measurements for X_p > 1.5 m as the flame now stands up like a plume due to increased buoyancy [1] and Eq. 1 is not strictly valid as it assumes the flame-surface heat flux to be constant between X_p and X_f, and zero beyond X_f.

REFERENCES

1. Apte V.B., Bilger R.W., Green A.R. and Quintiere J.G., "Wind-Aided Turbulent Flame Spread and Burning Over Large-Scale Horizontal PMMA Surfaces", Comb. Flame, 85 : 169-184, 1991.

2. Quintiere J.G., "The Application of Flame Spread Theory to Predict Material Performance", J. of Res. of National Bureau of Standards, 93 : 61-70, 1988.

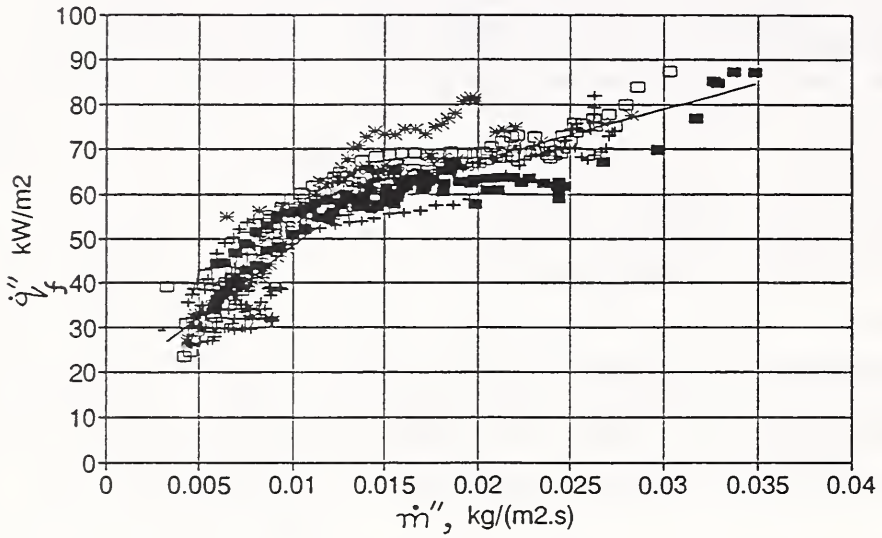

Figure 1 :

A correlation between flame-surface heat flux $\dot{q}''_f$ and pyrolysis mass loss flux $\dot{m}''$.
X_p = 0.5 - 2.5 m
Wind vel. = 1- 2.5 m/s

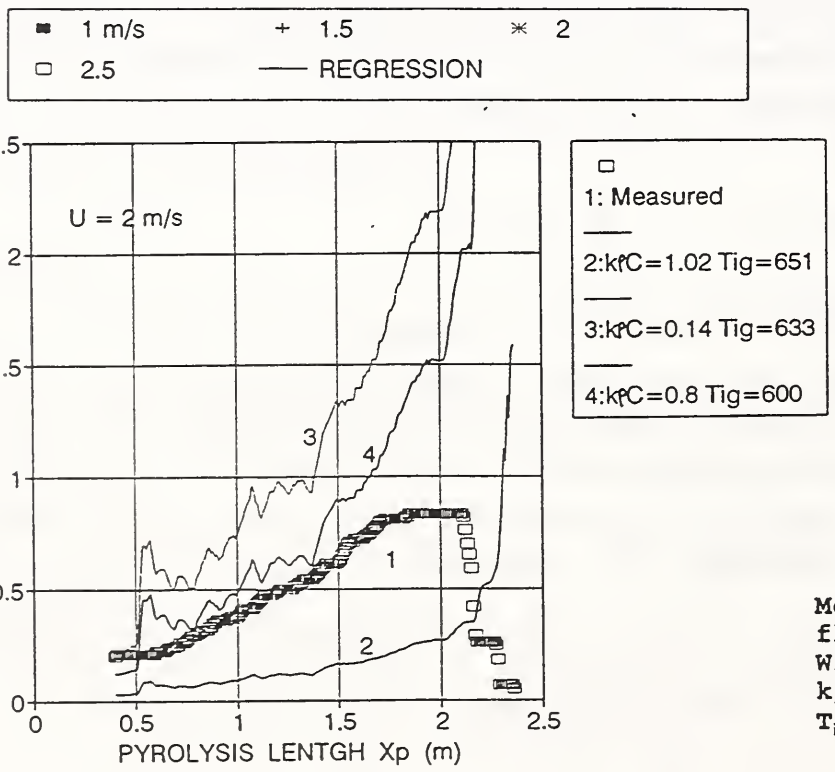

Figure 2 :

Measured [1] and predicted flame spread velocity.
Wind vel. = 2 m/s.
$k\rho c$ in $kW^2.m^{-4}.K^{-2}.s$
T_{ig} in K.

Characterization of Horizontal Flame Spread on Charring Surfaces

V. Motevalli and Y. Chen
Worcester Polytechnic Institute

M. A. Delichatsios
Factory Mutual Research Corp.

P. Tatem
Naval Research Laboratory

Introduction

A model for prediction of flame spread on horizontal surfaces has been developed for shipboard applications[1,2]. This is a general model appropriate for any simple material (as opposed to a composite), both charring and non-charring, in a horizontal orientation. This model may be extended to a composite material or used to predict lateral and downward flame spread. The flame spread prediction is primarily driven by a transient thermal model for heat transfer calculation and heating of the surface. This model is being coupled with an integral combustion model[3] which permits the calculation of the flame radiation[4] as the flame grows due to the increase in the burning area. The most important input to the model are the flame heat flux distribution and material properties. The flame flux distribution is divided into two components; a) radiation from the flame, and b) gas-phase conduction ahead of the flame front. Characterization of these two fluxes ahead of the flame as well as the surface temperature measurements are discussed herein.

Experiment and Instrumentation

Our experiment was primarily motivated by the strong need to determine the flame flux distributions. The methodology was inspired by a previous work[5]. A Constant Velocity Flame Spread Experiment (CVFSE), see Figure 1,was designed where a computer controlled slide mechanism is used to move a fuel sample at a constant velocity toward a stationary flame front. In doing so, the spread velocity is fixed and the external heat flux incident on the fuel surface is known at any given instance of time. While the flame front is stationary, the points on the sample surface, moving toward the flame front experience an increasing heat flux, same as the condition observed if the fuel sample was stationary and the flame front were to move toward the points of interest.

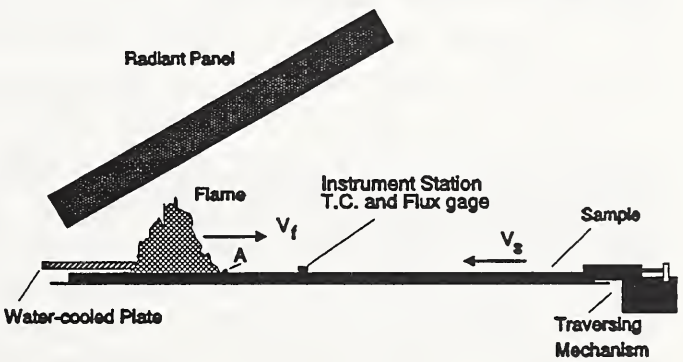

Figure 1 - Schematic of the constant velocity flame spread apparatus

The fuel samples were instrumented with thermocouples and total flux gages. At three stations, a thermocouple (K-type, 0.005" in diameter) was imbedded at the surface and another was mounted in the gas-phase above the sample (about 0.5 mm). Heat flux gages were also positioned flushed with the surface at two of the three instrument stations. A very small flux gage (1/16", 1.59 mm in diameter) was used to measure the total heat flux as the measuring station was moved toward the flame front.

Each fuel sample was initially pre-heated, then ignited, and finally the slider was moved when a pre-determined burning area was established. The predetermined slider velocity, would result in a constant burning area and flame spread rate since the external flux distribution is decaying with distance. At some location, away from the initial ignition point, the external flux level is just adequate to sustain a flame spread velocity matching the velocity of the slider mechanism. As the burning area is moved under the plate, the flame is quenched and burning is stopped.

Particle boards have been used as fuel samples in a number of constant flame spread tests. The samples were 800 mm long and 151 mm wide and the thickness of the particle board was 11.3 mm. The sample was first stationary and preheated during a prescribed time. A pilot ignition flame was then introduced to the sample leading edge. Three instrumentation stations were located at 200, 400 and 600 mm distances from the fuel sample edge. The material surfaces were painted with a known emissivity (0.92) black paint.

Results

The temperature measurements for a single test of particle board (charring) are shown in Figure 2. Time when the flame front location is reached is clearly indicated by the sudden jump in the temperature. The gas temperature close to the surface is very close to, but lower than, the surface temperature, as would be expected. The heating length ahead of the flame front can be estimated from the temperature history. The material pyrolysis temperature can also be deduced from the surface temperature measurements. The surface temperature measurements are used to validate the surface heating ahead of the flame front, which includes surface reradiation and convective heat transfer. In order to validate the flame spread model, the flame heat fluxes must be known. Figure 3 shows total the flame flux ahead of the flame and its decoupling into flame radiation and gas-phase conductive fluxes. The total flux is the measured flux by the water-cooled gage minus the known external flux. The total flux represents the combination of the flame radiation and gas-phase conduction. We have assumed that the flux distribution could be represented by:

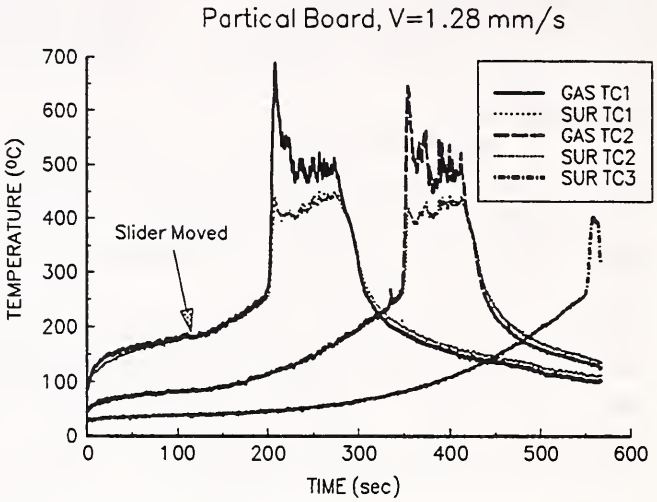

Figure 2 - Gas and surface temperature histories at 200, 400 and 600 mm from the sample edge.

$$\dot{q}''_{total} = \dot{q}''_g + \dot{q}''_R = \dot{q}''_{max,g}\, e^{-\frac{x}{\delta_g}} + \dot{q}''_{max,R}\, e^{-\frac{x}{\delta_R}} \qquad (1)$$

where δ_g and δ_R are the heating length scales. Here, we have taken the flame radiation flux to be equal to the total flame flux at distances much greater than δ_g. In order to obtain the gas-phase conductive flux, $\dot{q}_g$, we subtracted the radiation flux, which is assumed to increase linearly up to the flame front, and then corrected the flux for the fact that the flux gage is water-cooled. Using this approach, we hope to be able to determine $\dot{q}_{g,max}$ and δ_g from these measurements. Finally, we would use $\dot{q}_{g,max}$, $\dot{q}_{R,max}$, δ_R and δ_g as inputs to our flame spread model to compare the spread rate with the measured flame spread.

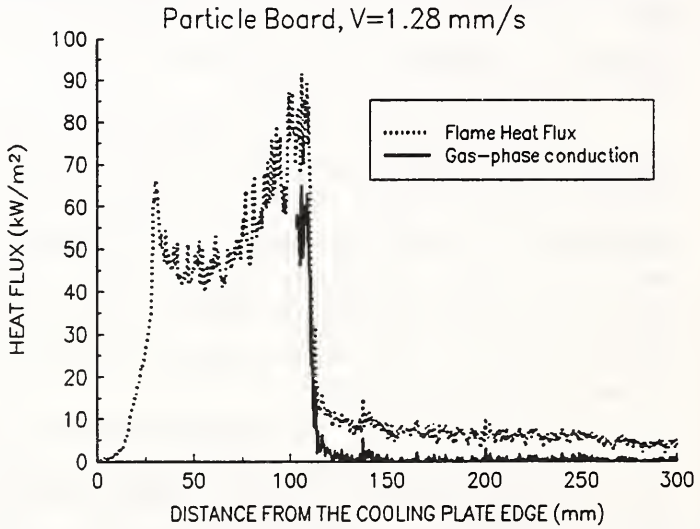

Figure 3 - Flame flux distribution ahead of the flame front.

References

1. Motevalli, V., Chen, Y. and Delichatsios, M.A., "Horizontal Flame Spread on Ship Compartment Surfaces", Annual Rpt. to the Naval Research Laboratory, Sept. 30, 1992.
2. Chen, Y., Motevalli, V. and Delichatsios, M.A., Joint Meeting of Eastern and Central Sections of the Comb. Inst., pp. 626-630, 1993, New Orleans.
3. Chen, Y., Motevalli, V. and Delichatsios, M.A., Joint Meeting of Eastern and Central Sections of the Comb. Inst., pp. 51-55, March 1993, New Orleans.
4. Delichatsios, M.A., Chen, Y., Motevalli, V. and Tatem, P., to appear in 4th Int'l Symposium of Fire Safety Science, Ottawa, Canada, June 1994.
5. Bhatnagar, S.K., Varshney, B.S., Mohanty, B. and Agarwal, C.P., 23rd Symp. (Int'l) on Comb., Comb. Inst., 1990, pp. 1693-1699.
6. Ito, A. and Kashiwagi, T., Combustion and Flame, April 1987.

CONCURRENT CEILING FLAME SPREAD: THE COMBINED EFFECT OF FLOW VELOCITY, TURBULENCE AND OXYGEN CONCENTRATION

Y. H. C. Chao and A. C. Fernandez-Pello

Department of Mechanical Engineering
University of California, Berkeley
Berkeley, CA 94720

ABSTRACT

Experiments have been conducted to study the mechanisms controlling the spread of flames over the surface of a thick solid fuel in an oxidizing gas flow moving in the direction of flame propagation. The parameters varied in the experiments are the oxidizer flow velocity, turbulence intensity and oxygen concentration, and the geometrical orientation (floor and ceiling). Their effect on the flame spread process is studied by measuring the rate of flame spread, flame length, surface heat flux, exhaust gas temperature, products of combustion and soot. Experimental results of the ceiling geometry will be presented in this paper. The results of the experiments show that the combined effect of flow velocity, turbulence intensity, and oxygen concentration has a complex influence on the flame spread process. At low flow velocity, the flame spread rate increases monotonically with turbulence intensity. At high flow velocity, however, the flame spread rate increases with flow turbulence at low turbulence intensities, but it decreases at high turbulence intensity values. The effect is more pronounced at high oxygen concentration. These trends appear to be due to a strong influence of the turbulence intensity on the flame temperature and length, and on the heat flux from the flame to the solid fuel. Turbulence enhances mixing, which increases the flame temperature and then the heat flux. It is shown that the heat flux data can be correlated in terms of a non-dimensional heat flux, $q''x/(\rho\alpha BL)$, that is approximately linearly proportional to the non-dimensional flow parameter, $aRe^{0.5}[1+b(u'/U)^{0.5}]$. The effect of turbulence on the flame length comes from two opposing factors. In one hand the enhanced mixing results in a stronger reaction with faster reactant consumption, which tends to produce a shorter but hotter flame. On the other hand , the higher flame temperature results in an increased mass burning rate, which tends to increase the flame length. It appears that at low flow turbulence, the latter effect dominates and thus there is an increase in the flame length. As the turbulence level continues to rise, the reactant comsumption dominates, which leads to a decrease in the flame length. For the present experiments, the transition between the two regimes shifts from $u'/U = 5$ % at $U = 2.0$ m/s, to $u'/U = 15$ % at $U = 1.0$ m/s, and no transition point is observed at $U = 0.5$ m/s within our experimental conditions. A flame length expression has been derived by performing a mass balance on the oxidiser content in the gas phase. Good correlation is obtained at high flow velocity and oxygen level, where the assumption of complete combustion is valid. The flame spread rate is the outcome of the combined effect of the flame length and the heat flux. Under all flow velocities and turbulence intensities, the flame spread rate increases with the oxygen concentration. For low oxygen concentrations, a linear dependence is observed between the flame spread rate and the oxygen concentration. For high oxygen concentrations, the dependence of the flame spread rate on the oxygen concentration follows a second power law. It has also been found that buoyancy has two opposite effects on the ceiling flame spread, one is enhancing the heat transfer to the surface by reducing the flame stand-off distance and the other reducing the chemical reaction

completeness by intensifying the flame quenching at the wall. The overall buoyancy effect on the flame spread and mass burning processes depends on the flow condition.

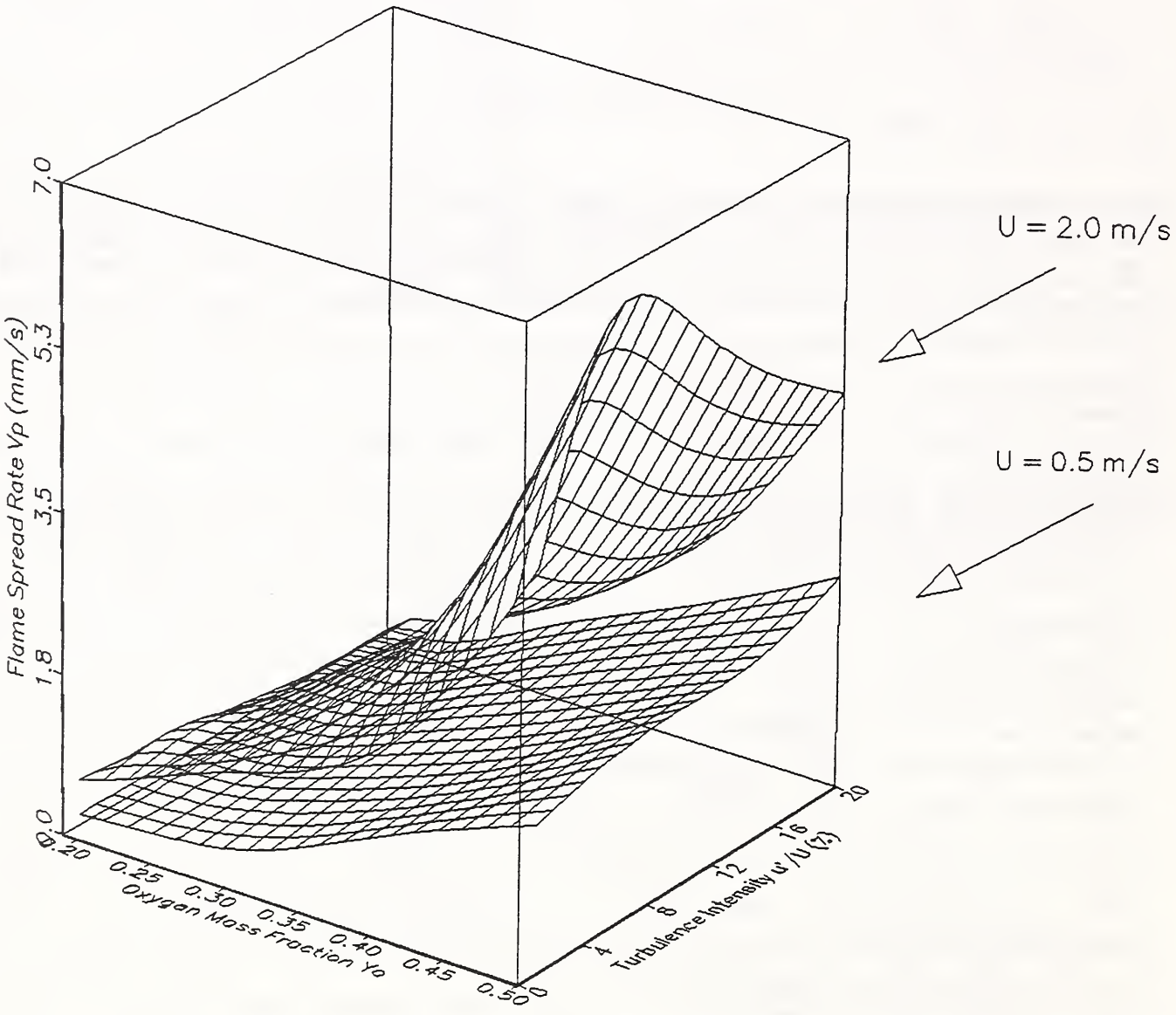

Flame spread rate at U = 0.5 m/s and 2.0 m/s

Similarity of Turbulent Wall Fires

J. de Ris and L. Orloff
FMRC

This study was undertaken to help resolve the general flammability problem - namely, to predict heat release rates and fire spread rates in terms of readily measured material flammability properties. At present much of the problem is understood; however we do not have established procedures for predicting the radiative heat transfer to adjacent fuel surfaces. These predictions must be quite accurate because upward spread and burning processes are very sensitive to flame heat transfer from the flames due to positive feedback. The present work parallels Markstein's[1,2] investigation of the radiant heat transfer blockage by the cold gas and soot near the fuel surface. Here we are concerned with the soot and temperature profiles responsible for the radiant emission from the flames. The results show the profiles remain geometrically similar for a fixed overall fuel to entrained air equivalence ratio corresponding to a fuel mass transfer rate, $\dot{m}''$, which increases with the square root of height, Z.

Various pyrolysis zone heights were simulated by supplying propylene to up to ten 132mm high and 320 mm wide water-cooled sintered-metal gas burners. The forward heat transfer zone was simulated by a 660mm high water-cooled heat transfer plate mounted above the gas burners. The flow was maintained two-dimensional by 150mm deep water-cooled side walls attached to the burner apparatus over its entire height.

The thickness of the soot layer, δ_s, was measured by inserting arrays of 5mm glass rods into the flames perpendicular to the wall surface and rapidly withdrawing them after a two second exposure to the flames. The soot layer thickness was determined from the average length of soot deposit on ten rods.

Figure 1 shows the length ratio, Z/δ_s, correlated against the inverse modified equivalence ratio $\rho_A(2gZ)^{1/2}/(\dot{m}''-\dot{m}_o'')$. The modification of the equivalence ratio is required because the soot vanishes and the flames become blue for mass transfer rates less than $\dot{m}_o''=4$ g/m^{2}s. As a result of wall cooling and dilution by the products of combustion at low mass transfer rates, the data show that the cut-off, $\dot{m}_o''$, is independent of Z. The turbulent motion typically transports the luminous soot (e.g. visible flames) out into the incoming air all the way to where the mean gas temperature drops to around 1000 K. The correlation says that the soot layer thickness is proportional to Z for a given ratio of entrained air, $\rho_A(2gZ^3)^{1/2}$ to supplied fuel $\dot{m}''Z$ above its blue flame value $\dot{m}_o''Z$. The correlation extends over a very wide range of flame equivalence ratios.

Temperature profiles across the flame boundary layer were measured by a thermocouple rake consisting of 15 insulated Chromel-Alumel thermocouples inside 1.6 mm diameter Inconel sheaths spaced 12.6 mm on center and protruding 1 cm downward into the rising flow. The measured temperatures inside the flame were significantly depressed by radiation heat loss. On the other hand, the thermocouple temperatures outside the flame were significantly increased by radiant heat transfer from the flame. We corrected for both these effects with a simple heat transfer model to obtain the correlations shown in Figure 2. The vertical dashed line at $y/\delta=1$ shows the boundary of the soot layer occurring at temperatures near T=1000K. Inside the soot layer, the presence of cold fuel is seen by the temperature drop near the wall. Outside the soot layer, the mixing of combustion products with the entrained air causes the corrected temperatures to asymptotically approach the ambient temperature as y/δ increases. These outer temperature profiles correlate reasonably well when plotted against $(y-\delta)/Z$.

Markstein[2] reports measurements of the extinction of infrared radiation, ε_o, by soot (at wavelengths λ_o = 0.9 μm and 1.0 μm) across the flame boundary layer. These measurements immediately provide the integral of the soot volume fraction, $f_v\delta_s$, across the flame, $f_v\delta_s=-\lambda_o\, ln(1-\varepsilon_o)/7$, which is replotted here in Figure 3 using coordinates similar to those in Figure 1. The factor of 7 in the above expression is recommended by Hottel and Sarofim[3] for soot. The correlation is not as good as for the soot standoff distance (Figure 2), apparently because the soot volume fraction, f_v, depends weakly on the flow time.

The faired curves in Figure 3 indicate that the fractional conversion of fuel carbon to soot, χ_s, at a fixed mass transfer rate (1) initially increases proportional to the flow time up to a height Z=0.75 m for the C_3H_6 flames, and then (2) becomes constant at greater heights.

Figure 4 shows the measured transverse temperature profiles for four C_3H_6 flames at two heights and two equivalence ratios, $\dot{m}/Z^{1/2}$ near 11 and 26 g/m$^{5/2}$s respectively. Notice the dependence of profile-shape on equivalence ratio, but almost perfect similarity at fixed equivalence ratios. Theory suggests that the heat release

by combustion per unit wall height increases with $Z^{1/2}$ at fixed equivalence ratio. The present data suggest that the soot and gas radiation initially increase almost linearly with height for small Z where radiation is unimportant, but convective heat loss is important. At somewhat greater heights the radiation increases more nearly with $Z^{1/2}$ due to radiant heat loss. Ultimately the radiation will level off at very large Z after the flames become optically thick.

The similarity of combustion observed in this study greatly eases the task of analyzing experimental data and will make it much easier to tailor future detailed semi-empirical turbulent combustion models, so that their predictions exactly agree with experiment (at least for situations having $\dot{m}'' \sim Z^{1/2}$). One rarely finds such true similarity (i.e. reducible to one-dimensional behavior) in combustion, especially turbulent buoyant combustion.

References

1. Markstein, G.H. and de Ris, J.: Twenty-Fourth Symposium (International) on Combustion, 1747, The Combustion Institute, 1992.
2. Markstein, G.H.: Personal Communication, 1994.
3. Hottel, H.C., and Sarofim, A.F. (1962), *Radiative transfer*, McGraw-Hill, New York, p. 199,

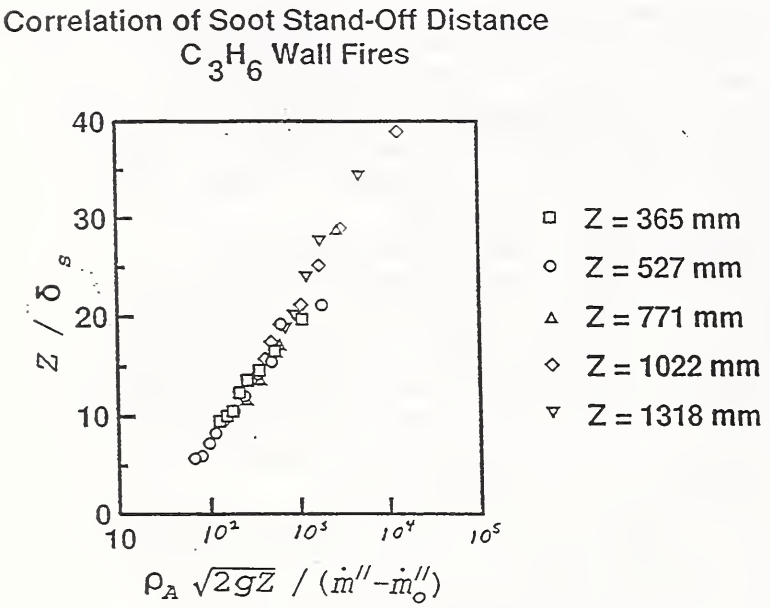

Figure 1.

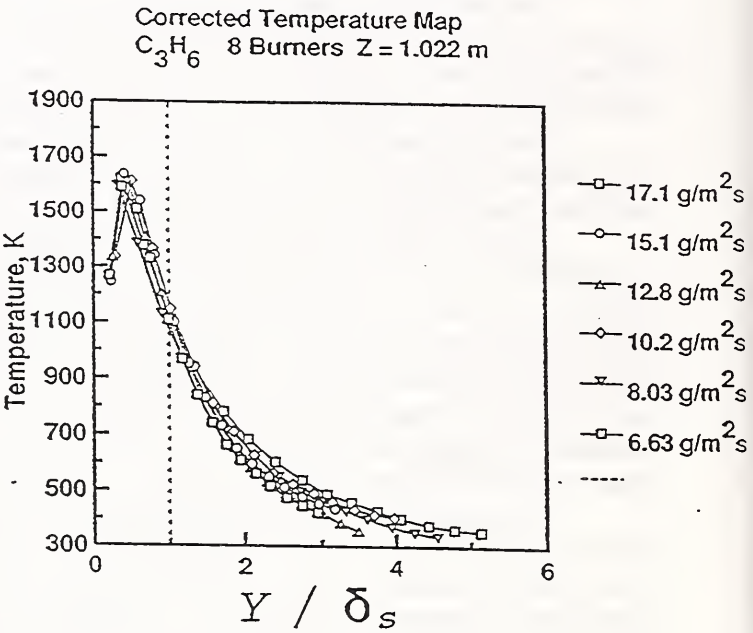

Figure 2.

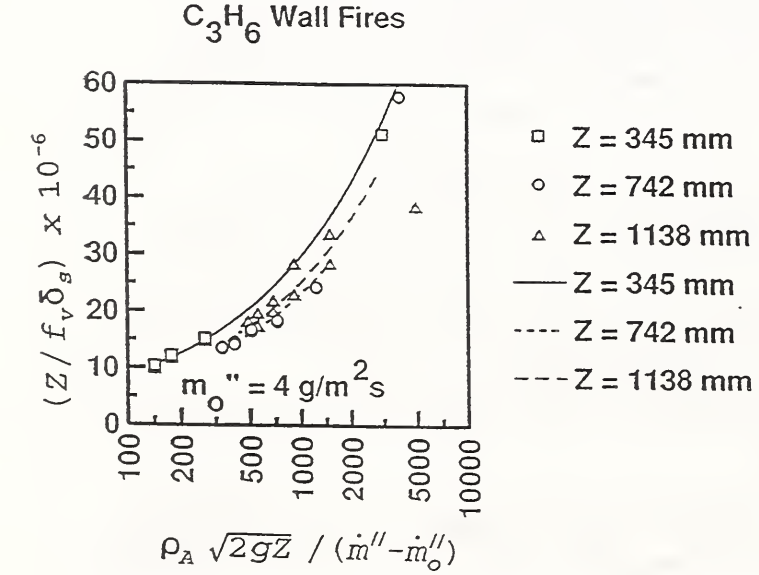

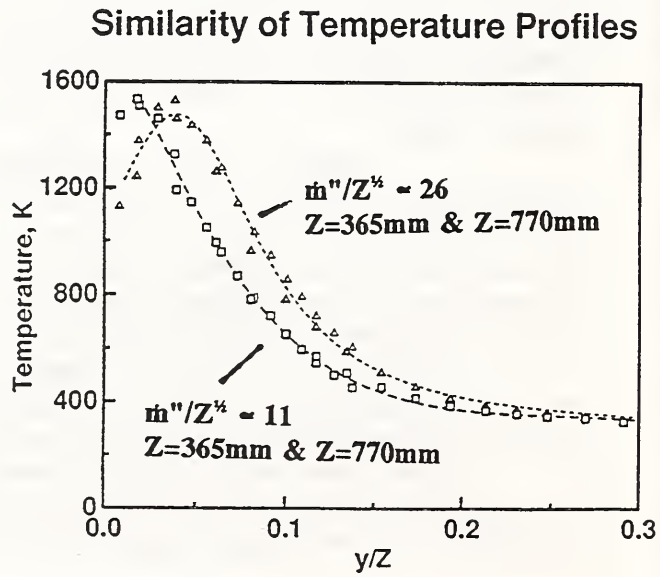

THE PHI-METER: A FUEL-INDEPENDENT INSTRUMENT FOR MONITORING COMBUSTION EQUIVALENCE RATIO

George Mulholland, Vytenis Babrauskas[1], William J. Parker[2], William H. Twilley
Building and Fire Research Laboratory
National Institute of Standards and Technology
Gaithersburg, MD 20899, USA

Gaseous carbon monoxide is mainly responsible for deaths due to unwanted fires[1]. This has been a major difficulty to specialists in fire protection engineering, since quantitative methods for predicting CO yields from building fires have not been available. Recent studies have indicated that the production of CO is primarily controlled by the equivalence ratio, φ, which is defined as

$$\phi = \frac{[fuel/oxygen]}{[fuel/oxygen]_{stoic}}$$

where 'stoich' denotes the stoichiometric fuel/oxygen ratio; it represents the actual fuel/oxygen ratio, compared to its stoichiometric value. Thus, $\varphi < 1$ implies fuel-lean and $\varphi > 1$ implies fuel-rich combustion.

Studies by Toner et al.[2] on methane, Morehart et al.[3] on methane and ethylene, and Beyler [4],[5] on hydrocarbons, alcohols, as well as several polymers indicate an abrupt increase in the CO concentration by more than a factor of 10 as the global equivalence ratio increases from about 0.5 to 2. By 'global,' we mean here the overall equivalence ratio for the combustion process and not any spatial variations of fuel or oxygen concentrations. These studies were steady state and involved the collection of the products of combustion in a hood. Under such circumstance the global equivalence ratio were obtained from GC measurements in the studies by Toner and Morehart and by the use of several real time gas analyzers by Beyler. Gas Chromatography is less useful for full scale enclosure fires for realistic fuels because of the presence of soot and a wide range of unburned hydrocarbons and because of both spatial and temporal variations in the species concentrations. Here we describe a device with a single gas analyzer that is able to monitor the local equivalence ratio during a large scale test.

The measuring principle is related to the Oxygen Consumption Method, which has been used to sense indirectly the heat released from combustion processes[6],[7],[8]. The basic concept is that the combustion products are sampled into a combustor to burn all of the carbon atoms in the fuel to CO_2 and all of the hydrogen atoms in the fuel to H_2O. The combination of 1000°C chamber temperature, the platinum catalyst, and the approximately 10 s residence time insures that the smoke and other gaseous products of incomplete combustion are converted to CO_2 and H_2O. The CO_2 and H_2O are scrubbed from the exhaust so that only O_2 and N_2 enter the oxygen analyzer.

With this method, the oxygen concentration is measured: (a) for the ambient air without oxygen addition ($X^o_{O_2}$), (b) for ambient air with oxygen addition ($X^i_{O_2}$), and (c) for the sampled combustion products with oxygen addition (X_{O_2}). Analysis of these measurements then yields φ through the following equation:

$$\varphi = \frac{X^i_{O_2} - X_{O_2}}{X^o_{O_2}(1 - X_{O_2})} .$$

From the equation it is seen that there is a simple relationship between the measured exhaust concentration of oxygen and the equivalence ratio. Furthermore the result is independent of the fuel type.

---

1 Fire Science and Technology Inc., 10900 Bethesda Church Rd., Damascus, MD 20872.

2 Fire technology consultant; previously a NIST employee.

The performance of the phi-meter has been evaluated by comparing the instrument results with the metered flow rate of fuel and air. Comparisons have been made for a variety of gases including methane, acetylene, and budadiene. The estimated uncertainty for the phi-meter is on the order of $\pm 3\%$ of full scale. The instrument response time is about 60 s and the measurement range extends from $\phi = 0.1$ to at least $\phi = 3$. The phi-meter has been successfully used with both reduced scale and full scale enclosure fires. The latest version of the phi-meter includes a microprocessor with a direct output reading in terms of equivalence ratio.

1. Babrauskas, V., Levin, B.C., Gann, R.G., Paabo, M., Harris, R.H. jr., Peacock, R.D., and Yusa, S., Toxic Potency Measurement for Fire Hazard Analysis (Special Publication 827). Natl. Inst. Stand. Technol., Gaithersburg (1991).

2. Toner, S. J., Zukoski, E. E., and Kubota, T., Entrainment, Chemistry, and Structure of Fire Plumes (NBS-GCR-87-528). National Bureau of Standards, Gaithersburg, MD (1987).

3. Morehart, J. H., Zukoski, E. E., and Kubota, T., Species Produced in Fires Burning in Two-Layered and Homogeneous Vitiated Environments (NIST-GCR-90-585). National Institute of Standards and Technology, Gaithersburg, MD (1990).

4. Beyler, C.L., Major Species Production by Diffusion Flames in a Two-Layer Compartment Fire Environment, *Fire Safety J.* **10**, 47-56 (1986).

5. Beyler, C.L., Major Species Production by Solid Fuels in a Two Layer Compartment Fire Environment, pp. 431-440 in *Fire Safety Science - Proceedings of the First International Symposium*, C.E. Grant and P.J. Pagni, eds., Hemisphere Publ., Washington (1986).

6. Parker, W.J., An Investigation of the Fire Environment in the ASTM E-84 Tunnel Test. NBS Technical Note 945. [U.S.] Natl. Bur. Stand. (1977).

7. Huggett, C., Estimation of Rate of Heat Release by Means of Oxygen Consumption Measurements. *Fire and Materials* **4**, 61-65 (1980).

8. Babrauskas, V., and Grayson, S.J., eds., *Heat Release in Fires*, Elsevier Applied Science Publishers, London (1992).

SELF-PRESERVING ROUND BUOYANT TURBULENT PLUMES: IMPLICATIONS FOR TURBULENCE MODELS

Z. Dai, L.-K. Tseng and G.M. Faeth
Department of Aerospace Engineering
The University of Michigan
Ann Arbor, Michigan 48109-2118

Introduction. Turbulence models are often used to analyze practical fires due to the computational intractability of fully resolved three-dimensional time-dependent simulations of practical buoyant turbulent flows. Developing reliable turbulence models, however, has been inhibited due to the absence of measurements; therefore, the objective of the present investigation is to complete measurements within round buoyant turbulent plumes, emphasizing self-preserving conditions far from the source. Present considerations include classical similarity concepts [1] and turbulence models of varying complexity [2,3]. Detailed discussion of the investigation can be found in [4-6].

Experimental Methods. Dense gas sources (carbon dioxide and sulfur hexafluoride) in still air were used to generate the test plumes. Mixture fraction and velocity statistics were measured using laser-induced iodine fluorescence (LIF) and laser velocimetry (LV), respectively.

Results and Discussion. The most significant finding has been that earlier plume measurements failed to reach self-preserving conditions [4-6]. This difficulty was not recognized in the past, causing controversy and impeding the development of turbulence models. The problem is illustrated in Fig. 1, where a similarity variable for mean mixture fraction, F, is plotted as a function of the radial plume similarity variable. The plots include turbulence model calculations and earlier measurements summarized in [2], as well as the present measurements. In order to match predictions and earlier measurements, the model constant, C_μ, was increased from 0.09, its well-established value, to 0.15-0.18 [2]. In contrast, present measurements of truly self-preserving plumes indicate a narrower flow and agree with predictions using the standard value of C_μ; consideration of velocities yielded similar results.

Quantities like the rms mixture fraction and streamwise velocity fluctuations, $\tilde{f}'$ and $\tilde{u}'$, must be known in order to treat developing flows but finding $\tilde{f}'$ is problematical for buoyant flows. This difficulty is illustrated in Figs. 2 and 3 where $\tilde{u}'$, and $\tilde{f}'$ are plotted for self-preserving conditions [4-6]. The behavior of $\tilde{u}'$, (Fig. 2) is similar to nonbuoyant flows [3] and is given reasonably well by the models used in [2]; however, $\tilde{f}'$ (Fig. 3) has large values near the axis due to buoyancy-turbulence interactions not treated in [2]. The difficulty is caused by the large streamwise gradient of mean mixture fraction which contributes a production term for $\tilde{f}'$ that normally is ignored using the conventional boundary-layer approximations.

Temporal power spectra are another interesting feature of buoyant turbulent flows. Examples of temporal spectra of $\tilde{u}'$ in the self-preserving region are illustrated in Fig. 4 but results for $\tilde{f}'$ are similar [4-6]. The spectra initially decay according to the -5/3 power of frequency similar to the inertial-convection region of conventional nonbuoyant turbulence, but then exhibit a -3 power decay rate within an inertial-diffusive subrange that only is observed for buoyant turbulent flows [4-6].

Acknowledgments. This research was supported by the United States Department of Commerce, National Institute of Standards and Technology, Grant No. 60NANB1D1175, with H. R. Baum of the Building and Fire Research Laboratory serving as Scientific Officer.

References

1. H. Rouse, C.S. Yih and H.W. Humphreys, Tellus 4:201-210 (1952).
2. M.A. Pivovarov et al., Combust. Flame 92:308-319 (1992).
3. N.R. Panchapakesan and J.L. Lumley, J. Fluid Mech. 246:197-247 (1993).
4. Z. Dai, L.-K. Tseng and G.M. Faeth, J. Heat Trans. 116:409-417 (1994).
5. Z. Dai, L.-K. Tseng and G.M. Faeth, Heat and Mass Transfer 94, Tata McGraw-Hill Pub., New Delhi, 1994, pp. 57-66.
6. Z. Dai, L.-K. Tseng and G.M. Faeth, J. Heat Trans., in press.

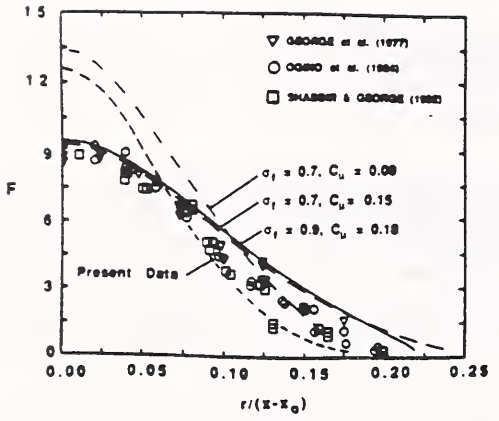

Fig. 1 Predicted and measured mixture fractions.

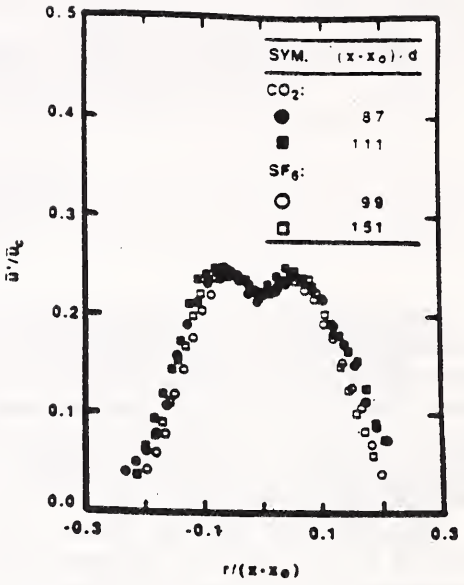

Fig. 2 Radial profiles of streamwise velocity fluctuations

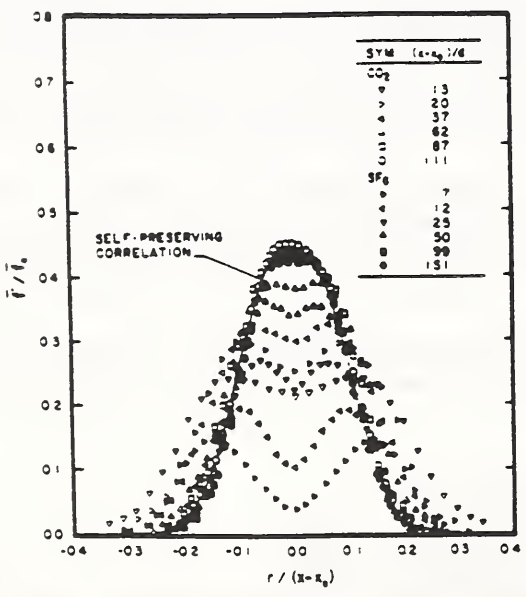

Fig. 3 Radial profiles of mixture fraction fluctuations.

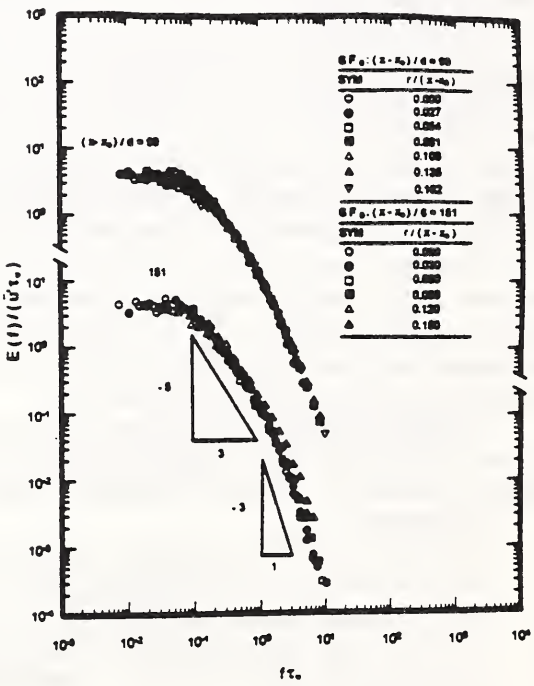

Fig. 4 Temporal power spectra of streamwise velocity fluctuations.

PHASE-RESOLVED VELOCITY FIELD MEASUREMENTS IN PULSATING BUOYANT PLUMES OF HELIUM-AIR MIXTURES

Baki M. Cetegen
Mechanical Engineering Department
University of Connecticut, Storrs, CT 06269-3139

It has been well-established that pool fires and highly buoyant non-reacting plumes undergo periodic oscillations near their source. Although many features of these oscillations have been characterized[1-3], there is still a need to understand driving mechanism of this phenomenon and its effects including entrainment. Thus, we present new experimental results on the periodic nature of plumes of helium-air mixtures established on a 0.10 m. diameter nozzle as shown in Fig. 1. The main reason for the study of nonreacting plumes is that (1) such plumes had been shown to exhibit the same phenomenon as simulated pool fires in terms of the periodic fluctuations[2] ; and (2) the relative ease with which laser measurements can be made in a non-reacting plume compared to pool fires. In our experiments, the helium-air mixture is seeded with small water droplets (≤ 2 μm) before discharging from the nozzle. A slow coflow, also seeded with similar water droplets, surrounds the nozzle to keep the plume seeded for the velocity measurements. Velocity field is measured with the technique of digital particle image velocimetry (DPIV). Measurements are performed in the near field of plumes within a height of 0.08 m from the nozzle exit at different phases of the plume pulsation cycle. Particle pair images in regions of 3.3 cm x 2.5 cm, spanning the radial-axial plane are obtained with a 1320 x 1035 pixel CCD array when illuminated with a light sheet from a modulated Ar^+ laser as shown in Fig. 2.. Digital images are analyzed on a computer to yield velocity vectors in the imaged region. The measurements are phase-locked to obtain the velocity field at different stages of the puffing cycle. This is accomplished by detection of small pressure fluctuations at one half diameter distance in the plume center and triggering the image acquisition from this sinusoidal signal with appropriate time delays. Three velocity field images are shown in Fig. 3 at different phase angles. The acceleration of the buoyant fluid near the plume centerline and the associated induction of the surrounding fluid into the plume can be clearly identified. This acceleration and induction evolves with the formation of the vortex ring which we see in the flames as the periodic vortical flame structures.

References:

1. Zukoski, E. E., Cetegen, B. M. and Kubota, T., *Twentieth Symposium (International) on Combustion*, The Combustion Institute, Pittsburgh, 1984, p.361
2. Cetegen, B.M. and Ahmed T. A., *Combustion and Flame*, 93: 157-184 (1993)
3. Hamins, A., Yang, J. C. and Kashiwagi, T., *Twenty-fourth Symposium (International) on Combustion*, The Combustion Institute, Pittsburgh, 1992,

Acknowledgements:

This work was started when I was on sabbatic leave at Yale University. I would like to thank Prof. Marshall B. Long for hosting me at his laboratory and providing the image processing software used in this work. I also would like acknowledge the help of Jonathan Frank and David Murran at Yale in various experimental diagnostic tasks.

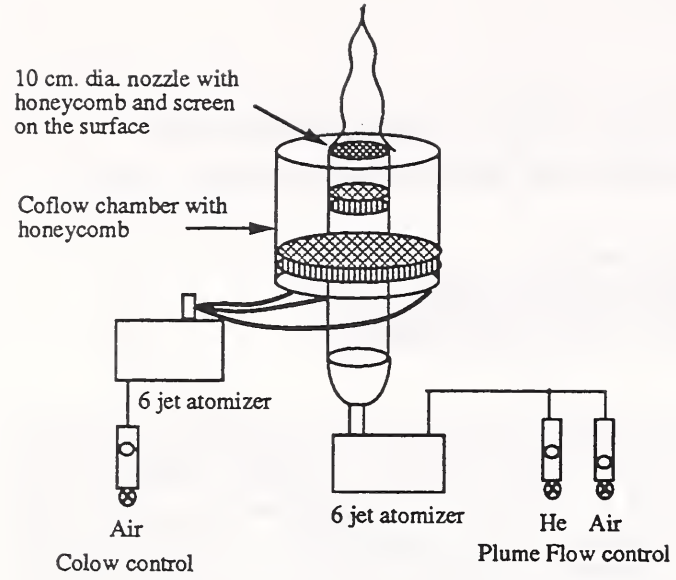

Figure 1. Transparent view of the nozzle set-up and its accessories

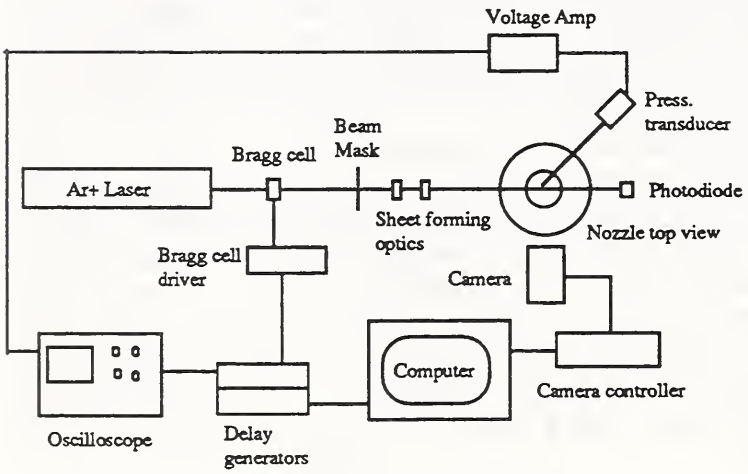

Figure 2. Schematics of the optical set-up

Figure 3. Velocity field at three instants during the puffing cycle as shown in the pressure trace below.

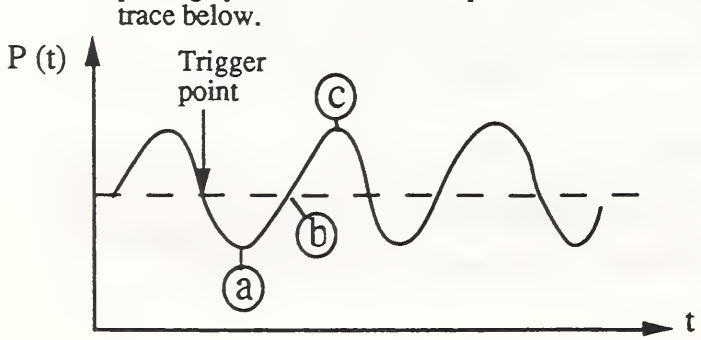

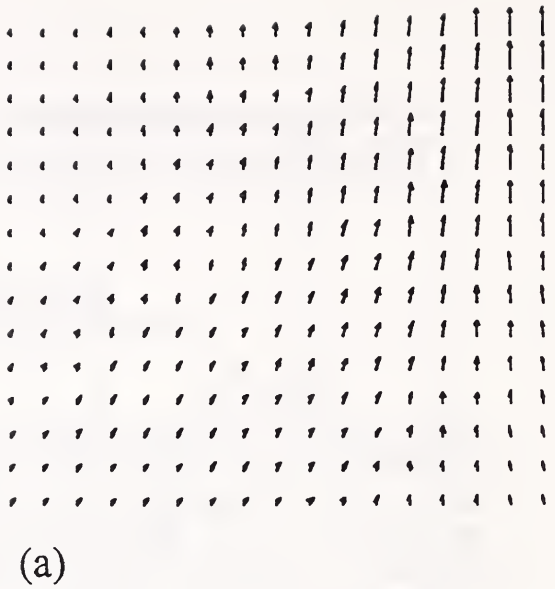

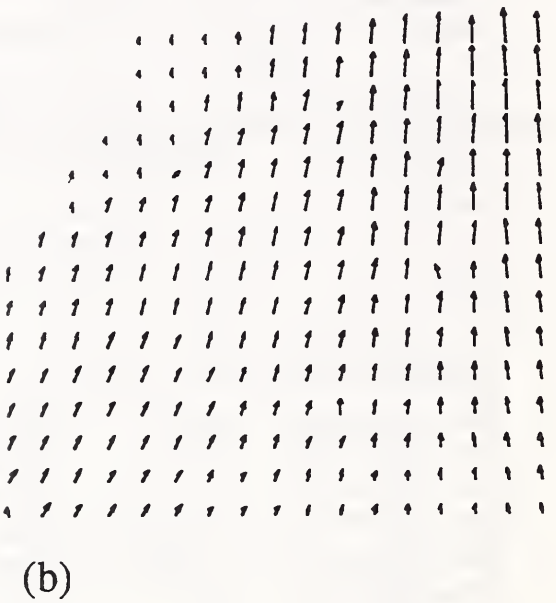

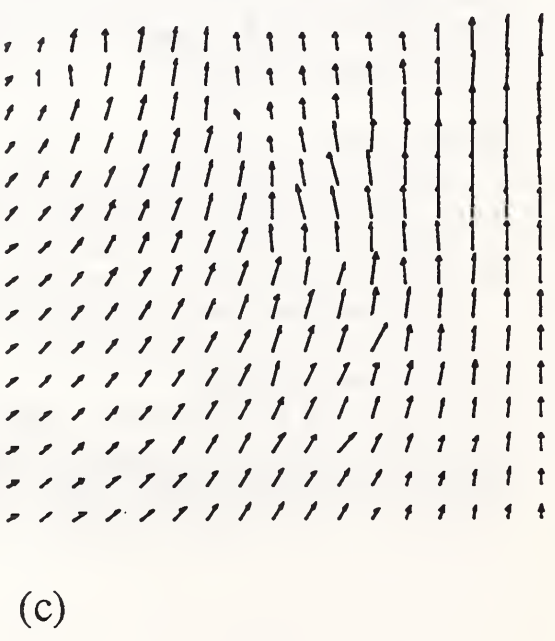

Simulation of a Jet Diffusion Flame using Lagrangian Thermal Elements

Ofodike A. Ezekoye and Ziji Zhang
University of Texas at Austin
Austin, TX 78731

Overview

An obstacle to the accurate simulation of the combustion processes in various turbulent combustion phenomena is the inability to model all scales of interactions on the computational grid. Several modeling strategies are presently used to overcome this obstacle (1). The laminar flamelet approach to combustion appears to provide a means of resolving many of the complexities associated with turbulent combustion. Unfortunately however, problems exist with the temporal and spatial temperature and soot species specifications in heavily sooting and radiating flames (2).

Ideally, any turbulent combustion process should be solved in such a way that the grid resolution is adaptive and provides sufficient resolution for the combustion/reaction processes while requiring less accurate resolution of the large scale convective processes. A Lagrangian formulation of the laminar flamelet approach may circumvent some of the difficulties associated with present turbulent combustion calculations (3).

Theory

One might imagine a Lagrangian method of combustion in which computational fuel elements are released into the large scale flow field. This concept may be justified since the singular issue in most turbulent combustion calculations is the "bookkeeping" of the fuel species through oxidation. A coarse grid Eulerian calculation is used to specify the mean mixture fraction (or extent of mixing with air that any individual fuel element undergoes). The coarse grid Eulerian calculation may also prescribe the local turbulence levels (scalar dissipation) at the location of any material element that originated as fuel species. A computation/look-up table from the element specifies the reaction rate, the amount of fuel remaining, the amount of various products generated from the initial mass of fuel, and the amount of soot generated by the initial mass of fuel. The temperature field may be computed on the Eulerian grid using the heat release rates of the small elements as source terms.

As a first approximation to a calculation in which information flows between the small and large scale processes, it is initially proposed that the sole input to the thermal element (i.e., to the small scale Lagrangian fuel element) be the large scale time variable. The thermal element is assumed to be a fuel sphere surrounded by an abundance of oxidizing air. The reaction process is computed on the element. As time progresses, the fuel is oxidized within the thermal element and various product species are formed. Thus, the fuel mass, products mass, and soot mass are all specified by the small scale processes. At any time, the mean mixture fraction of the element is taken from knowledge of the amount of fuel and product species. The convection time of the element in the large scale is equal to the diffusion time associated with combustion on the small scale. In a convective time of dt, the fuel species has been consumed at a rate specified by the diffusional processes within the element.

Practice

In the course of developing this approach for general applications, various canonical flow fields will be investigated using Lagrangian formulations. Thus, a turbulent jet diffusion flame is modeled using the first approximation of this technique. The combustion is modeled using Lagrangian elements in which a diffusion controlled reaction rate takes place. The flow field is decomposed into solenoidal and irrotational components. The jet solenoidal component is simulated using a two equation turbulence model based upon a GENMIX scheme. The irrotational component of the flow field is specified by the heat release rates specified by the thermal elements. It is important to note that although the solenoidal velocity is steady, the overall jet flow field is unsteady and fully three dimensional.

Particles with a precomputed burning history and self contained combustion field are released into the flow field at the jet inlet. At prescribed computational times, new particles enter the flow while older particles are convected downstream into the field. The conserved scalar field of the flame is determined by calculating the local mixture fraction of the individual elements and then interpolating these values onto the Eulerian grid. The various species mass fractions are also interpolated onto the Eulerian mesh in a similar fashion. The temperature field shown below is calculated by interpolating the individual particle temperatures onto the mesh. It is emphasized that an Eulerian or smooth temperature field can also be specified by computation of the energy equation on the Eulerian mesh. The temperature field specified by interpolation of the particle temperatures onto the mesh is relatively hot (i.e., the ambient temperature is not seen on the contour plot). This is consistent with the notion that only particles that originate from the fuel species are being tracked. These particles have recently

burned and are hot. A computation of the energy equation on the Eulerian mesh would provide the more often seen temperature profile with cool ambient temperatures. The results of these preliminary computations indicate that a Lagrangian modeling methodology may be appropriate for some turbulent combustion simulations. The next step is to further couple the mixing rates specified by the large scale processes to the combustion state within the local element.

Acknowledgments
The authors acknowledge the contributions of Dr. H.R. Baum. This research is supported by NIST Grant No.60NANB3D1436.

References

1. Bilger, R.W., "Turbulent Diffusion Flame," Annual Rev. Fluid Mechanics, 21, 1989.

2. Jang, J.H., Sivathanu, Y.R., and Gore, J.P., "Lagrangian Simulation of Radiative Cooling Processes in Acetylene/Air Jet Flames," Journal of Heat Transfer, 1992.

3. Baum, H.R., Ezekoye, O.A., McGrattan, K.B., and Rehm, R.G., "Mathematical Modeling and Computer Simulation of Fire Phenomena," Theoretical and Computational Fluid Dynamics, in press 1994.

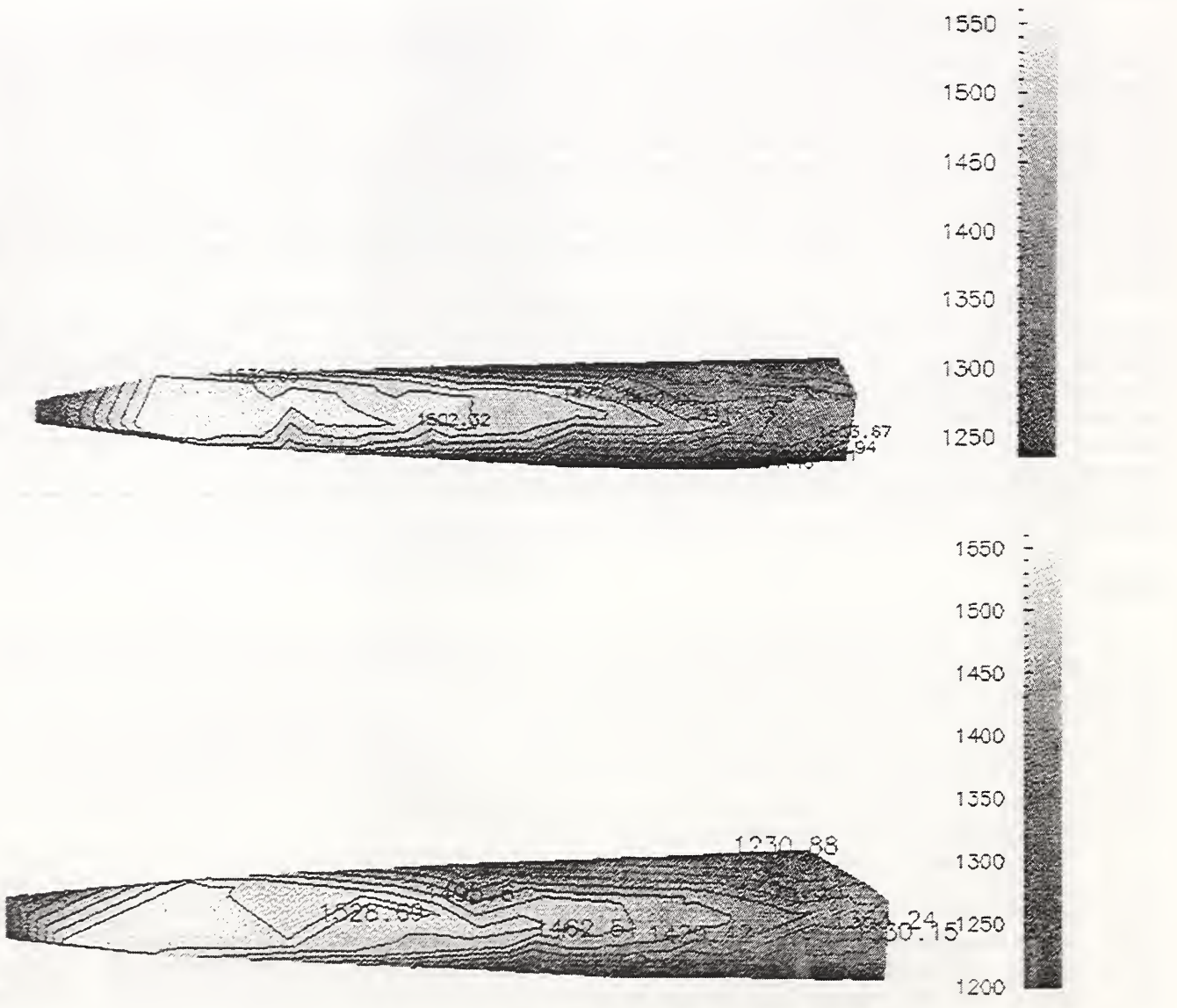

Figure 1. Isotherms at jet cross-section (Re= 20,000): a) t=0.6 seconds after "ignition", b) t= 0.8 seconds after "ignition".

FIRE WHIRL ENHANCED COMBUSTION

Cheng Qian, Ghassan Tashtoush, and Kozo Saito

Combustion and Fire Research Laboratory
Department of Mechanical Engineering
University of Kentucky
Lexington, KY 40506-0108

ABSTRACT

Crude oil spills at sea must be mitigated rapidly to deduce and prevent damage to the marine environment. Recent major oil spills such as the Exxon Valdez Spill in Prince William Sound Alaska on March 24, 1989 have demonstrated the difficulty and expenses in mitigating large oil spills at sea. In situ burning of spilled oil has been proposed as a technique which offers the potential to convert rapidly large quantities of oil into its primary combustion products, carbon dioxide and water, with small percentage of other residue by-products [1]. Because the direct burning of oil spills, which is generally collected and confined by a towed fire boom, produces a heavy smoke plume which may persist for many miles, the burning is questioned by many people from public healthier concerns. To control the combustion by-products and promote the burning rate, spinning of the entire flame by a concentrate vortex is proposed. The idea of this technique, fire-whirl-enhanced combustion, is to enhanced combustion rate by providing sufficient air from ambient, i.e., by increasing resident time for fuel and air to well mix, chemically react, and achieved complete combustion.

Mechanism of fire whirls is complex and is not clearly understood yet, although some studies were conducted [2]. The studies suggest that both wind and windshear needs to interact with fire-induced-buoyancy flow. This study is conducted to provide experimental data for use to design a fire-whirl-enhanced combustion apparatus.

The water pan is 76 cm long, 66 cm wide and 5 cm deep. The oil layer on the water surface was confined by a steel circular rim which diameter was 18 cm. The oil fuel was commercial diesel, the quantity of oil for each burn was 250 ml and the thickness of the oil layer was about 1 cm. As the oil was consumed, the water in unconfined area was free to flow under the circular rim. Because the area of the oil layer (254.5 cm^2) was very small compared with water area (4761.5 cm^2), the oil level was assumed remaining unchanged during burning. The pool fire was surrounded by a circular wall made of steel sheet. The wall was interrupted by four vertical slots arranged so as to admit air in a tangential

direction to produce a concentrated vortex in the flame. The fixed position instrumentation in the burn pan consisted of thermocouples and a heat flux meter. An array of 80.3 mm diameter K-type thermocouples were located vertically through oil layer and the water. A Gardon-gauge type heat flux meter was located at the center of the pan and at the same level of the oil surface to measure incident heat flux from the flame to the oil surface. Data from thermocouples and heat flux meter was recorded on a computerized data acquisition system every 0.5 seconds. To make comparison, tests were conducted with and without fire whirl receptively, and were repeated twice for each case. Burning time was recorded, the quantity of residue oil was measured to estimate the burning rate. Flame heights were measured and smoke production was observed.

The burning of oil layer on water was observed to take place in two different phases except ignition and extinction: 1) steady burning, 2) steady burning with boiling of water below the oil layer. The ignition and extinction took so short periods of time for these tests that they can be neglected compared with steady burning. The steady burn lasted 265 and 977 seconds respectively with and without fire whirl. As the fuel was consumed heat transferred through the fuel to the water bellow can result in boiling of the water. From previous experiments, it appears that boiling resulted in a great increase in regression rate with both fuel and water droplets being sprayed into the flame. The onset of boiling was characterized by a noticeable increase in sound and bubbles breaking through the oil layer. For these tests water boiling took place at 255 and 780 seconds after ignition was estimated from the burning time and the quantity of oil consumed. It was found that the burning rate was increased about 3.5 times by fire whirl. Surface regression rates were 0.0029 and 0.008 mm/s with and without fire whirl respectively. The height of the fire whirl was 175 cm in average, about 10 times of the oil pan diameter. The smoke production was also found decreased significantly.

Interaction of Large, Cold Objects with Engulfing Fires

V. F. Nicolette[1] and L. A. Gritzo
Department 1513, MS 0835
Sandia National Laboratories[2]
P.O. Box 5800
Albuquerque, NM USA 87185
Sandia Document #SAND94-1896A

J. Holen
Division Thermodynamics
SINTEF/NTH
Trondheim, Norway N-7034

Abstract

The interaction of large, cold objects with engulfing fire environments is poorly understood. Large, cold objects can have significant impact on the local temperature, combustion, and soot fields in a fire. The primary mechanism for this interaction is thermal radiation heat transfer between the object and the combustion products (specifically, soot, CO_2, and H_2O). As a result of this interaction, heat fluxes to the object can be significantly altered. An understanding of this phenomenon is especially important for the interpretation of heat flux measurements to large objects in fires.

A simple analytical model of the interaction between a large object and an engulfing fire environment has been developed previously (Nicolette and Larson, 1990). In that work, a one-dimensional thermal radiation model (a two-flux model) was coupled to the local flow, thermal, and combustion fields to characterize the interaction between an object and a fire. Many simplifying assumptions were invoked to derive the model. The combustion products were treated as a gray gas with uniform velocity. The model results demonstrated that a substantial thermal radiation boundary layer can develop adjacent to a large, cold object in a fire. Calculations with the model indicated that reductions in heat flux of 25-40% (relative to uncoupled blackbody heat flux calculations) were typical for a large flat plate in a fire, as a result of the thermal radiation boundary layer development. These results have successfully explained discrepancies observed in heat flux measurements to calorimeters of varying sizes (see for example, Keltner, Nicolette, Brown, and Bainbridge, 1990).

A second paper on this subject (Gritzo and Nicolette, 1993) built upon the previous work, but went further in adding the transient thermal response of a large object to the parameter space. In that work, the governing equations were non-dimensionalized and solved over a broad parameter space. The non-dimensional heat flux was found to be a function of a radiation number, a radiation Biot number, and the ratio of object temperature to fire temperature. The results were then utilized to delineate regimes in which this interaction was important, and others where it could be neglected. Also, a matrix of results in non-dimensional form was generated for design use.

The purpose of the present work is to investigate the validity of the results of the earlier work. There are two main aspects to this investigation. First, a more sophisticated two-dimensional discrete transfer radiation model (coupled to a two-dimensional flow field solver) is applied to problems previously investigated with the simple model, relaxing many of the assumptions of the earlier work. The effects of buoyancy, wall drag, non-uniform velocity field, and turbulence (via a k-ε turbulence model) are included. The results are in reasonable agreement with those

---

1. On temporary assignment at Federal Aviation Administration Technical Center, ACD-250, Bldg.204, Atlantic City Int. Airport, NJ, USA 08405. Telephone #: (609) 485-5132, Facsimile #: (609) 485-5785

2. Sandia National Laboratories is managed by Martin Marietta Corp. for the U. S. Department of Energy under contract DE-AC04-94AL85000.

of the simple model developed previously, and indicate that many of the assumptions used to derive the simple model are appropriate. The calculated thermal radiation boundary layer that develops along a vertical flat plate (Fig. 1) is very similar to that predicted by the simple model.

The second aspect of this investigation involves attempting to answer the more difficult question: how applicable is the simple model to actual fire environments, where combustion and soot generation processes are present, and the flow field may not be one-dimensional due to entrainment processes? To attempt to answer this question, a fire field model (based on the KAMELEON Fire model of Holen, Brostrom, and Magnussen, 1990) is used to simulate the actual fire environment. The effects of combustion, soot generation, and two-dimensionality in the flow field are included in the calculations. Direct comparison of the field model results with the simple model results is difficult due to the spatial and temporal variations in temperature, velocity, and soot concentrations that result from the combustion process. However, the results of the fire field model calculations provide a basis for discussion of the applicability of the simple model to actual fire environments.

References

Gritzo, L.A., and V.F. Nicolette (1993), "Coupled thermal response of objects and participating media in fires and large combustion systems,' ASME HTD vol. 250, Heat Transfer in Fire and Combustion Systems, pp. 161-172.

Holen, J., Brostrom, M., and B.F. Magnussen (1990), "Finite difference calculations of pool fires,' Twenty Third Symposium International on Combustion, pp. 1677-1683.

Keltner, N.R., Nicolette, V.F., Brown, N.N., and B.L. Bainbridge (1990), "Test unit effects on Heat Transfer in large fires,' Journal of Hazardous Materials, vol. 25, pp. 33-47.

Nicolette, V.F., and D.W. Larson (1990), 'The influence of large, cold objects on engulfing fire environments,' ASME HTD vol. 141, Heat and Mass Transfer in Fires, J.G. Quintiere and L.Y. Cooper (eds.), pp. 63-70.

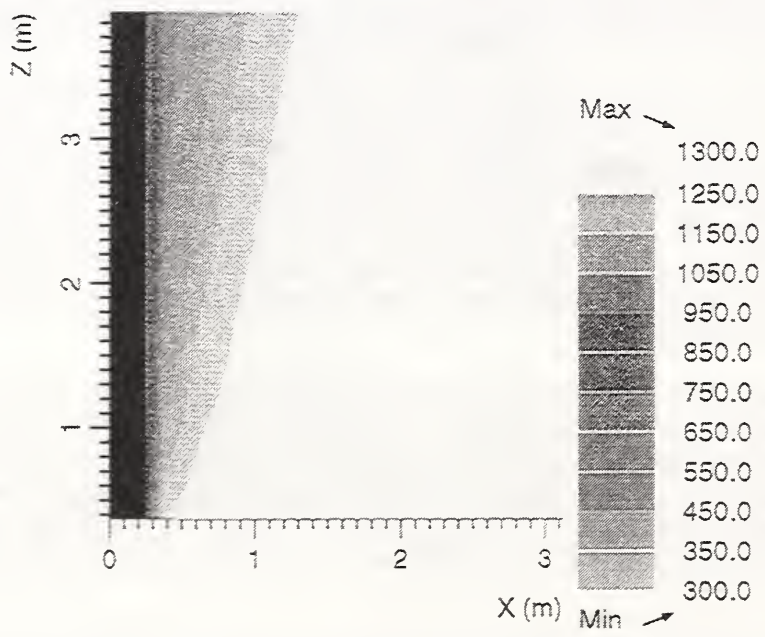

Figure 1: Calculated isotherms (K) showing radiation boundary layer along plate (2-D discrete transfer radiation, plate temp.= 300K, gas temp.= 1300K, gas velocity= 5m/s, extinction coeff.=5m^{-1}, k-ε turbulence model)

FLOW AND TEMPERATURE STRUCTURES INDUCED BY CORNER WALL FIRES

M. Daikoku, C. Qian, J.M. McDonough and K. Saito*

Department of Mechanical Engineering
University of Kentucky
Lexington, KY 40506–0108

(Corresponding Author: K. Saito, Fax: 606–257–3304/Tel: 606–257–1685)

ABSTRACT

A study on upward flame spread along the vertical corner walls is important in fire safety engineering because of its rapid spread rate and intense radiant emission. To understand the mechanism of heat transfer from a fire to corner walls, a room–corner model with 1/2 scale ratio to a NIST (National Institute of Standards and Technology) full–scale test–room was designed in the Combustion and Fire Research Laboratory at the University of Kentucky. A series of flow visualizations using smoke trace method was conducted. Later, based on a collaborative agreement, a duplicate room–corner model was designed at Hachinohe Institute of Technology (HIT). At the University of Kentucky, the focus was on flame spread, while at HIT the focus was on flow visualization. Marinite (inert) walls and Marinite ceiling were heated by a propane gas burner which was located on floor. This paper presents (1) experimental findings on flow visualization using two different (a smoke trace and a salt–water–model) techniques, and (2) temperature and heat flux distributions measured at a steady state both on the walls and ceiling as a function of burner stand–off distance and burner heat flux. The result from (1) confirms a sporadic occurrence of fire vortex along the corner. The result from (2) showed a bottle–neck pattern both for the heat flux and temperature distributions just below the ceiling indicating that the ceiling acts like a dumper to reduce the fire–induced convection.

This is a continuation of our experimental study on room–corner fires. As can be seen in a most recent review by Mitler and Steckler (Comparison of wall–fire behavior with and without a ceiling, **NISTIR 5380,** Building and Fire Research Laboratory, National Institute of Standards and Technology, Gaithersburg, MD 20899, 1994), upward flame spread is an important subject in fire safety engineering because of rapid spread rate and intense radiant emission from the flame. Past studies found that a one–dimensional spread model is applicable with reasonable accuracy for fires over flat vertical walls. Upward flame spread along the vertical corner walls, however, requires additional consideration due to the transient three–dimensional nature of the fire–induced flow. For example, Williamson et al (**Combust. Sci. Tech.**, 41:83, 1984) reports that a complex "T shape pattern" is the characteristic flame spread behavior in room corner fires. Because of the complex nature of the fire–induced flow and of the spread pattern, there are only a few prediction models proposed for corner fires. One of these examples is the Quintiere (**NISTIR 4840,** Building and Fire Research Laboratory, NIST, Gaithersburg, MD 20899, 1992) model which consists of concurrent–flow assisted vertical spread and opposed–flow assisted horizontal spread. Our recent study found that pyrolysis front shape for an upwardly spreading fire along the vertical corner walls was

always M–shape, i.e., no spread along the corner, and the maximum spread is within a few centimeters of the corner. This study clearly suggests a three–dimensional model is required to accurately predict the spread rate.

With the support from the Building and Fire Research Laboratory at NIST, we initiated an experimental project to investigate fires in room–corner walls. Our project consists of two phases: (1) characterization of fire–induced flow, and (2) understanding the mechanism of flame spread along the vertical corner walls. At the University of Kentucky, the initial part of the first phase was completed during 1990 through 1992 periods and the second phase has been undertaken since 1992. To complete the first phase, a joint research program was initiated between the University of Kentucky and HIT; this paper reports recent experimental results on fire–induced flow and temperature structures on Marinite corner walls.

In addition to the experimental work, we are conducting numerical simulation of room–corner fires, both with and without a ceiling. The numerical models very closely mimic the laboratory experiments in terms of geometry and physical conditions. However, the initial computations have been carried out in the absence of chemical reactions, and with radiation being neglected. In addition, all boundary solid surfaces are assumed to be adiabatic, and no treatment of turbulence has been involved. The main goal of this part of the study is to further elucidate details of the fluid dynamics of a room–corner fire, and to provide a rational explanation of differences between the ceiling and no–ceiling cases. In particular, the laboratory experiments indicate a somewhat counter–intuitive result of more heat flux to the walls near the corner for the case of no ceiling. We will attempt to explain this in terms of fundamental physical mechanisms by beginning with the fairly simple simulations described above (which does not exhibit this behavior), and proceeding to add more and more physics to the simulations in a stepwise fashion.

We have completed the first series of runs with this model for a stand–off distance of 5 cm and 80 W/cm^2 burner heat flux. Results are in general qualitative agreement with the experiment with the exception of enhanced heat flux in the no–ceiling case. In fact, we find the more intuitive result of increased heat flux in the presence of a ceiling. We have also shown that the flow field is three–dimensional and complex in the neighborhood of the flame. A fairly large vortex wraps around the flame with parcels of fluid originating near the flame being quickly spun out toward the wall and then circulating back toward the diagonal symmetry plane. The height of the main portion of this vortex continues to increase until it reaches a neighborhood of the ceiling and steady state is reached.

We will next begin to consider the influence of non–adiabatic walls, and then thermal radiation, and simultaneously study the effects of stand–off distance and heating rates on computed results.